Title

Analysis Tool for Fuel Cell Vehicle Hardware and Software (Controls) with an Application to Fuel Economy Comparisons of Alternative System Designs

Author

Hauer, Karl-Heinz

Publication Date

2001

Analysis Tool for Fuel Cell Vehicle Hardware and Software (Controls) with an Application to Fuel Economy Comparisons of Alternative System Designs

By

Karl-Heinz Hauer

Dipl. Ing. (University of Braunschweig, Germany) 1990

Dissertation

Submitted in partial satisfaction of the requirements for the degree of

Doctor of Philosophy

in

Transportation Technology and Policy

in the
Office of Graduate Studies

of the
University of California
Davis

Approved:

_____

_____

_____

Committee in Charge

2001

Meinem Vater

Table of Content

1. Introduction and Problem Context

The ever-growing demand for individual transportation leads to a larger and larger vehicle fleet and a steady increase in vehicle miles traveled (VMT) (National Research Council, 1997). Associated with this increase in VMT are increases in air pollution and carbon dioxide emissions, one possible reason for the observed global warming phenomena (The International Panel on Climate Change, 1995). Although emissions from new conventional vehicles with internal combustion engines and hybrid vehicles with internal combustion engines and additional electric motors are reduced, the air quality standards are not in attainment with federal regulations in many regions in the United States. Especially on the west coast in California with its rapid growth, booming economy, and special weather conditions that promote the formation of ozone, cities like Los Angeles and San Diego battle severe air quality problems (Lloyd, 1999). In addition, the energy efficiency and related carbon dioxide emissions are still far from the 80 miles/gallon goal for passenger vehicles set by the Partnership of New Generation Vehicles (PNGV) and seem to be difficult to achieve with conventional technology.

Widely discussed among the alternatives to the internal combustion engine vehicle are fuel cell vehicles. This vehicle type promises not only very clean operation (up to zero emission operation, but also higher energy efficiency than conventional vehicles without the range limitations associated with battery electric vehicles.[1] Although the fuel cell vehicle has been discussed since the 60's (Sievert 1968), fuel cell vehicles have not been seen as a likely replacement for the internal combustion engine vehicle until recently. In 1994 Daimler Chrysler (formerly Daimler Benz) introduced the first

New Electric Car (NeCar 1) in a series of five prototype fuel cell vehicles (Daimler Chrysler 1999). Despite the fact that these vehicles have prototype characteristics they demonstrated one path to a more environmentally friendly passenger vehicle and sparked public interest and a race into the market. Today all major car companies are investing heavily in this new and promising technology with ambitious plans to introduce it into the market (Panik 1999, GM Europe 1999).

Fuel cell vehicle modeling is one method for systematic and fast investigation of the different vehicle options (fuel choice, hybridization, reformer technologies). However, a sufficient modeling program, capable of modeling the different design options, is not available today. Shortfalls of the existing programs, initially developed for internal combustion engine hybrid vehicles, are:

- Insufficient modeling of transient characteristics;
- Insufficient modeling of advanced hybrid systems;
- Employment of a non-causal (backwards looking) structure;
- Significant shortcomings in the area of controls.

Modern simulation programs should be capable of serving as tools for analysis as well as development.

In the area of analysis, a modeling tool for fuel cell vehicles needs to address the transient dynamic interaction between the electric drive train and the fuel cell system. Especially for vehicles lacking an instantaneously responding on-board fuel processor, this interaction is very different from the interaction between a battery (as power source)

[1] Besides hydrogen fueled fuel cell vehicles, battery electric vehicles are the only other zero emission technology available today.

and an electric drive train in an electric vehicle design. Non-transient modeling leads to inaccurate predictions of vehicle performance and fuel consumption.

Applied in the area of development, the existing programs do not support the employment of newer techniques, such as rapid prototyping. This is because the program structure merges control algorithms and component models, or different control algorithms are lumped together in one single control block and not assigned to individual components as they are in real vehicles. In both cases, the transfer of control algorithms from the model into existing hardware is not possible.

The simulation program developed in this dissertation recognizes the dynamic interaction between fuel cell system, drive train and optional additional energy storage. It provides models for four different fuel cell vehicle topologies:

- A load following fuel cell vehicle;
- A battery hybrid fuel cell vehicle;
- An ultra-capacitor hybrid fuel cell vehicle in which the ultra-capacitor unit is coupled via a dc-dc converter to the stack;
- An ultra-capacitor hybrid fuel cell vehicle with direct coupling between fuel cell stack and ultra-capacitor.

The structure of the model is a causal and forward-looking. The model separates the modeling of control algorithms from the component models. The setup is strictly modular and encourages the use of rapid prototyping techniques in the development process.

The first half of the dissertation explains the model setup. In the second half of the dissertation, the simulation of different hybrid vehicle designs illustrates the capabilities of the model.

This study shows that, from the standpoint of fuel economy improvement, hybrid fuel cell vehicles have a potential advantage over the pure load-following fuel cell vehicle. Further, the study shows that among the modeled hybrid vehicles the vehicle with directly to the stack coupled ultra capacitor shows the largest benefit in terms of fuel economy compared to the pure load-following design. An additional benefit of this design is that it is the simplest of the three investigated hybrid vehicle concepts.

For all of the analyzed hybrid vehicles, the improvement of fuel economy results from the (averaged over a drive cycle) higher fuel cell system efficiency and the additional feature of regenerative braking. Besides the arrangement of the components, the realized fuel economy benefits depend significantly on the control schemes balancing vehicle performance, fuel cell system characteristics, and stress of the energy storage system. Due to the limited energy storage capacity of the ultra capacitor systems, the two vehicles hybridized with ultra capacitors are especially sensitive to the design of the control algorithms.

In addition to the potential improvement of fuel economy, hybrid designs offer the possibility to relax the transient requirements for the fuel cell system and the feature of a rapid cold start in the morning (increased customer benefit). Although not investigated, each of these two advantages is considered important and could, together with the higher fuel economy, spark the interest in hybrid fuel cell vehicle designs in the near future.

2. Literature Review

This chapter analyses different fuel cell vehicle models and compares them with each other on a qualitative basis. Quantitatively Hoefgen (Hoefgen 2001) compares a subset of the models listed in Table 2-3. For the qualitative comparison in this dissertation work first a metric of comparison was established. Second the most commonly discussed models are listed and relationships are identified. Based on the metric of comparison five of the listed modeling programs are described and advantages and disadvantages are highlighted. The comparison concludes that none of the investigated models is satisfactory in terms of modularity (separation of controls and component models), vehicle configurations modeled, and dynamic capabilities.

2.1. Introduction

The generic requirements for a fuel cell fuel vehicle model can be defined as follows and are not different to the requirements of other types of modeling work[2].

A fuel cell vehicle model has to be physically and mathematically sound. All relevant physical effects have to be considered and the model should stand on mathematical solid ground. Unless these two conditions are fulfilled we cannot rely on the results. In addition to the soundness the scope of the model should also be complete. Complete in this context means that it should enable the modeling of different types of vehicles (hybrids, non hybrids and different forms of hybrids) and fuel cell systems for different fuels. The resolution of the modeling effort should be high enough to capture all the effects of interest. For example some of the models listed in Table 2-3 simplify the

function of regenerative braking so much that the results become extremely inaccurate. In the context of Table 2-1, the resolution or depth of modeling these models provide is not sufficient. Also a fuel cell vehicle model has to be flexible enough to incorporate new trends and technologies without the need of starting from scratch. From a practical point of view: the necessary input data have to be available, the validation of the model should be possible, and the model should support its use as well as the issue of program maintenance. The runtime should be in context of the problem setup. Therefore for more complex questions a longer runtime seems to be acceptable. Last, but not least, the results have to be valid and (within tolerances) match the experimental results.

• Theoretically sound
  o Physically
  o Mathematically

• Complete scope
  o Consideration of different vehicle and fuel cell system concepts
  o Resolution (are all effects of interest modeled in a sufficient detail)
  o Flexibility (is the model flexible enough to incorporate future developments)

• Practicality
  o Are the required input data available?
  o Validation possible?
  o Ease of operation
  o Ease of program maintenance? (Logical structure)
  o Runtime

• Valid results

Table 2-1: Generic modeling requirements

[2] The listed requirements are basically taken from John L. Bowman and Moshi Ben – Akiva's paper "Activity - Based Travel Forecasting" (Bowman and Akiva, 1996) but translated into the context of this dissertation work.

Requirement	**Criteria**
Theoretical soundness	Is the model programmed in a forward or backwards approach?[3]
Complete Scope • Completeness	Is the model employing techniques supporting the coverage of a wide range of vehicle concepts (scaling, component libraries)?[4]
• Resolution	Does the model support the method of co-simulation?
• Flexibility	Is the model programmed in a modular way? [5]
Practicality • Input data	Are all required input data available?
• Validation	Does the program setup support the method of rapid prototyping? Are component models separated from control algorithms?
• Ease of use	Is a graphical user interface programmed? Is the documentation complete and useful? Is the runtime reasonable? Is the setup of the model transparent and logical?
Valid results	All the models investigated in this paper deliver valid results within tolerances. Therefore this requirement is not a measure of comparison.

Table 2-2: Translation of the original requirements into objective criteria that could be checked

For an objective comparison of the different simulation models the list of requirements in Table 2-1 is not beneficial. Therefore the content of Table 2-1 is translated into a number of key criteria that a "good" fuel cell vehicle-modeling program

[3] Limiting the requirement of theoretical soundness to the criteria above assumes that the model does not violate any elementary physical or mathematical laws. This assumption is justified for all of the models looked at in this dissertation.

[4] The issue of completeness looks towards the potential of a model to be complete, e.g.; the coverage of all vehicle configurations of interest. Because of the number of possible configurations and the unpredictability of future developments completeness is fulfilled if the model structure supports measures to incorporate a large number of designs.

has to fulfill (Table 2-2). The comparison is looking at these criteria assuming that the incorporation of them into the program guarantees the original requirements in Table 2-1. This systematic comparison emphasizes the (theoretical) potential of the simulation programs. This first comparison will be supported by a closer look at how much of the theoretical potential has already been realized in the current version of each model. This second measure of comparison is more subjective because of fact that due to the very different modeling approaches a direct comparison of functionality is not possible. However it still provides significant insight into the current state of fuel cell vehicle modeling.

After establishing the method of comparison the following paragraphs list the most important (and most used) electric, hybrid and fuel cell vehicle modeling programs. Among them only the UC-Davis hydrogen fuel cell vehicle model has been exclusively developed for fuel cell vehicle modeling. All the other programs incorporate functionality for the simulation of battery electric and IC hybrid vehicles.

[5] Flexibility describes the possibility to change the model structure in a time efficient manner. A modular structure supports flexibility.

Name	Source	Backwards/ Forwards	Fuel Cell Vehicles ?	Year
HYZEM	Ricardo Consulting Engineers Ltd.	Forward	No	1995
Elvis	Southwest Research Institute	Backwards	No	1993
Path	Southwest Research Institute	Forward	No	1996-1997
PSAT	Southwest Research Institute and Argonne National Laboratories	Forward	Yes	1996-1999
Advisor	National Renewable Research Laboratory (NREL)	Backwards	Yes	1994-2000
Simplev	Idaho National Engineering and Environmental Laboratory	Backwards	No	1990-1997
Avte	UC-Davis, ITS	Backwards	No	1996
UC Davis – Hydrogen	UC-Davis, ITS	Backwards	Yes	1999

Table 2-3: Overview about alternative fuel vehicle models

In addition to the vehicle models listed in Table 2-3 other models are under development or already completed. Most of these other, not listed, models are either propriety and internally developed by automotive manufacturers or contractors and only very limited information is publicly available or they are not completed yet. For this reason these models are not discussed in this dissertation work.

The next section compares the most important models listed in Table 2-3 with regard to the criteria explained in the appendix and derives, based on this comparison, the need for a new vehicle model that will be described in this dissertation work.

The comparison ends in a summery and concludes that a new fuel cell vehicle model is necessary.

The appendix provides the necessary background information about three major issues associated with fuel cell vehicle modeling. They are closely tied to the list of model requirements at the beginning of the chapter and have their origin in this list.

The issues discussed in the appendix are:

- The choice of the modeling approach. Two different modeling approaches have been realized in the existing fuel cell vehicle models. The forwards looking and the backwards looking approach. The physical and mathematical soundness of the model is significantly depending on the choice of the modeling approach.

- The incorporation of co-simulation techniques. Co-simulation techniques are the parallel operation of two different modeling programs, e.g. Matlab/Simulink for the overall vehicle and Saber for the electric drive train within the vehicle. Co-Simulation allows a higher depth of modeling or a higher resolution.

- The incorporation of rapid prototyping and hardware in the loop features. Both methods are well known development techniques for shortening the development time. From a modeling point of view the benefits are the fact that (through the involvement of the simulation program in the development process) a mutual validation of the model at all development stages occurs, and not only at the end of the development process.

2.2. Survey and Discussion of the existing vehicle models

Five different development lines could be identified looking at the model properties and the historical development of the models (Figure 2-1). These are:

- Ricardo Consultants with the Hyzem program system (Heath, 1996 and Sadler, 1998).
- Southwest Research Institute (SWRI) with the modeling program systems Elvis, Path, Apace and their final product PSAT (McBroom, 1996). PSAT has been originally developed as the modeling tool for the Partnership of New Generation Vehicles but will be soon made publicly available from Argonne National Laboratory for registered researchers[6].
- National Renewable Energy Institute with the program system Advisor (National Renewable Energy Laboratories, 2000). Since recently, Argonne National Laboratories is responsibility for the development lines PSAT and Advisor and incorporates them into a single graphical user interface for the ease of use.
- UC-Davis starting originally with the Advanced Vehicle Test Emulator (AVTE) and an (AVTE based) direct hydrogen fuel cell vehicle model (Fuel Cell Modeling Group, 1999). Both models are derived from Advisor. In addition to this modeling effort, UC-Davis started within the fuel cell vehicle modeling project a new forward looking fuel cell vehicle model that incorporates currently the fuels hydrogen, indirect methanol and indirect gasoline in hybrid and non- hybrid versions.

[6] The release, for registered researchers only, is scheduled for November 2000.

- Idaho National Engineering and Environmental Laboratory (INEEL) with Simplev. The program has only historical meaning - it was phased out in 1997 (Idaho National Engineering and Environmental Laboratory, 1993).

The final product of each of these development lines will be taken and benchmarked according to the criteria listed in Table 2-2. In addition the fuel cell vehicle modeling capabilities will be listed qualitatively, e.g.; which type of fuel cell vehicle models are included (hybrids, fuel choice).

Finally a statement about the current stand of the model with respect to depth of analysis will be made. For example, some of the vehicle models include a static fuel cell system model based on maps only while other models take dynamic aspects into account.

Based on this comparison it will be concluded that a new fuel cell vehicle simulation model is necessary.

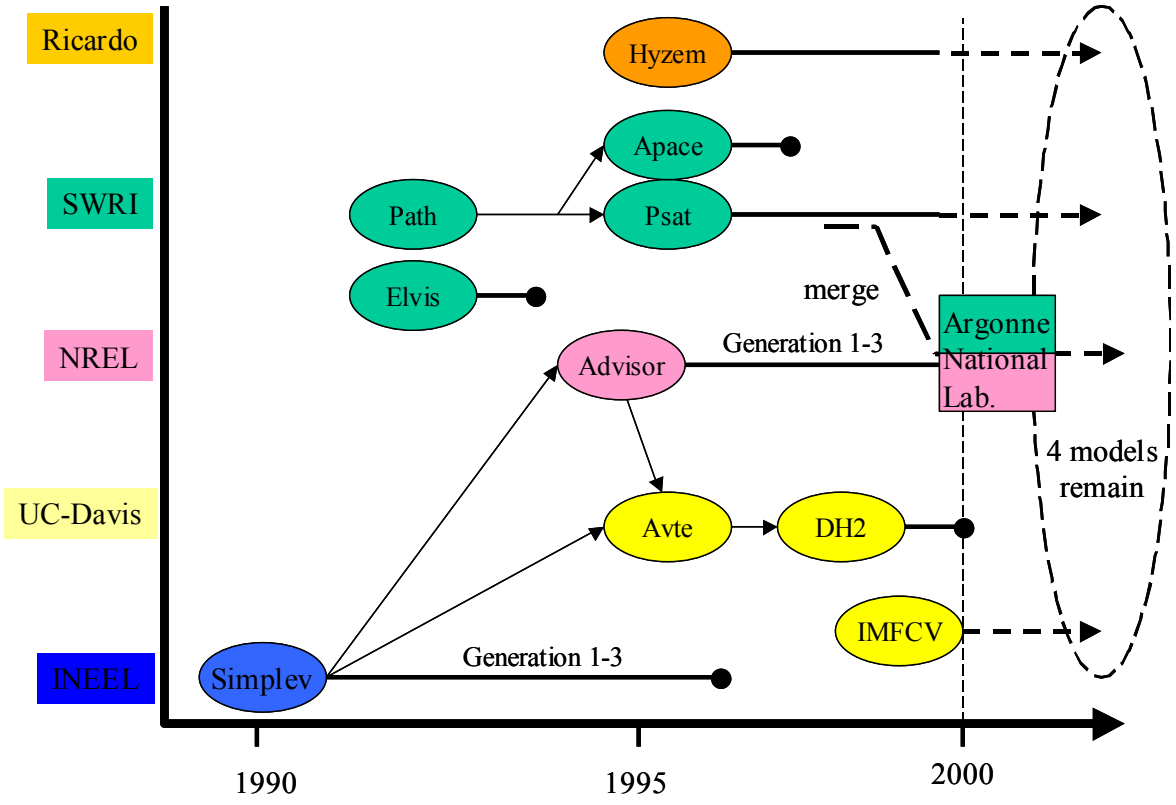

Figure 2-1: Model evolvement and history

2.2.1. The HY-ZEM (Hybrid-Zero Emission Mobility) Model

HY-ZEM has been programmed by Ricardo Consultants and is not commercially available as an off the shelf programming package[7]. The program will always be delivered in a project specific form as part of a development contract. The model is programmed in Simulink in a causal, forward looking, approach (Heath, 1996, Sadler, 1998). Figure 2-2 shows the program setup (highest level) for the example of a series hybrid electric vehicle with internal combustion engine.

The presence of a "driver" block indicates the forward-looking approach. Besides the driver the model consists of one main control Block "SH controller" and component blocks for every major component.

Each component model has three input and three output ports, each port could also be vectorized meaning it could combine several individual variables. The inputs and outputs are listed in Table 2-4. Control inputs and outputs are signals with no energy associated with them for example the value of a voltage or a current. Power outputs/inputs connect blocks on the physical level. One example is the battery voltage connected to the motor block. This connection is physical and could therefore be seen in a real vehicle. The third pair of inputs/outputs is also a physical connections but through these connections feedback loops among components are established. One example for such a feedback loop is the feedback of the motor current to the accessory block and finally to the battery block. Through these feedback loops dynamic behavior is incorporated into the model. Hyzem is set up in a modular form and includes a library for mechanical, electrical and control modules that all employ the same input /output

[7] Personal email exchange with Ricardo Consultants in October 2000

structure (Heath 1996). Input data for the modeling process are standard vehicle parameters and steady state maps for operating point dependent component properties (Sadler, 1998).

Input/Output	Label	Comment
Input 1	Controls input	Signals from the controller block
Input 2	Power input	Input values from a previous block
Input 3	Feedback input	Feedback values from a connected block
Output 1	Controls output	Signals looped to the controls block
Output 2	Power output	Output values to a succeeding block
Output 3	Feedback output	Feedback values to a connected block

Table 2-4: Overview of component models inputs and outputs.

No information could be found about the possibility of co-simulation. However in principle the causal, forward looking, approach supports co-simulation. Also the program package "wave" (Ricardo Consultants, 2000) has been suggested by Ricardo Consultants to UC-Davis for modeling the airside of a fuel cell system. Because of this suggestion it could be assumed that Ricardo also combines (or attempts to combine) Hyzem and wave[8].

Because of the fact that the model is not off the shelf available, and is only provided as part of a larger contract, the issue of "ease of use" becomes secondary. For example a graphical user interface, complete documentation and straight logic is not essential if the user gets assistance from Ricardo. The model has been validated with a Volkswagen Golf IC-hybrid vehicle and a Peugot 106 electric vehicle (Heath, 1996).

[8] Personal email exchange between members of the fuel cell modeling group (UC-Davis) and Ricardo

Modeling results for an indirect methanol fuel cell vehicle in load following and load leveling (hybrid) form have been presented by Sadler (Sadler, 1998). The model includes start up characteristics and emissions although it is not clear how detailed the model is[9].

Strengths:

- Strong modular approach using predefined components from a library (Heath, 1996),
- The model considers the dynamic interaction (feedback) between components (Heath, 1996).

Weaknesses:

- The combination of the library modules leads to a difficult to oversee system diagram, which does not always reflects the causalities within the vehicle. (Example: In the electric vehicle model the battery voltage does not directly feed back into the motor block).
- Control algorithms are not assigned to the individual components, such as the battery controller to the battery block. Instead the control algorithms are summarized in one single control block, which embeds the controls for all components. Embedding the controls of all components in one block makes rapid prototyping as one measure of continuous validation impossible[10]. However Ricardo claims that the recent versions are supporting rapid prototyping.
- The levels of information flow and physical component interaction are not separated.

[9] A version including fuel cell vehicle models was not available

[10] This is true for the 1996 version of HYZEM. However for recent versions of HYZEM Ricardo Consultants claim the possibility of rapid prototyping. Because neither the software itself nor any detailed information has been made available the statements could not be verified.

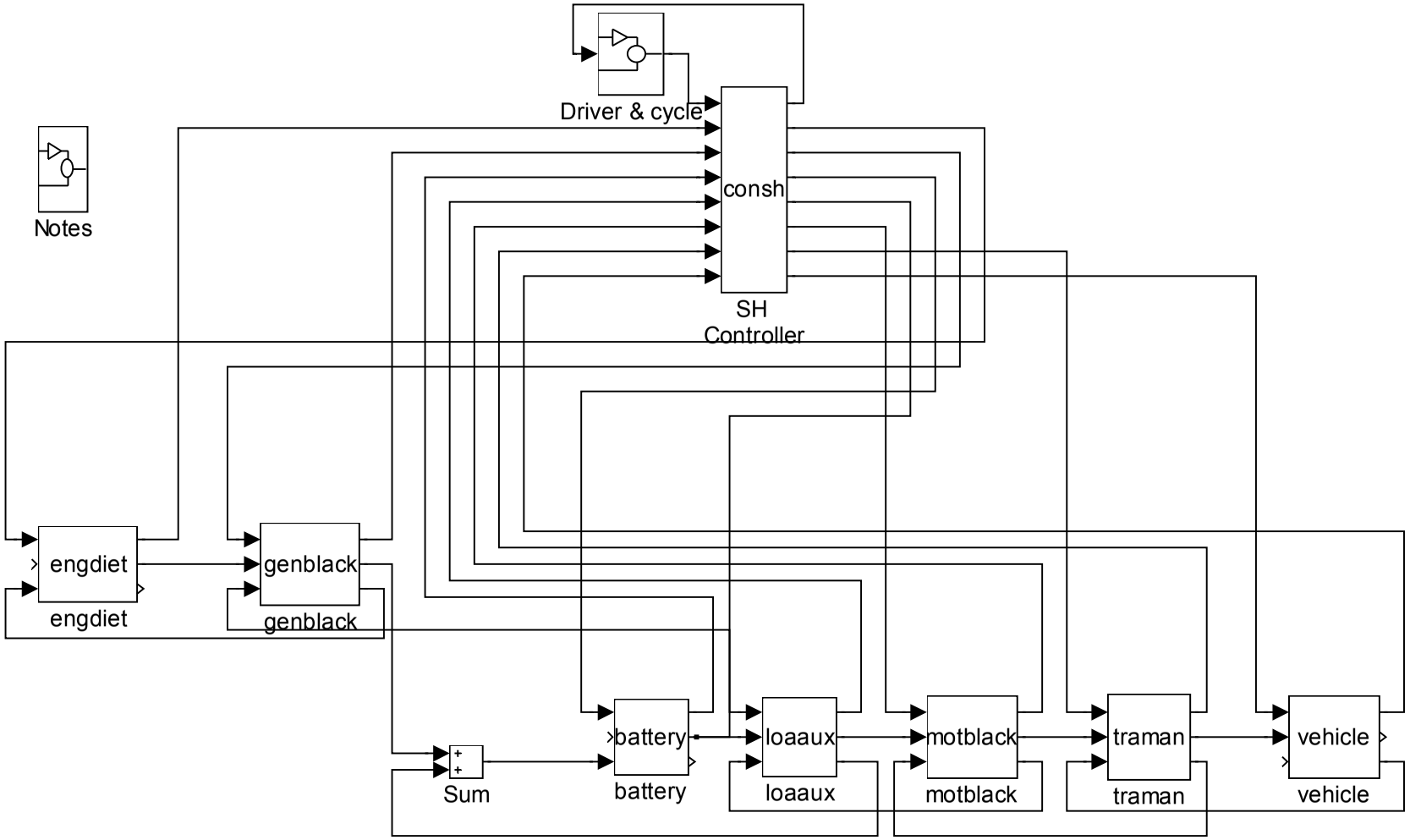

Figure 2-2: Hyzem vehicle model (most upper level of a series hybrid electric vehicle)

2.2.2. The PNGVSAT (Program for New Generation Vehicles Systems Analysis Toolkit) Model

The program PNGVSAT or PSAT has been originally developed by the Southwest Research Institute. Since August 2000 Argonne National Research Laboratories is responsible for program maintenance and further development. Since November 2000 PSAT 4.0 is available for registered researchers in the field of hybrid and electric vehicles (Rousseau 2000).

Figure 2-3 shows the most upper level of the model of an indirect methanol fuel cell vehicle with additional battery storage.

The existence of a driver model (the icon showing the steering wheel in Figure 2-3) indicates a causal, forward looking, modeling approach. The program documentation confirms the separation of driver and vehicle and the forward-looking modeling approach (Argonne National Laboratories 2000).

The general structure is similar to the model developed by Ricardo Consultants. Specific similarities are:

- A driver controls the velocity of the vehicle,
- One single controls block organizes the component interaction (Controller),
- Each individual component block employs three inputs and three outputs, which could be interpreted identical to the inputs and outputs defined by Ricardo Consultants. However the labeling in PSAT is different and orientated to the physical value each port carries, e.g. the current going into the battery is labeled “current in”, the resulting voltage at the battery terminals is labeled “voltage out”.
- Inputs and outputs of each block can be vectorized..

Despite these similarities PSAT employs more blocks than Hyzem. While Hyzem employs only one block modeling the drive train between motor shaft and wheels PSAT uses four blocks for the same task. PSAT models this part of the drive train with much higher accuracy than all other models compared in this dissertation work. One example is tire slip including modeling weight transfer, a feature important for modeling vehicles that exhibit a high power – weight ratio, such as the EV1.

The incorporation of advanced modeling techniques, such as co-simulation is possible (though not realized) in version 4.0.

Although PSAT follows the general setup of Hyzem it does not strictly separate component models from control algorithms. Because of this PSAT 4 does not qualify for the employment of rapid prototyping. The fast and mutual validation of the program in parallel to the development process of a physical vehicle employing rapid prototyping is not possible. Another consequence of the mix of control algorithm with component models is that a validation on the component level is not possible. One example for this is the validation of the stand-alone battery model. The battery model includes current limitations that are not part of the physical battery but realized in the motor controller software and power electronics. The effect is that even a short circuit of the battery model would not result in a voltage drop to zero volts and a current that exceeds the operational limits. In other words a largely oversized motor would still work fine with the battery without noticing that it draws a power much beyond what the battery is able to deliver. In fairness, is has to be said that PSAT as a complete model does not calculate anything wrong. However the result of the merge of a battery model with motor controller

characteristics is a difficult to oversee structure that makes changes and program maintenance time consuming.

A helpful feature of PSAT is the graphical user interface (Figure 2-4). This graphical user interface is very similar in appearance and logic to the one used in Advisor 3.0. It supports the following functions:

- Choice of vehicle topology (series, hybrid, conventional, split),
- Choice of vehicle and component data,
- Component choice (a list of predefined components is available),
- Component scaling (battery, fuel cell system and electric motor),
- Choice of control strategies,
- Choice of drive cycle,
- Parametric studies,
- Display of results (traces of values),
- Summery of results.

However the graphical user interface did not work in all cases and was therefore only of limited use. Also the use of a graphical user interface limits the flexibility of the program.

A fuel cell system model is provided. It has the following characteristics:

- The model covers warm up times and penalties associated with the warm up of the system.
- Emissions are considered in the model but currently all data for modeling emissions are set to zero.

- Transient characteristics of the reformer are modeled with a first order transfer function. The stack characteristics are modeled using a one-dimensional steady state lookup-table.
- The airside and water and thermal management characteristics are only considered through their impact on the overall fuel efficiency and transient effects are not taken into account.
- In summery it could be said PSAT provides a fuel cell system placeholder model that mimics the effects of a fuel cell system - instead of a model based on fundamental principles.

Strengths of PSAT are:

- Availability of a large variety of vehicle concepts
- Graphical user interface

Weaknesses of PSAT are:

- the merge of controls and component models, together with the not strict separation of functionality hurts rapid prototyping as one method of continuous validation
- the merge of controls and component models does not allow validation on the component level
- the merge of controls and component models lead to difficult to oversee interfaces and potentially problems in program maintenance and modifications

- The documentation references mostly to the graphical user interface. However many parts in the actual program are not explained[11].

[11] At the time of this dissertation the documentation was not finished yet.

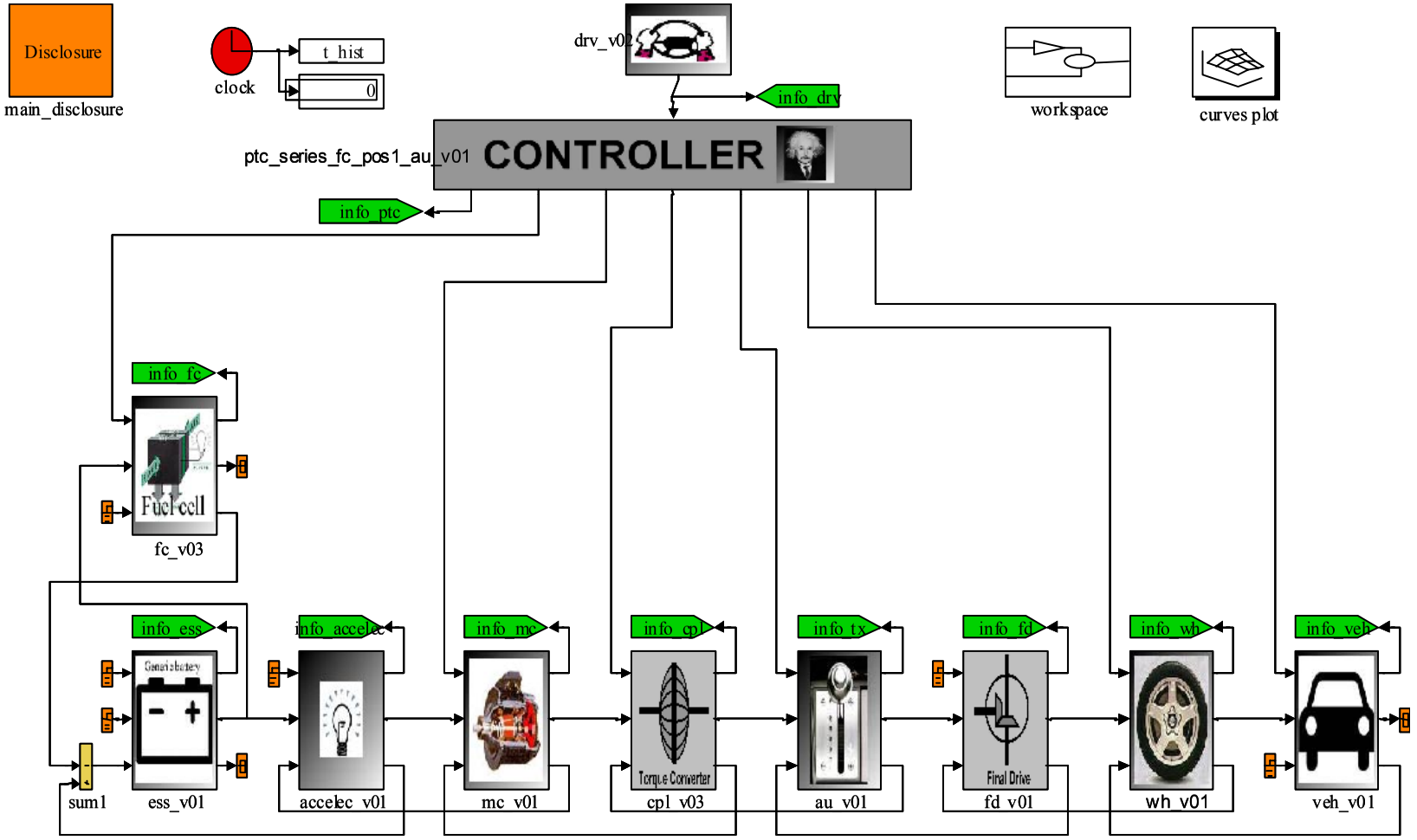

Figure 2-3: PSAT model (most upper level) for the example of an indirect methanol fuel cell hybrid vehicle.

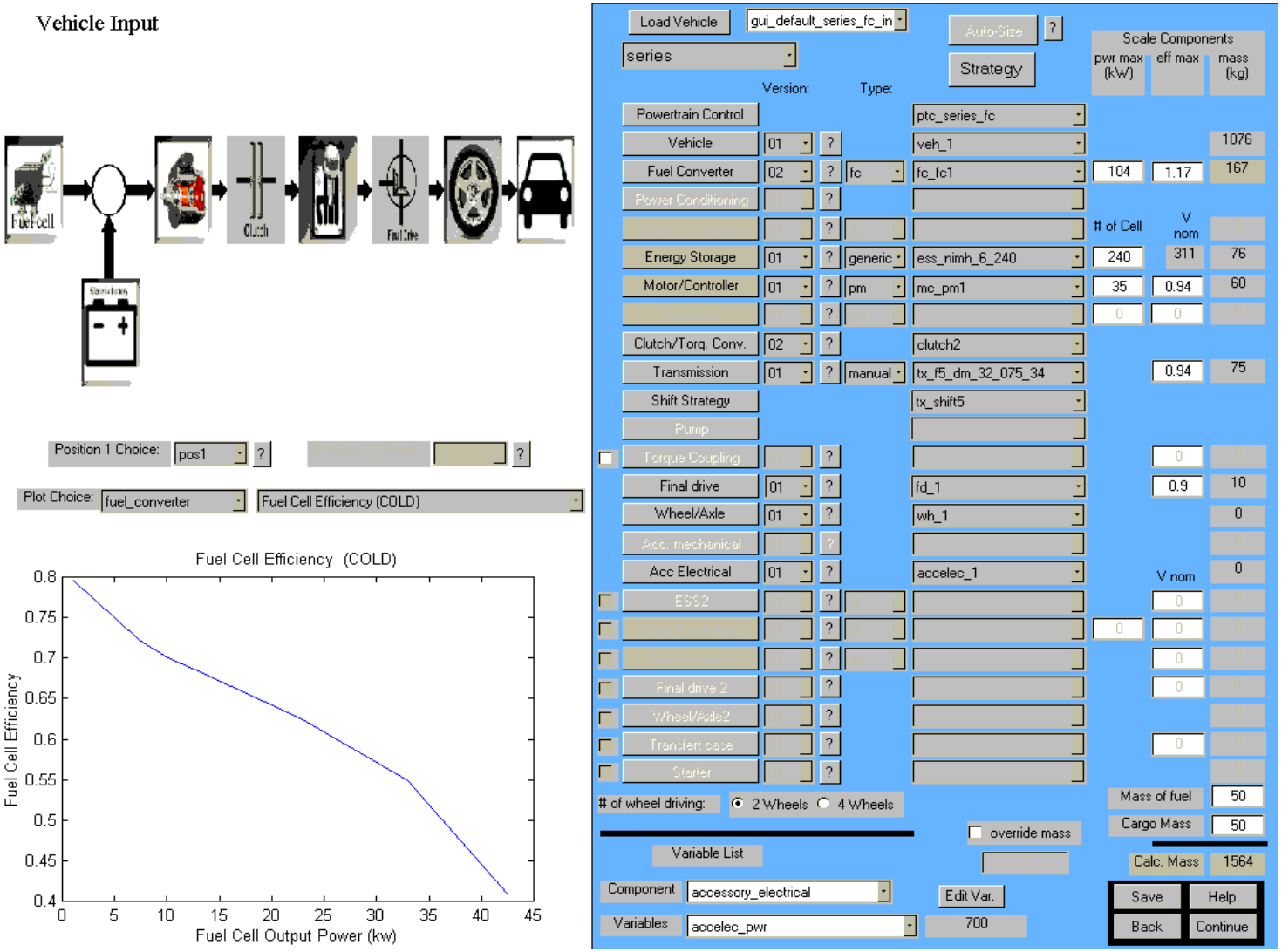

Figure 2-4: Graphical user interface PSAT.

2.2.3. The Advisor (Advanced Vehicle Simulator) Model

Advisor has been programmed by National Renewable Research Laboratory (NREL) and is, after registration, freely available on the Internet (National Renewable Research Laboratory, 2000). Figure 2-5 shows the most upper level of the Simulink code for the case of an indirect methanol fuel cell vehicle.

The program is setup in a backwards approach, e.g. the model is not causal. However according to the Advisor online documentation Advisor labels itself as a hybrid backwards/ forwards approach. This name is confusing because it does not recognize the inherent non-causality within the structure of the program, the key element of a backwards-facing model as defined by Ricardo Consultants (Heath, 1996), Southwest Research Institute (Mc Broom, 1999) and Bengt Jacobson (Jacobson, 1995)[12]. As a consequence of the reverse causality the model is considered to be less physical and less mathematically sound.[13]

Advisor is programmed in Matlab/Simulink. However for special modeling aspects the program has been linked to several program tools. John A. MacBain provides in his paper "*Co-Simulation of Advisor and Saber- A Solution for Total Vehicle Energy Management Simulation"* one example for co-simulation of Advisor and Saber (MacBain, 2000). However due to the reverse causality the employment of this method is limited. Furthermore MacBain describes the application of co-simulation as the only solution for simulating the closely coupled mechanical and electrical systems in series hybrid vehicles. This is not true. The UC Davis hydrogen model allows the simulation of

[12] Bengt Jacobson did not use the terms forward and backward looking models. Instead he used the terms driver controlled for the causal model and conventional model for the "unnatural causality". Important is that causality was his reason to distinguish both approaches.

this vehicle type without employing the method of co-simulation (UC-Davis, Fuel Cell Modeling Team, 1998). This fundamental misjudgment can be taken as one indicator how confusing the reverse causality of Advisor and other backwards-looking programs could be to users.

From a practical point of view the reverse causality is one major obstacle that has been already pointed out[14]. The program compensates this partly with an extensive graphical user interface and a large component library. Because of these features the standard user is not required to look into the details of the model. The good online documentation also provides good support in application questions. However, whenever the model itself needs to be modified the user is required to follow the logic dictated by the reverse causality. This could become more challenging than the physical issues involved with the desired modification. Because of this the model is considered neither flexible nor transparent compared with forward-looking models.

The reverse causality makes the use of control algorithms for rapid prototyping approaches impossible. Therefore this method of mutual validation of the model is not available to the user.

[13] See appendix.
[14] See appendix.

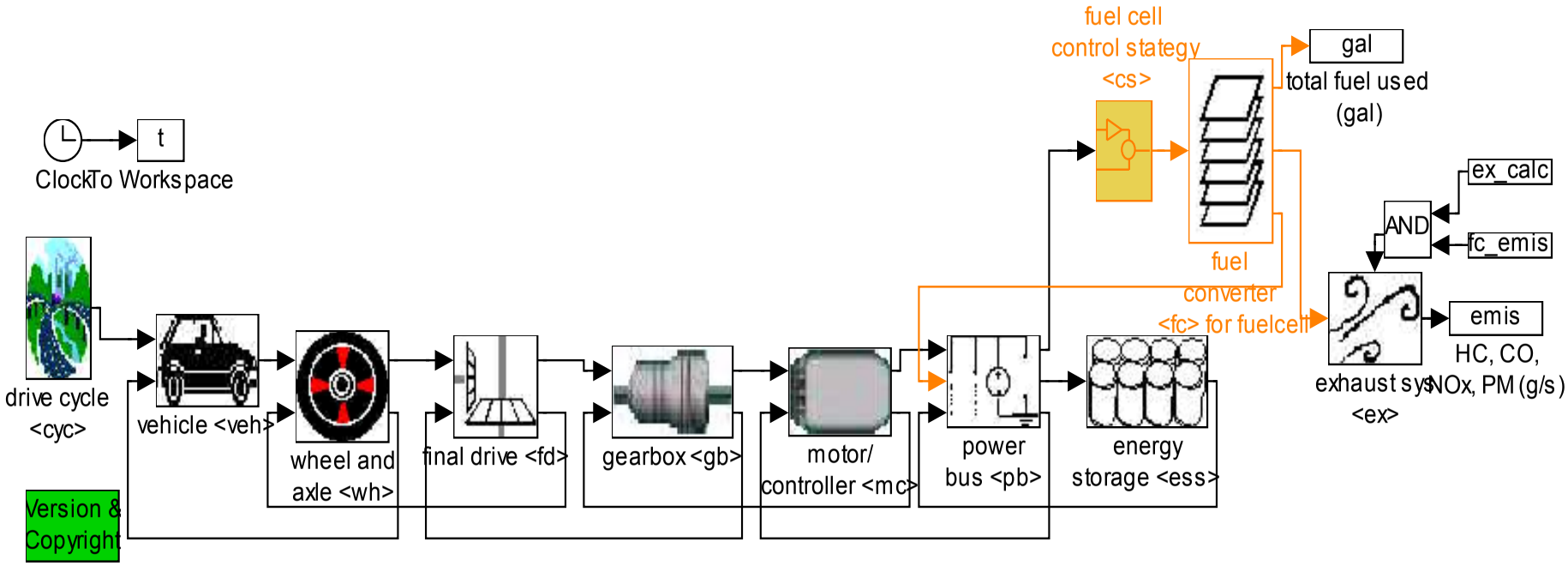

Figure 2-5: Advisor model of an indirect methanol hybrid fuel cell vehicle

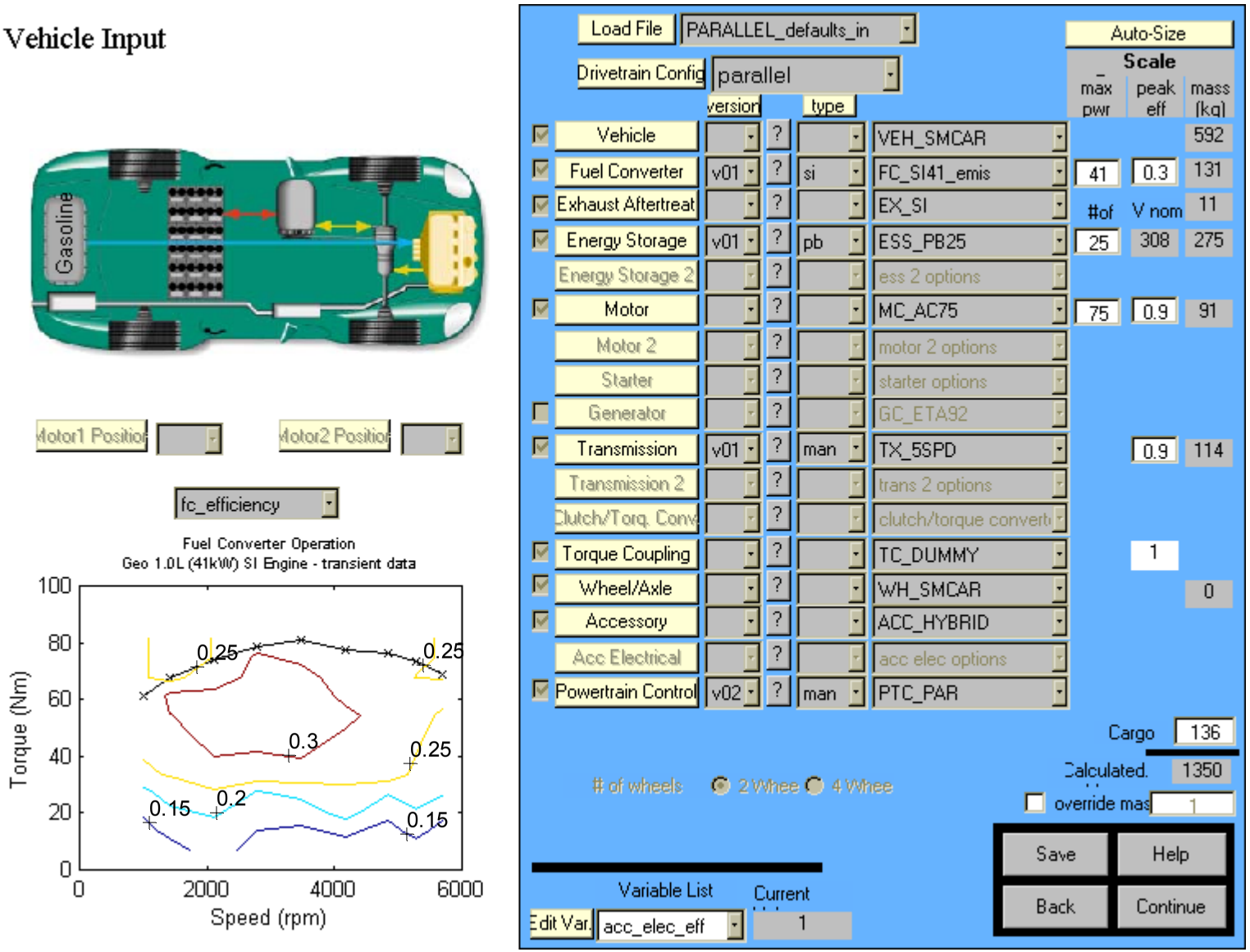

Figure 2-6: Graphical User Interface (GUI) of Advisor 3.0

According to the online documentation, Advisor provides direct-hydrogen, direct-methanol and indirect-hydrocarbon fuel cell vehicle models. In the current version an indirect- methanol system is not available (August 2000, 3.0).

The dynamic interaction among components, such as feedback effects, is limited. Subcomponents of the fuel cell system, such as the fuel reformer, air supply or water and thermal management are only modeled in terms of their impact on the net fuel cell system efficiency. Dynamic effects within the fuel cell system itself, such as reformer and air supply time lags, are not considered. For the case of the indirect-hydrocarbon system emissions, are not predicted.

Strengths:

- The strength of advisor is the detailed graphical user interface (Figure 2-6) that allows the setup and analysis of a wide range of vehicle configurations. The user can choose between 9 predefined drive train configurations. Each configuration allows the choice between 19 electric motors, 9 batteries and 7 fuel cell systems (Wipke, 1999 and National Renewable Energy Laboratories, 2000). The mentioned components are scaleable and could be combined in a vehicle. The user interface is intuitive and provides rapid access for the educated user to the capabilities of the model.
- Short runtime. Because Advisor is a backwards looking model it runs between 2.6 and 8.0 times faster in standard drive cycles than forward looking models (Wipke, 1999).

Weaknesses:

- Documentation helps only very little if the model needs to be modified.
- The reverse causality makes it difficult to follow the logic of the model. This is one major obstacle for future improvement and development.
- Interaction between fuel cell stack, fuel processor and drive train does not include feedback effects. For example it is assumed that the fuel processor is always able to deliver the by the stack required reformate in time. The effect of a drop in stack voltage because of a supply shortage of reformate gas is not modeled, and consequently the electric motor would not provide less torque because of the voltage drop. The feedback of the various components is essential for the modeling of one major issue of fuel cell system and vehicle analysis - transient behavior. The model allows one to investigate only in a very limited way the impacts of different component configurations, parameter variations and control strategies on transient behavior.
- If one component is not able to supply the value required by the previous stage, the operating point of the requesting component is not corrected. If component characteristics vary largely over the operating regime, then ignoring the change of the operating point could impose a large error on the results. An iteration process downstream of the limiting component could potentially solve this problem. However this would significantly complicate the model and is not realized in the current version of Advisor.

2.2.4. The UC-Davis Hydrogen (1998 Version) Model

The original direct hydrogen fuel cell vehicle model of University of California, Davis (UC-Davis) was programmed during 1998. It is part of a modeling effort sponsored by a group of industry and public sponsors and is not publicly available. It is essentially based on a previous version of Advisor and follows therefore the same structure of a backwards-facing model (Figure 2-7). From a practical point of view the complications are the same as with the Advisor model and are mainly a direct result of the reverse causality. The program employs also an extensive graphical user interface easing the simulation of the different vehicle configurations (Figure 2-8).

The model is specialized for direct hydrogen fuel cell vehicles in a load following and load leveling configuration. In addition pure battery electric vehicles could be modeled.

Similarly to Advisor, the fuel cell system is modeled in non-transient form employing steady state polarity plots characterizing the fuel cell stack (fuel cell system place holder model).

In addition to the actual fuel cell model, algorithms have been developed that optimize the interaction between various compressor technologies and the fuel cell stack. The results of this optimization process are then included into the vehicle model. However the combination of fuel cell stack and air supply with the optimization strategy makes it difficult to gain the necessary input data in a laboratory for a specific stack or compressor supplier.

A new forward-looking direct hydrogen fuel cell vehicle model has succeeded this program in 2000.

Strengths:

- Short runtime similar to Advisor,
- Graphical user interface including features for the automatic report generation.
- Attempt for the integration of an optimal compressor operating strategy. The direct hydrogen model of UC Davis is the only model (discussed in this overview) addressing and discussing the potential energy savings in this area.

Weaknesses (see Advisor):

- Reverse causality makes it difficult to follow the logic of the model and is one obstacle for further improvement and development,
- No feedback effects between motor and fuel cell system interaction modeled,
- No correction of the operating point if one component is unable to meet the request,
- Separate program required for the integration of new fuel cell stacks and compressors or the modification of the compressor control strategy ("config" model).

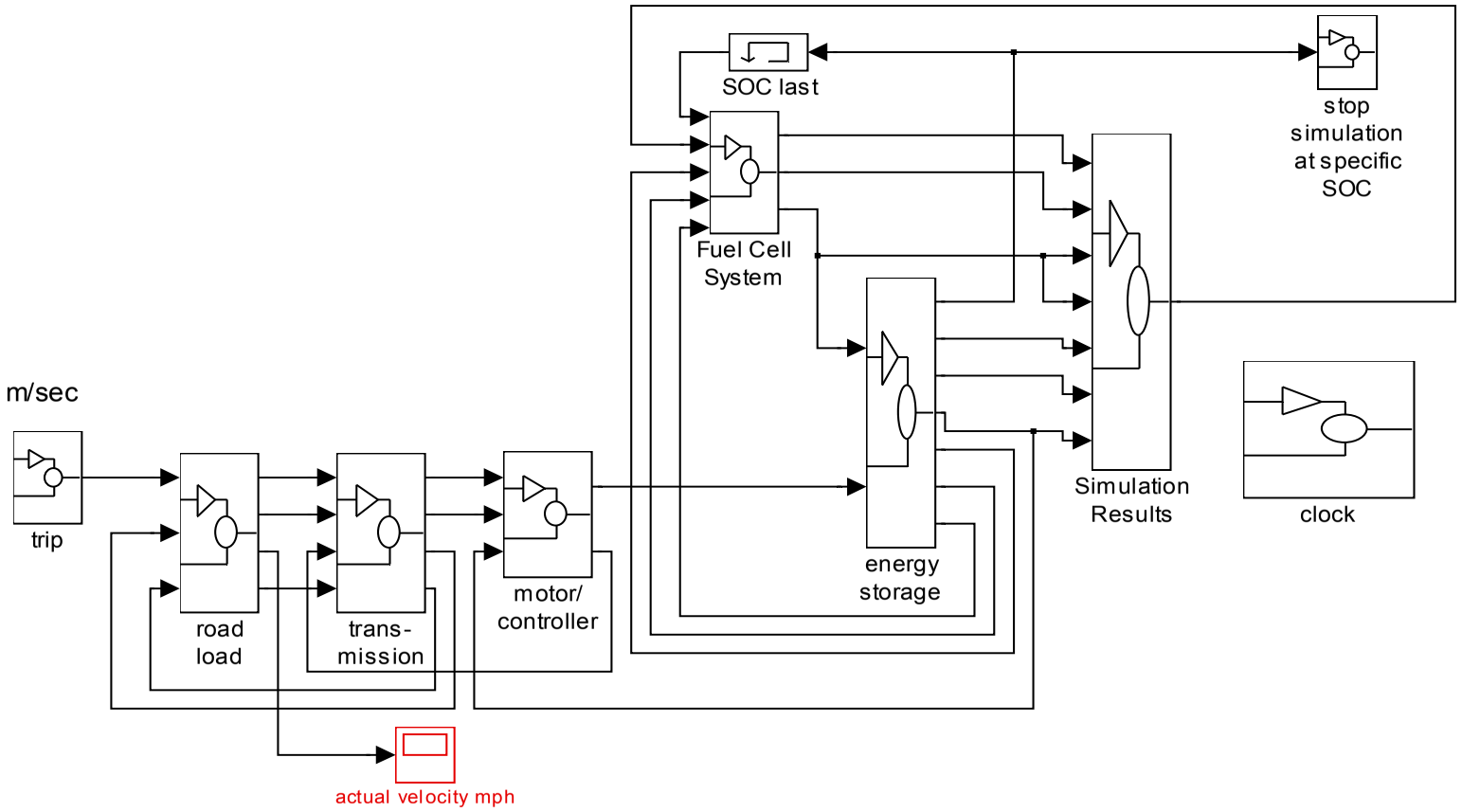

Figure 2-7: UC Davis Hydrogen Fuel Cell Hybrid Vehicle Model

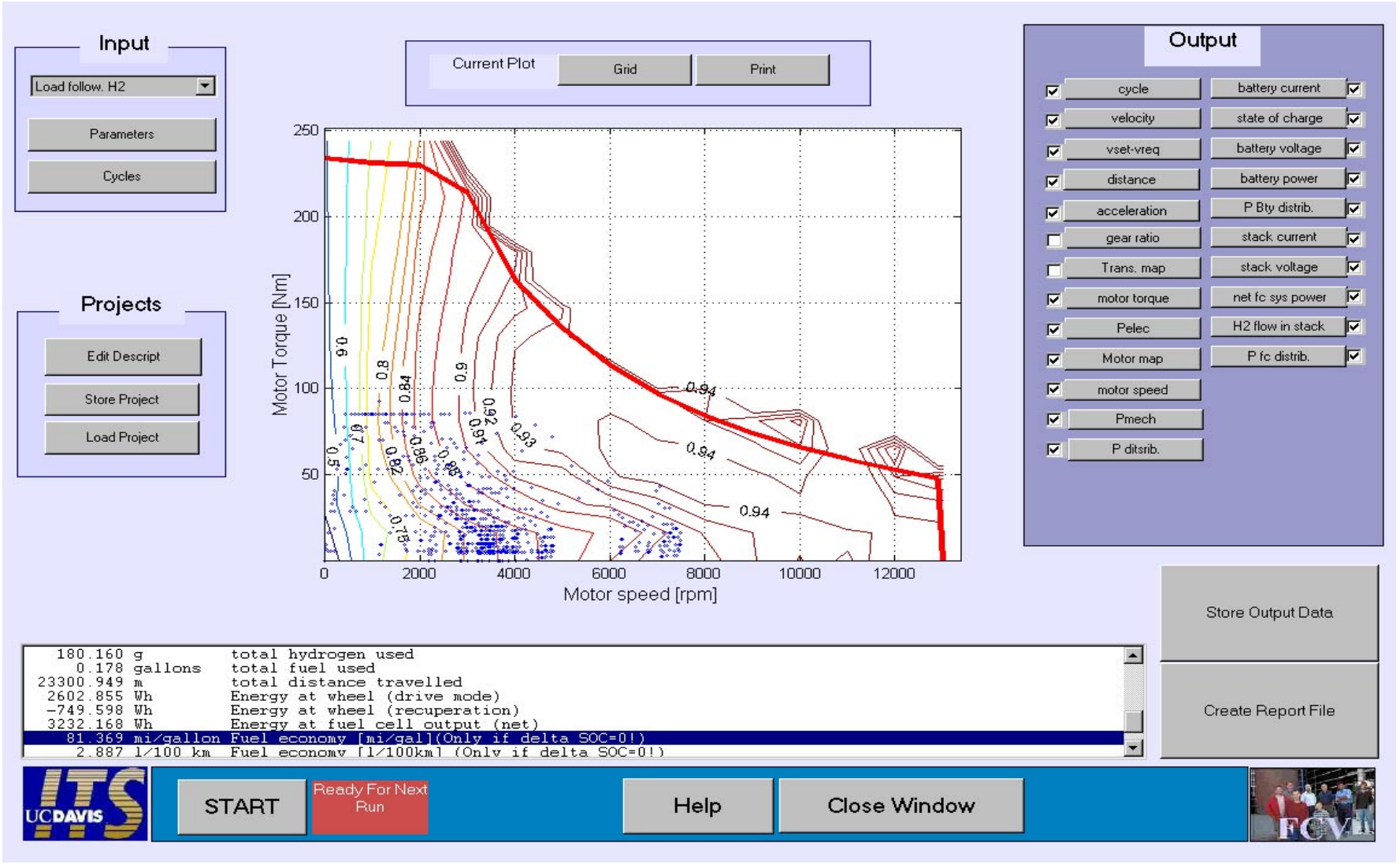

Figure 2-8: Graphical User Interface of the Hydrogen Fuel Cell Hybrid Vehicle Model of UC Davis

2.2.5. The Simplev (Simple Electric Vehicle Simulation) Model

Idaho National Engineering and Environmental Laboratories (INEEL) developed Simplev beginning in 1990. Since then several updates have been released. The latest update is Simplev 3.0. However the simulation package has been phased out in 1997.

It is programmed applying a backwards method (Idaho National Engineering and Environmental Laboratory, 1993). This programming approach is physically and mathematically less solid than the forward-looking approach[15].

Simplev does not support the method of co-simulation. Because Simplev is programmed in Basic, and the source code had not been made available, it is not possible for the user to expand and modify the initial program package.

Because of the reverse causality Simplev does not support rapid prototyping.

The required input data are standard vehicle and component parameter and steady state maps for motor efficiency, transmission efficiency etc. All the input data are either available or could be made available using standard methods, such as battery and motor bench tests. The program assists the user with a simple graphical interface. The runtime is very short compared with the other program packages.

Simplev is capable of simulating various types of internal combustion engine hybrid and battery electric vehicles. Simplev, in its original form, is not able to simulate fuel cell vehicle concepts.

It should be noticed that Simplev was introduced in 1990, and was among the first comprehensive programs modeling vehicles employing electric drive trains. Simplev was phased out by INEEL in 1997.

---

[15] See appendix

Strengths:

- Runtime

Weaknesses:

- Backwards approach,
- No fuel cell vehicle modeling capabilities,
- The electric drive train is not sensitive to voltage,
- Not flexible (Source code not available),
- No documentation for version 3.0,
- No longer available.

2.3. Summary

Several vehicle-modeling tools have been introduced and compared with each other. The points of comparison have been a list of generic requirements for mathematical modeling stated at the beginning of the chapter and restated in the first seven items in Table 2-5. These criteria define the theoretical potential of the modeling approach. In addition in the second half of Table 2-5 (items 8-10) the actual realized potential has been compared among the different models. Finally the last row states the public availability in October 2000.

The compared models could be classified in two different groups. Hyzem and Psat as forward looking models and Advisor, UC-Davis H2 (1998 version) and Simplev in the group of backwards looking models.

The items 1-5 in Table 2-5 state the theoretical potential of the models to incorporate future developments in an efficient and time saving manner. It can be seen that in this respect the group of causal forward-looking models offers a higher potential than the group of non-causal backwards looking models.

The item Nr. 6 “ease of use” includes two different aspects. First, the support the user receives through a graphical user interface and a good documentation, and second, the logical structure of the model and how it supports modifications. Table 2-5 shows that none of the models have an advantage regarding the ease of use. However this represents only the current state. Hyzem is valued neutral because it does not support the user with a graphical user interface but has a causal structure easing understanding and modifications. Advisor, UC-Davis H2 (1998 version) and Simplev are valued neutral because they employ a graphical user interface and a non-causal structure. Psat is valued

neutral although it offers a graphical user interface and a forward looking structure. The reason is that version 4.0 was still in the development state and the user interface was little flexible and unstable. Because a graphical user interface could easily be added to the causal models, while changing the non-causal structure of the backwards-looking models is not possible the theoretical potential for a better "ease of use" for the causal models is estimated to be higher.

The availability of input data (item 7), though important, is not a feature that distinguishes the models. Only the UC Davis Hydrogen model (1998 version) has a (minor) disadvantage in this area because of the combination of stack and air compressor data.[16]

Items 8-10 compare more specifically how much of the theoretical potential of each model has actually been realized in the current versions. Again the models could be separated into the causal and non-causal types.

Item 8 shows the vehicle concepts realized today. The differences shown should not be over interpreted. In principle all vehicle types could be modeled with each model. Most of the differences shown could be explained based on the history of the individual models and their sources of funding, primary objective, etc. However the fact that Advisor does not include an indirect methanol fuel cell vehicle model could be one hint towards the difficulties of incorporating non-instantaneous responding systems, such as a methanol steam reformer, into the model.

Item 9 compares the possibilities of incorporating dynamic characteristics in each model, on hand of the example of start up issues and fuel processor time constants.

Though the incorporation of these features is in principle possible in all models, the required effort for the case of non-causal models is much larger. Consequently none of the mentioned features has been realized in this vehicle group. The causal models have a significant advantage over the non-causal models. The reason is that the causal structure allows the incorporation of dynamic characteristics without difficulties if the physics of the system are understood.

Item 10, the issue of emissions, is not an area in which the models are fundamentally different. All models are in principle able to model emissions. However for models only considering hydrogen as a fuel (UC-Davis, H2) the task of modeling emissions is irrelevant. The applied method of modeling emissions in today's program versions is quasi-static with tables including the emissions depending on the emitters (anode gas burner, fuel processor) operating point.

Finally item 10 compares the availability of the individual models in October 2000. At this time only Advisor was publicly available (as free download on the Internet). However the Southwest Research Institute and Argonne announced that the PSAT model would be made available at a later time this year. Since October 2000 a beta version of PSAT is already available for researchers in the field of fuel cell vehicle modeling only.

From a fundamental point of view none of the above models are satisfying. The investigated models compromise in a number of different areas, such as separation of control algorithms from component models and causality. As a result the models become difficult to understand, non-modular (even if they appear modular on the surface) and difficult to validate.

---

[16] This comparison only considers the vehicle level. However in addition to the UC Davis H2 vehicle model a second model is existing generating the necessary vehicle model input data from standard data

Also, because of the number of compromises made, none of the investigated models appears suitable as a teaching instrument in companies or universities. Although this aspect is secondary for a professional use in industry, or in the policy arena, it seems important that long-term suitable tools for teaching in the area of fuel cell vehicles are available.

Based on this comparison a new fuel cell vehicle model is proposed. Key characteristics of this new model are:

- Emphasis on fuel cell vehicles,
- Incorporation of hybrid concepts including ultra capacitors,
- Causal structure,
- Preparation of rapid prototyping,
- Incorporation of dynamics aspects,
- Modular topology,
- Incorporation of the new indirect methanol and indirect hydrocarbon fuel cell system models of UC-Davis (Eggert, 2000, Fuel Cell Modeling Group, 2000),
- Incorporation of the new direct hydrogen fuel cell system model (Cunningham, 2000),
- Logical structure.

---

such as compressor maps and stack properties (config model).

Model / Requirement	HY-ZEM	PSAT	Advisor	UC-Davis H2	Simplev
1. Theoretical soundness	+	+	-	-	-
2. Completeness	+	O	O	O	O
3. Flexibility	+	O	-	-	-
4. Expanded resolution through co-simulation	+	+	O	-	-
5. Validation supported through rapid prototyping	+ (current version) - (1996 version)	-	-	-	-
6. Ease of use	O	O	O	O	O
7. Input Data Available	+	+	+	-	+
8. Realized fuel cell vehicle models (2000)	Indirect - Methanol and direct-H2 in hybrid and non-hybrid Versions, no ultra capacitor designs	Only battery hybrid fuel cell Vehicles, no ultra capacitor designs	Indirect-Gasoline and direct-H2 in hybrid and non hybrid versions, no ultra capacitor designs	Direct-H2 in hybrid and non - hybrid versions, no ultra capacitor designs	-
9. Dynamic Considerations (Start up, reformer time constants)	+ current version	- Place holder model	- Place holder model	- Place holder model	-
10. Modeling of Emissions	+ (maps)	+(maps)	-	Not applicable	+ (maps)
11. Availability (October 2000)	-	+(free[17])	+ (free)	-	-

Table 2-5: Benchmark (- negative or not possible, O neutral, + good).

Not emphasized are:

[17] For registered researchers.

- The employment of a graphical user interface,
- Large component libraries,

It is expected that through these key features a new fuel cell vehicle model could be developed with applications in

- Academia and government (in teaching and as a tool for policy analysis),
- The vehicle industry (for the analysis of different concepts),
- The component industry (for product planning and technology comparisons).

3. Applied Modeling Methodology

3.1. General Aspects

For a realistic and defendable vehicle model, only a physically and mathematically well-defined and documented modeling approach is acceptable. Therefore this dissertation work chose a causal forward looking[18] modeling approach.

For modeling of the control algorithms, an approach emphasizing the strict distinction between the controlled system and the controller controlling the system is proposed.

For the modeling of the components, either an approach based on first principles or an approach based on experimental data has been applied. Examples for the first principle approach are the modeling of the mechanical properties of the vehicle (inertia, friction, rotational inertia) or the modeling of the fuel cell stack. Examples for modeling based on experimental data are the use of efficiency maps for the electric motor and transmission.

The decision of which approach to follow depends on:

- The availability of experimental data;
- The complexity a first principle component model would add to the overall model and the effects on run time (practicality);
- The purpose of the model, e.g. what is the question asked. If the emphasis is towards aggregate vehicle properties, individual component models could eventually be simplified. If the emphasis is on one specific component, modeling

[18] See literature review (Hauer 2000).

in greater detail than in the first case might be necessary. Two methods to accomplish this are possible: First, by programming a more complex SIMULINK model, and second by employing a special programming tool for a specific component or characteristic. SIMULINK and the other, specialized, program, e.g. SABER for electric components, would then work together. This method is called co-simulation. Although not applied in this work, the modular, forward-looking structure of the model supports the method of co-simulation.

Because of the modular structure of the model, the modeling of each component is not limited to either the choice of a first principle model or an approach based on experimental data. Component models are exchangeable as long as the interfaces are compatible. Therefore the results of a detailed component model could be compared with a simpler one running both in the same overall vehicle model. If the differences between both models are neglect able and the focus of interest is on the vehicle and not the component itself one might decide to use the simpler component model for the benefit of a faster runtime.

In addition to the above-mentioned method of co-simulation, the model structure supports the use of rapid prototyping. In this context, rapid prototyping means the process of developing control algorithms in the software model, which are later transferred into existing hardware.

The model supports also the concept of “hardware in the loop,” allowing the replacement of component descriptions of the software model with hardware. From a modeling point of view, “rapid prototyping” and “hardware in the loop,” techniques offer the chance for faster model validation.

3.2. Mathematics

3.2.1. Introduction

The modeling, based on first principles, is done by applying a standard input/output approach as described by Leonhard (Leonhard 1985) and Foellinger (Foellinger 1985) for time invariant systems with one or multiple inputs x(t) and one or multiple outputs y(t). Mathematical component and hardware descriptions are formulated in the form of ordinary differential equations with the time t as the independent variable. The system description could be given in the form of one or several ordinary differential equations dy/dt = f(t,x(t), y(t)) for the output function y(t) (Figure 3-1).

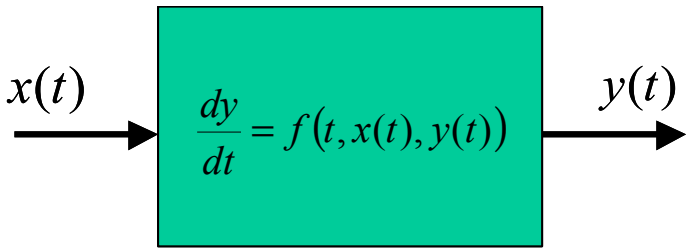

Figure 3-1: Time invariant input output system for one input x(t) and one output y(t) and a 1st order differential equation relating output and input function.

The input function x(t) could be of any form, including discontinuous functions, e.g. a step function or a pulse. The only limitation is that x(t) has to be defined for the complete time interval of interest [0,t].

The output function y(t) is calculated as a function of the input function x(t) applying the system description dy/dt = f(t,x(t),y(t)). For a physical system no singularities are expected. Therefore y(t) is defined for the whole time interval [0,t].

The differential equations describing the system could be either of linear or non-linear form. The equations describing the system are not limited to first order equations.

A system description with higher order differential equations is possible. In case that the component model requires a higher order differential equation, e.g. n^{th} order, it can be transformed into a first order system of n differential equations that could be solved easily in SIMULINK (Mathworks corporation, 2001). The general approach for the transformation of an n^{th} order equation is to substitute the higher order derivatives by introducing new variables.

Equation 3-1 shows a n^{th} order differential equation with the input function x(t) and the output function y(t).

$$\frac{d^{(n)}y(t)}{dt^n} = f\left(t, x(t), y(t), \frac{dy(t)}{dt}, \ldots, \frac{d^{(n-2)}y(t)}{dt^{n-2}}, \frac{d^{(n-1)}y(t)}{dt^{n-1}}\right)$$

where :

t = independent time variable

y(t) = system output

x(t) = system input

Equation 3-1

To solve Equation 3-1 in SIMULINK, it has to be rewritten into a system of n 1^{st} order differential equations for the n unknown functions $y(x,t), y_1(x,t) \ldots y_{n-1}(x,t)$ (Equation 3-2).

$$\frac{dy_1(t)}{dt} = g(t, x(t), y_1(t), y_2(t), ..., y_{n-1}(t))$$
$$\frac{dy_2(t)}{dt} = y_1(t)$$
$$\frac{dy_3(t)}{dt} = y_2(t)$$
...
$$\frac{dy_{n-1}(t)}{dt} = y_{n-2}(t)$$
$$\frac{dy(t)}{dt} = y_{n-1}(t)$$

where:

$$y_1(t) = \frac{d^{n-1}}{dt^{n-1}} y(t)$$
$$y_2(t) = \frac{d^{n-2}}{dt^{n-2}} y(t)$$
...
$$y_{n-1}(t) = \frac{dy(t)}{dt}$$

Equation 3-2

The resulting system in Equation 3-2 can be directly programmed in SIMULINK. Essentially SIMULINK provides the solution not only for the function of interest y(t) but also for the first n-1 derivatives of y, respectively $y_1 \ldots y_{n-1}$.

The algorithm to rewrite the n-th order differential equation does not require linearity in the original equation. It can also applied if the original equation is of non-linear form. The order of the system is also not a constraint, although physical systems are seldom of a higher order than two.

If the system has more than one input x(t), all inputs have to be considered. The first equation in Equation 3-2 is then a function of all inputs x_1, x_2 $\ldots x_m$, if m is the number of input variables.

If the system has more than one output function y(t), the above method can be applied for each output function.

An example of a multi input/output system is the air supply system in which pressure and flow rate set points are input variables and the actual pressure and flow rates in the stack form the output variables.

Start of the simulation (Initial values):

For the numerical solution, initial conditions for the integration of the system have to be considered. For a system of n^{th} order, n initial conditions are required. Initial conditions are the values of $y_1(t=0),\ldots,y_n(t=0)$. They are incorporated in the form of initial values of the integrator blocks in the SIMULINK diagram.

The so-derived first order system of differential equations could then be solved in SIMULINK. An example of a solution to a 2^{nd} order system in SIMULINK with one input and one output is provided at the end of the chapter.

Discontinuities:

A discontinuity in this context means that the derivative from the left side is different from the derivative from the right side in (at least) one point of a function. The function is then discontinuous in this point. An example would be if there is a kink in the function.

Discontinuities are common in the control algorithms applied for controlling the various components. They are introduced in the form of saturation blocks, switches, thresholds, and tables, and are necessary to model the applied control algorithm.

SIMULINK offers a vast number of functions to ease the incorporation of discontinuities into the model.

In an analytical approach, the presence of discontinuities makes it harder to solve the equation because it has to be solved for each continuous interval separately.

For the numerical approach applied in this work, the problem of discontinuities is less challenging. The applied method for solving the system is to work with one set of differential equations until the solution reaches a discontinuity. The simulation stops and continues then with a new (modified) set of equations, taking the old system's last vector of output values as vector for the initial values for the new system. After this, the simulation proceeds as usual until the next discontinuity arises.

Not considered in this model are time discontinuities. Realistically, due to the fact that most of the control algorithms are programmed in the software and run in discrete time steps in microprocessors, all control algorithms have to be modeled in discrete form. However, due to the high processor clock speed in comparison to the system time constants, the impact of time discontinuities is minimal and could be neglected. If the processor clock speed is in the order of magnitude of the inverse of the smallest time constant within the controlled system model, the control algorithm would have to be modeled in a time discrete form (Leonhard 1990).

Applied solving algorithm for solving differential equations:

SIMULINK offers several solvers supporting the numerical integration of ordinary differential equations.

The solvers provided could be classified as variable step solvers and fixed step solvers.

Fixed step solvers do not vary the simulation step size during the simulation. Therefore the step size has to be small enough to capture the most transient intervals of the solution with sufficient enough accuracy. On the other hand, a too small step size slows the simulation down. For the hybrid vehicles modeled in this work, the recommended method is the Euler method (ODE 1). The use of this algorithm for hybrid cases shortens the execution time significantly. Alternative fixed step solvers, available in SIMULINK, are listed in Table 3-1.

Variable step solvers vary the step size depending on the slope of the solution. In intervals with a small slope, the step size is increased, while in areas with steep slope (rapid change of the solution), the step size is decreased to minimize the computational error. The motivation of the variation in step size is to increase the speed of the simulation. Variable solvers provided by SIMULINK are listed in Table 3-1. Among the variable step solvers the ODE 45 method provides a good compromise between reliability (how likely is it that the simulation runs to the end) and efficiency (how fast does the simulation run) for the models discussed in this dissertation.

The standard solver applied in this work is the Euler algorithm (Bronstein 1985) for solving the system of differential equations that form the overall model.

Assuming the system that has to be solved is stated in explicit form (Equation 3-3) with the input function x(t) and the output function y(t) (Figure 3-1):

$$\frac{dy(t)}{dt} = f(x(t), y(t)) \qquad \textbf{Equation 3-3}$$

Applying the standard differentiation formula leads to (Equation 3-4).

$$\frac{dy(t)}{dt} = \frac{y(t + \Delta t) - y(t)}{\Delta t} = f(x(t), y(t))$$

where : **Equation 3-4**

$\Delta t = \text{step size}$

Solving for y(t+Δt) results in:

$$y(t + \Delta t) = y(t) + \Delta t \cdot f(x(t), y(t)) \quad \textbf{Equation 3-5}$$

The recursive algorithm in Equation 3-5 is named the Euler formula. Starting with an initial value y(t=0), Equation 3-5 allows the integration of the differential equation stated in Equation 3-3. The step size Δt stays constant in this algorithm. In some cases, especially if the solution has large intervals [t1, t2] with only little variation, the adjustment of the step size could decrease the overall runtime. In intervals with little variation, the step size is increased, while in areas with large variation (or high dynamic), the step size is decreased.

SIMULINK provides assistance for varying the step size offering variable time step solvers. Essentially, the absolute tolerance ε between two steps and the relative tolerance λ between two steps is calculated. If one or the other exceeds a (in the user interface adjustable) parameter, the iteration step is repeated with a smaller time step size Δt (Equation 3-6). For checking the relative step size at locations y(t) close to zero a special "zero crossing feature" could be activated to avoid difficulties in determining the step size in these situations (Simulink 2001).

$$\textit{if } \left|y(t+\Delta t)-y(t)\right| \geq \varepsilon \text{ or } \left|\frac{y(t+\Delta t)-y(t)}{y(t)}\right| \geq \lambda$$

then

decrease Δt and repeat step

Equation 3-6

where :

ε = absolute tolerance

λ = relative tolerance

Fixed step size solvers	**Description**
ode1 (Euler algorithm)	This method provides an efficient and reliable solution for all hybrid cases. The recommended step size is 0.005 sec. Recommended solver for all the models used in this dissertation.
ode5,ode4,ode3,ode2	For a detailed description see the Simulink web page (Simulink 2001). None of the listed solvers could (significantly) increase the reliability or runtime of the simulation.
Variable step size solvers	
ode45	Based on an explicit Runge-Kutta (4,5) formula, in general, ode45 is the best solver to apply as a "first try" for most problems.
ode23,ode113,ode15s, ode23s,ode23t,ode23tb	For a detailed description see the Simulink webpage (Simulink 2001). Depending on the exact configuration of the model one of the listed solvers might lead to a (i) more reliable, (ii) more efficient solution.

Table 3-1: Fixed and variable time step solvers.

Runtime:

Two different effects determine the run time of the overall vehicle model:

- The complexity of the model (this is the number of blocks forming the model);
- The system dynamics (this is how fast the solution including intermediate values change over time).

It appears obvious that the runtime increases with the system complexity. More blocks add essentially more equations to the overall system and more equations means that for every iteration step more computations have to be performed. For fixed computational resources, the runtime increases with increasing complexity.

Not so obvious is that the system dynamics can have a much stronger effect on runtime than the increase in complexity has. If a system is highly dynamic (e.g. if parts of the system are oscillating), in the interval of interest or shows rapid state changes only at certain times the runtime could increase significantly. In either case the reason for the increased runtime is that the simulation step size has to be small enough to capture all transient effects. If the solution shows highly transient behavior only at certain points in time (e.g. during an acceleration), a variable step solver could reduce the runtime. However, if the solution is transient over the complete interval of interest (e.g. oscillating), the step size has to be kept small all the time. For this case the number of calculations and therefore the runtime increases independent from the choice of the solver.

For the sake of a reasonable runtime and due to the finite computer power (floating point operations / second), the modeling has be constraint to the dominant time constants within the system.

A mixture of large and small time constants with a ratio of largest to smallest time constant of several orders of magnitude slows the simulation significantly down. The smallest time constant is effectively determining the step size and with this the total run time of the simulation. For example, the consideration of the cable inductivity and capacity between the fuel cell system and the electric drive train of a vehicle should be avoided because this time constant is significantly smaller than the mechanical time constants due to rotational inertia of the electric drive train or the vehicle mass.

On the other hand, in feedback systems it can be necessary to consider even secondary (small) time constants to avoid algebraic loops in the modeling process. The presence of algebraic loops in the simulation model can be interpreted as an indicator that the analysis of the system is not detailed enough. A significant aspect of the system has not been captured in the model.[19] In case of the presence of an algebraic loop how an additional time constant could be introduced into the system must be carefully analyzed. For the case that no algebraic loop is present, one must consider if the introduction of additional (smaller) time constants is necessary to describe the interesting properties of a system or if this just leads to an increase in run time. However, in this model it appears that considering the system determining time constants leads to a system model without any algebraic loops, which captures all dominant effects.

[19] This is true for physical systems. It can be said that in nature no algebraic loops exist (no immediate feedback from a system output to a system input).

3.2.2. Example and Transfer into SIMULINK

Equation 3-7 describes the horizontal movement of a vehicle with the mass m considering an aerodynamic drag, wheel inertia, tire friction, and an external acceleration Force F (Gillespie 1992).

$$m \cdot \frac{d^2 s(t)}{dt^2} + \mu_1 + \mu_2 \cdot \frac{ds(t)}{dt} + \mu_3 \cdot \left(\frac{ds(t)}{dt} \right)^2 + \frac{1}{2} \cdot cw \cdot \rho \cdot A \cdot \left(\frac{ds(t)}{dt} \right)^2 + \frac{\Theta}{r^2} \cdot \frac{d^2 s(t)}{dt^2} - F(t) = 0$$

Equation 3-7

Following the conclusions of the previous chapter the above 2nd order nonlinear differential equation can be rewritten into a system of two 1st order differential equations by the method of substitution (Equation 3-8).

$$m \cdot \frac{dv(t)}{dt} + \left(\mu_1 + \mu_2 \cdot v(t) + \mu_3 \cdot v^2(t) \right) + \frac{1}{2} \cdot cw \cdot \rho \cdot A \cdot v^2(t) + \frac{\Theta}{r^2} \cdot \frac{dv(t)}{dt} - F(t) = 0$$
$$\frac{ds(t)}{dt} = v(t)$$

Equation 3-8

Rearranging Equation 3-8 results in:

$$\frac{dv(t)}{dt} = \frac{1}{m + \frac{\Theta}{r^2}} \cdot \left[F(t) - \left(\mu_1 + \mu_2 \cdot v(t) + \mu_3 \cdot v^2(t) \right) + \frac{1}{2} \cdot cw \cdot \rho \cdot A \cdot v^2(t) \right]$$
$$\frac{ds(t)}{dt} = v(t)$$

Equation 3-9

In Equation 3-9 s(t) has the meaning of the distance traveled from t=0 until t and v(t) is the vehicle velocity at the time t. Because the system of differential equations has two unknown functions v(t) and s(t), two initial conditions have to be considered. These are the vehicle velocity at the beginning of the experiment (or simulation) v(t=0) = v_0 and

the location of the vehicle at the beginning of the experiment $s(t=0)=s_0$. Equation 3-9 can be seen as the description for an input / output system. System input is the acceleration force F(t) and system outputs are the vehicle velocity v(t) and the vehicle location s(t). Together with the above-mentioned starting conditions, the system can be easily solved in SIMULINK for all input traces F(t). Figure 3-2 shows the graphical representation of the SIMULINK algorithm.

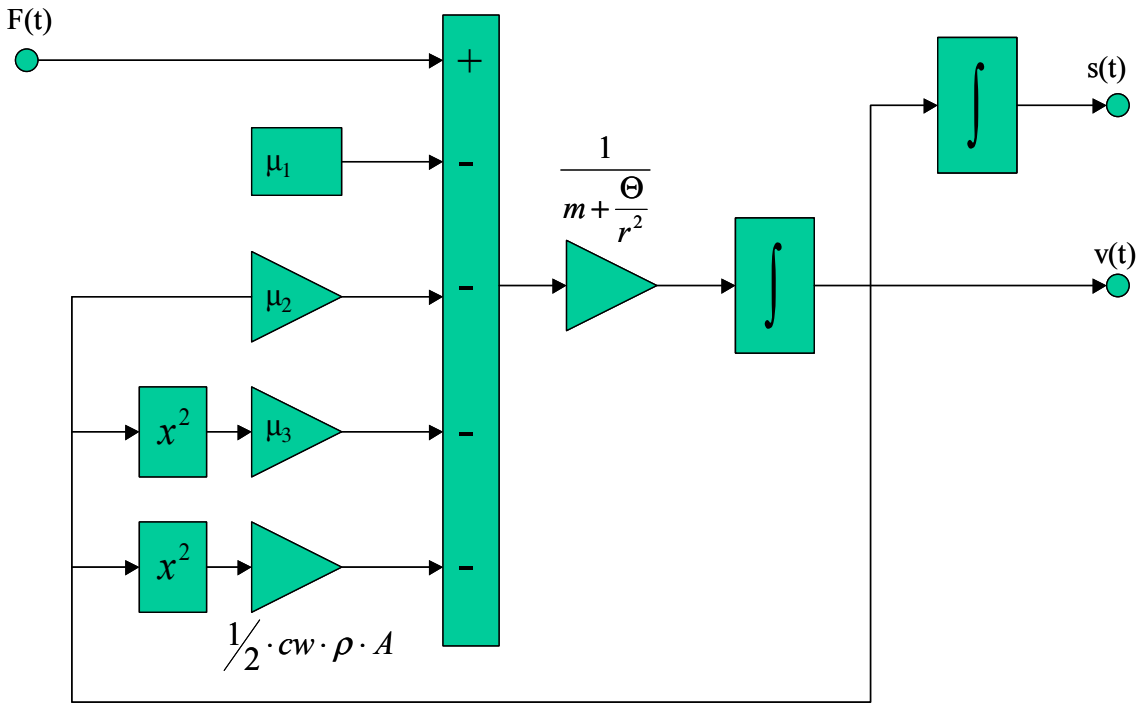

Figure 3-2: Graphical representation of Equation 3-9.

The initial conditions $s(t=0)=s_0$ and $v(t=0)=v_0$ are equivalent to the integrator status at t=0. Therefore the initial conditions can be directly programmed into the SIMULINK representation.

4. Model Description

4.1. Modeling Structure and Goals

This chapter explains the setup of the fuel cell vehicle model. The model is developed using a forward-looking approach (Hauer 2000). The model description starts with the most upper level, the vehicle. This level illustrates how the driver is interacting with the vehicle and how the drive cycle is fed into the model. After the establishment of this overall modeling frame, the models for all major components are explained in the chapter "Component models." The component models interface with each other and form, together with the vehicle properties, the overall vehicle model. One individual component could also consist of several subcomponents. One important characteristic of this model is that the component interfaces transfer only physical properties from one component to the other components. The limitation to "physical" interfaces qualifies the model for the use in rapid prototyping experiments. It also benefits the understanding and eases maintenance and further development because the model could be more easily associated with an image of the physical reality of the vehicle. Because of the strict modularity, individual component models could be tested off-line or replaced with a different model for the same component if the interfaces of the replacement model match the interfaces of the model replaced.

Besides the component models, the control strategies for the interaction of the individual components determine the overall vehicle characteristics. These control strategies are also explained under the headline "Component models." An example for a control strategy in a non-hybrid vehicle is the control algorithm for the fuel processor. An example for a control strategy in a battery hybrid vehicle is the activation of the fuel cell

system depending on the motor power and/or the state of charge of the battery and/or other parameters.

The modeling effort pursues two objectives:

First to estimate fuel consumption, energy flows and losses, and the vehicle dynamics (acceleration time and top speed) for different vehicle configurations (parameters) and different vehicle types (hybrid, non hybrid vehicles).

Second the safe and fast investigation and development of control strategies for the exploration of theoretical limits and the use in existing hardware later.

4.2. Vehicle Model

The uppermost level of the fuel cell vehicle model consists of the main blocks “Specified Drive Cycle”, “Driver” and “Vehicle" (Figure 4-1).

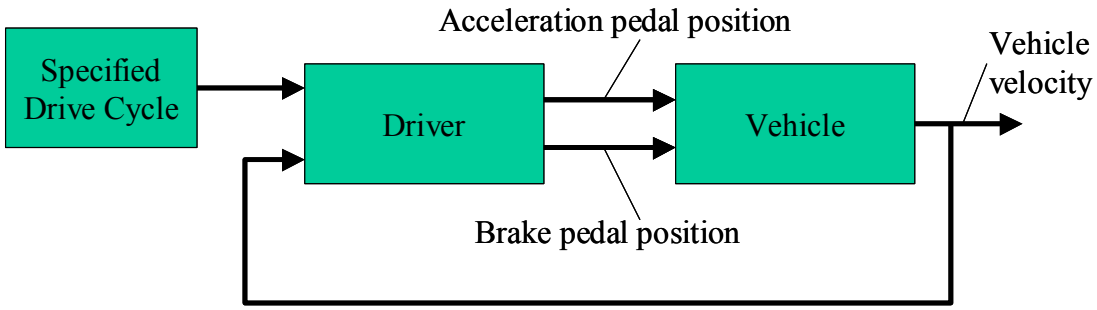

Figure 4-1: Uppermost level of the indirect methanol fuel cell vehicle model.

4.2.1. Drive Cycles and Driver Model

This chapter discusses the drive cycles available in the model and the algorithm that compares these drive cycles with the actual vehicle velocity and adjusts the acceleration and brake pedal position.

The block "Specified Drive Cycle" describes the demanded driving profile by specifying the velocity over the time. Standard drive cycles available in this simulation tool are the drive cycles listed in Table 4-1.

Available Drive Cycles	Length / Time	Max. speed / Avg. speed	Max. accel. Avg. accel.
Federal Urban Driving Schedule (FUDS)	7.45 mi / 1369 sec	56.7 mi/h / 19.6 mi/h	1.48 m/sec^2 0.34 m/sec^2
Federal Highway Cycle	10.26 mi / 765 sec	59.9 mi/h / 49.2 mi/h	1.43 m/sec^2 0.13 m/sec^2
US O6 Cycle	8.01 mi / 600 sec	80.3 mi/h 48 mi/h	3.75 m/sec^2 0.45 m/sec^2
ECE Cycle	0.62 mi / 195 sec	31.1 mi/h 11.4 mi/h	1.05 m/sec^2 0.43 m/sec^2
MVEG Cycle	6.79 / 1220 sec	74.6 mi/h 20.03 mi/h	1.05 m/sec^2 0.37 m/sec^2
EUDC 90	6.58 mi / 1220 sec	55.9 mi/h 19.4 mi/h	1.05 m/sec^2 0.39 m/sec^2
EUDC 120	4.32 mi / 400 sec	74.6 mi/h 38.9 mi/h	0.83 m/sec^2 0.26 m/sec^2
Japanese 10-15 cycle	2.59 mi 660 sec	43.5 mi/h 14.1 mi/h	0.79 m/sec^2 0.39 m/sec^2

Table 4-1: Available standard driving cycles with their main characteristics.

The block "driver" represents the driver properties and driver characteristics. The main task is the comparison of the velocity specified in the driving cycle with the actual vehicle velocity. In case the actual vehicle velocity is below the vehicle velocity specified in the drive cycle the driver sends an acceleration command to the vehicle block. In case the vehicle velocity is above the specified velocity the driver sends a brake command to

the vehicle block. In a real vehicle, the acceleration signal and the brake signal represent the position of the acceleration pedal and brake pedal. From a systems point of view the driver can be seen as a controller for the “system” vehicle. The inputs for the “system” vehicle are the acceleration and brake commands and the system output is the vehicle velocity. Although the presence of a driver model is important for the setup of the simulation, this analysis will not focus on the block "driver." The only criteria this block has to meet is to ensure that the vehicle follows the drive cycle as closely as possible whenever physically possible. In this respect the block "driver" has the same task as a driver on an emissions bench, namely following a given drive cycle.

The complete driver model is shown in Figure 4-2.

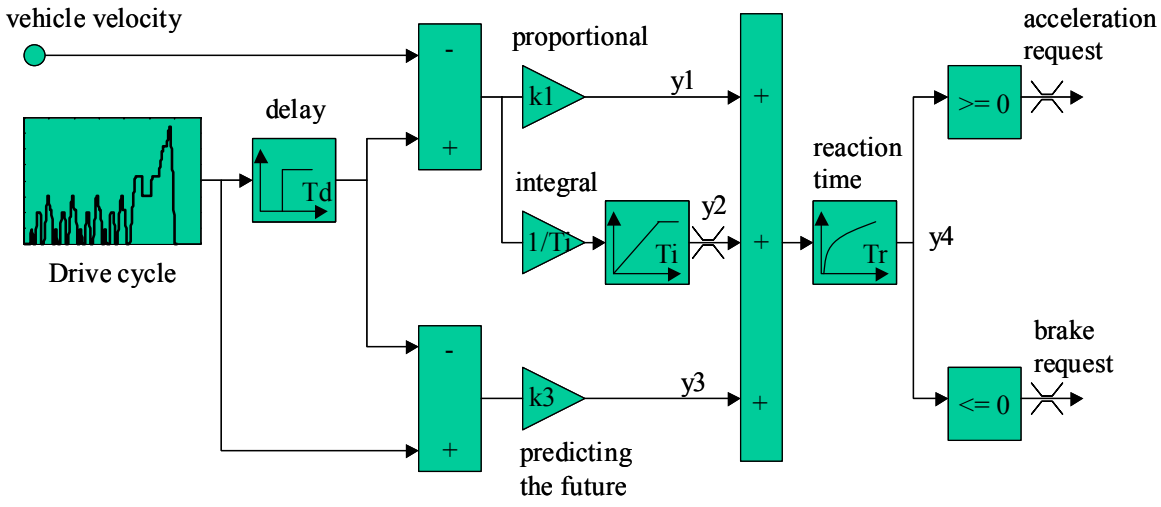

Figure 4-2: Driver model.

The model inputs are the specified drive cycle and the vehicle velocity. The model outputs are the normalized (between 0 and 1) acceleration request and the normalized (between 0 and –1) brake request.

The following steps are taken to calculate the output values in dependence of the input values. The (actual) vehicle velocity is subtracted from the (delayed) drive cycle

request. The difference between both values is fed into a proportional integral controller (PI controller). The proportional part is calculated according to Equation 4-1.

$$y_1(t) = k_1 \cdot \left(v(t) - v_{cycle}(t - T_d)\right)$$

where :

k_1 = proportional factor of the PI algorithm [1/km · h^{-1}]

v(t) = vehicle velocity [km/h] **Equation 4-1**

$v_{cycle}(t)$ = drive cycle velocity [km/h]

T_d = time is the time the driver looks into the future [sec]

t = time [sec]

The integral part of this PI controller is realized using an integral algorithm with a build-in anti-windup feature (Figure 4-3). The reason is to avoid the windup of the integrator to very high values in cases the vehicle is physically not able to meet the drive cycle, e.g. in an acceleration experiment). Equation 4-2 describes the algorithm of the integrator with anti-windup function.

$$y_2'(t) = \frac{1}{T_i} \cdot \int_0^t \left(v(t) - v_{cycle}(t - T_d) + c_1 \cdot (y_2 - y_2'(t)) \right) \cdot dt$$

where :

T_i = integration constant [h/km] **Equation 4-2**

c_1 = feedback constant [km/h]

$y_2'(t)$ = intermediate value [1]

$y_2(t)$ = output of the integrator with anti-windup [1]

The final output of the integrator with anti-windup is stated in Equation 4-3.

$$y_2(t) = y_2'(t) \qquad \text{if } |y_2'(t)| < \bar{y}_2$$
$$y_2(t) = \bar{y}_2 \qquad \text{if } |y_2'(t)| \geq \bar{y}_2 \qquad \textbf{Equation 4-3}$$

where :

$\bar{y}_2$ = upper and lower bound for y_2 [1]

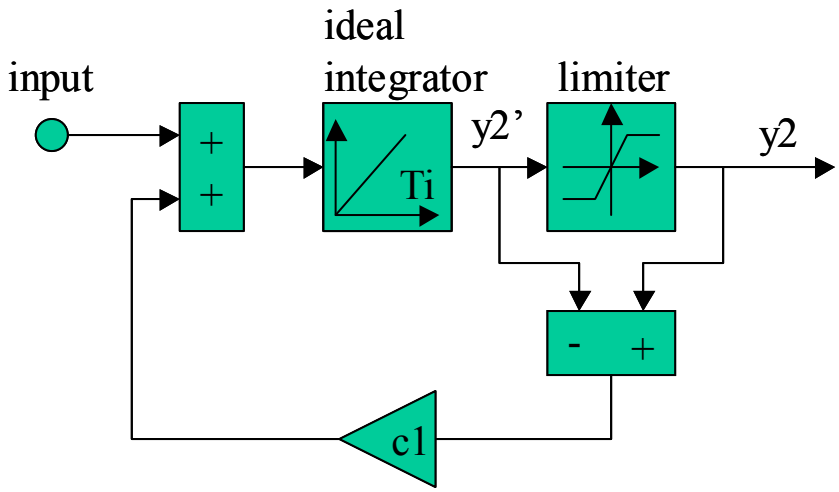

Figure 4-3: Integrator with "anti-windup function".

In addition to the PI algorithm, a third component impacting the driver request can be added (Equation 4-4). This third component takes into account that on an actual roller test stand the driver is able to foresee the future drive cycle.[20] This knowledge about the future can improve the driver's decision and allows a more accurate following of the drive cycle. The value the driver pays to the future is taken into account by a gain block. A gain of zero would mean that the driver does not pay any attention to the future at all. With increasing gain his attention increases. The delay determines how far the driver looks into the future. A delay of zero would be equivalent to a time horizon of zero seconds. If the delay time increases, the driver's time horizon increases.

[20] In a roller test stand the drive cycle request is communicated on a screen. This screen does not only show the current velocity request in digital form. Instead, the drive cycle, including the next few seconds of the drive cycle together with the actual vehicle speed, is displayed in the form of speed traces. Therefore, the driver is able to take the future velocity requests into account and base his current decisions on this additional knowledge. The net effect is that the driver can follow the drive cycle more accurately.

$$y_3(t) = k_3 \cdot \left(v_{cycle}(t) - v_{cycle}(t - T_d)\right)$$

where :

k_3 = constant for how the driver values the future [h/km]

$y_3(t)$ = intermediate value [1]

Equation 4-4

All three intermediate values y_1, y_2, and y_3 are summed and filtered through a low pass filter in the form of a first-order transfer function (Equation 4-5).

$$T_r \cdot \frac{dy_4(t)}{dt} + y_4(t) = y_1(t) + y_2(t) + y_3(t)$$

where :

T_r = filter time constant [sec]

$y_4(t)$ = intermediate value [1]

Equation 4-5

Finally, the filtered value is limited to values between -1 and 1, which are then interpreted as the driver's request for more or less acceleration. According to Equation 4-6, positive values are interpreted as a request for acceleration. Negative values are interpreted as a request for deceleration (braking).

$$\begin{aligned}
acc_request &= y_4(t) && \text{if } 0 \le y_4(t) \le 1 \\
acc_request &= 1 && \text{if } y_4(t) > 1 \\
acc_request &= 0 && \text{if } y_4(t) < 0
\end{aligned}$$

$$\begin{aligned}
brake_request &= y_4(t) && \text{if } -1 \le y_4(t) \le 0 \\
brake_request &= -1 && \text{if } y_4(t) < -1 \\
brake_request &= 0 && \text{if } y_4(t) > 0
\end{aligned}$$

Equation 4-6

where :

acc_request = driver request for acceleration [1]

brake_request = driver request for deceleration (braking) [1]

4.2.2. Physical Vehicle Model

In the previous chapter, the driver model and how the driver controls the actual vehicle velocity were discussed. In this chapter, the model for the vehicle and its main components and component arrangements will be explained. The block “vehicle” in Figure 4-4 contains the four sub-blocks “Drive Train,” “Vehicle Curb,” “Power Source,” and “Vehicle Controls” (Figure 4-4).

The inputs of this block are the brake pedal position and the acceleration pedal position. Both are derived in the previous chapter. The model output is the actual vehicle velocity. The acceleration pedal position feeds into the block "Drive Train" and determines the fraction of the maximum motor torque available supplied to the vehicle wheels. The brake pedal position feeds into the block “Vehicle Controls.” This block separates regenerative braking (in hybrid vehicles only) and mechanical braking. The request for regenerative braking is fed to the block “Electric Motor” and the request for mechanical braking is fed directly to the block “Vehicle Curb.”

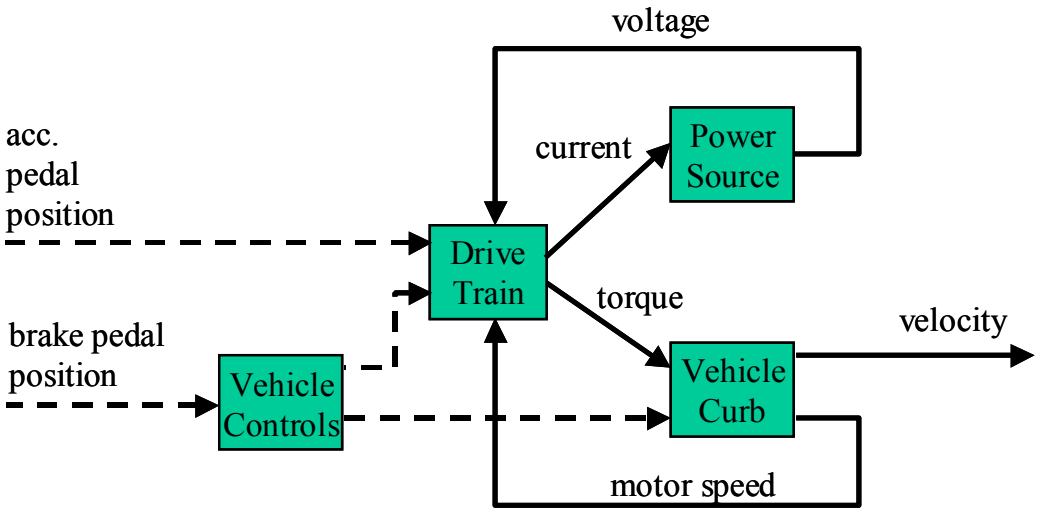

Figure 4-4: Content of the block "Vehicle".

The block “Drive Train” includes models for the power electronics for the electric motor, the electric motor itself, controls for the electric motor, and the transmission. Depending on the driver request, expressed by the acceleration pedal position and brake pedal position, the block “Drive Train” provides torque to the wheels and draws current from the power source (battery, ultra capacitor, or fuel cell stack).

The block “Vehicle Curb” models the mechanical properties of the vehicle curb such as aerodynamic drag, rolling resistance, mass, etc.. The inputs into this block are the applied wheel torque and the signal for the mechanical brake fraction. The outputs are the vehicle velocity and the motor speed. In designs not considering tire slip and a one-speed transmission, both values are directly correlated with each other.

The block “Power Source” could include models for a fuel cell system, a battery system, an ultra capacitor system, or a combination of all three systems. The input of this block is the electric current drawn by the motor. The output is the voltage seen by the dc terminals of the power electronics for the electric motor. For the case of a non-hybrid fuel cell vehicle this is the same voltage as the fuel cell stack voltage. In hybrid designs, this voltage could be the battery voltage or any other voltage depending on the exact design.

The overall design of the vehicle model incorporates two major feedback loops motivated by the dependence of the maximum motor torque of the electric drive train on the voltage supply and the motor speed. As soon as the driver signals a torque request the electric drive train starts providing torque to the wheels. Because of this torque supply, the vehicle accelerates and the motor speed increases. This increase in motor speed feeds back to the block “Drive Train” because of the sensitivity of the motor torque to

fluctuations of motor speed. This feedback loop represents the feedback on the mechanical side of the vehicle.

As soon as the motor starts spinning, it provides mechanical power to the wheels. It can only do this by drawing electrical power from the block "Power Source." As a result, the motor draws an electric current from the power source. Due to the internal resistance[21] of the power source, the voltage at the motor terminals drops depending on the load current drawn. Because of the sensitivity of the maximum motor torque on the supply voltage, the drop in voltage feeds back to the electric drive train. This feedback loop represents the feedback effects on the electrical side. Mechanical and electrical feedback together determine the overall characteristics of the combined system drive train, power source, and vehicle curb, which form the overall vehicle model.

This setup of the vehicle is close to the setup of a physical vehicle. The only interface[22] between the drive train and the source of electric power is the electric connection between both components. This interface can be fully described by change of voltage and current over time. On the mechanical side, the interfacing variables between the drive train and the vehicle curb are the wheel torque and the wheel speed. Similar to the electric side, the interface can be fully described by providing both values in time.

Properties of the vehicle and the vehicle environment

The overall vehicle is modeled according to the force balance stated in Equation 4-7. This equation accounts for the aerodynamic drag force; the friction force due to the rolling resistance of the tires; the vehicle inertia including rotational inertia of tires, motor, and transmission; and the climbing force necessary to climb a hill. The sum of all

[21] The internal resistance could vary over time.

these forces is the force required to operate the vehicle ("motor" force and friction brake force).

$$F_{motor} + F_{brake} = F_{friction} + F_{drag} + F_{inertia} + F_{climb} \qquad \textbf{Equation 4-7}$$

The individual forces can be expressed according to Equation 4-8 to Equation 4-13. Solving Equation 4-7 to 4-13 for the vehicle velocity and then integrating yields an equation for the vehicle velocity v.

The force necessary to accelerate or decelerate the vehicle is the force applied to the vehicle by the electric motor plus the braking force due to the mechanical brakes of the vehicle (left side of Equation 4-7). The applied motor torque is converted to a linear acceleration force accessing the vehicle. The same has been done for the brake force; although in reality this brake force is applied to the wheels, the model assumes a linear braking force that decelerates the vehicle directly (Equation 4-8).

$$F_{motor} + F_{brake} = \frac{T_{wheel}}{r_{wheel}} + q \cdot F_{brake\max}$$

$where$:

F_{motor} = Force induced by the electric motor [N]

F_{brake} = Force induced by the friction brakes [N] **Equation 4-8**

r_{wheel} = Wheel radius [m]

T_{wheel} = Wheel torque introduced by the motor [Nm]

q = Driver request for braking [1]

$F_{brake\max}$ = Maximum braking force [N]

The friction term represents the friction due to tire resistance and friction in the wheel bearings (Equation 4-9).

[22] Except information flow.

$$F_{friction} = m \cdot g \cdot (\mu + \mu_1 \cdot v + \mu_2 \cdot v^2)$$

where:

m = vehicle mass [kg]

g = gravity [$m \cdot sec^{-2}$]

μ = friction coefficient independant of velocity [1]

μ_1 = friction coefficient increasing linear with velocity [$m^{-1} \cdot sec$]

μ_2 = friction coefficient increasing with the square of the velocity [$m^{-2} \cdot sec^2$]

v = vehicle velocity [m/sec]

Equation 4-9

The aerodynamic drag is considered according to Equation 4-10.

$$F_{drag} = \frac{1}{2} \cdot \rho \cdot c_w \cdot A \cdot v^2$$

where:

ρ = density of air [$kg \cdot m^{-3}$]

c_w = coefficient of drag [1]

A = frontal area [m^2]

Equation 4-10

The force necessary to overcome the vehicle inertia is the sum of the force necessary for accelerating the vehicle mass plus the force necessary for the acceleration of the rotational inertia of the wheels.

$$F_{inertia} = m \cdot \frac{dv}{dt} + \frac{\Theta_{wheel}}{r_{wheel}} \cdot \frac{d\omega_{wheel}}{dt}$$

where:

Θ_{wheel} = Wheel inertia [$kg \cdot m^2$]

ω_{wheel} = Wheel speed in [rad/sec]

Equation 4-11

The wheel speed and the vehicle velocity are related to each other according to Equation 4-12. This equation assumes that the tires won't slip. In case of tire slip, this Equation has to be modified.

$$\omega_{wheel} = \frac{v}{r_{wheel}}$$

Equation 4-12

Finally, the climbing resistance (the force required to go uphill or the force gained going downhill) is considered in this model.

$$F_{climb} = m \cdot g \cdot \sin\left(\tan^{-1}\left(grade/100\right)\right)$$

where: **Equation 4-13**

$grade$ = grade the vehicle needs to overcome [%]

The sum of all forces impacting the vehicle determines, together with the vehicle mass, the vehicle acceleration. Equations 4-7 to 4-13 are used to calculate the vehicle acceleration as a function of time. The integration of the vehicle acceleration results in the vehicle velocity. The required starting value at t=0 sec represents the vehicle velocity at t=0 sec. This initial velocity is set to 0 km/h. Equation 4-14 shows the algorithm for the calculation of the vehicle velocity. Figure 4-5 is the graphical representation in form of a Simulink diagram of this algorithm.

The vehicle velocity can be calculated for a given wheel torque. The wheel torque itself depends on the vehicle velocity and is calculated in the block "motor." Because of the non-linear relationship between the provided wheel torque and the vehicle velocity, Equation 3-14 cannot be solved explicitly. The braking force F_{brake_max} in Equation 4-14 is less than or equal to zero.

$$v(t) = \frac{1}{\left(m + \frac{\Theta_{wheel}}{r^2_{wheel}}\right)} \cdot \int_{t=0}^{t} \left(\frac{T_{wheel}}{r_{wheel}} + q \cdot F_{brake\_\max} - m \cdot g \cdot \left(\mu + \mu_1 \cdot v + \mu_2 \cdot v^2 + \sin\left(\tan^{-1}\left(\frac{grade}{100} \right) \right) \right) - \frac{1}{2} \cdot \rho \cdot c_w \cdot A \cdot v^2 \right) \cdot dt$$

Equation 4-14

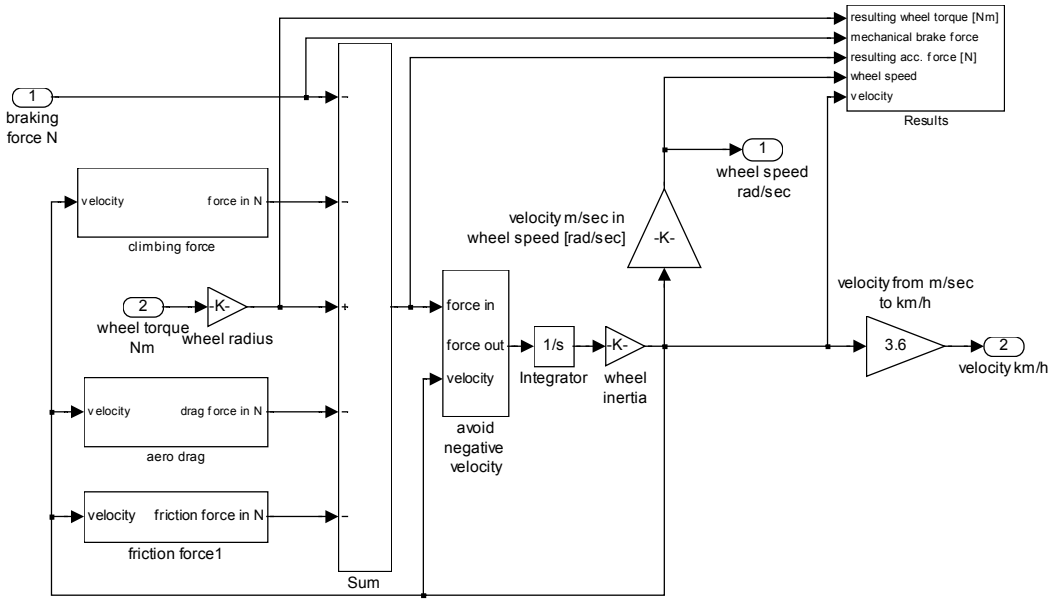

Figure 4-5: Simulink representation of the mechanical vehicle properties.

4.3. Component Models

4.3.1. Electric Motor Including Power Electronic

Many different motor technologies for electric vehicle drive trains are in use today. Among them are induction motors, permanent magnet brushless dc motors, dc-current motors, and switched reluctance motors (Nahmer 1996, Skudelny 1993).

Two different modeling philosophies are applied in today's vehicle models for the modeling of the electric drive train and the power electronics.

The first approach is based on fundamental physical principles. Motor torque and speed are calculated based on armature current and field current (armature current and magnetic field for permanent magnet motors). This approach requires a detailed motor model for each motor technology. A motor model for an induction motor would be fundamentally different from a motor model for a brushless dc motor. The input parameters for this approach are the motor geometry, material parameters, and the electrical parameters of the motor coil and power electronics. Li and Mellor (Li and Mellor 1999) describe such a modeling approach for the case of a brushless dc motor.[23]

The other possible modeling approach is based on static maps for the drive train efficiency in dependence of the motor torque and speed and the maximum motor torque in dependence of the speed and applied voltage. This second approach is followed by Ricardo Consultants (Heath 1996) and National Renewable Energy Laboratories (NREL, 1999). This modeling approach is technology independent, e.g. the same model could be used for different motor technologies. Only the motor describing parameters, such as maximum motor torque and maximum motor speed and the above-mentioned maps have

[23] In the paper, the brushless dc motor is referenced as a brushless ac motor .

to be adjusted for each specific motor technology and motor configuration (size, characteristic). The necessary input data for this approach could be gained on a motor test stand similar to the one described by Nahmer (Nahmer 1996). For gaining the efficiency map, the motor is operated at one specific operating point (torque and speed) and the electrical input power is measured. The efficiency is the ratio of mechanical output power over electrical input power. For gaining the map of maximum torque in dependence of speed and voltage, the motor is operated at one operating point (speed, voltage) and the maximum motor torque the motor is able to deliver is measured (increase of the mechanical load until the motor speed drops while holding the terminal voltage constant).

Due to the significantly shorter runtime and better availability of the necessary input data, the second modeling approach with static maps has been chosen in this dissertation. For modeling of the motor transient characteristics, the static approach has been modified and incorporates the mechanical time constant implied by the motor inertia. This time constant is the dominant time constant and exceeds the electrical time constant due to the coil inductivity and resistance, by far which is on the order of microseconds (Nahmer 1996).

The modeling based on static maps allows also the incorporation of all currently applied motor technologies without changing the model structure.

Interface:

On the electrical side the motor model including power electronics interfaces with the dc power source (battery system, fuel cell stack, or ultra capacitor system). The variables at this interface are the dc current and the dc voltage. On the mechanical side the motor shaft interfaces with the transmission. Interfacing variables are the shaft torque

and the shaft speed (Figure 4-6). On the information side (data bus) the motor receives the brake pedal position (only for hybrid vehicle designs with electrical energy storage) and the acceleration pedal position. However, if the motor controller is excluded from the actual motor, as shown in Figure 4-6, the motor receives a signal for the requested motor torque from the motor control algorithm.

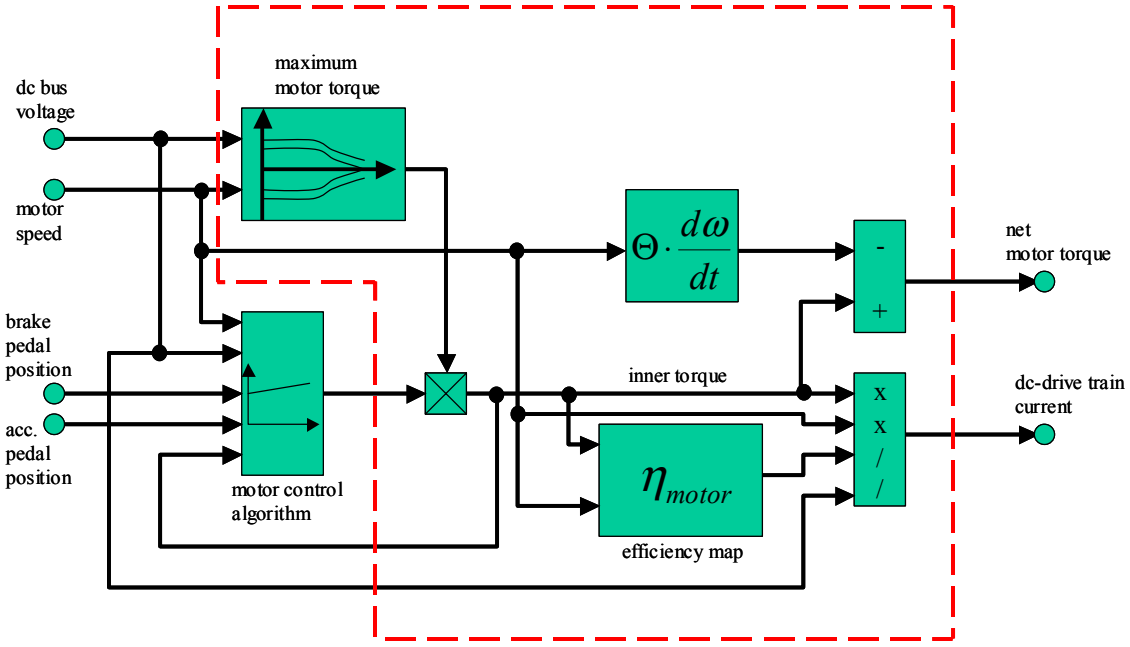

Figure 4-6: Structure of the motor block including power electronics and motor control algorithms. The characteristics of the motor and the power electronics are inside the by the dashed line marked area. Outside of this area is the motor control algorithm that takes the inputs shown and derives a signal for the requested motor torque.

Parameters:

For steady state operation, the motor including the power electronics is modeled with a two-dimensional efficiency map (Figure 4-7). This map shows the overall motor and drive train efficiency as a function of motor speed and motor torque for steady state conditions. The influence of voltage fluctuation on the peak efficiency and shape of the islands of constant efficiency is minor and can be neglected (Nahmer 1996). However, if

the motor is operated at lower voltages, not all operating points shown on the map are valid operating points. With decreasing voltage, the operating regime shrinks to the area within the lines of maximum torque shown in the Figure 4-8. Figure 4-8 shows a map for the maximum motor torque as a function of motor speed and terminal voltage. Both maps are derived from experiments for the case of a 75 kW induction motor. The efficiency map includes the power electronics. Therefore the maps represent not only the motor properties but also the properties of the combined system of power-electronic and electric-motor including control algorithm, such as torque limitation at lower voltages.

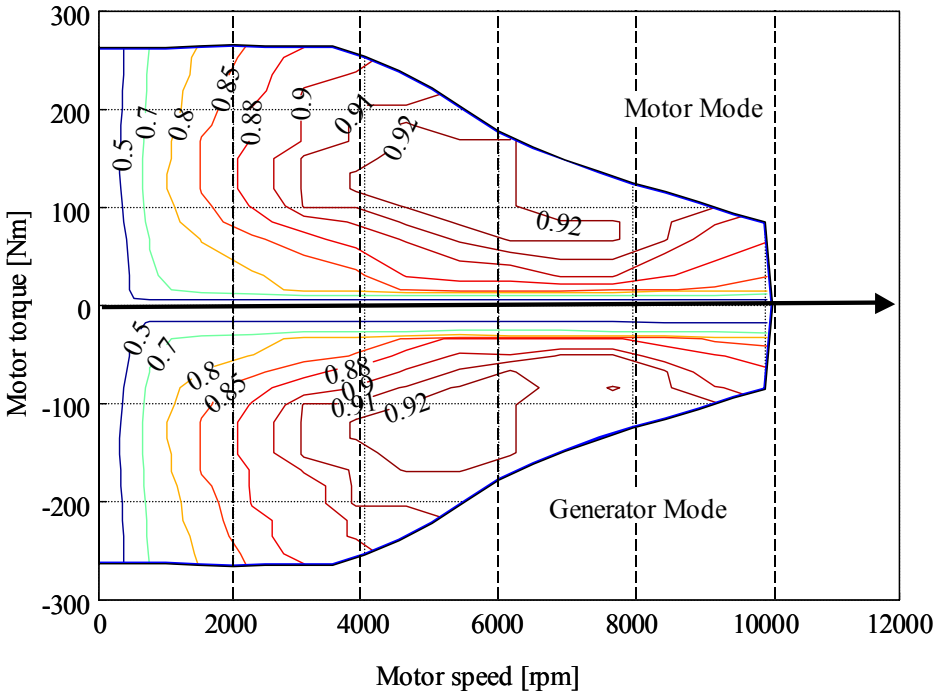

Figure 4-7: Motor efficiency map.

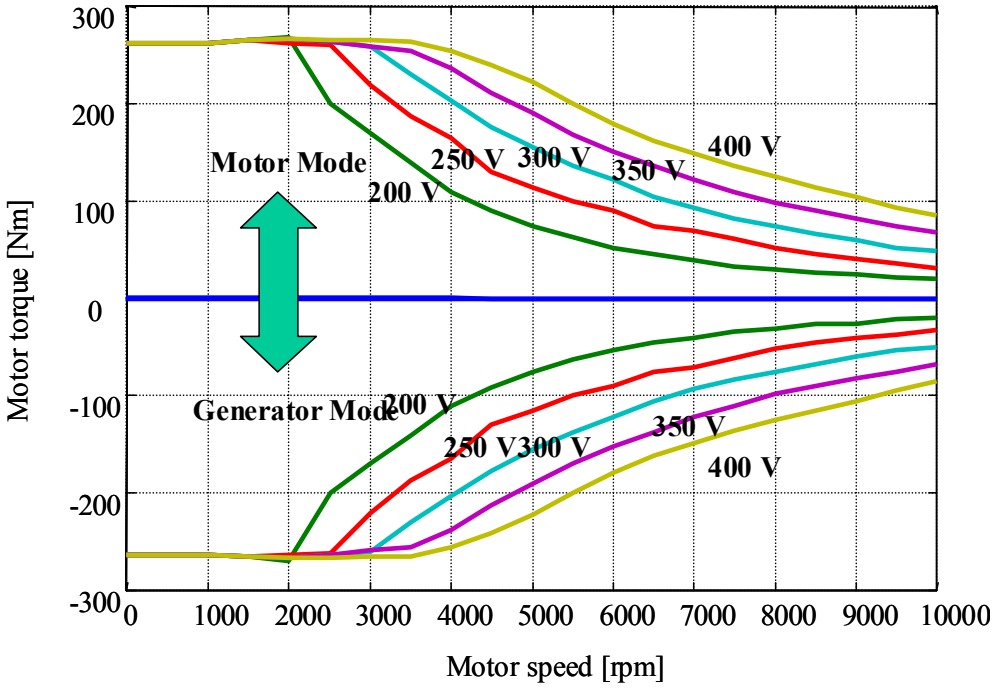

Figure 4-8: Map of maximum torque.

Besides the maps shown in Figure 4-7 and Figure 4-8, the only other parameters that characterize the electric motor including the power electronics are the rotational motor inertia and the motor mass. The motor inertia determines mechanical transients of the motor, e.g. the motor acceleration if no mechanical load is applied, and the motor mass influences the overall vehicle mass and with this the vehicle acceleration for a given configuration.

Algorithms:

For modeling purposes only the upper half (1st and 2nd quadrant) of both maps has been measured (acceleration mode). The lower half (regenerative braking) has been derived by mirroring the upper half. Because of friction within the motor bearings and frictional losses due to the aerodynamic drag (rotor) this assumption is not 100% correct. While in the acceleration mode the frictional losses reduce the available net motor shaft

torque, in the regenerative braking mode the frictional losses would provide additional shaft torque (Figure 4-9 and Figure 4-10). Only if the mechanical frictional losses could be neglected would the mirroring technique provide exact results. However, if the motor is not cooled by forced air through a fan sitting on the motor shaft, the frictional losses are much smaller than the provided net power. For this case the mirroring technique is justified and the maximum torque in the generator mode equals the maximum motor torque for the same speed and terminal voltage.

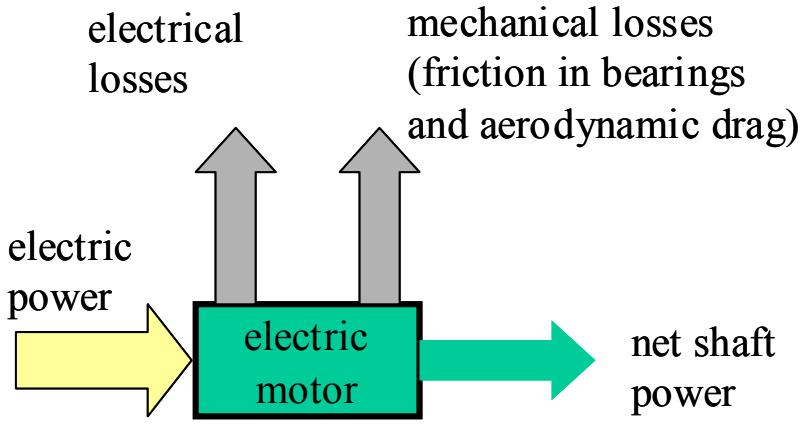

Figure 4-9: Power flow and losses in acceleration mode.

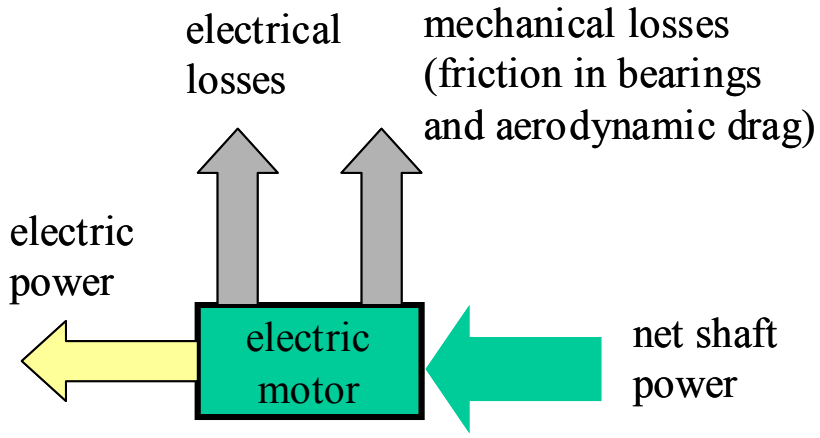

Figure 4-10: Power flow and losses in regenerative braking mode.

The motor efficiency during acceleration phases is stated in Equation 4-15.

$$\eta_{\text{motor}} = \frac{P_{mech\_net}}{P_{el}}$$

where :

η_{motor} = motor efficiency in acceleration mode [1] **Equation 4-15**

P_{mech_net} = accessable net mechanical power [W]

P_{el} = electrical power (dc) [W]

During phases of regenerative braking the motor efficiency is stated in Equation 4-16.

$$\eta_{\text{regen}} = \frac{P_{el}}{P_{mech\_net}}$$

where : **Equation 4-16**

η_{regen} = motor efficiency in regenerative brake mode [1]

The discussion above assumed the steady state operation of the electric motor. For the transient case, the motor inertia has to be considered (Equation 4-17). The usable motor torque supplied to the transmission is the motor shaft torque generated by the motor minus the product of motor inertia and angular shaft acceleration. During phases of vehicle acceleration, the torque supplied to the wheels is reduced and less torque is available for the acceleration of the vehicle. During phases of deceleration, the motor

inertia effectively acts as an energy storage that has to be discharged for the deceleration of the vehicle. The stored energy has to be dissipated in the brake system or converted into electrical energy if the vehicle concept allows for regenerative braking.

$$T_{trans} = T_{motor} - \Theta_{motor} \cdot \frac{d\omega_{motor}}{dt}$$

where:

T_{trans} = Torque supplied to the transmission [Nm]

Θ_{motor} = Motor inertia [$kg \cdot m^2$]

T_{motor} = Motor shaft torque [Nm]

ω_{motor} = Motor shaft speed [rad/sec]

Equation 4-17

The torque supplied by the motor to the transmission depends on the request of the motor control algorithm multiplied by the maximum torque the motor is able to provide (Figure 4-8). It is stated in Equation 4-18. The request of the motor control algorithm is derived from the inputs to this algorithm such as driver request and torque reduction due to high or to low voltage. The motor controller and the embedded control algorithms are described in the next chapter.

$$T_{motor} = T_{motor\_\max}(V_{dc}, \omega_{motor}) \cdot p$$

where:

$T_{motor\_\max}(V_{dc}, \omega_{motor})$ = Max. motor torque at this specific voltage and speed [Nm]

p = Torque request motor controller [1]

V_{dc} = Bus voltage [V]

Equation 4-18

On the electrical side of the motor, the dc motor current is derived by balancing mechanical power at the motor shaft and electric power at the motor terminals. The motor torque times the motor speed is equal to the product of drive train voltage times drive

train current times motor efficiency. Solving this power balance results in Equation 4-19 for the drive train current on the dc-side of the power electronics if the motor is in acceleration mode.

$$I_{motor\_dc} = \frac{\alpha_{motor} \cdot T_{motor}(V_{dc}, \alpha_{motor})}{V_{dc} \cdot \eta_{motor}(T_{motor,} \omega_{motor})}$$

$where:$ **Equation 4-19**

I_{motor_dc} = Dc current into drivetrain [A]

η_{motor} = Motor efficiency [1]

The motor efficiency in Equation 4-19 is taken from the motor efficiency map in Figure 4-7 for positive torque and positive speed (1st quadrant).

For the case of regenerative braking in hybrid vehicle designs, Equation 4-19 changes to Equation 4-20.

$$I_{motor\_dc} = \frac{\alpha_{motor} \cdot T_{motor}(V_{dc}, \alpha_{motor})}{V_{dc} \cdot \eta_{regen}(T_{motor,} \omega_{motor})}$$

$where:$ **Equation 4-20**

η_{regen} = Motor efficiency in the mode of regenerative braking [1]

The motor efficiency in Equation 3-20 is taken from the motor efficiency map in Figure 4-7 for negative torque and positive speed (4th quadrant).

4.3.2. Motor Controller and Motor Control Algorithm

According to the modeling philosophy, the control algorithms are separated from the component descriptions. This principle is also followed through for the electric drive train. The distinction allows greater flexibility and the use of advanced techniques such as rapid prototyping.

The motor control algorithm determines how the acceleration pedal position and the brake pedal position inputs determine the state of the electric motor, e.g. how much torque is requested. In addition to this "basic" functionality a number of safety and convenience features could be programmed and their impact on the vehicle characteristics tested. Generally, the algorithms could be either programmed in the vehicle controller or in the motor controller. From a pure modeling point of view the difference is not significant. However, in real vehicles, in some cases the supplier situation might require that "know how" be kept outside of the motor controller. If this is the case, specific motor control algorithms could be realized in the vehicle controller. In this work, it has been decided to place all motor related control algorithms into the motor controller. Figure 4-11 shows the graphical representation of the algorithm.

The overall algorithm splits up into two parts. The first part is responsible for the operation of the electric drive system in the motor mode. The second part is responsible for the operation of the electric drive system in the generator mode. The latter one is only active in hybrid configurations that allow for the regeneration of mechanical power during braking.

In the motor mode the relevant input variables are the motor speed, the motor temperature (or the temperature of the cooling system), the voltage at the dc-side of the power electronics, and the acceleration pedal position.

In the generator mode the relevant input variables are the terminal voltage at the dc-side of the power electronics, the motor speed, the motor temperature, and the brake signal indicating the request for regenerative braking.

In the motor mode the normalized acceleration pedal position requests the fraction of the peak motor torque available. This peak motor torque is a motor constant and is the maximum torque the drive train is able to provide at zero speed and maximum dc voltage at the dc side of the power electronics. This, by the driver requested torque value, can be reduced by several factors:

- If the motor speed is too high, e.g. in downhill situations, the motor centrifugal forces accessing the rotor increase and this increase could potentially damage the rotor. Therefore it is necessary to limit the accelerating motor torque beyond a maximum speed but below the critical motor speed that causes damage to the motor.
- If the motor temperature is too high, e.g. the losses in the electric motor led to an increase in the motor temperature above the critical temperature.
- If the supply voltage is too low. This function is not for the protection of the electric motor but for the protection of the power source (fuel cell stack, battery or ultra-capacitor). A too low voltage increases the possibility of cell reversal and with this a potential damage at the supply side.

In the generator mode the normalized electric brake signal derived from the normalized brake pedal position[24] determines the fraction of the maximum torque the motor is able to provide in the generator mode. This peak generator torque is the peak torque the drive train is able to provide in the generator mode at zero speed and maximum voltage. It is approximately the same torque as the maximum motor torque but with the opposite sign. Just as in the motor mode, in the generator mode the requested torque could be reduced and increased by several factors:

- if the voltage at the dc terminals of the power electronics is too high the generator torque and with this the recharged power needs to be decreased. This functionality protects the battery or ultra-capacitor storage from overcharging.
- if the temperature of the drive train or the associated cooling system is too high the torque in the generator mode needs to be reduced to avoid damage
- if the motor speed is too high, e.g. in downhill situations, the increasing centrifugal forces could destroy the electric drive train. To protect the drive train the generator torque could be increased if the energy storage could accept the additional power.

The derived acceleration torque request (in the motor mode) or the brake torque request for the braking mode is then compared to the actual torque the drive train provides. The result of this comparison is fed into a Proportional – Integral controller (PI –controller). The output of this controller is limited to upper and lower boundaries and filtered through a first order transfer function, which represents low pass characteristics of the control algorithm to avoid the impact of noise. Finally, the result of this algorithm

[24] See chapter “Vehicle controller.”

is the output of the motor controller and determines how much of the motor torque available is requested.

An additional function, not realized yet but possible to add, is the mimic of the compression torque of an IC-engine vehicle. Because of the fact that electric drive trains have very few frictional losses, the idle characteristics of electric vehicles and IC- engine vehicles are different. IC-engine vehicles decelerate if the acceleration pedal is released due to significant air compression losses in the engine. In contrast, electric vehicles don't show this deceleration because no compression losses are present and other frictional losses are small compared to the compression losses. Thus, for the driver of electric vehicles, unfamiliar behavior might lead to driver decisions less optimal for the overall energy consumption of the vehicle. If the driver sees an obstacle, e.g. a red light, he releases the acceleration pedal. However, the vehicle decelerates at a much slower rate than he is used to in IC engine vehicles. It is therefore possible that he approaches the obstacle faster than he thought and is forced to perform a rapid (last minute) braking maneuver to avoid a collision. In this rapid braking maneuver most of the kinetic energy stored in the vehicle mass is dissipated into heat in the friction brakes and not recovered by generatoric braking. The overall energy balance would be more optimal if the driver had decided to start a gentle braking maneuver as early as possible and recovered the maximum of the kinetic energy stored in the vehicle with generatoric braking. However, this driver behavior is unlikely because it is different from the conventional vehicles. For driver assistance, a function that automatically switches the drive train into the generator mode if the acceleration pedal is released could be implemented. In this case, the

requested brake torque simulates the compression losses of an IC engine vehicle. The torque could be constant and speed independent or varying with vehicle speed.

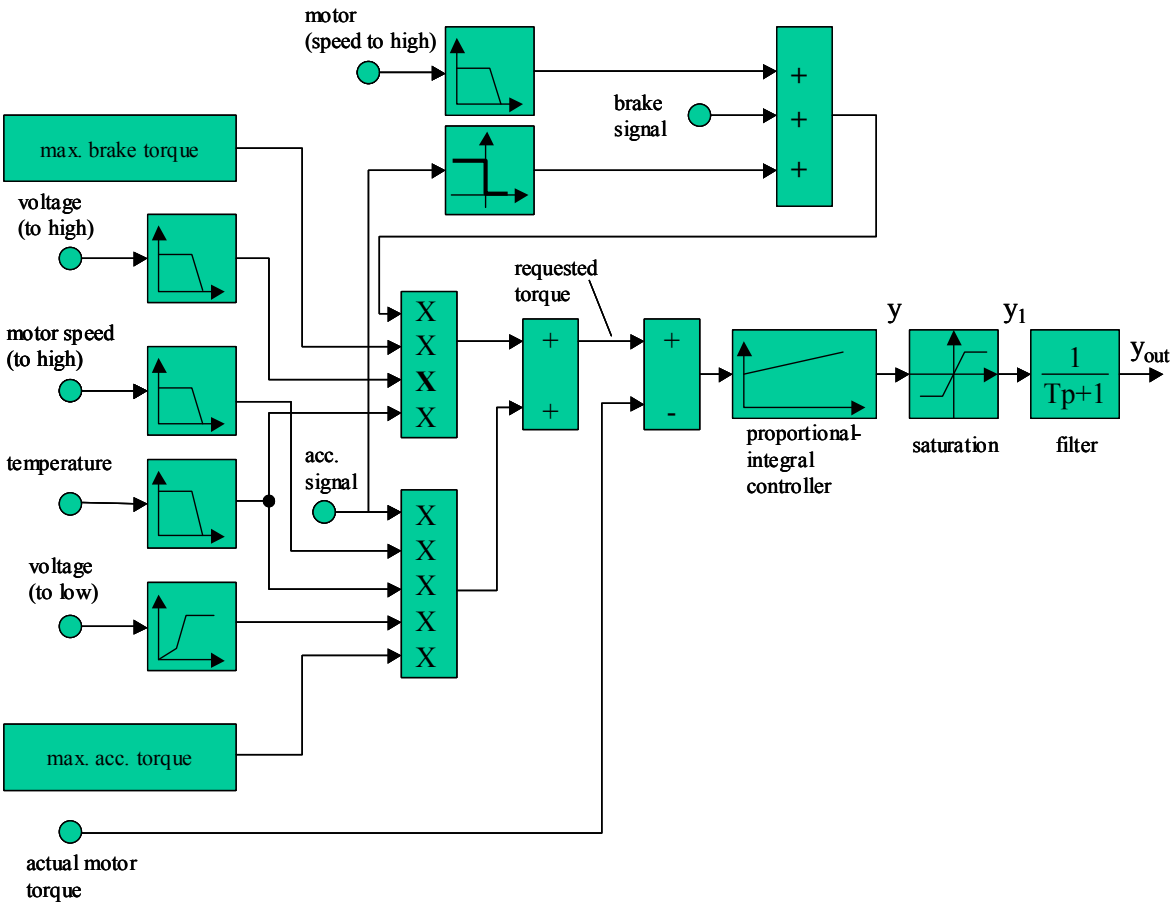

Figure 4-11: Motor control algorithm.

Equations 4-21 to 4-26 show the motor control algorithm illustrated in Figure 4-11 in mathematical form.

During regenerative braking the requested torque is computed according to Equation 4-21.

$$T_{request\_regen} = \left(p - p_{speed\_high}(n_{motor}) + p_{idle}(v)\right) \cdot T_{\max\_regen} \cdot r_{voltage\_high}(V_{ter\min al}) \cdot r_{temperature\_high}(\vartheta)$$

where:

$T_{request\_regen}$ = requested torque for the mode of regenerative braking

p = brake signal generated by vehicle controller

$p_{speed\_high}(n_{motor})$ = additional brake signal if motor speed is to high

$p_{idle}(v,q)$ = additional brake signal for simulating compression friction

$T_{\max\_regen}$ = maximum motor torque during regenerative braking

$r_{voltage\_high}(V_{ter\min al})$ = reduction factor due to high terminal voltage

$r_{temperature\_high}(\vartheta)$ = reduction factor due to high temperature

ϑ = temperature variable

Equation 4-21

During phases of acceleration the requested motor torque is calculated according to Equation 4-22.

$$T_{request\_accel} = q \cdot T_{\max\_accel} \cdot r_{speed\_high}(n_{motor}) \cdot r_{voltage\_low}(V_{ter\min al}) \cdot r_{temperature\_high}(\vartheta)$$

where:

$T_{request\_accel}$ = requested torque in the acceleration mode [Nm]

q = acceleration signal generated by the driver [1]

$T_{\max\_accel}$ = maximum motor torque during acceleration [Nm]

$r_{voltage\_low}(V_{ter\min al})$ = reduction factor due to low terminal voltage [1]

Equation 4-22

The requests for acceleration and braking are summed[25] and from the combined request the actual motor torque is subtracted. The difference between the requested and actual motor torque is the error and fed into the proportional integral controller (Equation 4-23). The output of this controller is limited to values between –1 (for maximum generatoric braking and +1 (for maximum acceleration) and then fed through a first order transfer function (Equation 4-24 and 4-25). This transfer function can be interpreted in several ways:

[25] Normally either the request for braking or for acceleration is zero. However, the possibility that the driver presses the acceleration pedal and the brake pedal at the same time is not excluded.

First it accounts for the filter time constants of the analog input low pass filters in a real power electronic design.

Second it accounts for the time constant imposed by the motor coil inductivity and resistance. The output of the motor control algorithm could be interpreted as an analog signal that determines the state of the power switches and therefore controls the average motor current.

$$\frac{\tau_{MC}}{K_{MC}} \cdot \frac{dy}{dt} = T_{MC} \cdot \frac{d\left(T_{request\_brake} + T_{request\_accel} - T_{actual}\right)}{dt} + \left(T_{request\_brake} + T_{request\_accel} - T_{actual}\right)$$

where:

y = intermediate value [1]

τ_{MC} = Time constant of proportional integral controller [sec]

K_{MC} = Gain proportional integral controller [1/Nm]

T_{actual} = actual motor torque [Nm]

Equation 4-23

After the limitation block the intermediate value y changes to the intermediate value y1.

$$y_1 = y \qquad if\ -1 < y < 1$$
$$y_1 = 1 \qquad if\ y \geq 1$$
$$y_1 = -1 \qquad if\ y \leq -1$$

Equation 4-24

where:

y_1 = intermediate request variable

Finally the output variable determining the requested motor torque is stated in Equation 4-25. The variable y_{out} determines the requested fraction of the maximum motor torque available.

$$T_{filter} \cdot \frac{dy_{out}(t)}{dt} + y_{out}(t) = y_1(t)$$

where :

Equation 4-25

T_{filter} = filter time constant [sec]

$y_{out}(t)$ = request variable for motor torque [1]

4.3.3. Transmission

The transmission modeled in this work is a 1-speed transmission including differential. Input variables are the motor shaft speed and the motor shaft torque. The output variables are wheel torque and wheel speed (Figure 4-12).

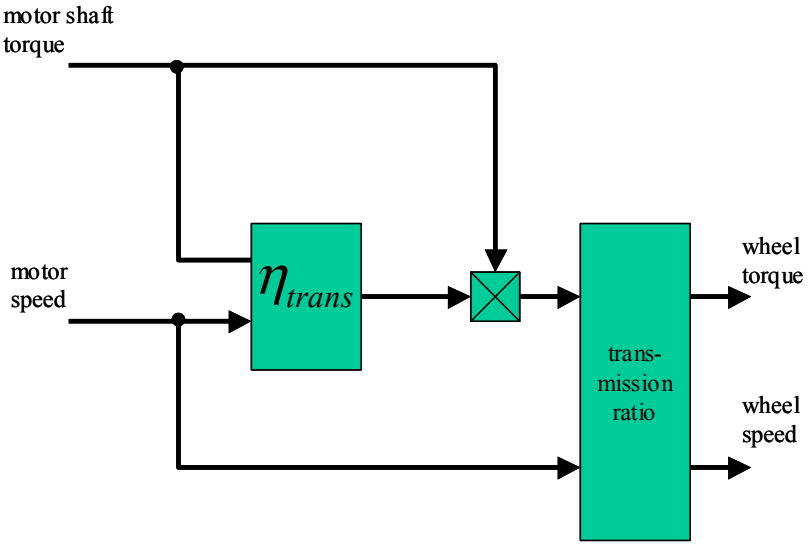

Figure 4-12: Block diagram of the transmission model.

Similar to the electric drive train, the transmission translates energy flows in both directions. During phases of acceleration or cruising with constant speed the energy flow is from the motor to the wheels. During phases of deceleration in hybrid designs the energy flow is reversed from the wheels to the electric motor.

The efficiency map has to describe both energy flow directions. Assuming that the motor speed and vehicle speed in this model are always positive, the two directions of energy flow result in a positive torque during acceleration phases and a negative torque during phases of regenerative braking (in hybrid designs only).

$$\eta_{\text{trans\_motor}} = \frac{P_{trans\_wheel}}{P_{trans\_motor}} = \frac{T_{trans\_wheel}}{T_{trans\_motor} \cdot i}$$

where:

$\eta_{\text{trans\_motor}}$ = Transmission efficiency in regenerative brake mode [1]

P_{trans_wheel} = Mechanical power at the wheels [W]

P_{trans_motor} = Mechanical power at the motor shaft [W]

T_{trans_motor} = Motor shaft torque [Nm]

T_{trans_wheel} = Wheel torque [Nm]

i = Transmission ratio [1]

Equation 4-26

$$\eta_{\text{trans\_regen}} = \frac{P_{trans\_motor}}{P_{trans\_wheel}} = \frac{T_{trans\_motor} \cdot i}{T_{trans\_wheel}}$$

where:

$\eta_{\text{trans\_regen}}$ = Transmission efficiency in regenerative brake mode [1]

Equation 4-27

Equations 4-26 and 4-27 describe the efficiency for both cases. The model assumes that the friction losses in the transmission are the same for both cases. These assumptions allow mirroring the 1st quadrant of the map (positive torque and positive speed) into the 4th quadrant (negative torque, positive speed). The complete efficiency map for the transmission is shown in Figure 4-13.

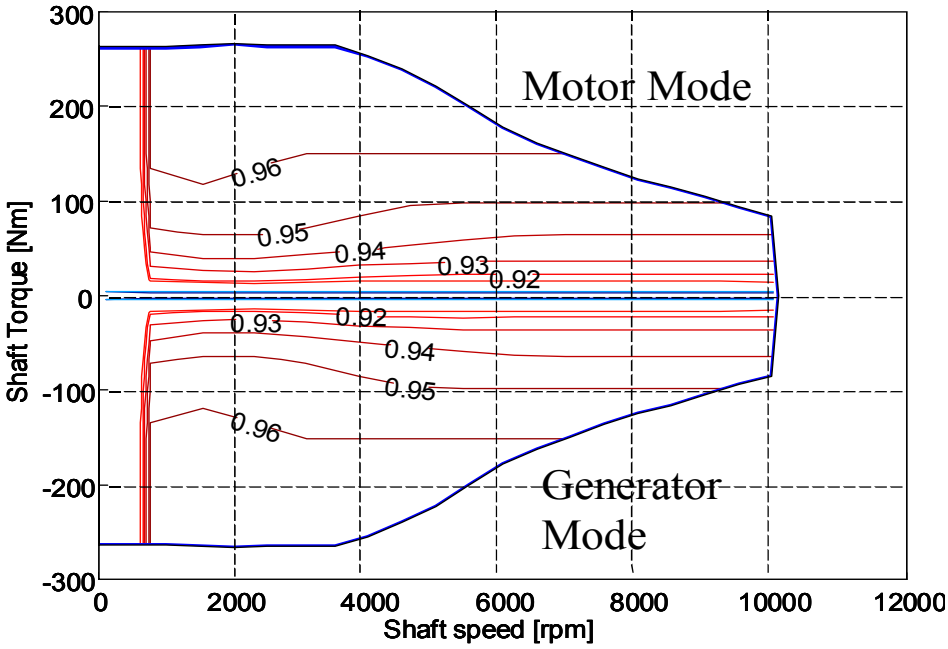

Figure 4-13: Efficiency map of the 1-speed transmission including differential.

The inertia of the transmission is not explicitly considered in the transmission block. However, the transmission inertia can be transformed without any constraints either to the wheel side and added to the wheel inertia or to the motor side and added to the motor inertia.

Equations 4-28 and 4-29 describe the transformation of the rotational inertia to the wheel side or to the motor side for the case of the two-stage transmission (reduction gear and differential). Figure 4-14 shows the rotational inertias at each stage.

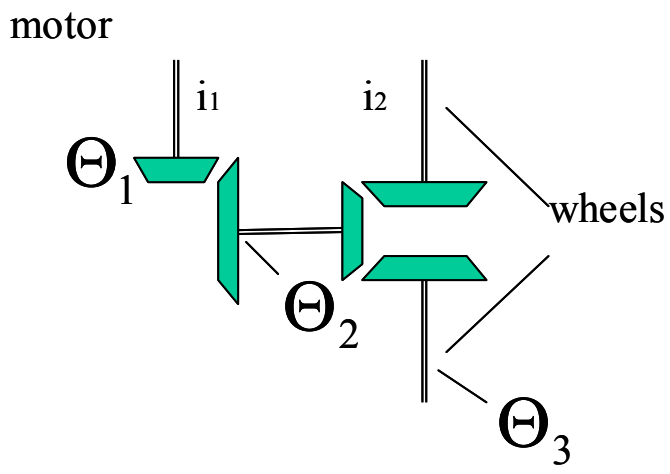

Figure 4-14: Schematic of the transmission.

$$\Theta_{trans\_motor\_side} = \Theta_1 + \frac{1}{i_1^2} \cdot \left(\Theta_2 + \frac{1}{i_2^2} \cdot \Theta_3 \right)$$

where :

$\Theta_{trans\_motor\_side}$ = Total transmission inertia transformed to the motor side $[\mathrm{kg} \cdot \mathrm{m}^2]$

Θ_1 = Inertia of transmission components spinning with motor speed $[\mathrm{kg} \cdot \mathrm{m}^2]$

Θ_2 = Inertia of transmission components spinning with the motor speed reduced by the ratio i1 $[\mathrm{kg} \cdot \mathrm{m}^2]$

Θ_3 = Inertia of transmission components spinning with wheel speed $[\mathrm{kg} \cdot \mathrm{m}^2]$

i_1 = Reduction ratio of the reduction stage $[1]$

i_2 = Reduction ratio of the differential stage $[1]$

Equation 4-28

$$\Theta_{trans\_wheel\_side} = \Theta_3 + i_2^2 \cdot \left(\Theta_2 + i_1^2 \cdot \Theta_1 \right)$$

where :

$\Theta_{trans\_wheel\_side}$ = total transmission inertia transformed to the wheel side $[\mathrm{kg} \cdot \mathrm{m}^2]$

Equation 4-29

4.3.4. Fuel Cell System

In this work, the term fuel cell system is used to refer to the combined system of fuel cell stack, water and thermal management, air supply (including compressor and expander), and fuel processor (including reformer, clean up stages, and the burner for the anode off gas).

Origin and Development

The individual component models that comprise the overall fuel cell system have different origins. Springer (Springer 1993 and 1998) described the fuel cell model fundamentals on the cell level. Friedman (Friedman 1998) took the original Springer model, expanded it to a complete stack model and programmed this into SIMULINK. Cunningham (Cunningham 1999) developed an air supply model for a direct hydrogen vehicle. Combining the stack model and the air supply model Friedman (Friedman 1999) and Cunningham (Cunningham 1999) developed an optimal operating strategy for the overall system of fuel cell stack and cathode air supply for the direct hydrogen case. Later, this initial model was expanded to cover the cases of indirect methanol fuel cell systems and indirect hydrocarbon systems (Friedman 2000). In addition, Cunningham discussed the implications of an additional expander into the air system of a PEM fuel cell engine (Cunningham 2000). Badrinarayanan developed a water and thermal management system, addressing the cooling loads and the issue of water sustainability. In a second step, Badrinarayanan added water and thermal management implications to the initial optimized operating strategy (Badrinarayanan 2000). Friedman (Friedman 2001) provided a complete discussion of the optimal control strategy, including water and thermal management implications and the air and fuel side for an indirect hydrocarbon

system. Two different fuel processor models have been developed and could be used in the fuel cell system model. The first fuel processor model models a fuel processor for a methanol steam reformation process including a water gas shift reaction and CO clean up stages (Ramaswamy 2000 and 2001). The second fuel processor model describes a fuel processor for the partial oxidation reformation process, of Iso-Octane. Similar to the first model, this second model includes also a water gas shift reactor and a preferential oxidation stage for the CO clean up (Ramaswamy 2001). Sundaresan (Sundaresan 2000) developed a burner model for the fuel cell stack anode exhaust and additional fuel (Methanol or Iso-Octane) if required.

Controls

In the area of controls, four main control loops control the states of the overall fuel cell system:

First, a controller for the fuel injected into the fuel processor controls the reformate production of the fuel processor. The controller input parameters are the stack current, the acceleration pedal position, and other parameters (Hauer 2000).

Second, a burner for the anode off gas provides the additional heat required for the evaporation of fuel and water as well as the necessary heat for the endothermic steam reformation process. Alternatively, to anode off gas the burner could also be fed with additional fuel (Methanol, Iso-Octane) if the anode off gas is not sufficient enough to provide the required heat. A burner controller controls the amount of additional fuel burned in the burner based on the heat requirements of the reformer.

Third, on the cathode side, the air supply system control scheme controls the cathode air pressure and airflow.

Fourth, a control scheme for an exit valve between the exit of the fuel processor and the fuel cell stack ensures that only the amount of hydrogen required for safe stack operation will be released from the fuel processor to the stack.

Eggert (Eggert 2000 and 2001) described the setup and simulation of the overall fuel cell system including all subcomponents. He also characterized the complete system with respect to its steady state efficiency and its dynamic characteristics.

Figure 4-15 shows a (simplified) diagram of the overall system, including the controllers for the provision of fuel to the fuel processor and the burner and the controller for the air supply system.

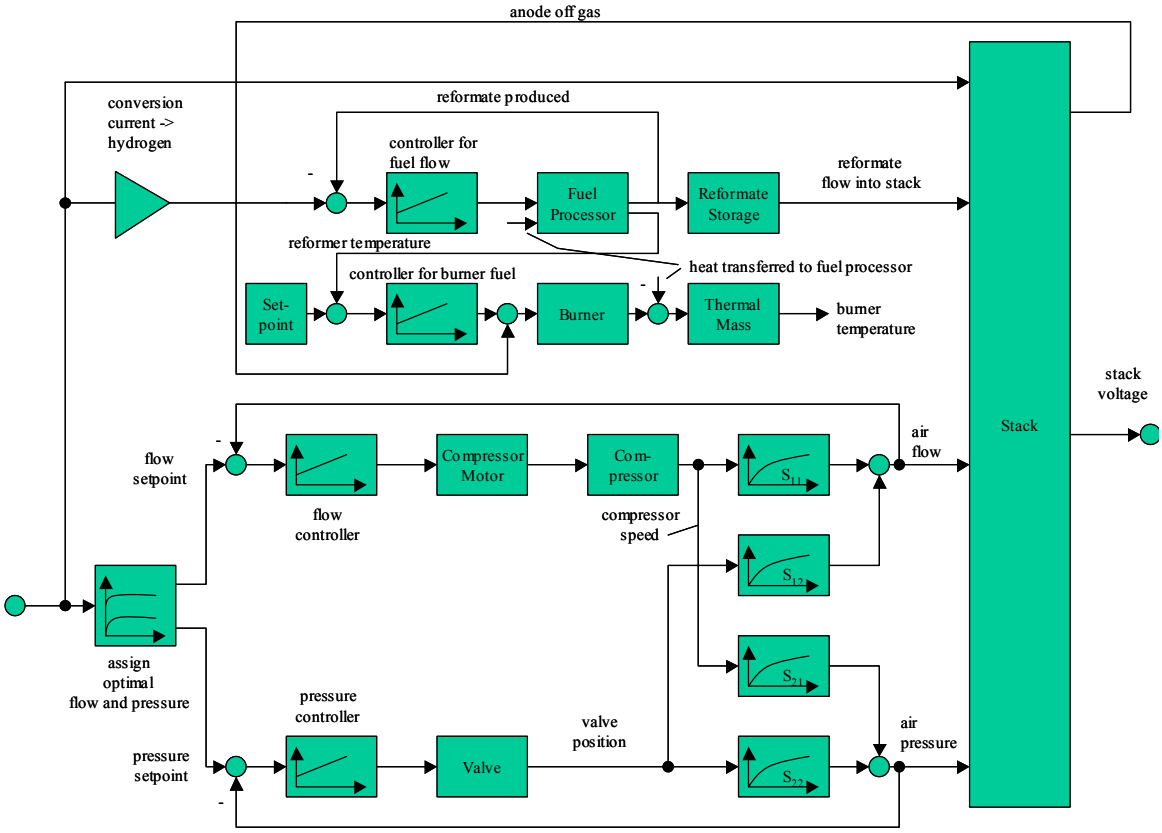

Figure 4-15: Fuel cell system overview.

The following sections explain the components of the fuel cell system model in greater detail. However, for a more complete discussion of the individual aspects, the reader is encouraged to study the provided references.

4.3.4.1. Fuel Cell Stack Model

The fuel cell stack model used in the overall fuel cell system model is based on a cell model initially developed by Springer (Springer 1993 and 1998). Based on this initial cell model Friedman (Friedman 1998) developed an extensive stack model allowing the prediction of the stack voltage for varying stack current, anode fuel flow, and cathode air supply conditions (pressure and air mass flow). In the following explanation this complete stack model is referred to as the "config" model. The "config" model accounts for the following effects:

- Anode overpotential losses: Reaction losses due to oxidation of the hydrogen at the anode catalyst,
- Diffusion losses in the anode backing layer,
- Cathode overpotential losses: Reaction losses due to the reduction of oxygen at the cathode,
- Cathode diffusion losses in the cathode backing layer,
- Ionic membrane resistance,
- Water management in the membrane,
- Electronic resistance of the catalyst, backing layer, and bipolar plates,
- Pressure drop in the anode channel and its effect on the partial pressure of hydrogen at the catalyst layer,
- Pressure drop in the cathode channel and its effect on the partial pressure of oxygen at the catalyst layer,
- Anode air bleed to mitigate effect of CO poisoning,

- Hydrogen dilution effects if reformate gas is supplied to the stack instead of hydrogen.

Summarizing, it could be said that in the "config" model the stack voltage is derived from basic material parameters and first principles. Due the high computational requirements of this detailed model, a simplified table-based version has been derived which is included in the vehicle model. In the context of this work, only the simplified version included in the overall vehicle model will be discussed. For an explanation of the detailed model, the reader is encouraged to study the listed references.

In the vehicle stack model, three different loss mechanisms are considered in principle (Friedman 2000). These are: (a) the anode losses due to the mass transport limitations and reaction losses on the anode, (b) ohmic membrane losses, and (c) the cathode losses due to mass transport and reaction losses on the cathode.[26] In the vehicle model the overall stack potential available at the stack terminals is calculated according to Equation 4-30.

The tables for the anode and cathode voltage losses as a function of current and partial pressures of hydrogen and oxygen respectively are derived from the more detailed "config" model.

[26] The net output power of the combined system of stack and air supply has been maximized, adopting an "optimal control strategy" for the variation of pressure and stoichiometric ratios of the cathode air supply.

$$V_{stack} = n_{cell} \cdot \left(V_0 - \eta_{anode}(p_{H_2}, I) - R_{cell} \cdot I - \eta_{cathode}(p_{ox}, I)\right)$$

where :

V_{stack} = Stack voltage [V]

n_{cell} = Cell number [1]

V_0 = Open circuit cell voltage [V]

η_{anode} = Anode overpotential [V] **Equation 4-30**

p_{H_2} = Partial pressure of hydrogen [Pa]

I = Stack current [A]

R_{cell} = Cell resistance [Ω]

$\eta_{cathode}$ = Cathode overpotential [V]

p_{ox} = Partial pressure of oxygen [Pa]

On the anode side, the impact of the fuel supply, through providing limited hydrogen to the stack, is accounted for in the stack characteristic by a map of anode voltage drops as a function of hydrogen (reformate) mass flow rate and current. Each particular flow and current results in a different partial pressure of hydrogen and in a different anode voltage loss. The maximum absolute cell current for each hydrogen (reformate) flow rate is typically indicated by a sharp increase in the anode voltage loss, due to starvation of the anode. As a result, the cell voltage drops sharply. Consequently, the maximum cell current (current at which the cell voltage drops) increases with increasing hydrogen (reformate) flow (Figure 4-16).

On the cathode side, the impact of air supply is accounted for in the stack with a map of cathode voltage losses as a function of the partial pressure of oxygen and the stack current. Similar to the anode side, the maximum cell current for a particular constant supply of oxygen is indicated by an increase in cathode voltage losses. However, this increase in cathode voltage losses is more gradual than on the anode side.

The third loss mechanism considered on the vehicle level is the ohmic voltage loss due to the ionic resistance of the membrane plus the electronic resistance in the catalyst layer, the backing layer, and the bipolar plates. This loss is proportional to the applied stack current.

Figure 4-16 shows the typical shape of the V-I curve of a fuel cell stack. For small currents the curves are not influenced by the different hydrogen mass flow rates until almost all of the supplied hydrogen is converted (utilization =1). With a further increase in stack current, to the points nearing a utilization of 1, the stack voltage drops sharply due to the increase in anode voltage losses. This characteristic distinguishes a fuel cell stack supplied with pure hydrogen (supplied from an onboard hydrogen storage) from a stack supplied with reformate.

The gentler roll off of the stack voltage at high currents has its origins in the above mentioned cathode losses.

The shape of the polarity plot has significant impact on the vehicle acceleration due to the dependence of the motor torque from the supply voltage at the terminals of the power electronics.

A complete discussion of the model used to derive the magnitude of the different loss mechanisms considered in the stack model, including humidification and CO-poisoning effects, will be provided by Friedman (Friedman 2001) in his doctoral dissertation.

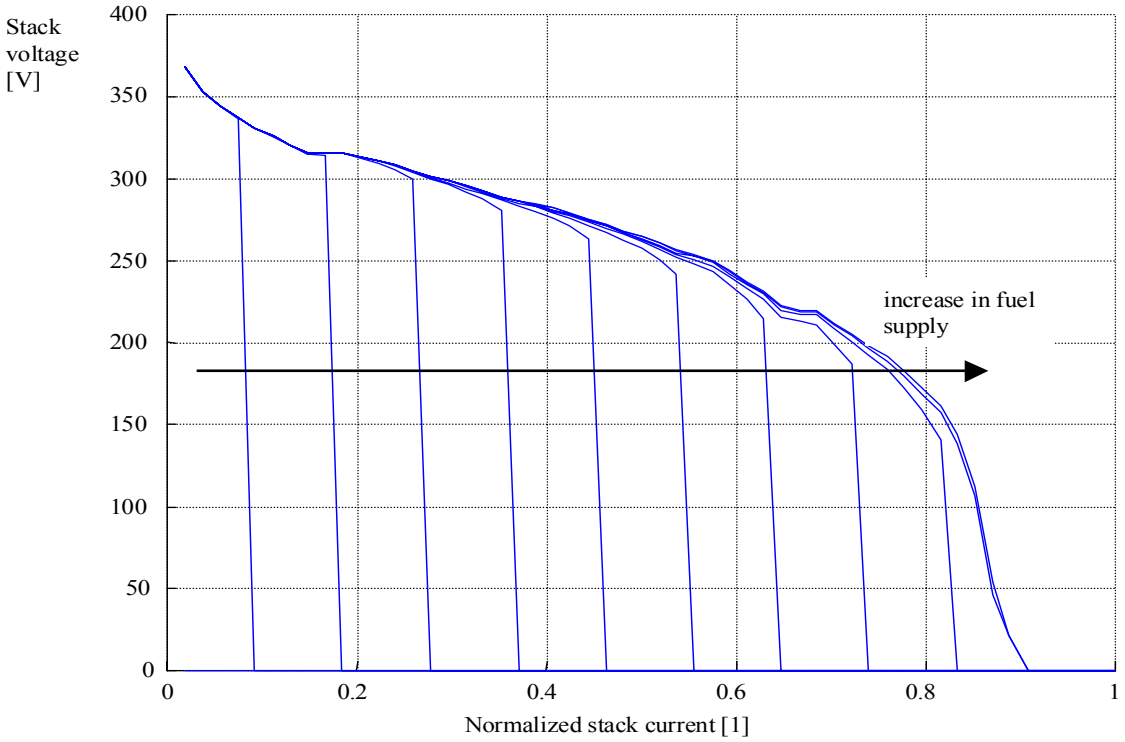

Figure 4-16: Polarization curves for a fuel cell stack fed with a fuel composition of 75% H_2 and 25% CO_2 and assuming the adoption of the earlier mentioned optimal control strategy for the air supply at the cathode side. The total fuel mass flow is varied.

4.3.4.2. Fuel Processor (Reformer) Model

Two different fuel processor systems are available for the integration into the overall fuel cell system model. One model describes the steam reformation process of Methanol including the evaporator/superheater for the fuel, the water gas shift reactions, and CO clean up stages (Ramaswamy 2000). The second model describes the partial oxidation process of Iso-Octane, also including the water gas shift reaction and the gas clean up stages (Ramaswamy 2001).

Because of the complexity of the fuel processor models and the significant impact on run time, a simplified model has been proposed supporting the system analysis if the main objectives are vehicle dynamics and not fuel consumption or emissions.

The analysis of an indirect-methanol system shows that the dominant factor in the dynamic response of the vehicle is the transient response of the specific methanol steam reformer design that is included in the system (Hauer 2000). Therefore, if the focus is on vehicle dynamics, e.g. acceleration time and elasticity, a simplified fuel processor model accounting for the dynamic fuel processor properties only could be included in the simulation.

For this case, the reformer dynamics (including the evaporator-superheater and gas clean up stage) are modeled by assuming a second order transfer function as suggested by Peters (Peters 1998). Using this second order transfer function model, the dominant characteristic of the fuel flow response to an input step of methanol flow is an exponential increase over time (Figure 4-17). The exact shape of this curve and the magnitude of the 10-90% response time (the metric used herein) depend on the specific reformer design. In the case of steam reformers, the heat transfer limitations within the reformer dominate the overall reformer dynamics together with the reaction kinetics at

the catalyst sites (Ohl 1995). Table 4-2 shows the 10-90% response times associated with various time constants using the assumed second order transfer function. The reformer model used here assumes a damping factor D=1 to ensure that no physically unrealistic overshoot occurs in the uncontrolled (open loop) reformer model (i.e., the output hydrogen flow exceeds the hydrogen content of the input feedstock flow). The conversion rate (molar ratio) from Methanol to hydrogen for the steam reformer is assumed to be cv=3.[27]

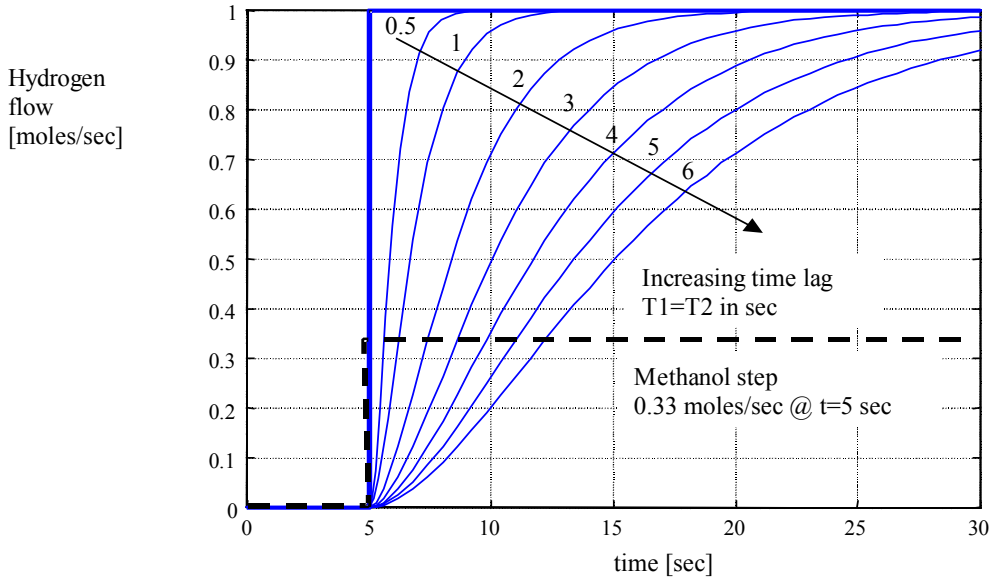

Figure 4-17: Normalized reformer response (input: Methanol step at t=5sec; output: hydrogen at reformer exit). The labels at the curves are the assumed time constants T1 and T2 in sec (see also Table 4-2); the damping factor of the open loop system is set to 1 (T1=T2).

[27] In reality the conversion rate is lower than the ideal conversion rate of three (three moles of hydrogen for each mole of methanol). However, assuming a lower conversion rate would only influence the efficiency but not the transient characteristic of the reformer model. However, because the reduced fuel processor model is used for transients only, the exact conversion rate is secondary.

time constant of the transfer function in sec (T1=T2)	10 to 90 % response time in sec
1	3.4
2	6.7
3	9.6
4	13.5
5	16.8
6	20.1

Table 4-2: 10-90 response times of the reformer if modeled as a 2nd order transfer function.

Equation 4-31 shows the reformer model in equation form for this simplified case.

$$\frac{\dot{m}_{H2}}{\dot{m}_{methanol}} = \frac{cv}{T_{fp1} \cdot T_{fp2} \cdot p^2 + (T_{fp1} + T_{fp2}) \cdot p + 1}$$

Equation 4-31

where :

$T_{fp1} = T_{fp2}$ = time constants [sec]
($T_{fp1} = T_{fp2}$ leads to $D = 1$)

p = complex frequency [1/sec]

$\dot{m}_{H2}$ = hydrogen flow at the reformer outlet [moles/sec]

$\dot{m}_{methanol}$ = methanol flow at the reformer inlet [moles/sec]

cv = conversion rate (moles of hydrogen per mole of methanol in steady state conditions) [1]

4.3.4.3. Fuel Processor Controller

The fuel processor controller is separately modeled from the actual fuel processor hardware. The fuel processor controller determines the amount of hydrogen generated by the fuel processor based on several control variables (inputs). The output of the controller is the same as the methanol flow into the fuel processor. A separate actuator, e.g. a fuel injector, has not been modeled.[28]

The amount of hydrogen requested from the fuel processor is dependant on three input variables. These are:

- The stack current,
- The derivative of the acceleration pedal position,
- The stack voltage.

The motivation for choosing these three control variables for the fuel processor is to ensure good vehicle acceleration and reasonable fuel consumption at the same time under all operating conditions.

The stack current is the dominant control variable during steady state or nearly steady state vehicle operation e.g. cruising on the highway with constant speed. The actual stack current is taken and converted into a molar hydrogen request (Equation 4-32).

[28] The injector time constant is small compared to the reformer time constant and could be neglected. Also, the energy losses due to the injection of the fuel are negligible in this context. Both assumptions together allow accurate modeling without considering the injection process.

$$\dot{m}_{H_2}^{req\_current} = \frac{I_{Stack}}{4 \cdot F \cdot u} \cdot n_{cell}$$

where:

$\dot{m}_{H_2}^{req\_current}$ = requested hydrogen due to the stack current [moles · sec^{-1}]

I_{Stack} = Fuel cell stack current [A] Equation 4-32

F = Faraday constant [A · sec · mole^{-1}]

u = utilization rate [1]

n_{cell} = number of cells in stack [1]

During positive transients, e.g. vehicle acceleration, the derivative of the acceleration pedal position dominates the operation of the fuel processor. In this mode, a large amount of hydrogen is requested from the reformer to guarantee high stack voltages leading to high motor torque and therefore good vehicle acceleration. This request is almost zero during periods of low vehicle dynamics (Equation 4-33).

$$T_1 \cdot \frac{d\dot{m}_{H_2}^{req\_pedal}}{dt} + \dot{m}_{H_2}^{req\_pedal} = K_1 \cdot T_2 \cdot \frac{dp}{dt}$$

where:

K_1 = controller time constant [moles/sec] **Equation 4-33**

T_1, T_2 = controller time constants [sec]

$\dot{m}_{H_2}^{req\_pedal}$ = requested hydrogen due to the derivative of the acceleration pedal position [moles · sec^{-1}]

p = normalized acceleration pedal position [1]

The third input variable into the fuel processor controller is the stack voltage. The stack voltage is compared to a minimum stack voltage and, depending on this comparison, additional hydrogen is requested from the fuel processor (Equation 4-34). In some respect, this control variable is only a backup for situations in which the first two request variables would not request sufficient enough hydrogen. It guarantees the robustness of the overall algorithm.

$$\dot{m}_{H2}^{req\_voltage} = f(V_{stack})$$

where:

$\dot{m}_{H2}^{req\_voltage}$ = requested hydrogen flow due to low fuel cell stack voltage $[\text{moles} \cdot \text{sec}^{-1}]$ **Equation 4-34**

$f(V_{stack})$ = table for the hydrogen request as a function of stack voltage [moles/sec]

V_{stack} = stack voltage [V]

The aggregated hydrogen request is then used to derive the methanol injected into the reformer. For this the hydrogen request is compared with the actual hydrogen flow at the reformer outlet (downstream towards the fuel cell stack). A Proportional Integral (PI) control algorithm (Equation 4-35) determines the methanol flow into the reformer.

$$T_3 \cdot \frac{d\dot{m}_{CH3OH}}{dt} = K_3 \cdot \left(T_3 \cdot \frac{d}{dt} x + x \right)$$

$$x = \left(\max\left(\dot{m}_{H_2}^{req\_current}, \dot{m}_{H_2}^{req\_pedal} \right) + \dot{m}_{H_2}^{req\_voltage} - \dot{m}_{H_2}^{actual} \right)$$

where: **Equation 4-35**

T_3 = time constant for reformer controller [sec]

K_3 = controller gain [moles of $\mathrm{CH_3OH}$ / mole of $\mathrm{H_2}$ difference]

$\dot{m}_{CH3OH}$ = methanol flow into reformer $[\text{moles} \cdot \text{sec}^{-1}]$

$\dot{m}_{H_2}^{actual}$ = actual hydrogen flow at the reformer exit [moles/sec]

The complete control algorithm in graphical form is shown in Figure 4-18. Equations 4-32 – 4-35 represent the full set of equations allied to derive the hydrogen flow request from the reformer depending on the above-mentioned measures.

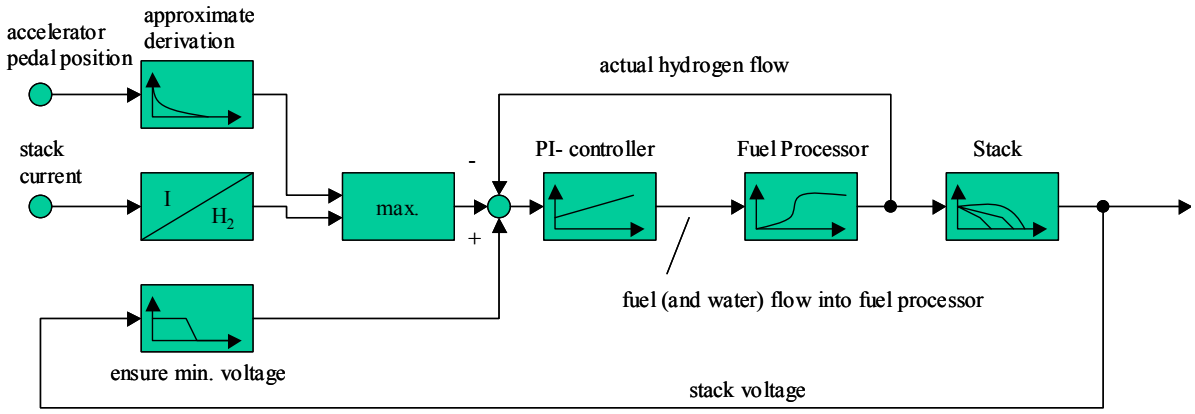

Figure 4-18: Control algorithm for fuel processor (without additional storage for reformate).

For practical purposes, controller parameters are always chosen to ensure a damping factor D=1/sqrt(2) for the closed loop system of reformer and controller. The reasons for this setting are:

- Reasonable good fuel processor dynamic,
- Maintaining stability for different reformer time constants and conversion rates.

With the system assumptions in the previous discussion, the controller parameters K_3, T_3 for the Methanol controller could be calculated according to Leonhard (Leonhard 1985). For a given fuel processor system gain cv and reformer time constants T_{fp1} and T_{fp2}, the control parameters for the PI controller in Equation 4-35 could be calculated according to Equation 4-36. The in Equation 4-36 calculated parameters assume a closed loop damping factor of D=1/sqrt(2).

$$T_3 = T_{fp1}$$

$$K_3 = \frac{1}{cv} \cdot \frac{T_{fp1}}{2 \cdot T_{fp2}} = \frac{1}{2 \cdot cv}$$

Equation 4-36

4.3.4.4. Burner Model Including the Controller Model

For the case of steam reformation of methanol, the burner supplies the necessary heat for the endothermic steam reformation process in the fuel reformer as well as for the evaporation of fuel (methanol and water) in the fuel evaporation unit.

For the partial oxidation of gasoline (Iso-Octane), no additional heat is required. For this case the burner supplies only heat for the evaporation of fuel and water (water gas shift reaction).

Hence for both cases the utilization of hydrogen in the fuel cell stack is less than 100%. The gas from the anode exit contains a fraction of hydrogen, which could be utilized in the burner for heat generation. For achieving high fuel efficiency, only if this hydrogen fraction contains not enough heat for maintaining the reformer (and evaporator) temperature, supplemental methanol has to be burned in the burner. Figure 4-19 shows the integration of the burner and the burner controller (this is the controller which decides if supplemental fuel should be added to the burner) into the fuel processor model.

The burner controller compares the reformer set point temperature (this is the temperature at one carefully chosen location inside the reformer) with the actual reformer temperature at this location. Depending on this comparison, more or less additional fuel is injected into the burner. In addition to the fuel supplied, the hydrogen content in the anode off gas coming from the fuel cell stack is combusted in the burner.

The burner model used in this work consists of 10 Continuous Stir Tank Reactors (CSTR). The supplied constituents are fed into the first CSTR and react. The products form an outlet stream and feed into the second CSTR. The outlet of the 10^{th} CSTR goes finally into the exhaust. Sundaresan (Sundaresan 2000) describes the overall burner model in detail. It is assumed that no afterburner heat exchanger is installed to utilize the

heat contained in the burner off gas. The heat transferred from the burner into the fuel reformer (or the fuel evaporation unit), the heat losses into the environment, and the heat in the burner exhaust are subtracted from the heat of combustion. The difference between the four energy streams determines the temperature of the burner structure. The difference between reformer temperature and burner temperature together with the wall parameters (heat transfer area and heat transfer coefficients) determine the heat transferred from the burner into the reformer.

At the reformer side, the heat required by the reformation process plus the heat required by the evaporation unit plus the transferred heat minus heat losses into the environment and minus heat losses through the exit flow to the fuel cell stack determine the temperature of the reformer structure.

This simplified view of the reformer burner integration assumes that the constituents are in thermal equilibrium with the structure.

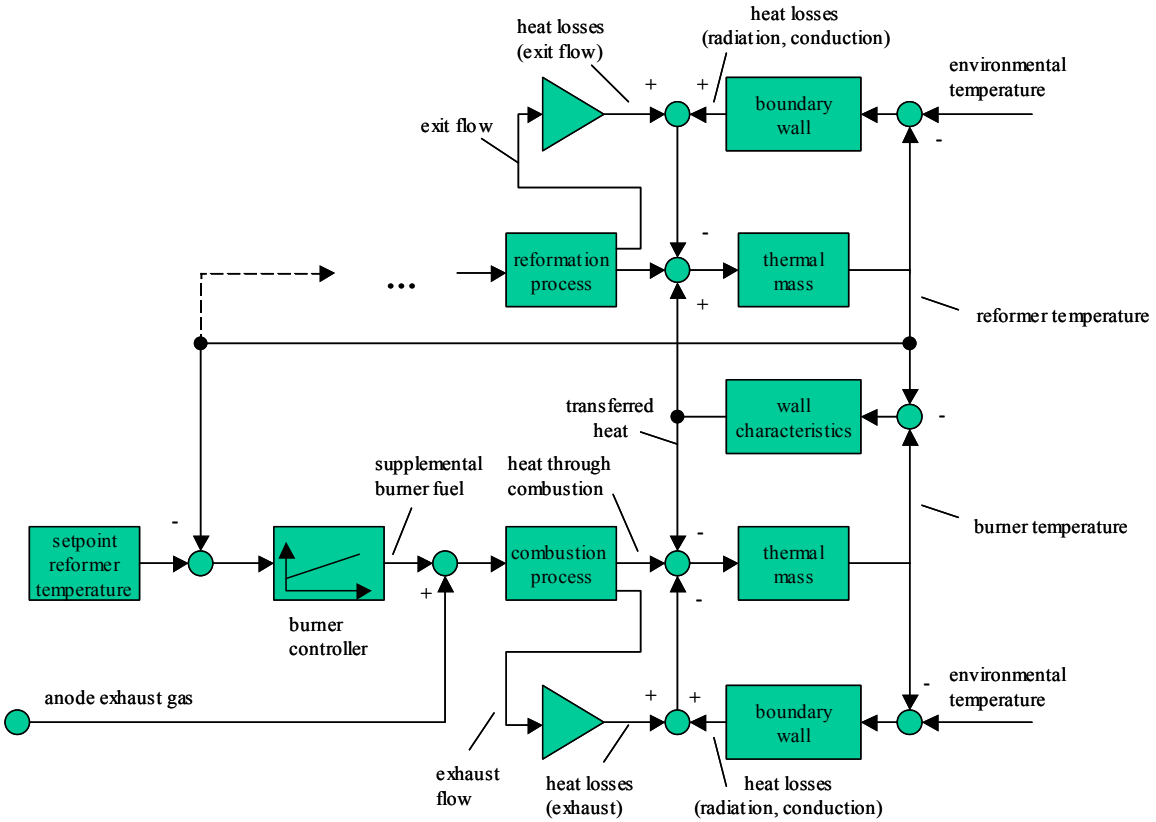

Figure 4-19: Integration of the burner in the fuel processor unit.

4.3.4.5. Reformate Storage Including Controller for the Exit Valve

The model provides the capability for the activation of a separate buffer for reformate between the exit of the fuel processor unit and the inlet of the stack anode. The motivations for the incorporation of this reformate buffer are (1) the improvement of the transient response time of the overall fuel cell system and (2) improvement of the overall fuel cell system efficiency during transient operation.

The improvement of the fuel cell system dynamics has its reason in the capability of the reformate storage to supply reformate almost immediately (without time lag) to the fuel cell stack. In contrast, the system response time without integrated reformate storage is limited because of the reformer response time.

The improvement of the average system efficiency is due to the ability to control the reformate supply to the stack during downwards transients. Without the storage device, reformate generated in the fuel processor due to already injected fuel would be wasted and therefore reduce the overall fuel cell system efficiency. The reformate storage allows the reformate flow to be buffered for later use in an upwards transient.

Figure 4-20 shows the integration of the reformate buffer together with the modified control scheme for the fuel processor. In addition to the fuel processor controller, a controller for the exit valve of the reformate storage is necessary.

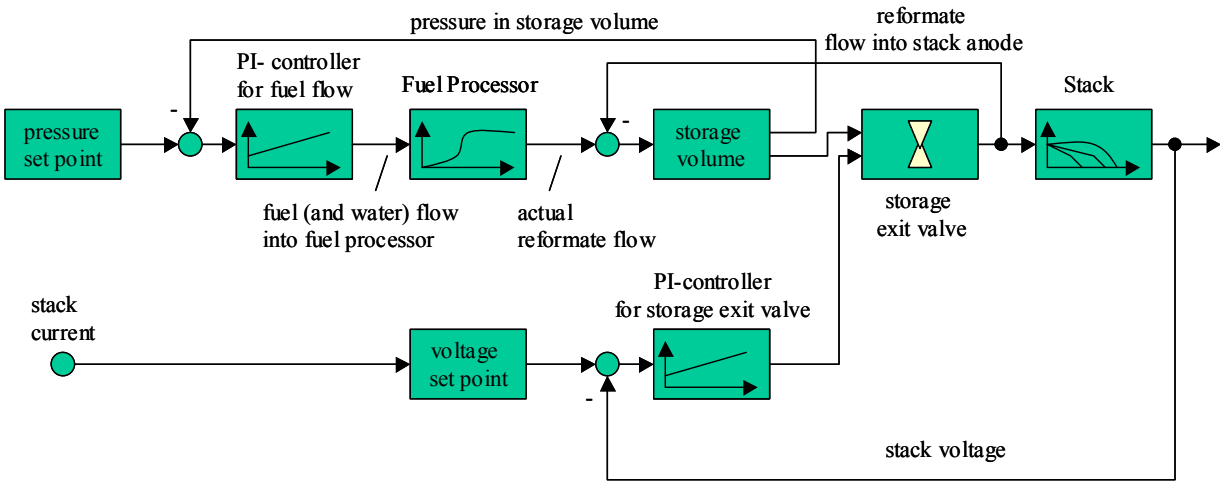

Figure 4-20: Integration of the reformate buffer and control scheme for the exit valve and fuel processor for the case of a reformate buffer.

With an integrated reformate buffer within the system, a different control strategy for the fuel processor than in systems without reformate storage has been applied. For the case of a reformate storage the fuel processor controller maintains a constant storage pressure within the storage volume (Figure 4-20). In addition, the reformate flow downstream to the fuel cell stack is controlled by an exit valve located either at the exit of the buffer or the exit of the fuel cell stack.[29] In this work the controller for the state of the exit valve compares the difference between the minimum stack voltage for a given stack current and the actual stack voltage as input variable and controls the position of the exit valve (and with this the reformate flow from the storage into the stack). If, for a given current, the stack voltage drops below the minimum stack voltage, the controller opens the exit valve and supplies more reformate to the stack. If the stack voltage exceeds the target stack voltage for a given current, the controller reduces the reformate flow into the stack.

It is assumed that the described control loop is fast compared to the ramp up and ramp down times of the fuel processor. The time for an increase in hydrogen supply from 0 to 100% is determined by the speed the valve can be operated.

Figure 4-20 shows the closed loop control system for the exit valve. Besides the speed limitations and gain of the valve, the overall system characteristic depends on the controller characteristics and the stack gain(depending on the operating point of the stack). In this context the stack gain is defined as the sensitivity of the stack voltage to hydrogen flow fluctuations. Friedman (Friedman 2000) shows that this gain parameter is almost zero in the regime of low hydrogen utilization (below a utilization of 0.9) and high in the regime of high hydrogen utilization (Figure 4-16).

In the following section, the controller parameters for this control loop will be derived. It will be shown that the system parameters will lead to a controllable system if a proportional integral controller is used.

Equation 4-37 states the transfer function of a proportional integral controller. This controller type is applied for controlling the exit valve.

$$F_{Controller} = K_{Controller} \cdot \frac{T_i \cdot p + 1}{T_i \cdot p}$$

where:

$F_{Controller}$ = controller transfer function

$K_{Controller}$ = controller gain [actuator current / volt]

T_i = controller time constant [sec]

p = complex frequency [rad/sec]

Equation 4-37

[29] The current fuel cell stack model does not account for channel length within the stack. Therefore the results for placing the valve at the anode stack inlet or outlet are equal.

The exit valve is characterized with a first order transfer function (Equation 4-38). The valve contains the actuator (electric motor or magnet) and the actual mechanic that opens or closes the reformate storage volume. The valve transfer function takes the controller output signal (actuator current) and translates this signal into the reformate flow going into the stack.

$$F_{valve} = \frac{K_{valve}}{T_{valve} \cdot p + 1}$$

where:

F_{valve} = transfer function for the valve including actuator

K_{valve} = valve gain [mole/actuator current]

T_{valve} = valve time constant [sec]

Equation 4-38

For the purpose of the controller design, the stack is characterized by an algebraic gain only. The gain is a function of the stack current and the anode and cathode conditions, including the flow of reformate and air (Equation 4-39).

$$F_{stack} = K_{stack}(\text{stack current, reformate flow, air flow})$$

$$K_{stack} = \frac{1}{V_0} \cdot \left(I_0 \cdot \frac{\partial V_{stack}}{\partial I} + \dot{m}_{H2} \cdot \frac{\partial V_{stack}}{\partial \dot{m}_{H2}} + \dot{m}_{air} \cdot \frac{\partial V_{stack}}{\partial \dot{m}_{air}} \right)$$

where:

F_{stack} = transfer function for the fuel cell stack from the reformate flow into the stack to the stack voltage [1]

K_{stack} = stack gain [1]

$V_0, I_0, \dot{m}^0{}_{H2}, \dot{m}^0{}_{air}$ = normalisation factors

Equation 4-39

For optimizing the dynamic behavior of the closed loop system, the analysis of the transfer function of the closed loop system is required (Equation 4-40).

$$F_{total} = \frac{V_{stack}}{V_{setpo\,int}} = \frac{F_{controller} \cdot F_{valve} \cdot F_{stack}}{F_{controller} \cdot F_{valve} \cdot F_{stack} + 1}$$

where: **Equation 4-40**

F_{total} = transfer function for the closed loop system [1]

Combining Equations 4-37 through 4-40 and setting the controller time constant equal to the valve time constant results in Equation 4-41. The setting the controller time constant equal to the valve time constant optimizes the transient characteristic of the combined system. The resulting system is of first order and of (potentially) higher dynamic than the characteristic of the uncontrolled reformer stack characteristic.

$$F_{total} = \frac{1}{\frac{T_{valve}}{K_{controller} \cdot K_{valve} \cdot K_{stack}} \cdot p + 1}$$ **Equation 4-41**

It can be seen that for a given valve characteristic (T_{valve}, K_{valve}) and a given stack characteristic (K_{stack}), a higher controller gain ($K_{controller}$) would result in a faster responding system. However, due to the limited output of the controller (current supplied to the valve coil), the controller gain cannot be increased above an upper limit.

Because of this the minimum time constant of the closed loop system is T_{min} as defined in Equation 4-42.

$$T_{\min} = \frac{T_{valve}}{K_{controller}^{\max} \cdot K_{valve} \cdot K_{stack}}$$

where: **Equation 4-42**

$T_{\min}$ = minimum time constant of the closed loop system

$K_{controller}^{\max}$ = maximum controller gain

Because of the fact that the stack gain K_{stack} is not a constant but depends on the operating point of the stack, the closed loop time constant is variable. The system is fast

responding if K_{stack} is large and slow if K_{stack} is low. However, if K_{stack} is low the stack is not operated at an operating point in which rapid supply of hydrogen is necessary. On the other hand, if K_{stack} is high (large voltage variations due to changes in the hydrogen flow into the stack) the overall system dynamic is fast. Therefore it can be expected that the overall system dynamics are satisfying. The control scheme will allow the control of the hydrogen flow into the stack such that the stack voltage follows the voltage set point dynamically.

4.3.4.6. Air Supply System

This chapter discusses the cathode air supply system. From a controls point of view the air supply system could be separated into three major parts. These are:

- The air supply controller including the control strategy,
- The actuators necessary for realizing the control strategy (compressor, cathode exit valve),
- The air system itself (stack and piping).

The input for this controller is the fuel cell stack current. The outputs are the air flow and air pressure at the stack exit. The air supply control strategy has been designed for maximizing the net fuel cell stack power available at the terminals (Friedman 2000).

For maintaining flow and pressure at the same time, two actuators need to be controlled. The actuators are the air compressor with its output compressor speed and the exit valve (located at the stack exit) with its relative position.

The system is cross-coupled, e.g. if the valve is operated, the airflow and the pressure in the stack change. Similar, if the compressor speed changes, flow and pressure in the stack also change. The coupling is described by the transfer functions S_{12} and S_{21} as defined in Equations 4-43 and 4-44 and shown in Figure 4-15.

$$S_{12} = \frac{\Delta\Phi_{air}}{\Delta\alpha_{valve\_position}}$$

where:

S_{12} = transfer function describing the change of air flow through the stack as a function of the valve position

$\Delta\Phi_{air}$ = change in air flow [moles/sec]

$\Delta\alpha_{valve\_position}$ = change in the position of the exit valve[1]

Equation 4-43

$$S_{21} = \frac{\Delta p_{air}}{\Delta \Omega_{compressor}}$$

where:

S_{21} = transfer function describing the change of air pressure at the stack exit as a function of the change in compressor speed

Equation 4-44

Δp_{air} = change in air pressure [Pa]

$\Delta \Omega_{compressor}$ = change in the compressor speed [rad/sec]

The transfer function S_{11} relates the compressor speed to the airflow at the compressor exit. It is defined in Equation 4-45.

$$S_{11} = \frac{\Delta \Phi_{air}}{\Delta \Omega_{compressor}}$$

where:

Equation 4-45

S_{11} = transfer function for the transfer of the air compressor speed into the air flow

The transfer function S_{22} relates the change in the position of the (stack) exit valve to a change in pressure.

$$S_{22} = \frac{\Delta p_{air}}{\Delta \alpha_{valve\_position}}$$

where:

Equation 4-46

S_{22} = transfer function for the transfer from the valve position into a pressure fluctuation

With this setup, the control of the air supply system could be treated as a controls problem with two inputs (set points for air flow and air pressure depending on the stack current) and two outputs (airflow and pressure in the stack). Leonhard (Leonhard 1985) describes the sizing of the controllers for the case of a coupled system with linear

elements and two inputs and two outputs. For the linear case, he finds that linear control algorithm could be found such that flow and pressure are decoupled and independently controllable. However, this is not possible for the general non-linear case.

The solution pursued in this work assumes an instantly responding compressor and valve. Consequently dynamic aspects of the compressor system are neglected. This is possible for configurations with significantly faster responding air systems than reformer systems.

Cunningham (Cunningham 2000) describes the characteristics and the modeling of different compressor (and expander) technologies including the compressor motor and design specifics (piping, pressure drops) in detail.

4.3.4.7. Overall Fuel Cell System Characteristics

From the view of an overall vehicle, the complete fuel cell system can be seen as a power source (similar to a battery) for the electric drive train. With this view, the primary interface variables between the fuel cell system and the rest of the vehicle are the stack current and the stack voltage. Beyond these primary interface variables, the acceleration pedal position, and in the case of a hybrid vehicle with batteries and/or ultra-capacitors, the auxiliary load of the system is interfacing with the vehicle (Figure 4-21).

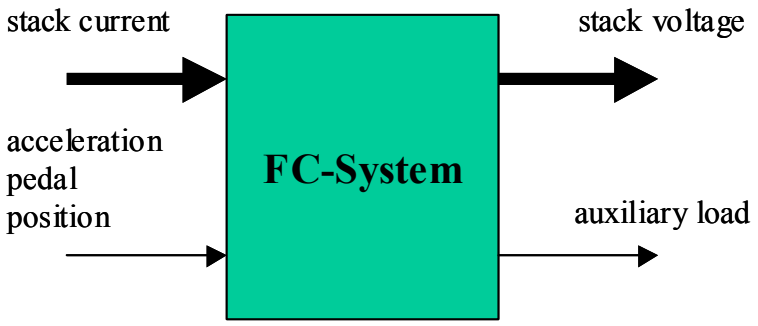

Figure 4-21: Interface between the fuel cell system and the vehicle (conceptional). The stack current together with the acceleration pedal position determines the stack voltage and auxiliary load.

The fuel cell system can be characterized with a steady state efficiency map showing the efficiency versus the stack current (Figure 4-22).

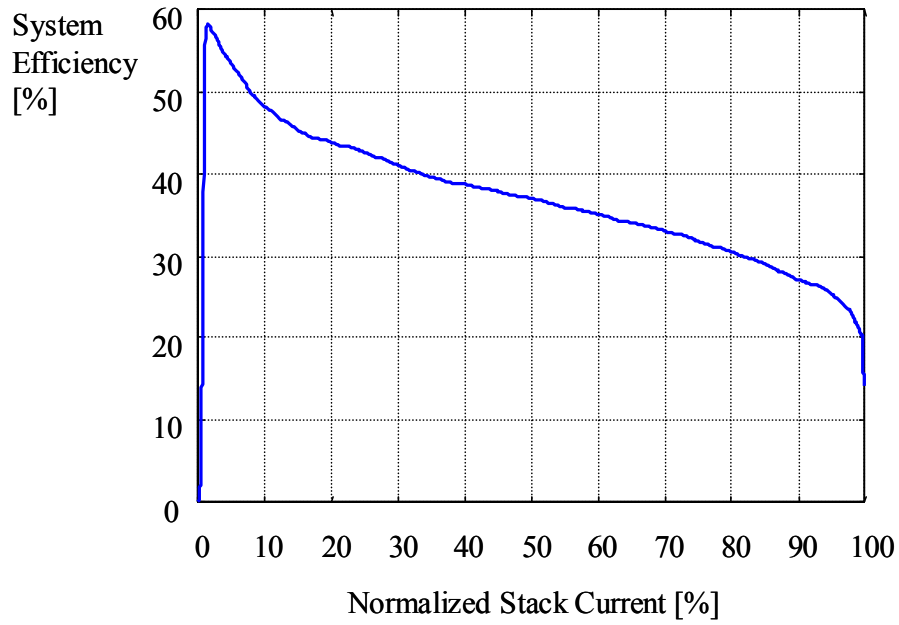

Figure 4-22: Steady state efficiency of the fuel cell system versus gross stack current (the acceleration pedal is hold constant equal to 0, the auxiliaries are supplied from a constant voltage source with V_{source}=300V).

Alternatively to Figure 4-22, the steady state efficiency could be plotted versus the gross stack power Figure 4-23).

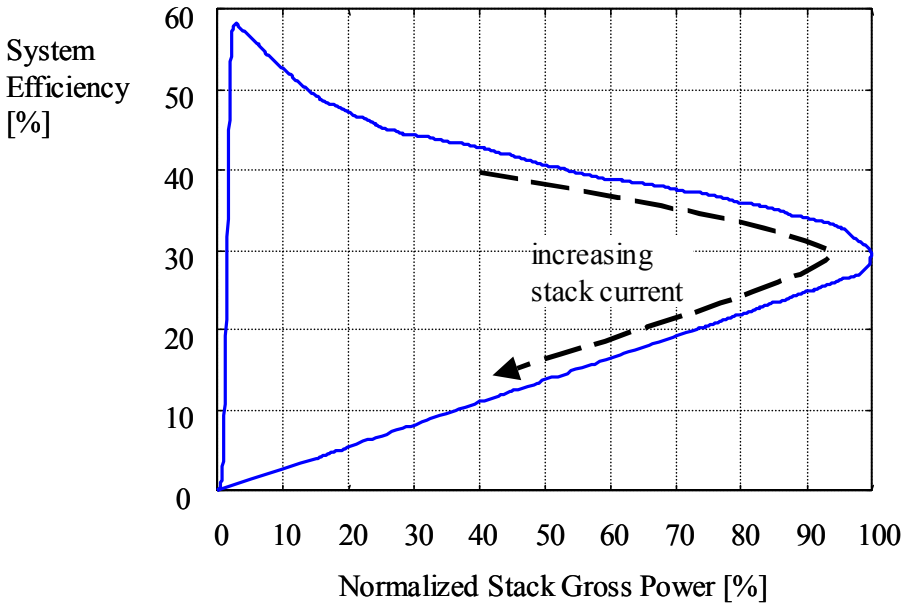

Figure 4-23: Steady state system efficiency of the fuel cell system versus gross stack power (the acceleration pedal is kept constant, equal to 0; the auxiliaries are supplied from a constant voltage source with V_{source}=300V)

The steady state efficiency plotted in Figure 4-22 and Figure 4-23 has been defined according to Equation 4-47. The equation assumes that the auxiliary power for running the compressor and pumps and fans for the water and thermal management are supplied by an outside energy storage (battery or ultra-capacitor).

$$\eta_{system} = \frac{P_{stack}}{P_{LHV\_fuel} + P_{auxiliaries}}$$

$where$:

η_{system} = steady state fuel cell system efficiency [1]

P_{stack} = gross electric stack power at the fuel cell stack terminals [W]

P_{LHV_fuel} = Input power in form of fuel (Lower heating value) [J/sec]

$P_{auxiliaries}$ = fuel cell system auxiliary power [W]

Equation 4-47

Figure 4-24 shows the model setup for the determination of the steady state system efficiency.

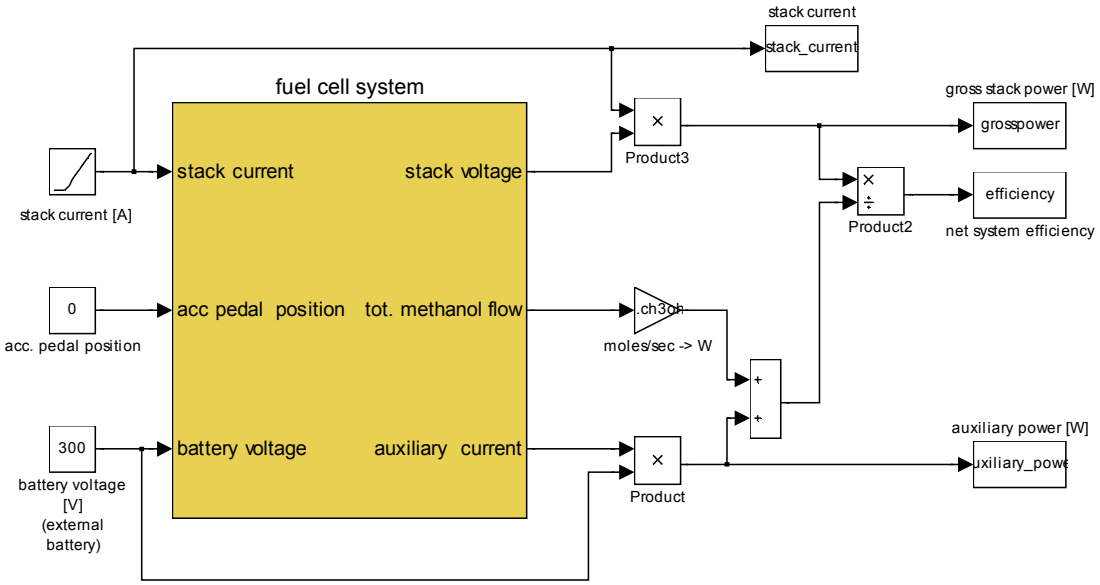

Figure 4-24: Model setup for determining the steady state fuel cell system efficiency. For ensuring steady state conditions, the stack current is increased with 1 A/ sec (about 0.2% of the maximum stack current /sec) only. The efficiency calculation is based on the lower heating value of methanol of 640.8 kJ/mole.

The dynamic properties of the system can be illustrated by applying a current step as an input while assuming a constant acceleration pedal position.[30] The system output is the stack voltage (Figure 4-25). However, because of the non-linear characteristics of the system the single system step response is not sufficient for the full characterization. For capturing the system dynamics for small and large input (current) steps, different step sizes have been chosen and the corresponding system responses have been plotted.

It is also important to notice that the above-described system characterization is only recommended for numerical experiments. For the characterization of a physical system, the input function (stack current) should be modified so that the stack voltage

[30] Note: The system integrated in the vehicle will continuously receive a varying current and varying acceleration pedal position as input signals and respond with the resulting stack voltage and auxiliary load.

never drops below a minimum stack voltage to avoid cell reversal within the stack. Electronic loads, such as the ABC 150 from Aerovironment (Aerovironment 2001), include the necessary functionality for this.

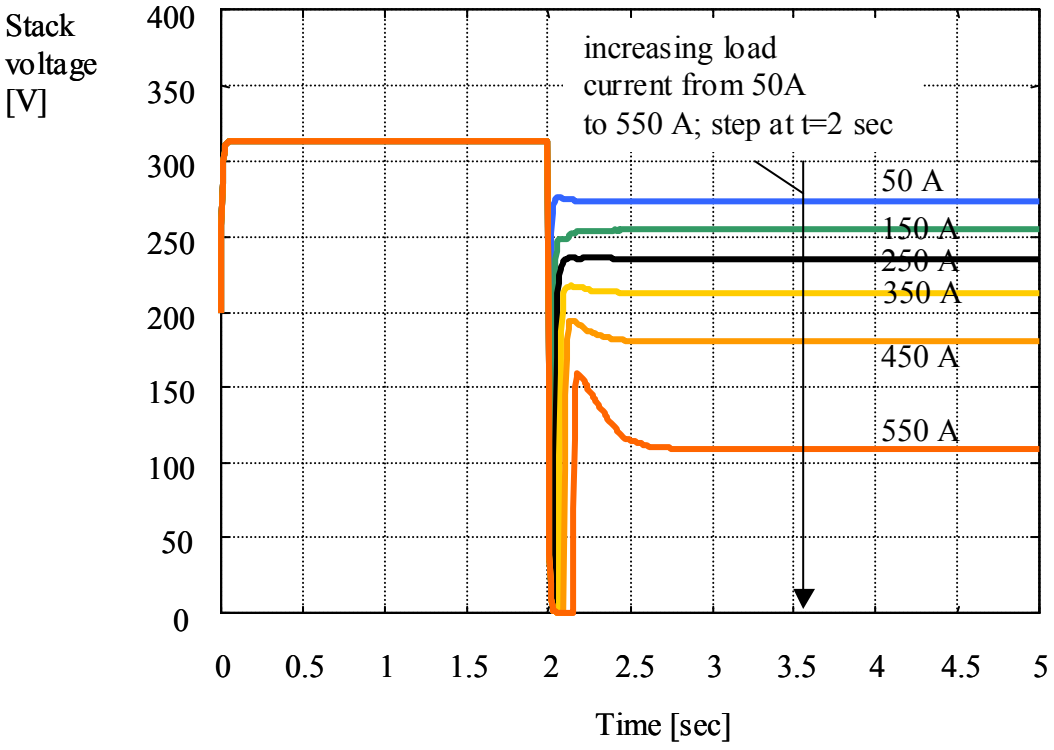

Figure 4-25: Output voltage for various input current requests (with back pressure control). [31]

[31] The voltage overshoot at high currents is due to the cathode air supply characteristics as determined by the associated optimized control scheme.

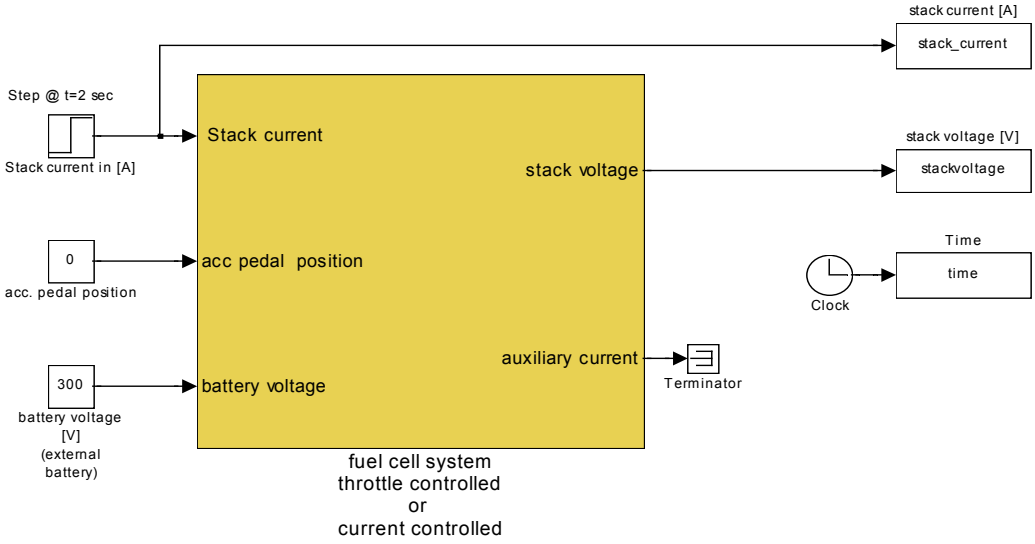

Figure 4-26: Model setup for determining the dynamic fuel cell system characteristics. The internal reformate buffer has been disabled. The current step occurs at t=2 sec.

4.3.5. Battery System

4.3.5.1. Battery Integration

The battery effectively decouples the fuel cell system from the dynamics of the electric drive train in a hybrid vehicle design. The battery model is integrated into the overall vehicle model outlined in Figure 4-27 in the block "power source". The vehicle structure is the structure of a series hybrid vehicle (Wallentowitz 1999). The fuel cell system provides power to a dc-dc converter, which decouples the fuel cell stack from the battery. It allows the fuel cell system to operate steady state even though the electric load and the battery voltage are varying. The output of the dc-dc converter is connected to the battery. The total electric load is the sum of motor power, vehicle auxiliary power, and fuel cell auxiliary power. Figure 4-27 shows the arrangement of the different components together with the energy flow.

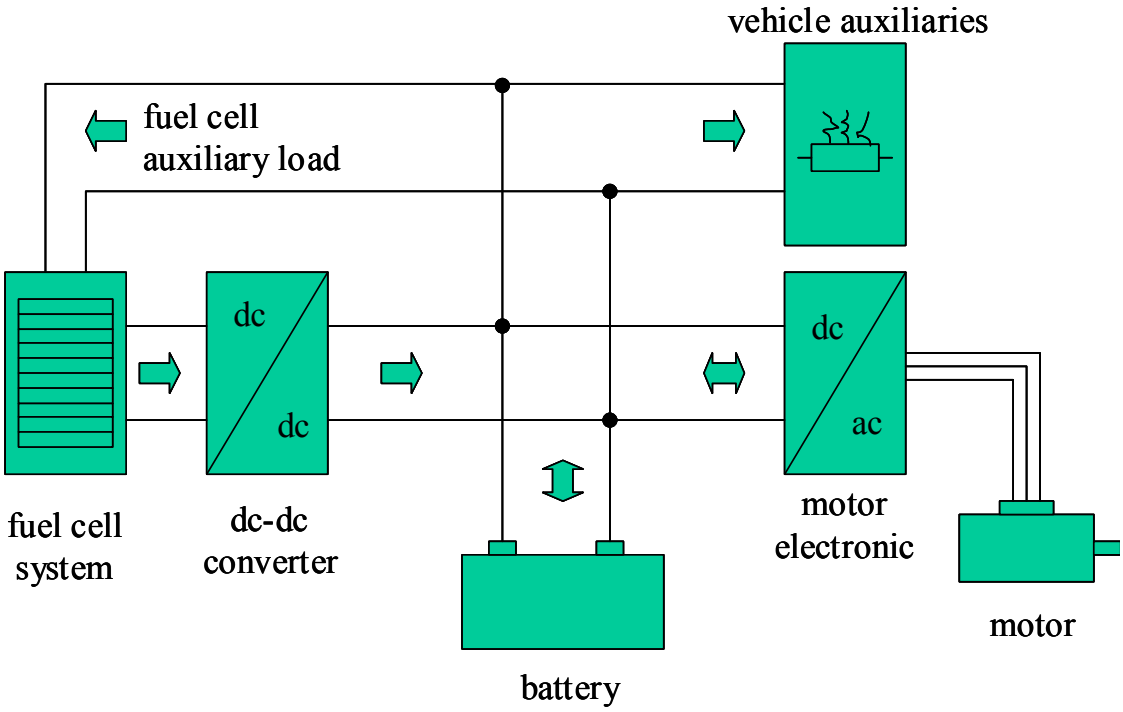

Figure 4-27: Component arrangement and energy flow for the case of a battery hybrid fuel cell vehicle (physical component arrangement)

The component arrangement in Figure 4-27 can be redrawn in a more suitable form for programming purposes (Figure 4-28). The differences are:

- a battery controller has been added;
- the law of current conservation is emphasized (Kirchhoff's law). The battery current is the difference between recharge current from the dc-dc converter and the load current;
- the component models are shown as input /output systems. The battery has the input battery current and the output battery voltage. The motor controller, the vehicle auxiliaries, and the fuel cell auxiliaries have as input the battery voltage and as output the current they draw. The fuel cell system has the input stack current and the output stack voltage. The dc-dc converter has the inputs stack voltage, stack current, and battery voltage and the output battery current. The battery controller measures the battery current and computes a current request for the fuel cell system (enforced by the dc-dc converter);
- it is assumed that the fuel cell stack always delivers the current requested by the battery management system. This assumption makes sense. In case the fuel cell system is not able to meet the requested current value, the stack voltage drops (in severe cases until it reaches zero) and the dc-dc converter output current also goes down to zero.

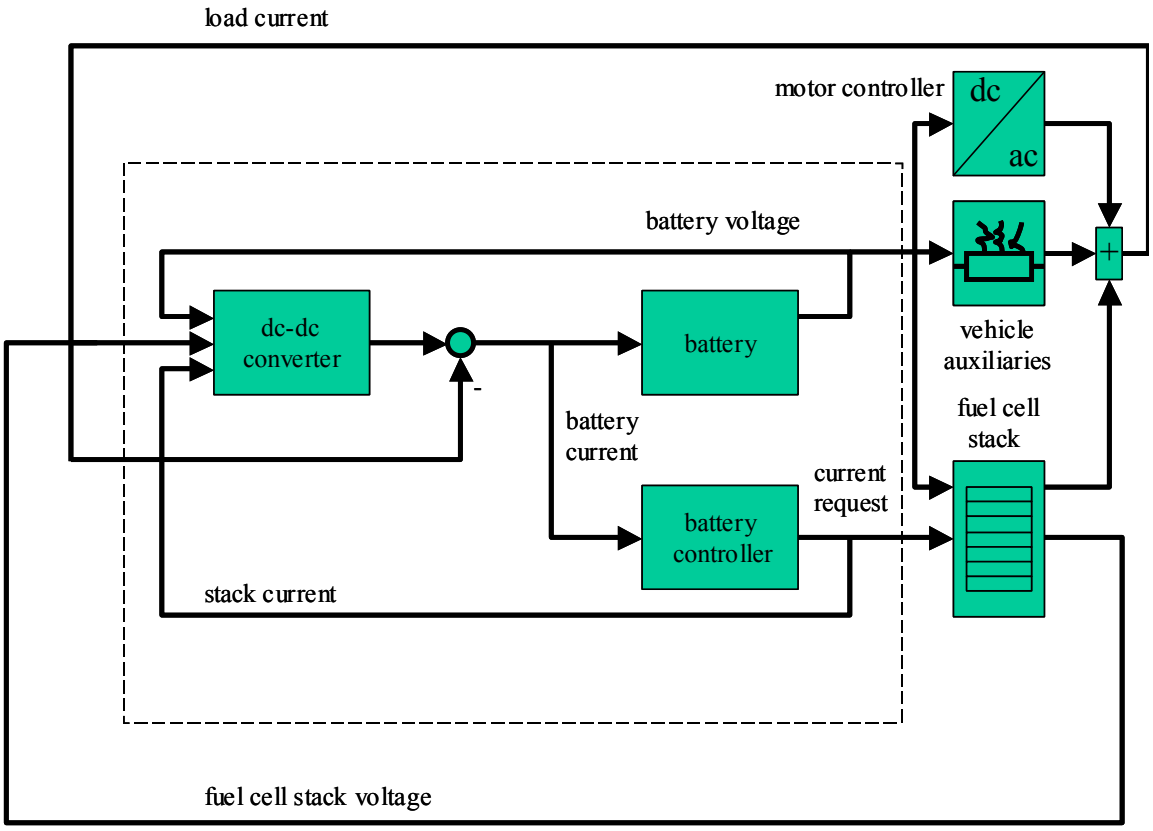

Figure 4-28: Component arrangement in form of input-output systems.

The advantage of the view in Figure 4-28 is that it establishes simple interfaces between components. The interfacing variables are based on physical values. This simplifies the validation of the model on a component level. The input-output approach allows the application of standard control theory as described by Leonhard (Leonhard 1985 and 1996) or Ogata (Ogata 1998) if dynamic component models are used. In the following section, the battery model and the battery controller model will be explained. The dc-dc converter model for the battery hybrid fuel cell vehicle model will be discussed in the chapter "Dc-Dc converter" together with the dc-dc converter necessary for the ultra-capacitor hybrid fuel cell vehicle.

4.3.5.2. Battery Model

Because the objective of the vehicle model is to determine fuel economy and dynamic characteristics of specific vehicle designs, the charging and discharging losses and open circuit voltage of the battery system are important parameters for the vehicle analysis. Since charging and discharging losses and the open circuit voltage depend on the state of charge of the battery, it is important to determine the state of charge as accurately as possible. One way to determine the state of charge is the method of current integration and correcting the effect of high currents with a Peukert relation. The calculated battery state of charge can then be used to determine the actual resistances and open circuit voltages V_{oc}. The battery current finally determines the battery terminal voltage V_{bty} relevant for the connected components, such as the electric drive train (Figure 4-29).

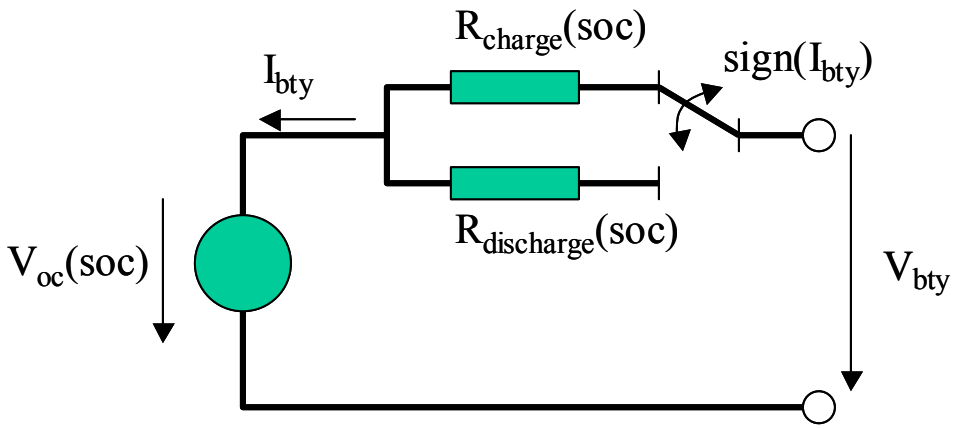

Figure 4-29: Electric diagram of the battery model.

The advantages of this modeling setup are that the basic structure of the model is technologically invariant, e.g. nickel-metal-hybrid, lead-acid and Li batteries can be incorporated into the model without the need of a change of algorithm. In addition, this setup relies only on data that could be relatively easily gained in a battery laboratory.

Similar battery algorithms have been applied for the simulation of electric vehicle batteries and batteries in hybrid vehicles employing internal combustion engines (Wiegman 2000). The results have been good if the input parameters have been chosen carefully. It should also be acknowledged that for the processing of the algorithm only few computational resources are required.

Not incorporated into the battery model are dynamic battery effects related to diffusion and double layer capacities at the surface of the electrodes. However, compared to the vehicle dynamics, these dynamic effects are fast, with time constants in the order of msec (Huet 1998). It is therefore not expected that they have a significant impact on the overall vehicle characteristics.

The Peukert correction used in the model is defined for discharge with constant current. However, in a fuel cell hybrid vehicle the discharging current is fluctuating over a wide range and sometimes is even negative (when recharging the battery). To account for this, the mean of the battery current is fed into the Peukert relation for the determination of the state of charge. Although the algorithm is technically not a pure Peukert correction anymore, it is still assumed that the effect on the battery state of charge is the same for discharge with constant current and discharge with an average current with the same mean. Finally, no temperature influences are considered in this model.

All battery parameters, including the Peukert constant and Peukert exponent, are stored in a separate file for battery parameters.

The Equations 4-48 to 4-50 describe the overall calculation of the battery state of charge.

$$\bar{I}(t) = \frac{1}{t} \cdot \int_0^t \left| I(t) \right| \cdot dt$$

$I(t) = \text{normalized current}[\text{A}]$

$\bar{I}(t) = \text{average normalized current}[\text{A}]$

$t = \text{time}[\text{sec}]$

Equation 4-48

The nominal capacity of the battery is calculated based on the Peukert relation and depends on the average charge and discharge current. The parameters K_1 and K_2 have to be gained in laboratory tests.

$$C_{actual} = K_1 \cdot | \frac{\bar{I}(t)}{I_{nom1}} |^{K_2}$$

where:

$K_1 = \text{Peukert constant (1 hour discharge capacity)}[\text{Ah}]$

$K_2 = \text{Peukert Exponent}[1]$

$I_{nom1} = \text{nominal 1 hour battery discharge current}[\text{A}]$

$C_{actual} = \text{actual battery capacity}[\text{Ah}]$

Equation 4-49

The state of charge of the battery is calculated according to Equation 4-50. The actual state of charge of the battery is referenced to the actual battery capacity calculated based on average battery current up to this point in time.

$$SOC = \frac{\int_0^t I(t)dt}{C_{actual}} + SOC_{initial}$$

where:

$\text{SOC} = \text{state of charge}$

$\text{SOC}_{\text{initial}} = \text{initial state of charge}[\text{Ah}]$

Equation 4-50

Depending on the state of charge the discharge resistance, charge resistance and open circuit voltage can be calculated (Equation 4-51).

$$\begin{aligned} R_{charge} &= R_{charge}(soc) \qquad \text{for } I_{bty} \geq 0 \\ R_{dischage} &= R_{dischage}(soc) \quad \text{for } I_{bty} < 0 \\ V_{oc} &= V_{oc}(soc) \end{aligned}$$

Equation 4-51

Finally Equation 4-52 determines the terminal voltage depending on the battery current.

$$\begin{aligned} V_{bty} &= V_{oc} + R_{charge} \cdot I_{bty} \qquad \text{for } I_{bty} \geq 0 \\ V_{bty} &= V_{oc} + R_{dischage} \cdot I_{bty} \qquad \text{for } I_{bty} < 0 \end{aligned}$$

Equation 4-52

4.3.5.3. Battery Controller

In most hybrid electric vehicles and pure electric vehicles, the battery is monitored and controlled by a battery controller or battery management system. The battery controller has the following functionality (Table 4-3).

Function	Realized in the model	Not realized yet
Temperature Management		√
Monitoring state of charge (SOC)	√	
Avoid overcharging during regenerative braking	√	
Avoid over-discharging	√	
Avoid overload	√	
Controlling the charging process through the on-board fuel cell system (Range extender design)	√	
Controlling the charging process through the on-board fuel cell system (Power assist design)	√	
Controlling the battery charging process with an on board charger		√
Controlling the battery charging process with an off-board rapid charging system		√

Table 4-3: Functionality of the battery management system (overview)

The functionality for the temperature management is not realized yet because the current battery model does not take temperature effects into account. The functions for battery charging with an on-board charger or an off-board rapid charging system are not realized yet because all hybrid designs discussed in this work are charge-sustaining designs.

Realized functions are:

- The battery controller monitors the state of charge of the battery system and activates and deactivates the fuel cell system depending on this. Superposed to this mode of activation is the activation of the fuel cell system if the average

power, drawn by the electric drive train plus auxiliaries, exceeds a lower power threshold or if the acceleration pedal position exceeds an upper threshold.

- The battery controller generates a signal that deactivates the ability of regenerative braking for situations in which continuing regenerative braking could lead to overcharging of the battery. This signal is received and interpreted by the motor controller.
- The battery controller limits the motor power if the state of charge is below a lower threshold.
- The battery controller limits the motor power if the maximum battery power is exceeded.
- the battery controller sets the current request to the fuel cell system to zero if the system is not ready to supply energy, e.g. during the warm-up phase.

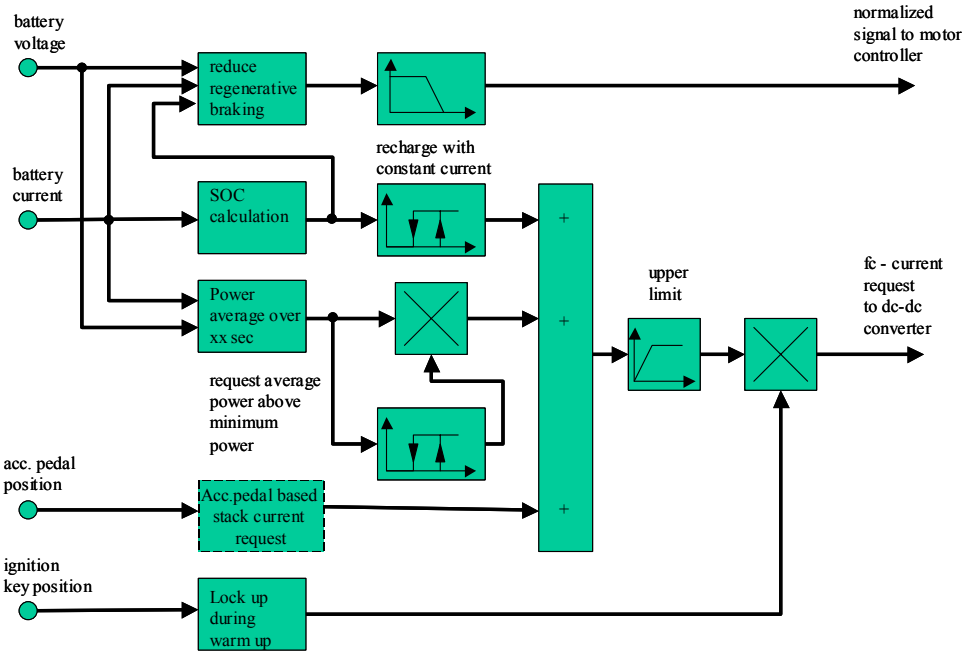

Figure 4-30: Basic structure of the battery controller (the stack current request based on the accelerator pedal position is not realized yet).

Figure 4-30 shows the battery controller functions in graphical form. It is possible to expand this initial set of functions, if required, for specific vehicle designs.

The battery controller supports two operating strategies different in principle. These are the “range extender” operating strategy and the “power assist” operating strategy.

The range extender operating strategy is named after the so-called range extender battery electric vehicle type. In this vehicle type, a small (in terms of maximum power provided) Auxiliary Power Unit (APU) recharges the battery pack of a battery electric vehicle. Through this recharged energy, the range of the battery electric vehicle is extended. However, the maximum power available for the drive train stays nearly unchanged due to the low power ratio of range extender power and battery power. The APU operates in an on/off mode and is solely controlled by the state of charge of the battery.[32] Because of the limitation to an on/off operation, the APU does not have to meet any dynamic requirements.

The power assist operating strategy relies on the superposition of battery power and fuel cell system power. In this strategy, the battery assists the fuel cell system with the power provision for the electric drive train. Steady state, the maximum motor power, is the sum of the maximum fuel cell power plus the maximum battery power.

Dynamically, the power assist strategy relies on the capability of the fuel cell system to follow fully or almost fully the transient requirements of the drive train. During low power drive train operation, the battery could compensate the transient shortfalls of the fuel cell system providing the power difference between the drive train and fuel cell system. However, at high power operation the transient shortfalls of the fuel cell system

result directly in a voltage drop at the terminals of the motor electronic and finally in reduced vehicle performance. Therefore, for the power assist design the fuel cell system needs to be as transient as possible. Besides the necessity of a dynamic fuel cell system, the key for a successful power assist fuel cell design is to minimize the charging and discharging losses of the battery while operating the fuel cell system (in average) at an optimal operating point. Both requirements have to be pursued at the same time. Minimizing only the charging and discharging losses in the battery by minimizing the current flow in the battery terminals underutilizes the battery. In the extreme case, the battery could be taken out if no current is flowing in the battery terminals (equivalent to zero battery losses). This extreme would be the case of a load-following vehicle with the additional feature of regenerative braking (impossible in praxis). On the other hand results the operation of the fuel cell system at the point of highest efficiency only in an (inferior) range extender design with significant battery losses.

Summarizing it could be said that a power assist design is a compromise between a range extender design and a load following vehicle design. It tries to incorporate most of the positive features of both vehicle types (Table 4-4).

Property	Range Extender Fuel Cell Vehicle	Load Following Fuel Cell Vehicle	Power Assist Fuel Cell Vehicle
Fuel cell system dynamic requirements	Low	High	Medium
Battery losses	High	-	Medium
Operation of Fuel cell system in the regime of high efficiency	Yes	No	In some degree

Table 4-4: Comparison of different fuel cell vehicle concepts.

[32] The literature is not clear about the definitions of range extender vehicles. Different sources may define range extender vehicles differently.

The final operating strategy for the fuel cell system depends on the fuel cell system characteristics (maximum power and dynamics), the battery characteristic (maximum power), the drive train characteristics (maximum power) and the drive cycle the vehicle is operated at. Because of the dependence on the drive cycle a general optimization is not possible. Any operating strategy is only optimal for one drive cycle and a trade off for all other drive cycles.

The battery controller allows the adjustment of the operating strategy over the full range from the pure range-extender design to the “load-following” vehicle design with the additional regenerative braking feature. However, as already said, the most promising control strategy is a blend between the two extremes.

4.3.6. Ultra-Capacitor System

As an alternative to the integration of a battery, an ultra-capacitor system can be used for the hybridization of the vehicle. The motivation for doing this is the same as for the step from the load-leveled vehicle to the battery hybrid fuel cell vehicle. These are:

- Support of regenerative braking,
- Decoupling of the fuel cell system and the drive train (release of the fuel cell system from dynamic requirements),
- Superposition of fuel cell power and ultra-capacitor power (power boost),
- Provision of energy for the fuel cell system start-up (compressor, pump).

However, the ultra-capacitor system does not add the feature of rapid drive-away to the vehicle because the energy density of ultra-capacitors is significantly smaller than the energy density of batteries.

The section about the ultra-capacitor model is organized in three subsections.

The first subsection discusses two possible methods to integrate an ultra-capacitor system into a fuel cell vehicle, one with dc-dc converter and one in which the dc-dc converter is directly coupled to the fuel cell stack terminals.

The second subsection describes the development of an ultra-capacitor model for one single capacitor.

Finally, the last subsection discusses the build-up of a larger system from individual small capacitors.

4.3.6.1. Ultra-Capacitor System Integration

In principle an ultra-capacitor system could be integrated in two different ways into the overall system.

The first method is the integration of the ultra-capacitor system via a dc-dc converter. Among others, Burke (Burke 1995) proposed the basic principle of this method of integration. Figure 4-31 shows the electrical circuit diagram of the main components for this type of design.

The second method of integrating an ultra-capacitor system into a fuel cell vehicle is the connection of the ultra-capacitor to the stack terminals via a diode. This design has been proposed by Honda (Honda, 2000) and is realized in Honda's demonstration vehicle for the California Fuel Cell Partnership. Although the vehicle for the California Fuel Cell Partnership is a direct hydrogen fuel cell vehicle, the principle idea is not limited to this vehicle type and could also be applied to fuel cell vehicles employing an on-board reformer. The principle component configuration of this second design is shown in Figure 4-32.

The direct connection of fuel cell stack and dc-dc converter is attractive because it does not require a high power dc-dc converter, resulting in significant reduction of complexity, cost, weight, and volume. At the same time, the efficiency of the overall system increases because the losses in the diode are significantly smaller than the losses in a dc-dc converter. On the other hand, some of the advantages are partly compensated because of the need to design the ultra-capacitor system for the voltage level defined by the fuel cell stack and the electric motor.

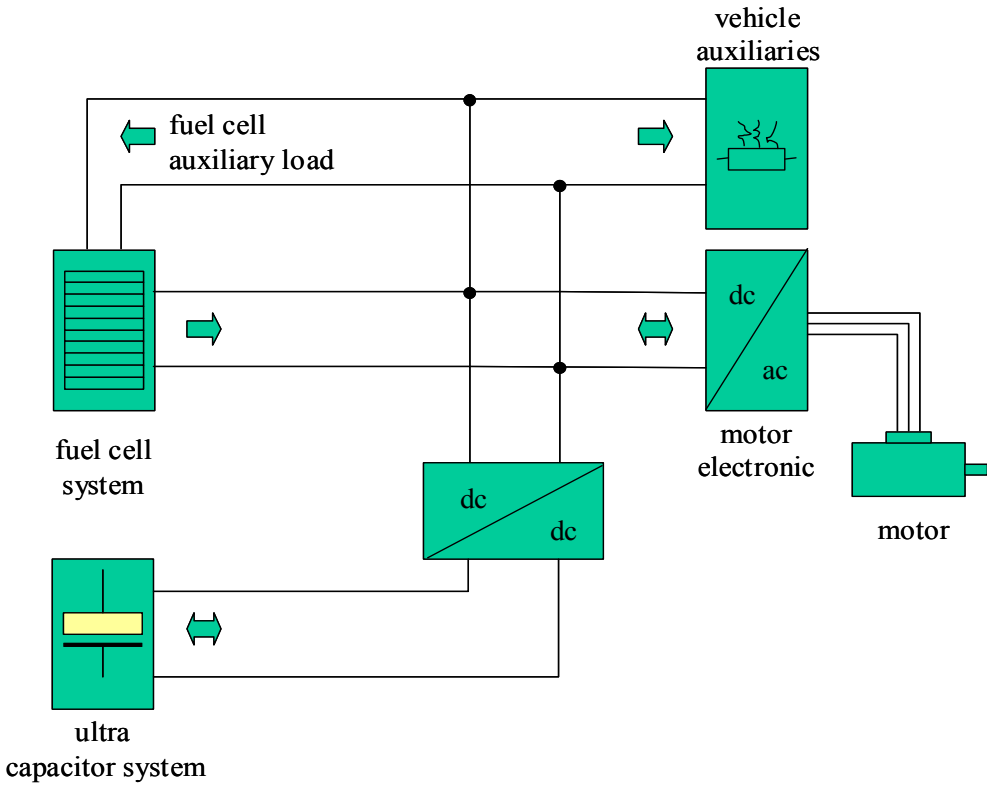

Figure 4-31: Component arrangement and energy flow for the case of an ultra-capacitor hybrid fuel cell vehicle (physical component arrangement).

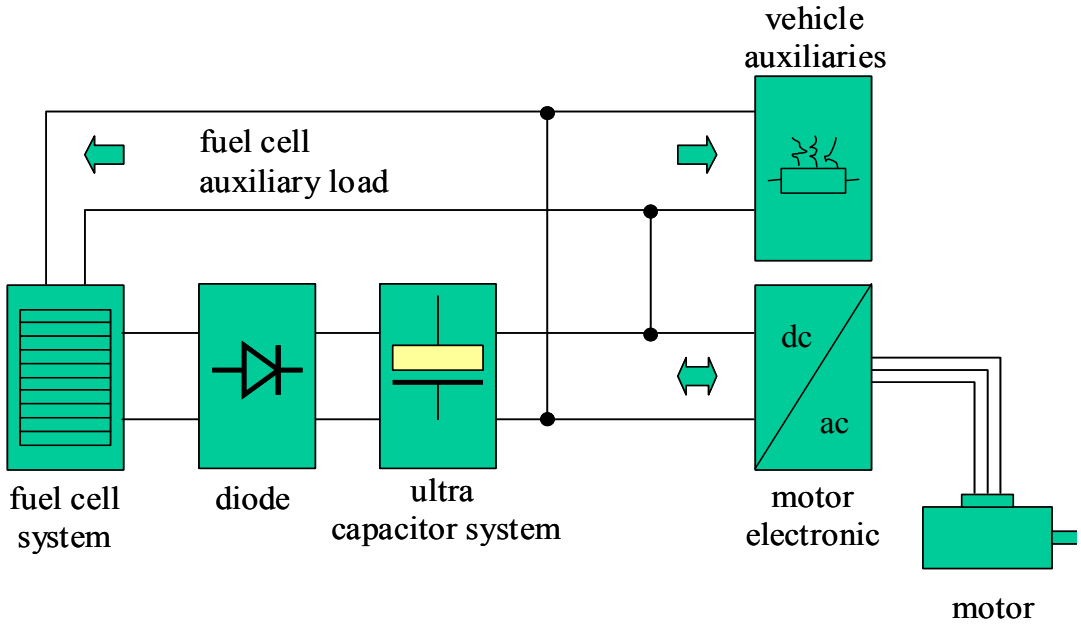

Figure 4-32: Fuel cell vehicle with directly connected ultra-capacitor system as suggested by Honda.

Similar to the battery hybrid case, it is beneficial for the modeling of the ultra-capacitor vehicles to redraw the diagrams 3-31 and 3-32, transforming them into an arrangement of input /output systems. The following two sections discuss this transformation for the designs with and without integrated dc-dc converter.

System with Integrated DC-DC Converter

Figure 4-33 shows the transformation of Figure 4-31. The differences between both figures are:

- A controller (dc-dc controller) has been added.[33] The task of the controller is to decide how much power will be supplied by the fuel cell system and how much power will be supplied by the ultra-capacitor.
- Kirchoff's law has been emphasized. The current supplied by the fuel cell system plus the current supplied by the ultra-capacitor system equals the total load current.
- All components are shown as input/output systems. The ultra-capacitor has as input the total system current and as output the total system voltage. The dc-dc converter takes as inputs the ultra-capacitor voltage, the bus voltage (equal to fuel cell stack voltage), and the current the dc-dc converter draws from or supplies to the bus. The controller takes as input the total load current and computes the request for the current the dc-dc converter draws from the bus. The electric load, consisting of drive train, vehicle auxiliaries and fuel cell system auxiliaries, takes as input value the bus voltage and provides the load current as output value.

[33] The controller is labeled dc-dc controller. However, it could also be labeled ultra capacitor controller because it also oversees the state of the ultra capacitor system. In this respect, the controller is the equivalent of the battery controller for the battery hybrid fuel cell vehicle.

Note: The assumption for this approach is that the dc-dc controller requests only the dc-dc converter current the ultra-capacitor system is able to deliver. Therefore the controller has to consider the state of charge of the ultra-capacitor system. If the ultra-capacitor is discharged below its minimum voltage, the dc-dc converter would not supply the requested current. As a result, the fuel cell stack alone would have to provide the full load current. The stack voltage (equal to the bus voltage) would drop and the motor would provide less torque. For controlling this situation, the dc-dc controller has a (communication) link to the motor controller limiting the motor power if the ultra-capacitor system is discharged. A very similar situation occurs during regenerative braking if the ultra-capacitor system is already fully charged. In this situation, the dc-dc controller sends a signal to the vehicle controller (and based on this the vehicle controller would send a signal to the motor controller) limiting the amount of regenerative braking. For simplicity, these additional control loops are not shown in Figure 4-18. However, they are incorporated into the model and are important to guarantee stable behavior under all conditions.

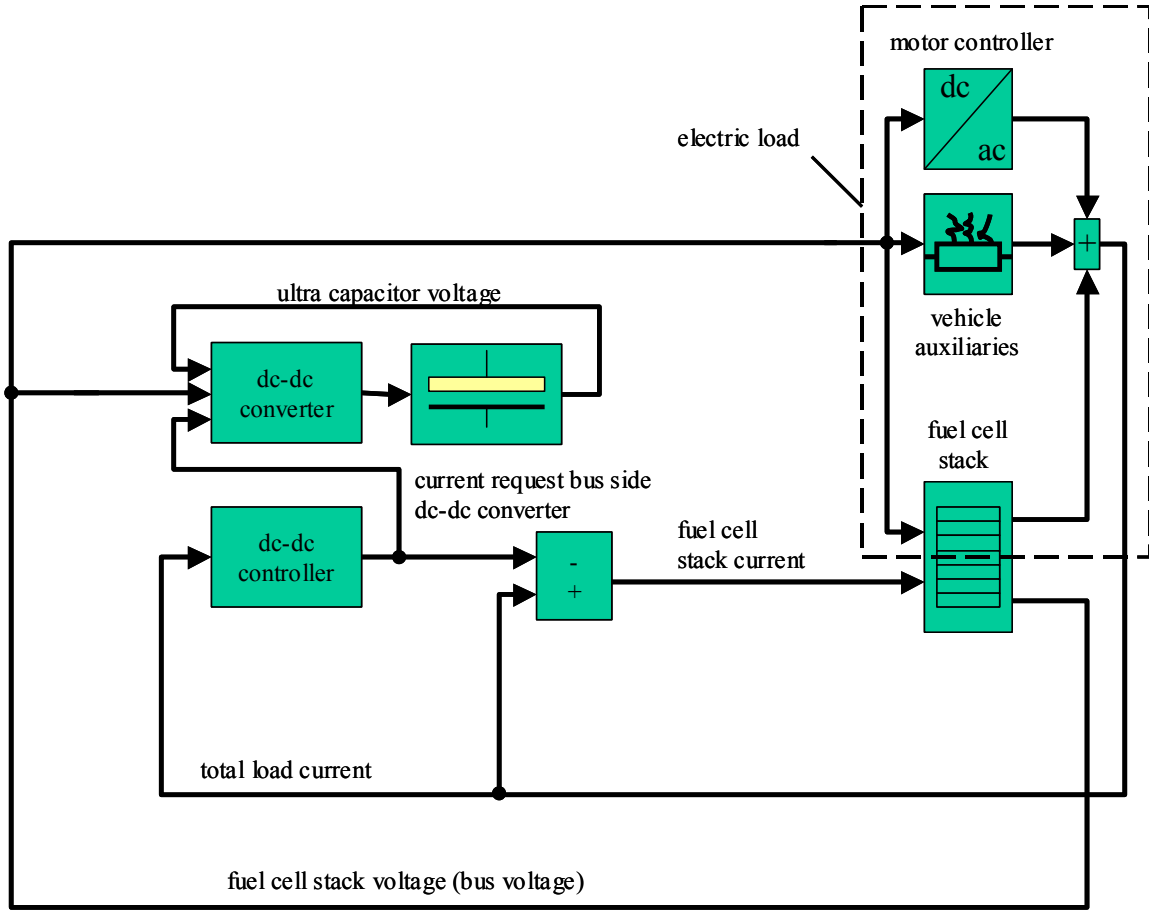

Figure 4-33: Component arrangement in form of input/output systems.

Direct coupling between fuel cell stack and ultra-capacitor system

Figure 4-34 shows the transformation of Figure 4-32 in a more suitable form for programming purposes, an input/output system. The transformation process is similar to the transformation for the case of the vehicle with dc-dc converter.

The fuel cell stack and the ultra-capacitor are connected with each other via a diode. This diode avoids the flow of a reverse current from the ultra-capacitor into the fuel cell stack. Without such a diode this could occur if the fuel cell system were switched off or if, in phases of regenerative braking, the ultra-capacitor voltage were higher than the fuel cell stack voltage.

The current from the fuel cell stack into the ultra-capacitor system is not directly controlled and depends solely on the voltage difference between the fuel cell stack terminals and the ultra-capacitor terminals divided by the total resistance between both systems. However, due to the limitations of the stack current (due to the finite supply of hydrogen), the stack current will not exceed its limits as long as the ultra-capacitor voltage is above the minimum stack voltage. In this respect the situation is very different to the (hypothetical) situation of a battery and an ultra-capacitor directly connected with each other. If the (initial) battery voltage is only slightly different from the ultra-capacitor voltage, a very high balancing current would be the result, which could easily go up to several thousand ampere and induce high stress on the coupling diode, the battery, and the ultra-capacitor system. For the combination of a fuel cell system and an ultra-capacitor system, no component damaging currents are expected as long as the ultra-capacitor voltage is above the minimum fuel cell stack voltage.

Therefore it is necessary to avoid the discharge of the ultra-capacitor below the minimum stack voltage to prevent stack damage due to the reversal of individual cells in the stack. On the other hand, the ultra-capacitor voltage should be kept low enough to allow the ultra-capacitor to store the energy regained during phases of regenerative braking.

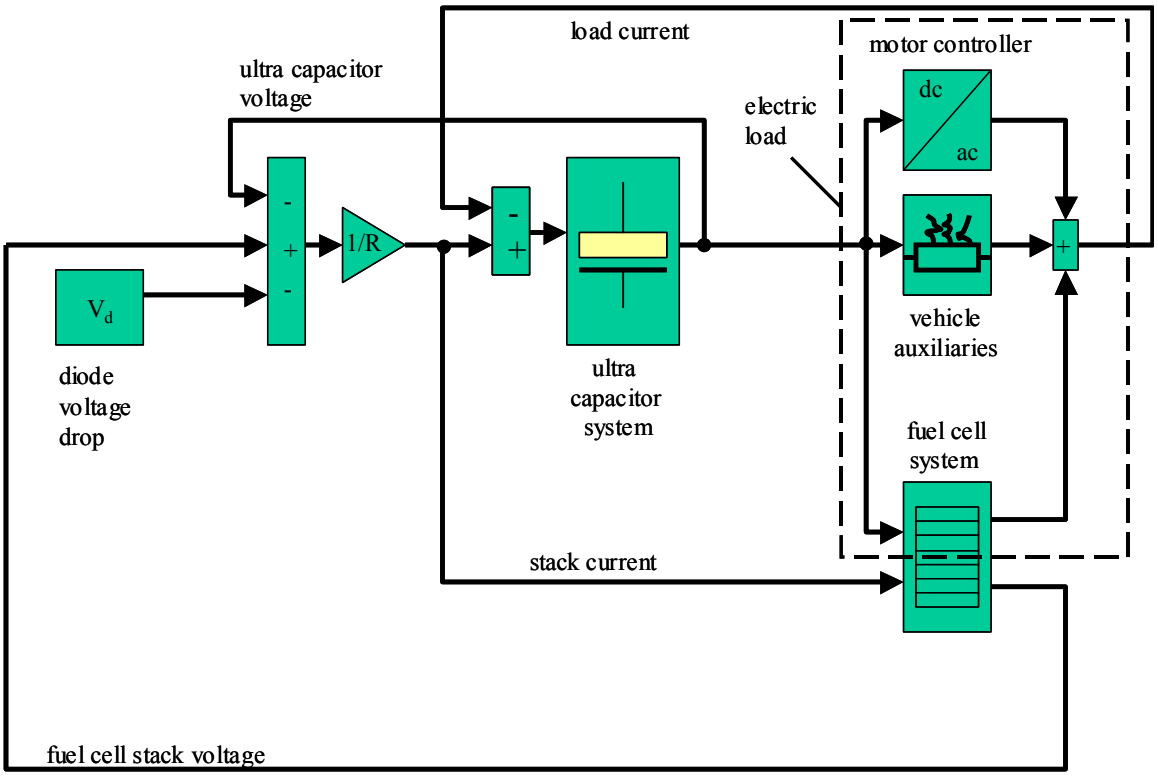

Figure 4-34: Fuel cell vehicle with directly to the stack coupled ultra-capacitor system.

4.3.6.2. Ultra-Capacitor Model

In this section, the mathematical description of the ultra-capacitor used in the simulation program will be developed. Figure 4-35 shows the circuit diagram of the physical model. The model consists of three elements. The (ideal) capacity C represents the capacity of the (loss free) ultra-capacitor. R_1 represents the charging and discharging resistance of the ultra-capacitor and accounts for the associated losses. R_2 represents the self-discharging losses.[34]

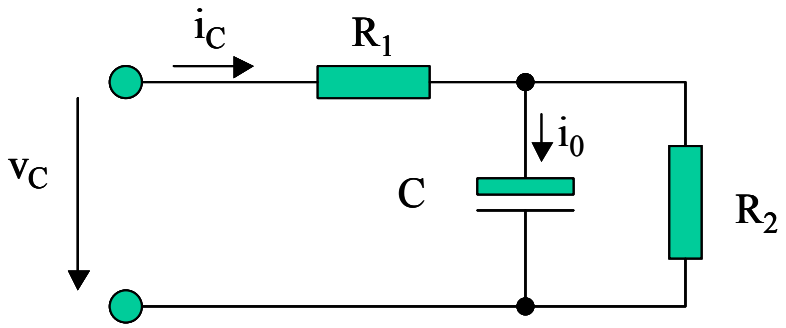

Figure 4-35: Physical model of the ultra-capacitor system.

Equations 4-53 and 4-54 describe the model in Figure 4-35 in equation form.

$$i_c = i_0 + \frac{1}{R_2 C} \cdot \int_0^t i_0 \cdot dt$$

where:

i_c = current into the ultra capacitor system [A] **Equation 4-53**

i_0 = net current stored in the ultra capacitor system [A]

R_2 = discharge resistance [Ω]

C = capacity [F]

[34] The self-discharge rate of an ultra capacitor is an important parameter influencing the balance of a system of several ultra capacitors. High self-discharge rates lead to more difficulties in keeping the system balanced than low self-discharge rates. However, because R_2 is significantly larger than R1 (Maxwell 2000), self-discharge does not play any role for energy and efficiency calculations. Because of this, R_2 is set to infinite for most of the discussion and the simulation runs.

$$v_c = R_1 \cdot i_c + \frac{1}{C} \cdot \int_0^t i_0 \cdot dt$$

where: **Equation 4-54**

$R_1 = \text{charge resistance}[\Omega]$

For the coding in Simulink and the integration, it is beneficial to transform the model into a form in which the terminal voltage v_c is a function of the input current i_c. For this, first the current into the capaciter C has to be calculated (Equation 4-53), and second the voltage v_c at the terminals has to be calculated based on this current (Equation 3-54). Figure 4-36 shows the complete algorithm as coded in Simulink. The figure shows the ultra-capacitor model as an input / output system with the input parameter current (i_c) and the output parameter terminal voltage (v_c).

For the case that the influence of the discharge resistance can be neglected (R_2=infinite), the charge and discharge efficiencies of the system can be calculated according to Equation 4-55 (charge) and 4-56 (discharge).

$$\eta_{charge} = 1 - \frac{i_c \cdot R_1}{v_c}$$

where: **Equation 4-55**

$\eta_{charge} = \text{charging efficiency of the ultra capacitor system}[1]$

$$\eta_{discharge} = \frac{v_c}{v_c - i_c \cdot R_1}$$

where: **Equation 4-56**

$\eta_{discharge} = \text{discharge efficiency of the ultra capacitor system}\ [1]$

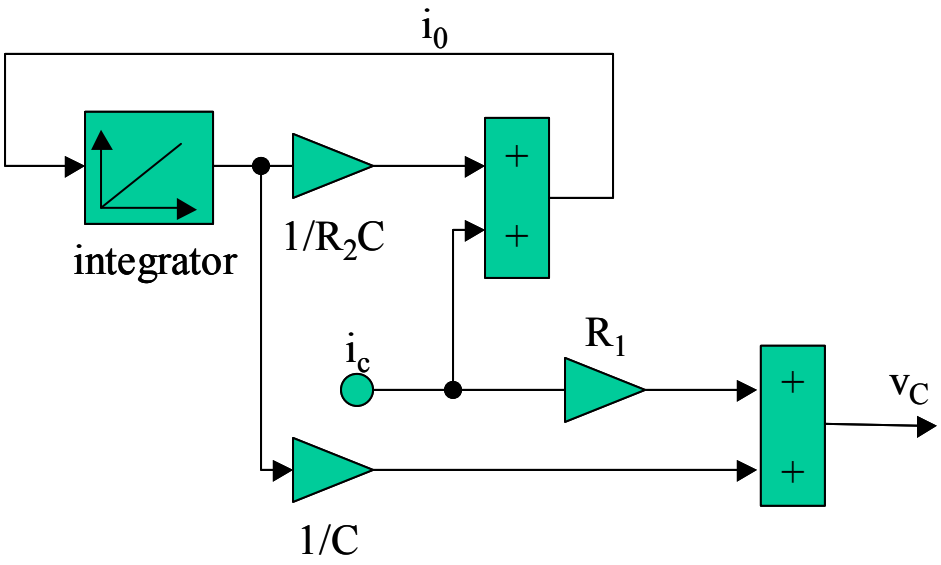

Figure 4-36: Model of the ultra-capacitor system

4.3.6.3. System Design With Individual Capacitors

In practical applications, an ultra-capacitor storage system for a hybrid vehicle would not consist of one individual large capacitor as assumed in the model derived above. Instead a real system would be build through the arrangement of many smaller devices in parallel and series to achieve the necessary properties (terminal voltage, capacity). Figure 4-37 illustrates how a number of (smaller) ultra-capacitors could be arranged to build systems that are able to meet the requirements of a fuel cell vehicle.

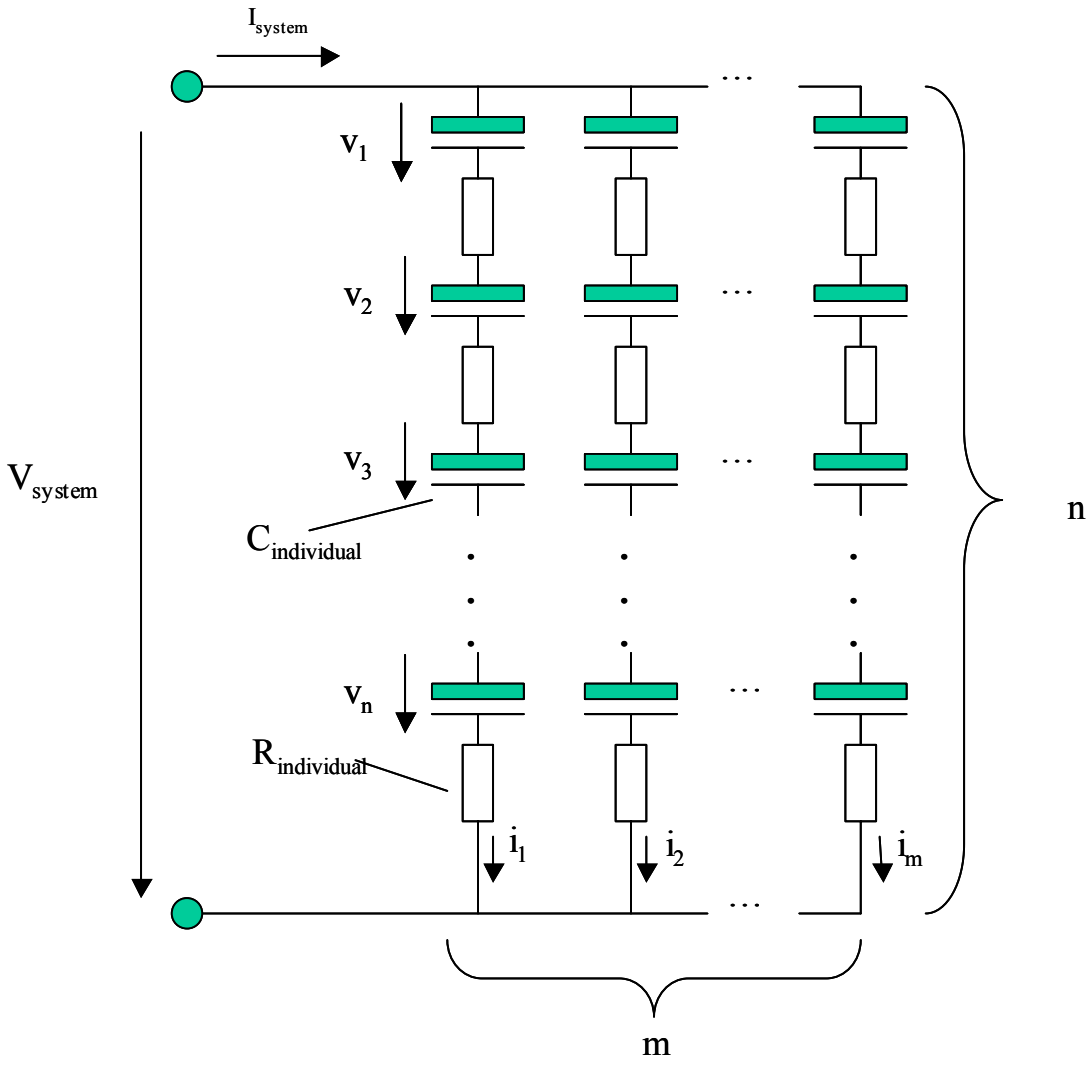

Figure 4-37: Ultra-capacitor system build from a number of smaller capacitors.

The total system capacity of the system in Figure 4-37 is calculated according to Equation 4-57. It is assumed that all individual capacitors have the same capacity.

$$C_{system} = C = \frac{m}{n} \cdot C_{individual}$$

where:

C_{system} = system capacity [F]

m = number of parallel branches [1]

n = number of capacitors in series [1]

$C_{individual}$ = capacity of each individual capacitor [F]

Equation 4-57

The total system resistance is calculated according to Equation 4-58. The assumption is that the internal resistance for all capacitors is the same.

$$R_{system} = R_1 = \frac{n}{m} \cdot R_{individual}$$

where:

R_{system} = system resistance [Ω]

$R_{individual}$ = resistance of each individual capacitor [Ω]

Equation 4-58

The terminal voltage and terminal current for the system are stated in Equation 4-59 and 4-60. They could directly replace the corresponding values in the model for the single ultra-capacitor. With the assumption of symmetry across parallel branches the total system voltage is shown in Equation 4-59.

$$V_{system} = \sum_{j=1}^{n} v_j$$

where:

V_{system} = system voltage [V]

v_j = individual capacitor voltage [V]

Equation 4-59

The total system current into or out of the system is shown in Equation 4-60.

$$I_{system} = \sum_{j=1}^{m} i_j$$

$where:$ **Equation 4-60**

I_{system} = total current into the ultra capacitor system [A]

i_j = current into one individual capacitor [A]

The system properties are represented by the elements C_{system} and $R_{system.}$ They could be directly plugged into the model derived in the previous chapter.[35]

[35] The self-discharge resistance has not been considered.

4.3.7. DC-DC Converter

For the two different vehicle designs shown in Figure 4-27 (battery hybrid fuel cell vehicle) and Figure 4-31 (ultra-capacitor hybrid fuel cell vehicle), different dc-dc converters are required.

For the battery hybrid fuel cell vehicle case as suggested by Burke and Hauer (Burke 1995, Hauer 2001), a one-directional dc-dc converter is required (the energy flow is always from the fuel cell stack into the battery). In this design, the stack voltage could be either higher than the battery voltage or lower than the battery voltage. Therefore, depending on vehicle parameters and the vehicle state, the dc-dc converter has to be able to function as both an upwards and downwards converter.

For the ultra-capacitor hybrid fuel cell vehicle case, a two-directional dc-dc converter is necessary. The energy flow is from the fuel cell stack (or the electric motor during phases of regenerative braking) into the ultra-capacitor during recharging. In phases of acceleration, the ultra-capacitor is discharged and the energy flow is from the ultra-capacitor system towards the electric motor. Independent from the direction of the energy flow, the voltage at the ultra-capacitor side could be higher or lower than the voltage on the motor side. Therefore, the dc-dc converter has to function for both directions of energy flow as an upward or downward converter.

The following section explains the hardware design and the modeling for both types of dc-dc converters. After this, the control strategy for each design will be discussed.

4.3.7.1. DC-DC Converter for a Battery Hybrid Fuel Cell Vehicle

The principle circuit diagram of a one directional dc-dc converter is shown Figure 4-38.

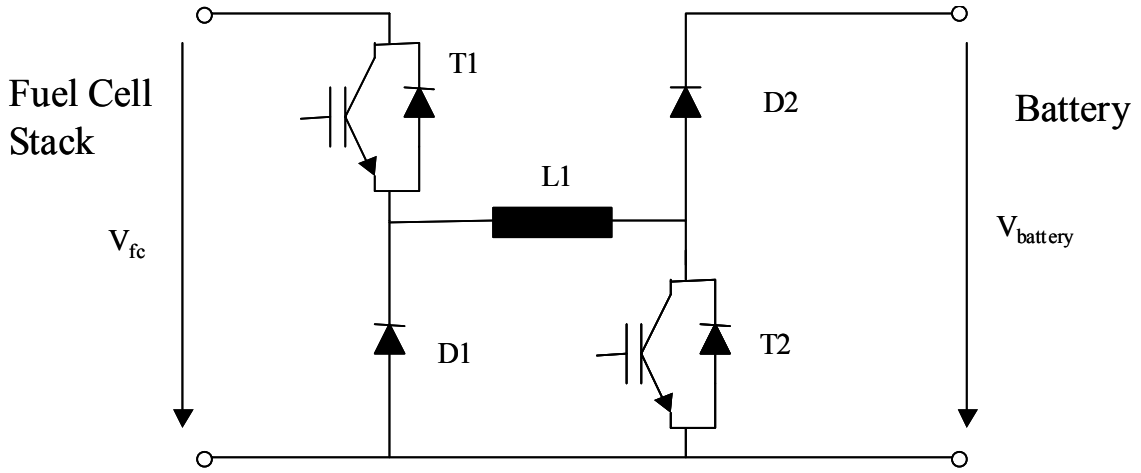

Figure 4-38: Dc-dc converter for the battery hybrid fuel cell vehicle.

The energy flow is always from the fuel cell stack side to the battery side.

For the case that the fuel cell stack voltage is higher than the battery voltage, transistor T2 stays switched off while transistor T1 is pulsing and controlling the current flow from the fuel cell stack via T1, L1, D2, the battery, and back to the fuel cell stack. The current through the battery charges the battery.

For the case that the fuel cell stack voltage is lower then the battery voltage the inductor L1 has to be first charged from the fuel cell stack and than discharged, charging the battery. For charging the inductor, the current flow is from the fuel cell stack via transistor T1, inductor L1, transistor T2 and back to the fuel cell stack. The discharging process begins when the inductor current reaches its upper limit. The transistor T2 is switched off and the current through the inductor L1 commutes to the diode D2 and recharges the battery until it is declined below the minimum current. If this is the case, the next cycle begins. The transistor T2 is switched on and the inductor is recharged again.

4.3.7.2. Modeling of the DC-DC Converter for a Battery Hybrid Fuel Cell Vehicle

The dc-dc converter is modeled with a two-dimensional efficiency map[36] (Figure 4-39). Because of the almost immediate response of the dc-dc converter, transient effects are not taken into account. Consequently, the model does not consider the effects of current ripple on the fuel cell stack. In an actual design, a capacitor between the fuel cell stack and the dc-dc converter would reduce the current ripple in the stack imposed by the dc-dc converter. In this case, the stack current ripple is comparable to the stack current ripple in a load following vehicle design caused by the switching of the motor electronics.

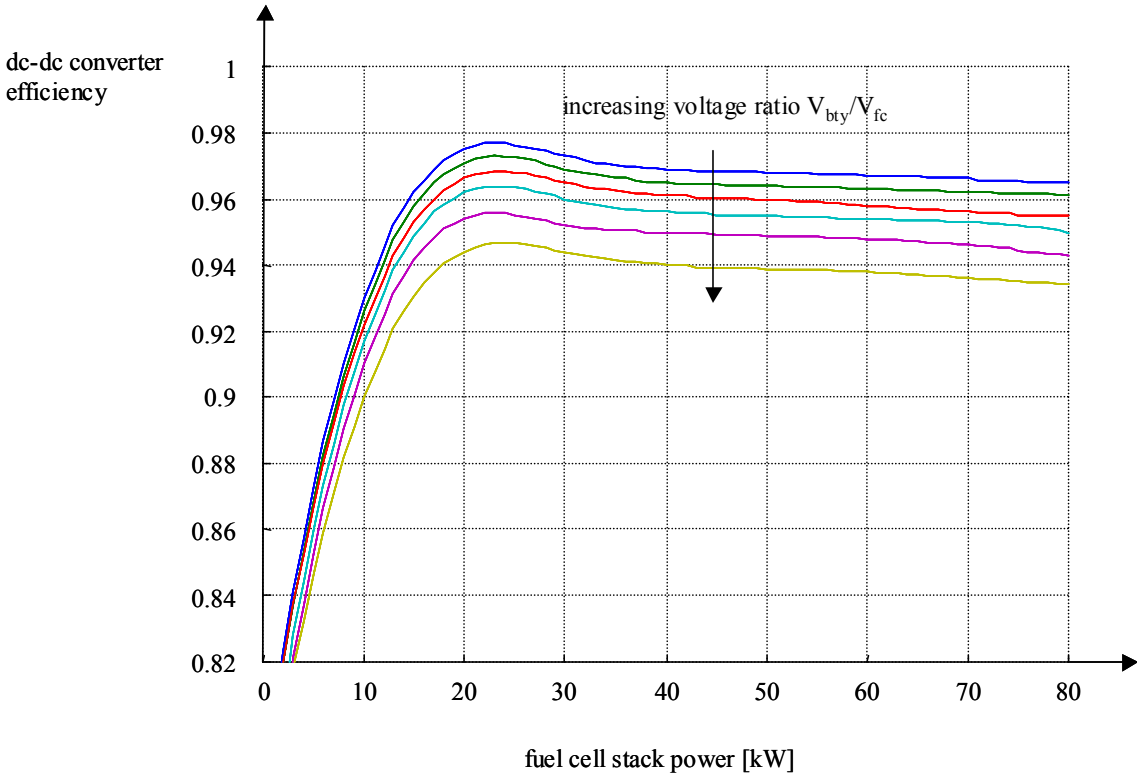

Figure 4-39: Efficiency map of the dc-dc converter. The ratio of output voltage (battery side) to input voltage varies from 1.0 to 2.0. The transferred power varies from 1 kW to 80 kW.

[36] Alternatively, the dc-dc converter could be modeled applying principles. Li (Li 1999) followed this approach for modeling a bi-directional dc-dc converter with a determined high and low voltage side. The disadvantage of such an approach is the increase in computational time because of the requirement of small iteration time steps to resolve the high switching dynamics.

The efficiency of the dc-dc converter is defined as the ratio of output power on the battery side over the input power on the fuel cell system side (Equation 3-61). King (King 1998) found that the efficiency depends on the transferred power and the voltage ratio between input (fuel cell stack voltage) and output (battery voltage).

Because in this model the efficiency is not derived from first principles, the modeling approach relies on access to experimental data, e.g. efficiency data for different operating points. However, because only limited experimental data were available for the power level and voltage range required in the model, the map in Figure 4-39 is the result of a scaling and extrapolation process based on data provided by King (King 1998) for a smaller dc-dc converter. Additional assumptions made are:

- The efficiency of the dc-dc converter depends only on the ratio of output voltage over input voltage, and not on the absolute voltage levels itself;
- The efficiency is lower for the upwards conversion (two transistors in current path) than for the downwards conversion (only one transistor in current path);
- For a constant voltage ratio, the efficiency increases with increasing power until it reaches it peak and then drops slowly with further increasing power.

Although the above assumptions are significant, due to the relative flatness of the curves, and because the operating regime of the dc-dc converter is limited by the operating strategy, it is not expected that a complete dc-dc converter map would significantly alter the results.

$$\eta_{dc-dc} = \frac{P_{dc-dc-bty}}{P_{dc-dc-fc}} = f\left(\frac{V_{bty}}{V_{fc}}, P_{dc-dc-fc}\right)$$

where:

η_{dc-dc} = efficiency of the dc – dc converter [1]

$P_{dc-dc-bty}$ = output power of the dc - dc converter on the battery side [W]

$P_{dc-dc-fc}$ = input power of the dc - dc converter on the fuel cell stack side [W]

V_{bty} = battery voltage [V]

V_{fc} = stack voltage [V]

Equation 4-61

The simulation model for the dc-dc converter takes as input values the battery voltage, the fuel cell stack voltage, and the net fuel cell stack current. Based on these inputs, the voltage ratio between battery and fuel cell stack voltage and the net fuel cell stack power drawn by the dc-dc converter is calculated. Both values together determine the efficiency at the specific operating point. The output current on the battery side is finally calculated, balancing the output and input power under consideration of the efficiency (Equation 4-62). Figure 4-40 shows the model in graphical form.

$$I_{bty-dc-dc} = \frac{\eta_{dc-dc} \cdot V_{bty} \cdot I_{fc-dc-dc}}{V_{fc}}$$

where:

$I_{bty-dc-dc}$ = current from dc - dc converter on the battery side [A]

V_{bty} = battery voltage [V]

$I_{fc-dc-dc}$ = current from the fuel cell stack into the dc - dc converter [A]

V_{fc} = fuel cell stack voltage [A]

Equation 4-62

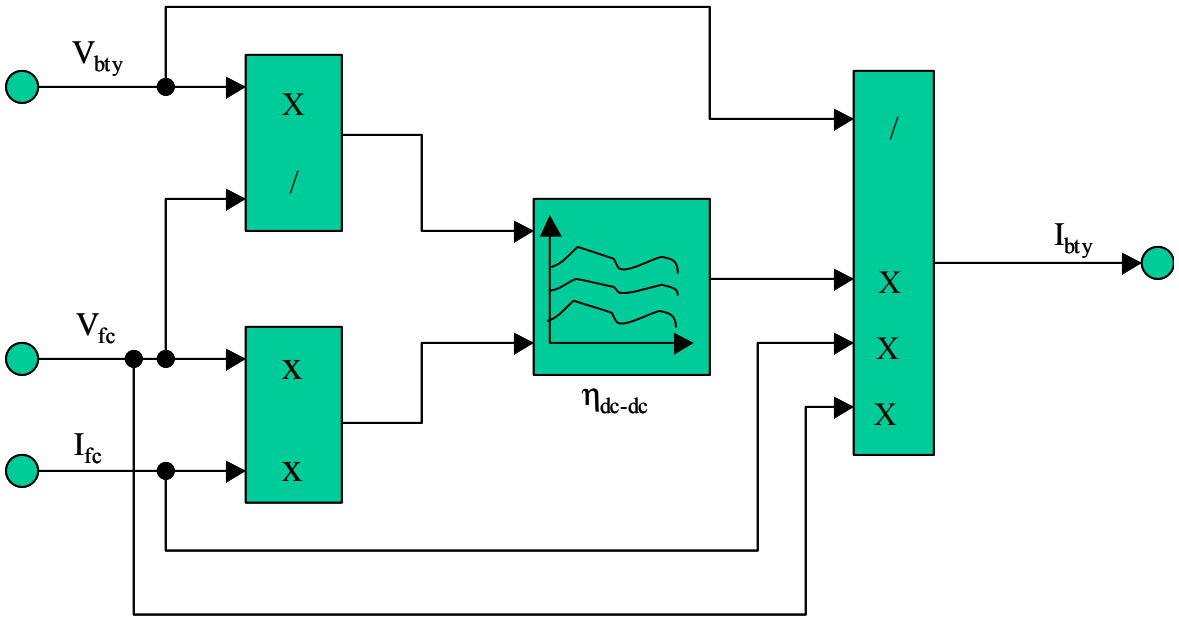

Figure 4-40: Simulation model of the dc-dc converter.

4.3.7.3. Controls for the DC-DC Converter for the Battery Hybrid Fuel Cell Vehicle

For the case of the battery hybrid fuel cell vehicle, the vehicle configuration allows the operation of the fuel cell system at one specific predetermined current independent from the battery voltage (Li 1999, Hauer 2001). Without a dc-dc converter between the fuel cell stack and battery, such an operation mode would not be possible because the fuel cell stack current is determined by the voltage difference between the stack and battery terminals divided by the total load resistance. The total load resistance is the sum of stack resistance (R_{fc}) plus cable resistance (R_{cable}) plus the battery resistance ($R_{battery}$) in parallel to the resistance of the electric drive train (R_{motor}) (Figure 4-41). Without a control device between the fuel cell stack and the dc–dc converter, fluctuations in the electric motor load would impose battery voltage fluctuations and finally impact the fuel cell stack current. Therefore, a steady state operation of the fuel cell system would not be possible.

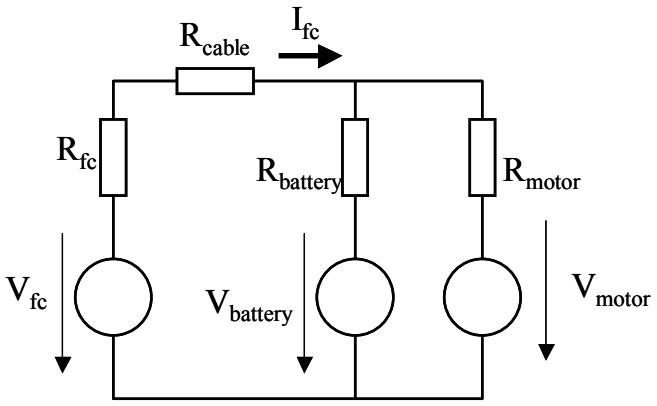

Figure 4-41: Fuel cell stack current as a function of resistances and voltages in the overall electric system for the configuration without dc-dc converter.

The control strategy for the dc-dc converter for this (load leveling) operating mode is implemented in the battery controller (Chapter 3.3.5.3).

Alternatively to the steady operation of the fuel cell system, fuel cell system power and battery power could be superposed in phases of high motor power demand. Such an operation strategy is called power assist strategy and requires a fuel cell system able to follow transient requests. In this context, the control strategy for steady state fuel cell operation and the power assist strategy represent the two extremes of possible control strategies for the fuel cell system. In most designs a compromise between these two extremes will be pursued. The compromise has to be found, considering fuel cell system efficiency, limitations of fuel cell system dynamics, and charge and discharge losses of the battery system. Further the estimated drive cycle (how the driver is most likely to drive) has to be taken into account.

4.3.7.4. DC-DC Converter for the Ultra-capacitor Hybrid Fuel Cell Vehicle

Figure 4-42 shows the circuit diagram of a bi-directional dc-dc converter integrated in the indirect ultra-capacitor hybrid vehicle concept shown in Figure 4-31. In this vehicle concept, the energy flow can be from the ultra-capacitor into the electric motor and vice versa. For both directions of energy flow it is possible that the voltage at the ultra-capacitor terminals is higher or lower than the voltage on the motor controller side of the converter.

The principle functionality is similar to the functionality of the one-directional dc-dc converter explained in the previous chapter.

For the case of energy flow from the ultra-capacitor towards the electric motor, only the transistors T1 and T4 are active. The transistors T2 and T3 stay inactive in this operation mode. The switching pattern of T1 and T4 and the current path is the same as for the one directional dc-dc converter used in the battery hybrid vehicle.

For the case of energy flow from the electric motor (or fuel cell stack) into the ultra-capacitor system, the symmetry of the dc-dc converter allows the same switching patterns for T3 and T2 as assumed for T1 and T4 for the other direction of energy flow.

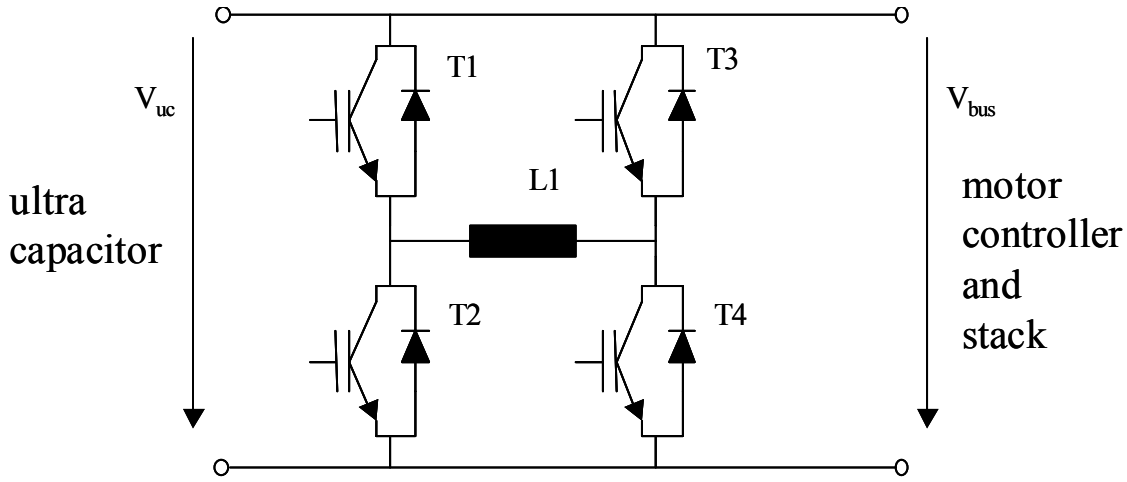

Figure 4-42: Principle schematic of the dc-dc converter for the case of an ultra-capacitor hybrid fuel cell vehicle.

4.3.7.5. Modeling of DC-DC Converter for the Ultra-Capacitor Hybrid Fuel Cell Vehicle

Similar to the one-directional dc-dc converter, the model of the bi-directional dc-dc converter also relies on a (static) efficiency map for the different operating points (Figure 4-43). The main difference is that the power through the dc-dc converter is not only positive but could also become negative if the direction of power flow reverses. Besides this difference, the modeling is similar to the one-directional case. After establishing the operating point, a power balance between input and output power is used to determine the current from the dc-dc converter into the electric motor. Depending on the operating point, this current could be positive (acceleration) or negative (regenerative braking or recharging of the ultra-capacitor system from the fuel cell system).

The graphical representation of the model is equal to the graphical representation of the one-directional case shown in Figure 4-40. The only differences are the expanded efficiency map and the that the current I_{fc} in Figure 4-40 is not the fuel cell current (as in the previous case) but the current on the bus side flowing into the dc-dc converter. This current could be positive or negative and is controlled by the controller for the dc-dc converter.

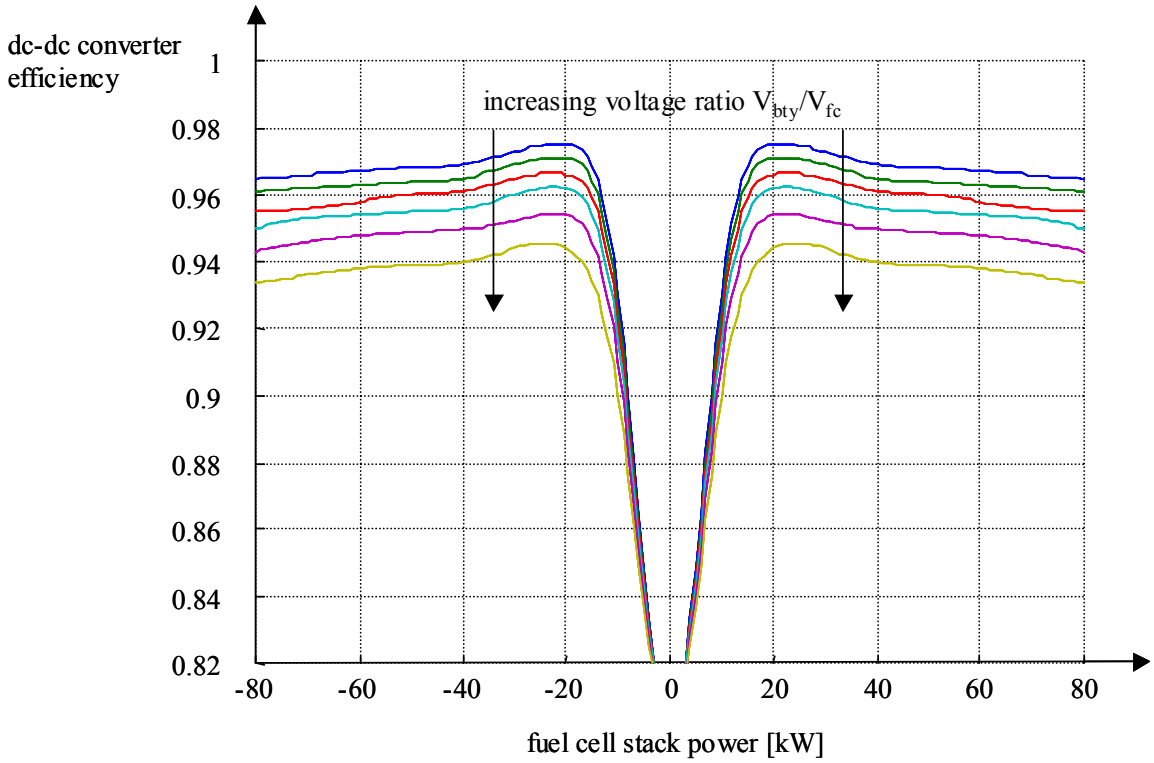

Figure 4-43: Efficiency map for the dc-dc converter for the bi-directional case.

4.3.7.6. Controls for the DC-DC Converter for the Ultra-capacitor Hybrid Fuel Cell Vehicle

Equivalent to the battery hybrid fuel cell vehicle, two different operation modes are possible. These are the load leveling mode in which the fuel cell stack current is aimed to stay as constant as possible and the power assist mode in which fuel cell power and ultra-capacitor power are superposed and feed together into the electric motor. Despite these similarities with the battery fuel cell vehicle, the control issues for both vehicle configurations are very different. For the case of the battery electric vehicle the motor voltage is determined by the battery voltage. For the case of the ultra-capacitor vehicle the motor voltage is determined by the fuel cell stack voltage. Especially in fuel cell vehicles with on-board reformer the stack voltage is expected to be much softer during transient phases compared with the battery voltage in a battery hybrid fuel cell vehicle. The reason is that the ability of power provision of the fuel cell stack depends on the fuel supply. In vehicle designs with on board fuel processor the provision of fuel is not instantaneous and because of this the transient power characteristics of fuel cell systems are inferior compared to batteries. As a consequence the power split between the ultra-capacitor system and the fuel cell stack needs to be carefully controlled to avoid overpowering the fuel cell stack.

The control strategy used in this work is a compromise between the load leveled strategy and the power assist strategy.

The control strategy incorporates the following main operating modes:

- Power assist mode (the power flow from the ultra-capacitor through the dc-dc converter into the electric drive train during phases the fuel cell system alone is not able to meet the power demand of the electric drive train),

- Regenerative braking (the power flow from the electric motor through the dc-dc converter into the ultra-capacitor during phases of regenerative braking),
- Recharge mode (the power flow from the fuel cell system through the dc-dc converter into the ultra-capacitor system during phases of low power demand).

Figure 4-44 shows the overall dc-dc controller in the form of a Simulink diagram. The controller considers the input variables:

- Total load current (this is the sum of the drive train current, vehicle auxiliary current, and fuel cell system auxiliary current),
- The fuel cell stack voltage (equivalent to the voltage at the terminals of the motor electronics),
- The voltage at the terminals of the ultra-capacitor system.

The output variables are:

- The dc-dc converter current at the bus side,
- A signal for the limitation of the motor power,
- A signal for the limitation of regenerative braking.

The functionality of the dc-dc converter controller is formulated in Equations 4-63 to 4-69.

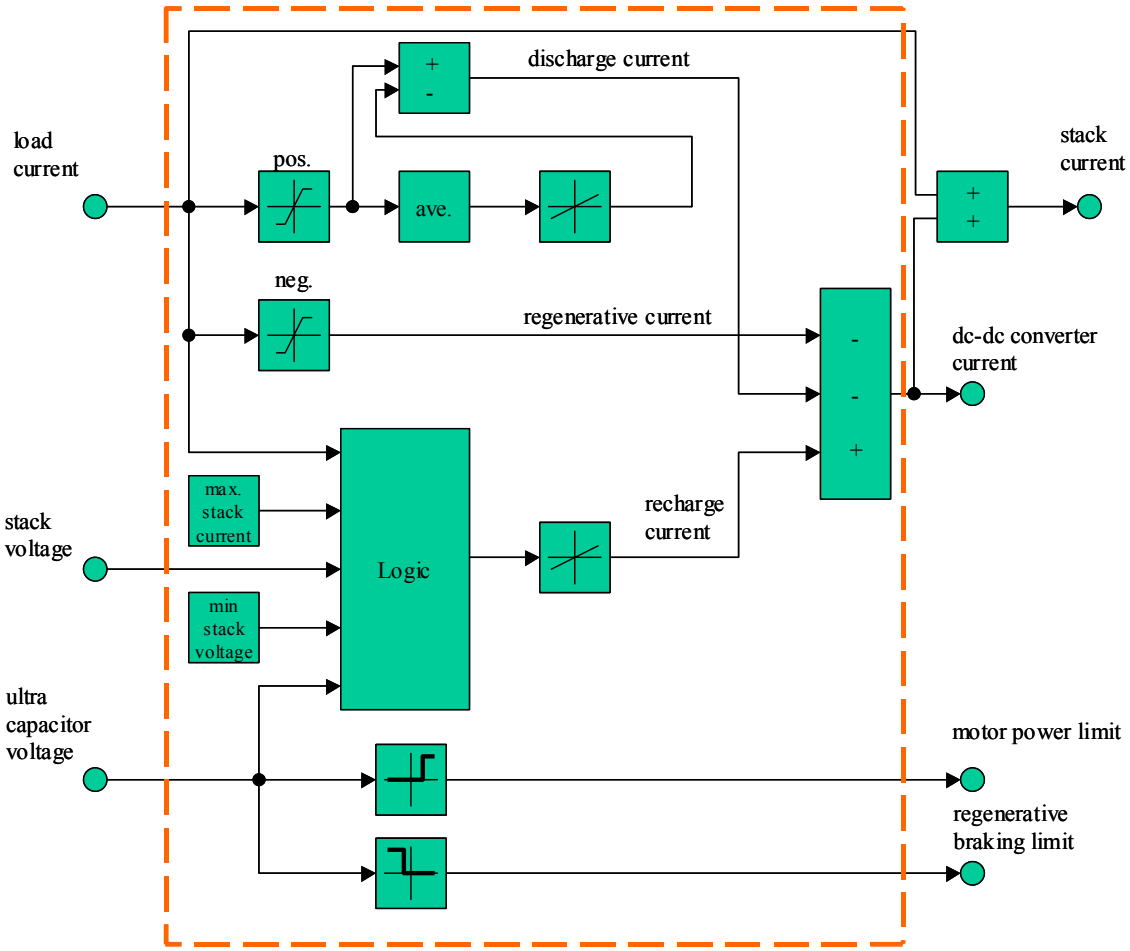

Figure 4-44: Scheme of the dc-dc converter controller. The stack current is not directly controlled and therefore the summation block calculating the stack current is not part of the controller algorithm.

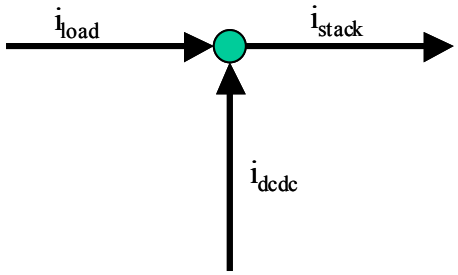

Figure 4-45: Definition of current directions. The diagram shows the current flow into the bus for the acceleration case (discharge of the ultra-capacitor system)

During phases of acceleration the fuel cell current can be calculated according to Equation 4-63. Note that the stack current is uncontrolled and determined by the load current and the current on the bus side of the dc-dc converter (this is the only current that

can be directly controlled by the dc-dc converter). The signs of the individual currents are defined in Figure 4-45.

$$i_{stack} = \frac{1}{T} \cdot \int_{t}^{t+T} i_{load}(t) \cdot dt$$

$where$:

i_{stack} = stack current **Equation 4-63**

i_{load} = load current

T = average time for averaging the load current

Applying Kirchhoff's law and the definitions in Figure 4-45, the current flowing on the bus side out of the dc-dc converter could be calculated according to Equation 4-64. Note that this current is the current controlled by the dc-dc converter.

$$i_{dcdc\_bus} = i_{load} - i_{stack} = i_{load} - \frac{1}{T} \cdot \int_{t}^{t+T} i_{load}(t) \cdot dt$$

$where$: **Equation 4-64**

i_{dcdc_bus} = dc - dc converter current on the bus side [A]

During phases of regenerative braking the fuel cell stack current is 0 and the dc-dc converter current on the bus side equals the (dc) total load current (Equations 4-65 and 4-66).

$$i_{stack} = 0$$ **Equation 4-65**

$$i_{dcdc\_bus} = i_{load}$$ **Equation 4-66**

If the state of charge of the ultra-capacitor voltage is below a certain threshold, the ultra-capacitor system could be recharged to prepare for future load conditions. This operation mode is the recharging mode. For the case of recharging the ultra-capacitor system, the conditions stated in Equation 4-67 have to be fulfilled. The resulting dc-dc converter current is calculated in the second half of Equation 4-67. Note: Similarly to the

normal load case, the fuel cell stack current is not directly controlled. The stack current is the difference between the load current and dc-dc converter current flowing out of the dc-dc converter (bus side).

$$
\begin{aligned}
&\textit{if } (i_{\text{stack}} < i_{\text{stack\_recharge\_max}}) \,\&\, (V_{stack} \geq V_{\text{stack\_recharge\_min}}) \,\&\, (V_{\text{uc\_min}} \leq V_{uc} \leq V_{\text{uc\_max}}) \\
&\textit{then} \\
&i_{stack} = i_{rech\,\text{arg}\,e} + \frac{1}{T} \cdot \int_{t}^{t+T} i_{load}(t) \cdot dt \\
&i_{dcdc\_bus} = i_{load} - \frac{1}{T} \cdot \int_{t}^{t+T} i_{load}(t) \cdot dt + i_{rech\,\text{arg}\,e} \\
&\textit{where}: \\
&i_{\text{stack\_recharge\_max}} = \text{maximum stack current for recharge mode [A]} \\
&V_{\text{stack\_recharge\_min}} = \text{minimum stack voltage for recharge mode [A]} \\
&V_{\text{uc\_min}} = \text{minimum ultra capacitor voltage for recharge [V]} \\
&V_{uc\_\max} = \text{maximum ultra capacitor voltage for recharge [V]} \\
&i_{\text{recharge}} = \text{recharge current [A]}
\end{aligned}
$$

Equation 4-67

In addition to the main functionality above, the control strategy ensures also the power reduction of the electric motor for the case that the ultra-capacitor is already discharged and the fuel cell system is not able to provide the full requested motor power (avoidance of deep discharge of the ultra-capacitor system). Similar to the avoidance of over- discharging the ultra-capacitor, the controller also has to avoid the overcharging the ultra-capacitor system during phases of regenerative braking.

The limitation of the motor power at low ultra-capacitor voltages is described in Equation 4-68.

$$
\begin{aligned}
&\textit{if } V_{uc} \leq V_{uc\_\min} \\
&\textit{then} \\
&L_{factor} = f(V_{uc}) \qquad \text{(limitation)} \\
&\textit{else} \\
&L_{factor\_motor} = 1 \qquad \text{(no limitation)} \\
&\textit{where}: \\
&V_{uc\_\min} = \text{minimum ultra capacitor voltage [V]} \\
&L_{factor\_motor} = \text{limiting factor for motor power request [1]}
\end{aligned}
$$

Equation 4-68

The limitation of regenerative braking at high ultra-capacitor voltage is described in Equation 4-69.

$$
\begin{aligned}
&\textit{if } \mathrm{V_{uc}} \geq V_{uc\_\max} \\
&\textit{then} \\
&L_{factor\_regen} = f(\mathrm{V_{uc}}) \qquad \text{(limitation)} \\
&\textit{else} \\
&L_{factor\_regen} = 1 \qquad \text{(no limitation)} \\
&\textit{where}: \\
&V_{uc\_\max} = \text{maximum ultra capacitor voltage [V]} \\
&L_{factor\_regen} = \text{limiting factorfor regenerative braking request [1]}
\end{aligned}
$$

Equation 4-69

For all these cases the controller assumes that the fuel cell system cannot immediately respond to transient loads. The maximum upwards slew rate of the stack current is therefore limited and impacts the control scheme for the dc-dc converter. For example, if due to steep increase in motor current the (uncontrolled) stack current would exceed the maximum slew rate of the fuel cell system, the controller would control the dc-dc converter to avoid this overload situation. The controller has two principle methods of achieving this.

- If the ultra-capacitor system is charged and able to provide current, the dc-dc converter will be controlled, supplying enough current from the ultra-capacitor to the bus. Doing this, the slew rate of the stack current would be reduced below the specified maximum slew rate.
- If the ultra-capacitor is already discharged, the dc-dc converter controller would reduce the motor current request and with this the motor power.

Alternatively to the control strategy described above, a control strategy relying solely on the fuel cell stack voltage could be developed for controlling the current in and out of the ultra-capacitor system. Such a strategy would also lead to stable conditions if supported by the controls for motor power reduction and the reduction of regenerative braking as described above. The main difference of the solely voltage controlled strategy compared to the strategy in which the average load current is requested by the fuel cell system is that for the voltage based control strategy no system knowledge has to be included in the dc-dc converter controller. In this respect, the fuel cell system could therefore be treated as a black box. However, the voltage controlled control strategy would also pass all transients directly to the fuel cell system, while the strategy described here effectively smoothes the transient loads for the system.

4.3.8. Vehicle Controller

Several car companies propose a so-called vehicle controller in addition to controllers for each individual component (Volkswagen 1999). Although a vehicle controller is not a necessary device for the function of the overall vehicle, its presence could simplify the development of software, especially during the development and market introduction phase.

The main objectives of the vehicle controller are:

- Hosting of software algorithms which could not be directly assigned to a component controller,
- Hosting of diagnostic functions,
- Hosting of driver information functions,
- Hosting of proprietary algorithms that reflect core knowledge of the car manufacturer and should not be handed over to suppliers,
- Hosting of temporary algorithms for test and development purposes only.

In this work, the only function the vehicle controller hosts is the decision process as to which fraction of the drivers brake request will be translated into frictional braking and regenerative braking respectively.

For hybrid configurations, the model allows two different braking modes, namely mechanical braking with the conventional brake system of the car, and electric or regenerative braking (operating the electric motor as a generator). The former generates heat at the brake pads and discs, while the latter recharges the battery the battery or ultra-

capacitor. The mode of regenerative braking is limited to hybrid designs with electrical energy storage (batteries, ultra-capacitors) because in non-hybrid designs the generated energy could not be stored.

The block “vehicle controller” is responsible for dividing the brake pedal signal (as the expression of the drivers desire) into two different brake signals. One determines the electric brake mode and the other determines the mechanical brake mode. Optionally, to realize this functionality in a vehicle controller, it could be integrated into the control devices of the Anti-Lock Brake System (ABS) or into the motor controller.

From an energy point of view, it seems logical to choose the maximum fraction of electric braking, since mechanical braking only dissipates the energy into heat. However, due to the fact that electrical braking only works for the wheels connected to the electric motor, electric braking has its limits. These limits are dictated by both safety and convenience. Another limit is the limited torque that the motor can provide, which is normally not enough for hard decelerations or emergencies.

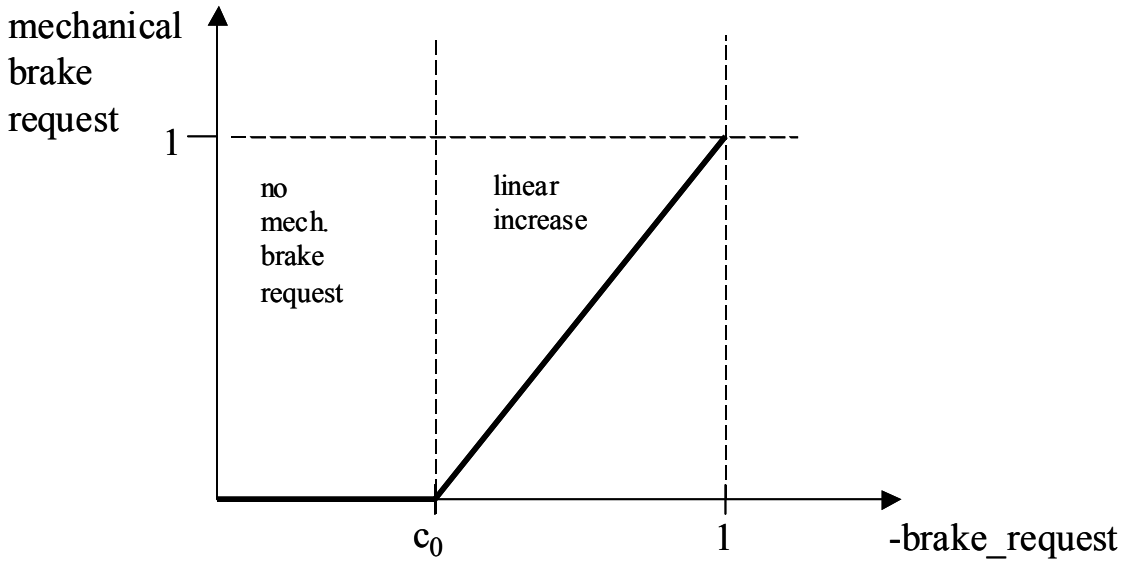

Figure 4-46: Mechanical brake request as a function of the driver's brake request.[37]

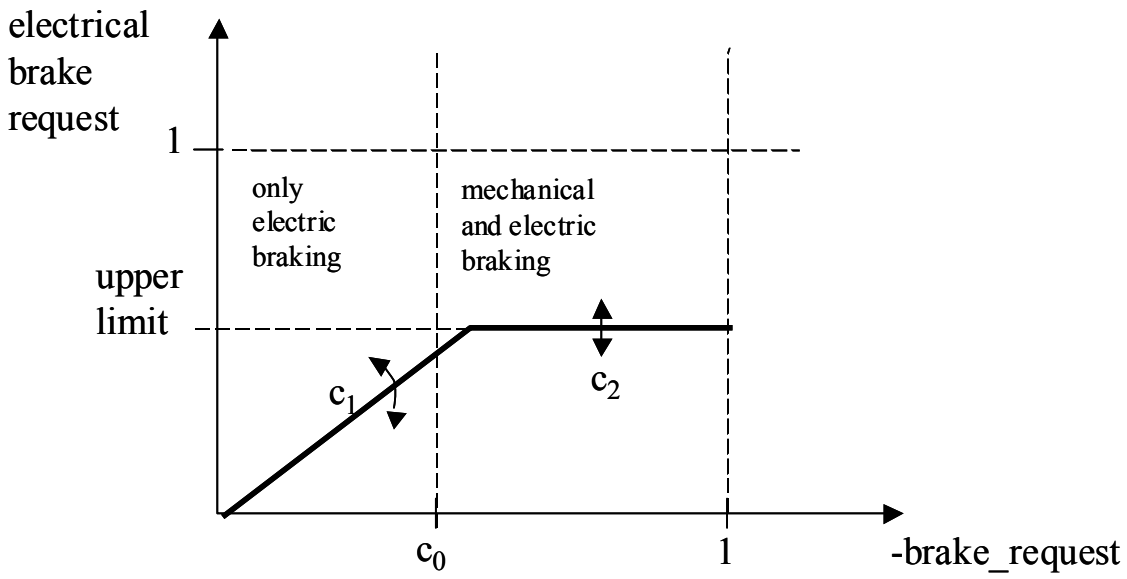

Figure 4-47: Electrical brake request (regenerative braking) as a function of the driver's brake request.

Figure 4-46 and Figure 4-47 illustrate how the vehicle controller splits the driver's brake request into individual requests for the mechanical and electrical brake system. Three different parameters allow the configuration of the overall brake characteristics in the vehicle controller unit.[38]

The parameter c_0 sets the regime for exclusive regenerative braking only. If the driver of a vehicle with regenerative braking possibilities generates a brake signal below the value specified through parameter c_0, the mechanical brakes are not active and all the

[37] Note that the braking characteristic shown is only conceptual. It is not a suggestion of an optimal braking characteristic for hybrid vehicles. In this example setup, the varying slope of the characteristic could be disturbing for the driver.

[38] The maximum mechanical torque is always applied at the maximum brake pedal position and zero for brake pedal positions below c_0. Therefore no separate parameter is necessary to specify the slope of the mechanical brake torque.

braking will be done with regenerative brakes only. A brake pedal signal above c_0 generated by the driver results in mechanical and electrical braking.

The parameter c_1 allows the adjustment of the regenerative braking requested for a given driver request. Essentially c_1 determines the sensitivity of the output value regenerative braking request as a function of the input value driver's brake request.

The parameter c_2 determines the maximum value of the regenerative braking request. In the vehicle controller this value is fixed (independent from other inputs). It could be derived from safety considerations or component constraints. However, additionally the regenerative braking request is also limited inside the motor controller.

The requests for mechanical and electrical braking generated in the vehicle control block are fed to the motor control block (request for electrical braking) and to the block "vehicle curb" (request for mechanical braking). The motor control block computes the final regenerative brake torque from the request value together with other input values. In the block "vehicle curb" the request for mechanical braking is multiplied with the maximum brake force. The result is essentially the brake force applied to the vehicle and determines, together with the other forces accessing and the vehicle mass, the final vehicle acceleration.

The mechanical brake request is derived according to Equation 4-70. The input value is the driver's request p and the output value is the request for mechanical braking p_{mech}.

$$p_{mech} = 0 \qquad \text{if } (-p) \le c_0$$

$$p_{mech} = \frac{1}{1-c_0} \cdot (-p) - \frac{c_0}{1-c_0} \qquad \text{if } (-p) > c_0$$

where :

p_{mech} = request for mechanical brakes

- p = driver's brake request (normalized brake pedal position)

c_0 = parameter

Equation 4-70

The mechanical brake force applied by the friction brakes is the product of the requested value for mechanical braking times the maximum brake force F_{brake_max} (Equation 4-71).

$$F_{brake} = p_{mech} \cdot F_{brake\_\max}$$

where :

F_{brake} = mechanical brake force

$F_{brake\_\max}$ = maximum mechanical brake force

Equation 4-71

The request for regenerative braking is calculated according to Equation 4-72.

$$p_{regen} = c_1 \cdot (-p) \qquad \text{if } p_{regen} < c_2$$

$$p_{regen} = c_2 \qquad \text{if } p_{regen} \ge c_2$$

p_{regen} = request for regnerative braking

c_1 = *parameter*

c_2 = *parameter*

Equation 4-72

Based on the request for regenerative braking, the motor controller algorithm finally computes the regenerative motor torque.

Unless otherwise stated, all the simulation runs in this work use the setting c_0=0.3, c_1=0.5 and c_2=0.5 (limitation of the brake torque to 50% of the maximum motor brake torque). The reason is that this parameter set recaptures for the vehicles analyzed in this work the majority of the energy potential of regenerative braking (for all cycles). On the

other hand, the parameter choice guarantees that the driver could conveniently adjust the mechanical brakes (for example this would be difficult for a parameter setting of c_0=0.99). The limitation of the maximum electric brake torque to half of the maximum motor brake torque (parameter c_2) guarantees that the energy storage will not be overpowered if charged by the fuel cell system and the regenerative braking system at the same time.

5. Model Application

5.1. Vehicle Requirements

A vehicle can be designed and optimized in a variety of ways, depending on how the various vehicle performance metrics are prioritized. The final project goals for a specific vehicle design depend largely on market demands and the purpose for which the vehicle is designed. In this dissertation the vehicle targets of the Partnership of New Generation Vehicles (PNGV[39]) have been chosen to serve as design goals for the vehicles simulated. The goals are progressive and are originally set for the 3X[40] car defined by the PNGV. These targets primarily relate to the performance of the vehicle, though there are many other attributes, e.g. noise, comfort, safety, reliability, package etc., which are not addressed explicitly but are considered qualitatively as far as it is possible in this discussion.

For this work, as primary design targets for designing PNGV type vehicles, the 0-60 mph acceleration time and the minimum top speed requirement of 85 mph have been chosen. The other vehicle attributes are required to be similar among the different concepts but allowed to differ from the PNGV requirements. This simplification eases the design process significantly while still allowing the comparison of the fuel economy (the primary metric of comparison) among the different vehicle types. Despite the fact that not all vehicle requirements in Table 5-1 are met, the vehicles are still referenced as “PNGV type” vehicles.

---

[39] The Partnership for a New Generation of Vehicles (PNGV) is a public/private partnership between the U.S. federal government (7 agencies and 20 federal laboratories) and Chrysler, Ford, and General Motors that aims to strengthen the United States' competitiveness by developing technologies for a new generation of vehicles.

[40] PNGV's long term goal, dubbed the "Supercar" goal , is to develop an environmentally friendly car with up to triple the fuel efficiency of today's midsize cars - without sacrificing affordability, performance, or safety.

PNGV Requirements	Target	Load follow	Battery Hybrid	Ultra Cap. Hybrid indirect	Ultra Cap. Hybrid direct
0..60 mph time	12.0 sec	12.3 sec	11.2 sec	12.6 sec	12.1 sec
Maximum speed	85 mph	94 mph	94 mph	94 mph	94 mph
Peak acceleration	17 ft/sec^2 (5.18m/sec^2)	4.6 m/sec^2	3.4 m/sec^2	3.7 m/sec^2	3.8 m/sec^2
5 sec distance	140 ft (42.7 m)	44 m	36 m	37 m	37 m
40 .. 60 mph pass time	5.3 sec	6.2 sec	5.1 sec	6.6 sec	5.4 sec
0..85 mph time	23.4 sec	31 sec	25.3 sec	33 sec	33 sec
Gradability[41]	30%	> 30 %	> 30 %	> 30 %	> 30 %
Gradability	6.5% at 55mph for 20 min	> 6.5 %	> 6.5 %	> 6.5 %	> 6.5 %
Emissions[42]	EPA Tier II	-	-	-	-
Range[43]	380 mi	393 mi	393 mi	420 mi	448 mi
Efficiency[44]	80 mpg	60 mpg	60 mpg	64 mpg	69 mpg

Table 5-1: PNGV targets (PNGV 2001)

The PNGV fuel efficiency goal in Table 5-1 is stated in miles per gallon of gasoline. However, all of the vehicles under consideration in this dissertation use methanol as a fuel. For the purpose of gaining comparable fuel economy we convert the energy content of the consumed methanol into a gasoline equivalent.

[41] Initial velocity of 5 km/h assumed.
[42] Not investigated in this dissertation.
[43] Range in the combined cycle with 50 l tank volume.
[44] Combined cycle.

5.2. Vehicle Parameters and Vehicle Design

At the beginning of the modeling process, it is necessary to specify a number of different vehicle parameters. These are essentially the model input values describing either the vehicle or component properties (Table 5-2). Additionally, the vehicle characteristics are influenced by the choice of controller parameters, which also need to be specified (Table 5-3). The vehicle parameters are either single-valued (the aerodynamic drag coefficient), vectors (e.g. battery resistance as a function of the state of charge), or two-dimensional maps (e.g. motor and transmission efficiency). It is important to understand that the values of these parameter or the technologies used (with their inherent parameters) are chosen so that the complete vehicle is able to meet the vehicle requirements as stated in Table 5-1. Therefore, the process of "designing" the vehicle is inherently iterative, and the parameter values in Table 5-2 and Table 5-3 are partially the result of this iteration process.

Vehicle Type	Load following vehicle	Battery hybrid Vehicle	Ultra-capacitor hybrid vehicle (direct)	Ultra-capacitor hybrid vehicle (indirect)
Vehicle				
Drag Coefficient	0.2	0.2	0.2	0.2
Frontal area	2.00 m^2	2.00 m^2	2.00 m^2	2.00 m^2
Wheels Radius Inertia Rolling friction coefficient	 0.3556 m 4 kg*m*m 0.01	 0.3556 m 4 kg*m*m 0.01	 0.3556 m 4 kg*m*m 0.01	 0.3556 m 4 kg*m*m 0.01
Vehicle hotel load	0.2 kW	0.2 kW	0.2 kW	0.2 kW
Maximum mechanical brake force	10.000 N	10.000 N	10.000 N	10.000 N
Test weight	See end of table	See end of table	See end of table	See end of table
Battery				
Technology Number of cells Energy content Maximum power Weight Open circuit voltage Model data	-	Li Ion (Shin Kobe 4 Ah)[45] 84 x 2 2755 Wh 75 kW 50.4 kg (only cells) 344 V See appendix	-	-
Ultra-capacitor System				
Manufacturer Number of cells Energy content[46] Power Weight	-	-	Maxwell PC 2500 85 x 1 161 Wh 43 kW[47] 61 kg	Maxwell PC 2500 136 x 1 258 Wh 69 kW 98 kg

[45] The test data have been borrowed from Burke and Miller (Burke, Miller 2000).
[46] Discharging the ultra capacitor from maximum voltage to half of the maximum voltage.
[47] The power rating of 43 kW corresponds to 95% efficiency (Burke 2000). The matched impedance power is higher than 200 kW.

Model data			See appendix	
Dc-Dc converter				
Technology	-	Uni-directional Up and down	Bi-directional up and down (-)	-
Dc-Dc converter efficiency map	-	Figure 4-39	Figure 4-43	-
Fuel cell system				
Net Power Power density Static efficiency map 10-90% response time	75 kW 0.25 kW/kg Figure 4-22 2 sec			
Fuel cell stack technology Number of cells Cell area Membrane Resistance Open circuit voltage Polarity plot	PEM 350 600 cm^2 0.07 Ohm cm^2 0.9 V/cell Figure 4-17			
Fuel processor and clean up	Methanol steam reformer with water gas shift reactor and preferential oxidation stage			
Burner	Catalytic - for anode exhaust and additional methanol			
Reformate buffer Volume Maximum pressure Minimum pressure	 60 l 3 atm absolute 1.2 atm absolute			
Compressor	Vairex Twinscrew			
Expander	Without expander			
Water and thermal management system	Water sustainable 80^{O}C stack temperature			
Transmission				
Number of gears	1			
Total gear ratio incl. differential	8.9			
Transmission efficiency map	Figure 4-13			

Electric Motor				
Basic Technology	Induction Motor			
Maximum Torque	260 Nm *1.15	260 Nm *0.9	260 Nm	260 Nm
Maximum Speed	10,000 rpm	10,000 rpm	10,000 rpm	10,000 rpm
Characteristic speed	2750 rpm @ nominal voltage	2750 rpm @ nominal voltage	2750 rpm @ nominal voltage	2750 rpm @ nominal voltage
Nominal voltage	312 V	312 V	312 V	312 V
Motor efficiency map	Figure 4-7	Figure 4-7	Figure 4-7	Figure 4-7
Torque as a function of voltage	Figure 4-8	Figure 4-8	Figure 4-8	Figure 4-8
Motor inertia	0.1 kgm^2	0.1 kgm^2	0.1 kgm^2	0.1 kgm^2
Scale factor (for torque only)	1.15	0.9	1.0	1.0
Mass balance				
Shell mass	970 kg	970 kg	970 kg	970 kg
Payload (driver)	75 kg	75 kg	75 kg	75 kg
Fuel cell system mass[48] (0.25 kW / kg)	300 kg	300 kg	300 kg	300 kg
Battery mass	-	50.4 kg	-	-
Ultra-capacitor mass	-	-	61 kg	98 kg
Dc-dc-converter mass[49]	-	37.5 kg	37.5 kg	-
Motor mass (including power electronic and transmission)	126.5 kg (110 kg*1.15)	99 kg (110 kg*0.9)	110 kg	110 kg
Fuel (ca. 3/4 of the tank volume of 50 l)	30 kg	30 kg	30 kg	30 kg
"Test" weight incl. driver	1501 kg	1562 kg	1583 kg	1583 kg

Table 5-2: Vehicle Parameters

[48] Includes water and thermal management system. Excludes fuel tank, fuel and dc-dc converter.
[49] King (King 1998) estimates a power density of 2000 W/kg for a liquid cooled dc-dc converter.

List of Controller Parameters

Vehicle Type	Load following vehicle	Battery hybrid vehicle	Ultra-capacitor hybrid vehicle (direct)	Ultra-capacitor hybrid vehicle (indirect)
Driver				
Algorithm	Proportional-Integral for present drive cycle Prediction of the future drive cycle			
Input(s)	Vehicle velocity, drive cycle, drive cycle xx sec ahead from now			
Output(s)	Normalized acceleration pedal position Normalized brake pedal position			
Parameter	Integral: 0 Proportional: 0.3 Prediction time for the future drive cycle: 0.5 Weight of the future drive cycle: 0.1 Driver reaction time: 0.2			
Vehicle controller				
Algorithm	Algebraic, Split up of the brake request into the electric brake request and mechanic brake request			
Input(s)	Normalized brake pedal position			
Output(s)	Normalized electrical brake request Normalized mechanical brake request			
Parameter	Regime of exclusive regenerative braking: c_0=0.3 (30%) Gain factor (regenerative strength): c_1=0.5			
Motor controller				
Algorithm	Proportional Integral controller for the control of the motor torque			
Input(s)	Normalized acceleration Pedal position Normalized electric brake request Dc - terminal voltage Motor speed Motor torque			
Output(s)	Fraction of the maximum motor torque requested			

Parameter	Integral: 0.1 Proportional: 0 Time constant: 0.01 Characteristic for torque limitation due to too low voltage Characteristic for regenerative braking limitations due to too high voltage Characteristic for speed limitations due to too high speed (optional)			
Battery controller				
Algorithm	-	State of charge determination, Control of the Dc-Dc converter current (stack side)	-	-
Input(s)	-	Battery current Load current (motor + auxiliaries) Battery voltage	-	-
Output(s)	-	Stack current request	-	-
Parameter	-	See appendix	-	-
DC-DC converter controller				
Algorithm	-	Functionality included in the battery controller	Power assist if stack voltage drops below threshold, Recharging, Regeneration	-
Input(s)	-	-	Stack voltage Regenerative current	-
Output(s)	-	-	Dc-dc converter control signal for assistant current	-
Parameter	-	-	See appendix	-

Fuel processor controller	
Algorithm	Proportional Integral controller for the Methanol flow into the reformer (based on stack current) Approximate derivation of the acceleration pedal position (optional) Pressure control in reformate storage Stack voltage control
Input(s)	Stack current Stack voltage Pressure Acceleration pedal position
Output(s)	Methanol flow into reformer
Parameter	Proportional: 0.05 Integral: 0.33 See appendix
Back pressure controller	
Algorithm	Proportional / Integral controller for the control of the reformate flow into the fuel cell stack
Input(s)	Stack voltage
Output(s)	Valve position (Reformate flow from buffer into stack)
Parameter	Proportional: 1 Integral: 0.1
Burner controller	
Algorithm	Proportional Integral controller for supplemental methanol
Input(s)	Reformer temperature
Output(s)	Burner methanol into the burner
Parameter	Proportional: 0 Integral: 0.1
Air compressor controller	
Algorithm	Optimized set points for pressure and air flow as a function of stack current

Input(s)	Stack current
Output(s)	Compressor Speed Stack exit valve position
Parameter	(Cunningham 2000)

Table 5-3: Controller parameters

5.3. Component Sizing

5.3.1. Choice and Sizing of the Battery System

In this work the term "battery system" refers to the battery together with the battery controller and additional temperature management systems.[50] The battery system integrated in the hybrid vehicle has to fulfill the following criteria:

- The battery system should be able to supply the maximum power the electric drive train and the vehicle auxiliaries draw for the minimum time of 10 sec and for a battery state of charge above 50%.
- The battery system should be able to accept the maximum regenerative power up to a state of charge of 90%.
- A minimum energy capacity of ca. 2 kWh is required to guarantee the instant operation of the vehicle if the fuel cell system is started at ambient temperatures (cold start).[51]
- The battery system should be self-protecting. If the battery condition does not allow further discharge, the battery controller limits the power draw, guaranteeing safe battery operation. If the battery condition does not allow further charge, the battery controller limits the charging power (regenerative braking and charging through the fuel cell system). Both limitations are realized through communication of the battery controller with the motor controller, the fuel cell controller and the dc-dc converter.

[50] Battery temperature management, although important in a real vehicle, has not been modeled yet.
[51] The value of 2 kW is secondary to the power requirements. The battery configuration in Table 4-4 allows the operation (of the vehicle described in the previous chapter) over one complete FUDS cycle.

Based on this list of requirements, a Shin Kobe Li-Ion Battery was configured based on Shin Kobe's 3.6Ah high power cells. Two parallel strings each with 84 cells in series were assumed. The battery configuration and data are summarized in Table 5-4.

Because of the availability of a complete set of data, the model is based on the experimental test results of Burke and Miller (Burke and Miller 2000). The complete data set, including cell resistance and open circuit voltage as a function of state of charge, is listed in the appendix.[52]

Property	**Value**
Battery Manufacturer	Shin – Kobe
Battery Technology	Li-Ion
Nominal cell capacity (1h)	3.6 Ah
Nominal cell voltage	3.6 V
Cell mass (bare cell)	300 g
Number of cells per string	84
Number of strings in parallel	2
Rated energy of the complete battery (rated capacity times rated voltage)	2.2 kWh
Battery mass (only cells)	50.4 kg
Battery rated power (Shin Kobe 2001)	43.75 kW
Battery peak power (Burke and Miller 2000)	68 kW (90% efficiency)

Table 5-4: Battery data for the battery composition using the Shin Kobe Li-Ion 3.6 Ah high power cell.

[52] The resistance of the cell connecters has not been modeled. However, the consideration of this additional resistance would not significantly alter the results.

5.3.2. Choice and Sizing of the Ultra-capacitor System

The ultra-capacitor systems for the fuel cell hybrid vehicles proposed in this dissertation have been sized according to the following criteria:

For both ultra-capacitor vehicle concepts (with and without dc-dc converter):

- The ultra-capacitor system should be able to provide enough power to satisfy the PNGV standards for the overall vehicle (acceleration, elasticity) while maintaining a reasonable charge and discharge efficiency (above 90 %).
- For minimizing the change of the vehicle characteristics with the state of charge of the ultra-capacitor, the energy content in the ultra-capacitor system should be large enough that at least three accelerations from 0 to 60 mph are possible without significantly altering the vehicle characteristics (acceleration time). In addition, the vehicle should be able to follow all the standard drive cycles in Table 4-1 without any problems.
- Practicality: For practicality and cost reasons the maximum current at the ultra-capacitor system terminals should not exceed 400A significantly (Figure 5-1d).
- The ultra-capacitor system should be self-protecting. In the case of the indirect coupled capacitor, this means that if the ultra-capacitor condition does not allow further discharge the ultra-capacitor controller limits the power draw guaranteeing safe operation. If the ultra-capacitor condition does not allow further charge, the ultra-capacitor controller limits the charging power (regenerative braking and charging through the fuel cell system). Both limitations are realized through communication of the ultra-capacitor controller with the motor controller and the fuel cell controller (respectively the dc-dc converter). In the case of the direct coupling of the stack and

ultra-capacitor, the ultra-capacitor system has no designated controller. For this case the required functionality is integrated in the motor controller.

For the vehicle concept without dc-dc converter, an additional criterion for sizing the ultra-capacitor system has been defined:

- The maximum ultra-capacitor voltage is 1.15 to 1.2 times higher than the open circuit stack voltage. This criterion allows for regenerative braking even if the capacitor is charged to the open circuit stack voltage level.

The criteria defined are in some respects arbitrary and depend largely on the designer's decisions regarding how to compromise vehicle features, such as regenerative braking, efficiency, and performance, with cost for the overall system. Additional constraints are package limitations dictated by the overall vehicle package. Because of all this, the absolute numbers provided are not a recommendation for an optimal ultra-capacitor system design. In fact, the optimum system size could be different for different vehicles, markets and scenarios. However, the sizing process tried to take all this into account without having complete knowledge about the vehicle.

The energy storage requirement of the ultra-capacitor system is not only dependent on the demand side (how will the ultra-capacitor be discharged by the drive train and auxiliaries) but also on the supply side. Meaning how fast the ultra-capacitor system can be recharged for fixed fuel cell system characteristics (maximum power and transient response).

Figure 5-1 shows the interaction of drive train, fuel cell stack, and ultra-capacitor system at the electrical interface for the case of an ultra-capacitor coupled via dc-dc

converter. As drive cycles three vehicle accelerations from 0 – 60 miles/hour have been chosen (Figure 5-1a).

The control strategy for the dc-dc converter is such that above a certain stack voltage the fuel cell stack alone supplies the motor current to the motor. Only at low stack voltages does the dc-dc converter assist the fuel cell system with the provision of current (Figure 5-1h and Figure 5-1d).

It can be seen that the (average) ultra-capacitor voltage drops slowly from acceleration to acceleration (Figure 5-1e). The ultra-capacitor has been sized for three accelerations. A fourth acceleration immediately following would result in an acceleration time longer than the target of 12 sec. The lower supply voltage at the terminals of the stack (Figure 5-1h) results in lower motor torque (Figure 5-1b) and finally in a longer acceleration time.

The control strategy guarantees that the efficiency of the ultra-capacitor stays above 90% most of the time (Figure 5-1e). Given that the drive cycle is extreme, this efficiency is considered to be high enough.

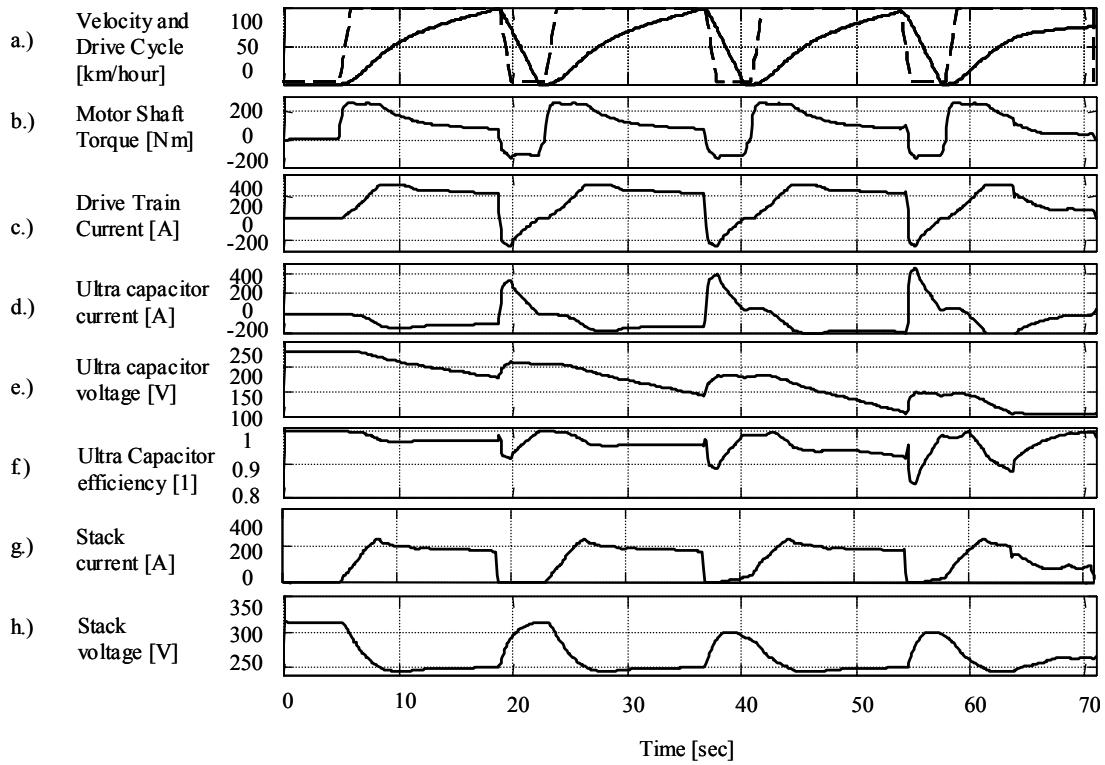

Figure 5-1: Indirect coupled ultra-capacitor system. Vehicle states for four accelerations from 0 – 60 miles / hour. The standard parameters for regenerative braking have been applied. The initial voltage level of the ultra-capacitor system is 90% of the maximum voltage.

The ultra-capacitor current always stays below the target value of 400 A (Figure 5-1d).

Summarizing, it could be concluded that the ultra-capacitor system chosen is large enough to satisfy the requirements stated in the beginning of the chapter. The ultra-capacitor system characteristics are summarized in Table 5-5.

Figure 5-2 shows the same acceleration cycle as Figure 5-1 for the vehicle with direct-coupled ultra-capacitor system. For both designs, the basic requirements in Table 5-1 are fulfilled.

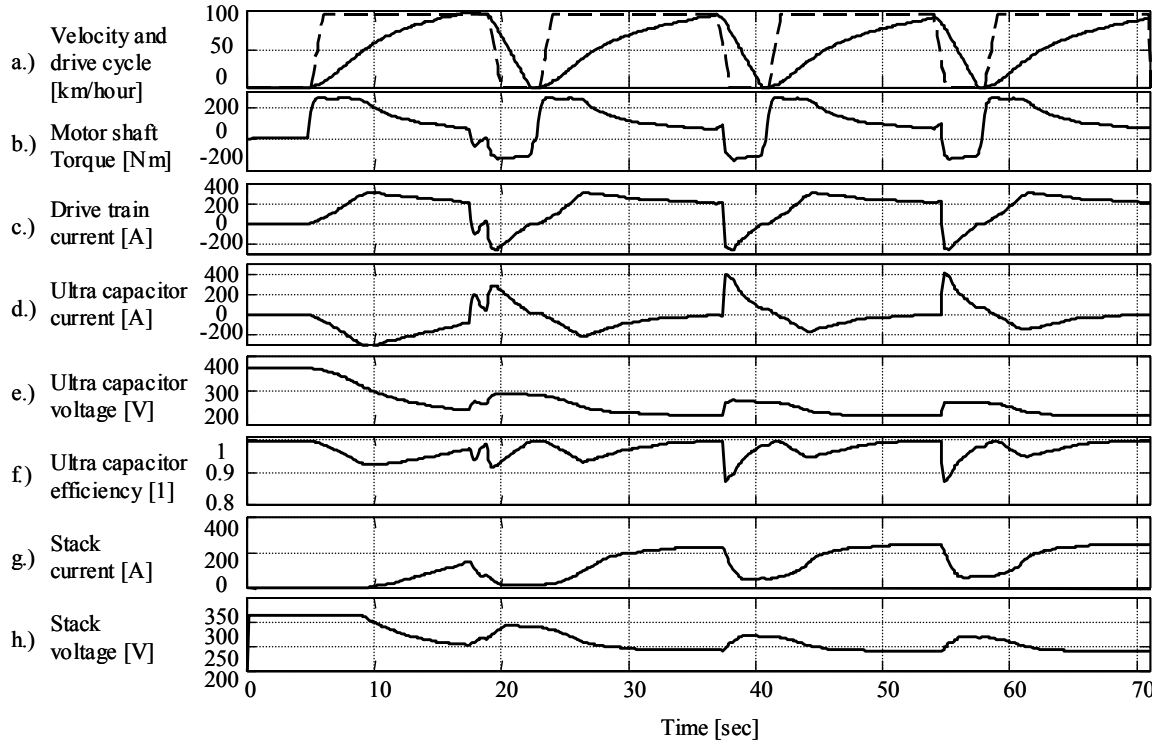

Figure 5-2: Vehicle with direct coupled ultra-capacitor system. Vehicle states for four accelerations from 0 – 60 miles / hour. The standard parameters for regenerative braking have been applied. The initial voltage level of the ultra-capacitor system is 100 % of the maximum voltage.

Table 5-5 shows the ultra-capacitor system characteristics for both vehicle designs.

	Vehicle concept with dc-dc converter (indirect coupling)	Vehicle concept without dc-dc converter (direct coupling)
Ultra-capacitor type	Maxwell PC 2500	Maxwell PC 2500
Number of cells	85 (in series)	136 (in series)
Maximum cell voltage	2.7 V (3.0V short term)	2.7 V (3.0V short term)
Lowest cell discharge voltage	1.35 V	1.35 V
System energy content (from maximum cell voltage to lowest discharge voltage only)	164 Wh	258 Wh
Maximum system voltage	229.5 V (255 V short term)	367 V (408 V short term)
Minimum system voltage (below this voltage discharge is disabled)	115 V	183 V
Ultra-capacitor mass	61 kg	98 kg
System resistance (no cell interconnections considered)	48 milli Ohm	82 milli Ohm
Matched impedance power at lowest voltage (highest voltage)[53]	68.5 kW (274 kW)	102.8 kW (408 kW)
Maximum power for maintaining 95% (90%) efficiency for discharging from maximum voltage to minimum voltage	31 kW (62 kW)	46 kW (92 kW)
DC-DC converter weight (2kW/kg)	37.5 kg	0 kg
System weight including dc-dc converter	98 kg	98 kg

Table 5-5: Ultra-capacitor system configuration for the indirectly (via a dc-dc converter) and directly coupled ultra-capacitor systems.

[53] According to Burke (Burke 1999)

5.4. Simulation Results

As an example application for the model developed in this chapter, the fuel economy for the four different vehicle setups defined in Table 5-2 will be listed for the drive cycles stated in Table 4-1.

The modeled vehicle types are:

- A load following vehicle with internal buffer for reformate,
- A battery hybrid fuel cell vehicle,
- An ultra-capacitor hybrid fuel cell vehicle with indirectly coupled ultra-capacitor system,
- An ultra-capacitor hybrid fuel cell vehicle with direct coupled ultra-capacitor system.

All the vehicles analyzed meet (almost) the PNGV requirements stated in Table 5-1. They are comparable vehicles with respect to their utility for the user.

Besides the comparison of fuel economy, all major energy flows and losses in the vehicle will be stated. The results will be briefly discussed and compared for different drive cycles and for the different vehicle concepts.

The content of this section is not meant to be a vehicle analysis. The results provided are only illustrative and should be understood as an exemplary introduction into the application of the model described in the previous chapter. In addition, they should underline the importance of proper energy management in fuel cell vehicles and how this, if well done, could significantly improve the vehicle fuel economy.

5.4.1. Load Following Fuel Cell Vehicle Model

The first vehicle modeled is the load following vehicle (Figure 5-3). In addition to the main components of this vehicle concepts Figure 5-3 highlights also the energy flows among them.

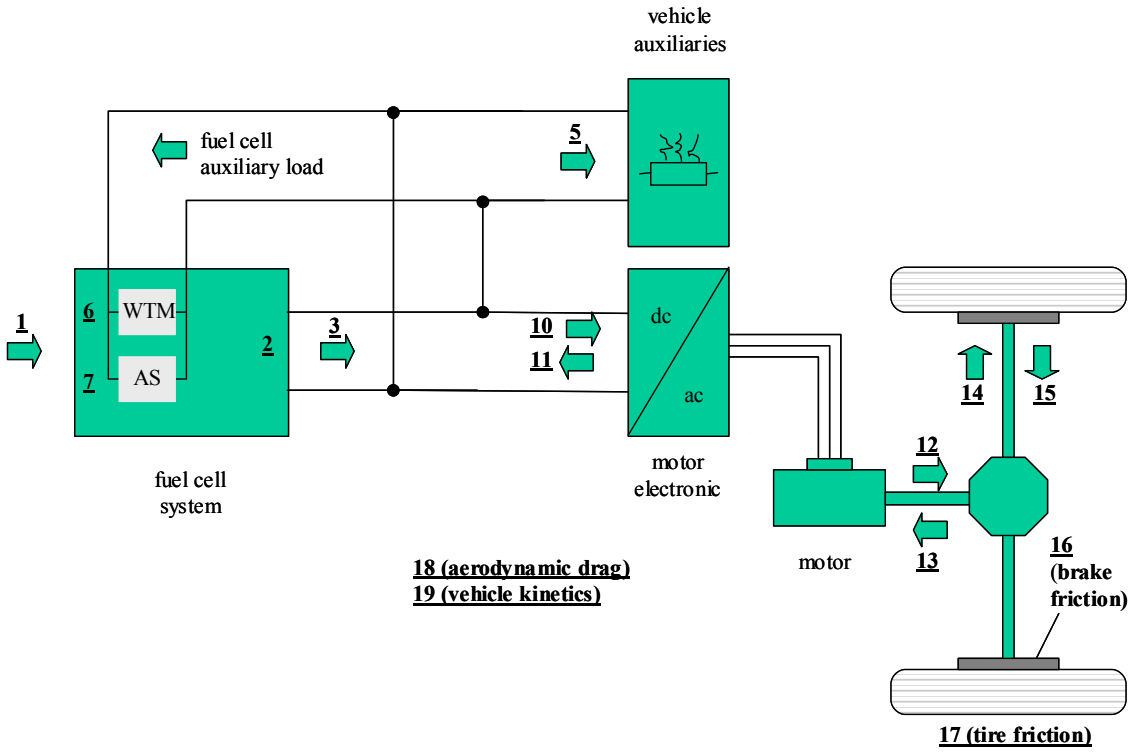

Figure 5-3: Load following fuel cell vehicle. The numbers in the diagram indicate energy flows and component efficiencies and correspond to the columns in Table 4-8.

Corresponding to Figure 5-3, Table 5-6 lists the fuel economy and the energy flow at the various stages of the vehicle for different drive cycles. The results summarized in Table 5-6 will be discussed in the next paragraphs.

Column 1 shows the fuel economy of the vehicle in gallons of gasoline equivalent. Because the vehicles researched in this dissertation are methanol fueled fuel cell vehicles, the heating value of the consumed methanol has to be converted into a

gasoline equivalent to allow a direct comparison with gasoline fueled vehicles. For the conversion from methanol to gasoline equivalent, the conversion factors listed in the appendix have been assumed.

Column 2 shows the fuel cell system efficiency as defined in Equation 4-47. This definition considers that the "cost" of electricity at the stack is not only the methanol converted but also the electric energy consumed by the water and thermal management and the air supply.

Column 3 shows the electric energy / mile drawn from the stack including the fuel cell system auxiliary loads.

Columns 4, 8, and 9 are not addressed for this vehicle type because no additional electric storage device is considered. For the start-up of the fuel cell system a model for a small battery integrated into the fuel cell system has been programmed. The charge difference of this auxiliary battery between start and end of the simulation is zero.

Columns 5, 6 and, 7 represent the auxiliary loads in Wh/mile. The vehicle auxiliary load is assumed to be constant. The air supply and water and thermal management loads depend on the state of the fuel cell system.

Column 10, and 11 state the electric energy provided to the power electronics of the drive train in Wh/mile. The values in parentheses are the regenerated energy (at the motor terminals) in Wh/ mile. For the load following vehicle this energy is 0 Wh/mile because the load following vehicle does not have the feature of regenerative braking. On the electrical side, the following energy balance has to be fulfilled, which could be used as a crosscheck for the consistency of the model:

The energy generated by the fuel cell stack is equal to the sum of all auxiliary loads plus the energy supplied to the electric drive train.

Column (3) = column (5) + column (6) + column (7) + column (10)

Column 12 shows the mechanical energy at the motor shaft supplied to the transmission. The energy ratio of Column 12 and Column 10 is the motor efficiency for the specific cycle. For the case of the FUDS cycle, the efficiency is 77.6%. This efficiency number includes the losses in the power electronics of the inverter. For the FUDS cycle, the efficiency matches the efficiency reported by Ogden (Ogden 1998) of 77%. For the ECE cycle, the motor efficiency of 72.0% matches the motor efficiency reported by Nahmer (Nahmer 1996) of 72.2 % for an induction motor of similar size. However, it has to be acknowledged that an exact comparison is not possible because the differences in the vehicle characteristics (weight, transmission ratio, aerodynamic drag) force the motor to operate at different operating points even if the cycle is the same. Also, the electric motor itself (size, technology) has a significant impact on its efficiency.

Column 13 shows the mechanical energy (in Wh/mile) the transmission provides to the wheels. Similar to the motor efficiency, the transmission efficiency can be calculated (column 13 over column 12). Depending on the drive cycle, the range of the transmission efficiency is changes between 88% to 92%. This corresponds closely to the cycle efficiencies reported by Skudelny (Skudelny 1993) between 85% and 90%. However, no details were provided.

Column 14 shows the energy dissipated in the friction brakes (Figure 5-5). Because the load following vehicle does not have the capability of regenerative braking during phases of deceleration, all the excess kinetic energy has to be dissipated in the

brakes. The braking losses are higher for cycles with more decelerations and accelerations per mile. For example, the braking losses per mile in the USO6 cycle are five times higher than for the Highway cycle. For hybrid vehicles, the braking losses build the potential for regenerative braking.

Column 15 shows the tire friction losses (see also Figure 5-5). It can be seen that the tire friction losses per mile are the same for all drive cycles. The reason is that a constant (velocity independent) friction coefficient was assumed in this calculation. Therefore, the tire friction losses stated in Table 5-6 are only a function of the total vehicle test weight.

If the friction coefficient is velocity dependent, the tire friction changes (increases) with the vehicle velocity. The impact on fuel economy of modifying the tire friction model to a model with a friction coefficient increasing with velocity has been investigated for two cases. In the first case, a friction coefficient increasing linear with velocity has been assumed and in the second case with a friction coefficient increasing with velocity by the power of 2.5 has been assumed[54]. The results of these model variations are summarized in Figure 5-5.

[54] All three tire friction models are discussed in the literature (Gillespie 1992).

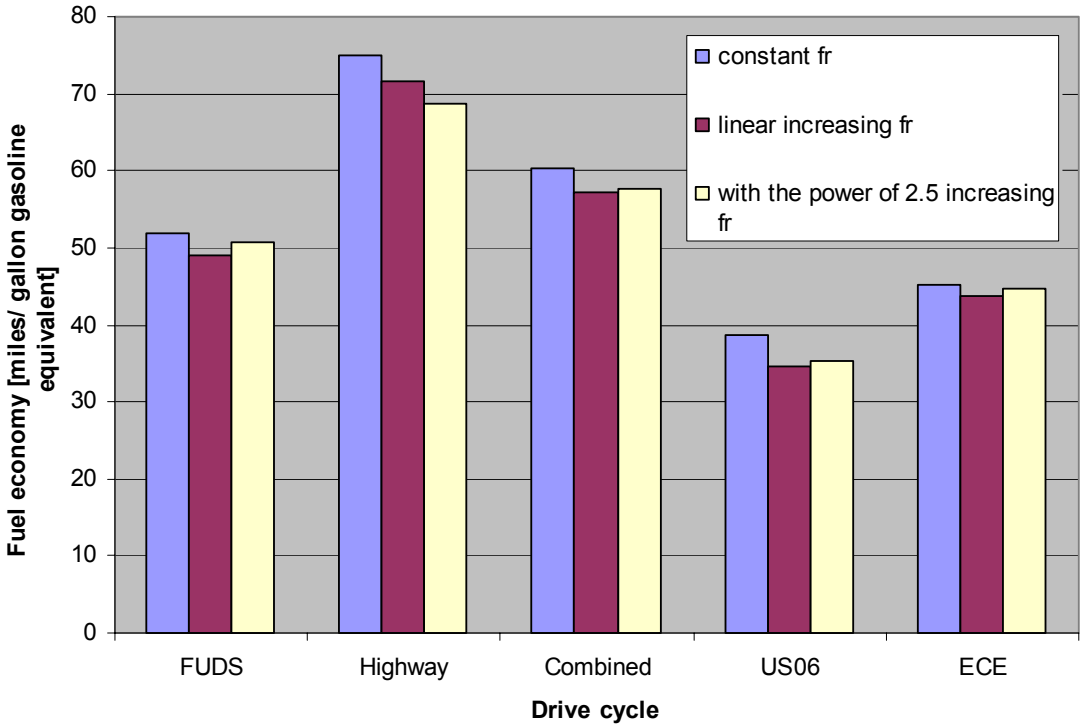

Figure 5-4: Fuel economy of the load following vehicle for different tire friction models: a.) constant friction coefficient fr=0.01 ; b.) friction coefficient increasing linear with velocity, fr=0.01*(1+v/100) ; c.) friction coefficient increasing with velocity into the power of 2.5, fr=0.01*3.24*0.05*(v/100)$^{2.5}$

Figure 5-5 shows that the choice of the tire friction model is especially important for drive cycles with higher average speeds while the impact of the tire friction model on the fuel economy is smaller for low speed cycles. In this analysis, a velocity independent tire friction model (constant friction factor fr) has been applied for all cases.

Column 16 shows the losses due to the aerodynamic drag relative to the brake friction losses and tire friction losses (Figure 5-5). For all cycles except the US06 cycle, the losses are smaller than the losses due to tire friction. The reason is that a relatively small aerodynamic drag coefficient has been assumed (cw=0.2, frontal area A=2m^2). It could be seen that cycles with higher average speeds or with high-speed phases (Highway, US06, EUDC 120) require more energy to overcome the aerodynamic drag than cycles with lower average speeds (ECE, FUDS or J10-15).

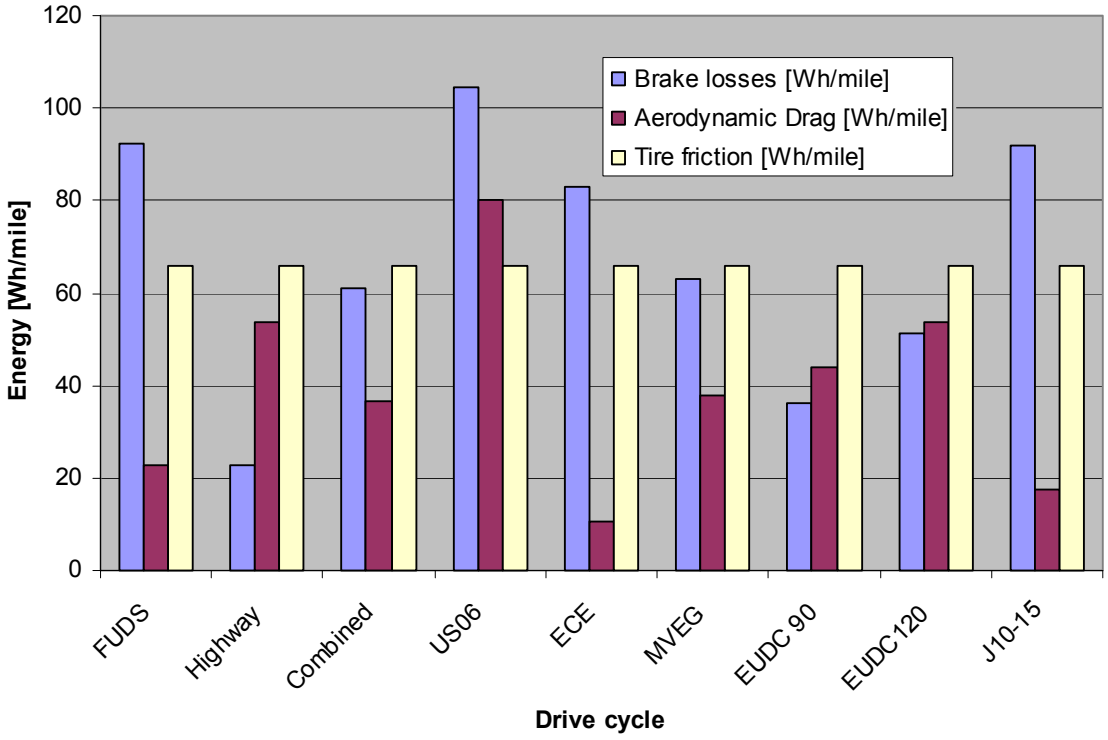

Figure 5-5: Brake losses, aerodynamic drag losses, and tire friction losses for different drive cycles.

At the wheel, a second energy balance has to be fulfilled and could be used as a crosscheck for the consistency of the model.

The energy supplied to the wheels is equal to the sum of brake friction losses, tire friction losses, and aerodynamic drag losses. This energy balance assumes that the vehicle velocity at the end of the cycle is equal to the velocity at the beginning of the cycle. This assumption is unproblematic for the pure load following vehicle because all of the standard cycles start and end with zero velocity and the simulation is normally terminated after one complete cycle. However, for hybrid vehicles this is not necessarily the case. A termination criterion for hybrid vehicles is the equal state of charge of the energy storage at the beginning and end of the simulation. The fulfillment of this criterion might lead to a vehicle velocity at the end of the simulation different to the velocity at the beginning of the simulation. In other words, the kinetic energy stored in the vehicle mass

and wheel inertia is not zero at the end of the cycle. Therefore, for this case, the energy balance has to consider the kinetic energy of the vehicle.

However, for the load following case the simpler energy balance as worded above could be used for crosschecking the results in Table 5-6.

Column (13) = column (14) + column (15) + column (16)

The calculation of the brake, tire friction, and aerodynamic drag losses is purely mathematical and is essentially the solution of Equations 4-9, 4-10, and 4-14. Therefore if:

- The input parameters into the equations are known (vehicle mass, drag coefficient, frontal area, tire friction model, wheel inertia, air density etc.),
- The expressions for the approximation of rolling resistance and aero dynamic drag are considered sufficiently accurate,
- The drive cycle is known,

then the individual losses could be determined within the numerical accuracy of the simulation program. Therefore in such a scenario a validation of the stated energies at the wheel becomes secondary.[55]

The fuel economy for the combined cycle has been derived from the fuel economy of the highway and the FUDS cycle (Equation 5-1).

[55] See also the chapter discussion of the results and model validation.

$$mpg_{combined} = \frac{1}{\frac{0.55}{mpg_{fuds}} + \frac{0.45}{mpg_{hiway}}}$$

Equation 5-1

where:

$mpg_{combined}$ = fuel economy in the combined cycle
[miles/gallon gasoline equivalent]

	1	2	3	4	5	6	7	8	9	10+11	12+13	14+15	16	17	18
Drive Cycle	Equivalent gasoline consumption [miles/ gallon]	Fuel cell system efficiency [1][56]	Electric energy generated by the fuel cell stack [Wh/mile]	Electric energy after dc-dc converter [Wh/mile]	Electric energy into vehicle auxiliaries [Wh/mile]	Electric energy for WTM [Wh/mile]	Electric energy for air supply [Wh/mile]	Electric energy charged into electric storage [Wh/mile]	Electric energy discharged From electric storage [Wh/mile]	Electric energy into drive train [Wh/mile] (regenerative)	Mechanical energy at motor shaft [Wh/mile] (regenerative)	Mechanical energy at wheels [Wh/mile] (regenerative)	Friction losses in brakes [Wh/mile]	Tire friction [Wh/mile]	Losses because of aero drag [Wh/mile]
Federal Urban Driving Schedule (FUDS)	52.0	40.2	295.5	N/A	10.3	5.8	23.1	N/A	N/A	256.3 (0)	199.0 (0)	181 (0)	92.4	65.8	22.8
Federal Highway Cycle	75	44.2	214.2	N/A	4.1	2.9	10.6	N/A	N/A	196.6 (0)	157.4 (0)	142.2 (0)	22.6	65.8	53.8
US O6 Cycle	39	36.4	351.1	N/A	4.2	6.4	22.4	N/A	N/A	318 (0)	271.8 (0)	250.4 (0)	104.7	65.8	80.0
ECE Cycle	45	35.6	321.3	N/A	21.3	9.5	41.6	N/A	N/A	249.0 (0)	179.3 (0)	158.9 (0)	82.8	65.8	10.4
MVEG Cycle	56	41.2	275.5	N/A	10.0	5.6	22.3	N/A	N/A	237.6 (0)	185.2 (0)	166.4 (0)	62.9	65.8	37.8
EUDC 90	70	44.3	229.3	N/A	5.5	3.3	12.9	N/A	N/A	207.6 (0)	162.1 (0)	145.9 (0)	36.3	65.8	43.9
EUDC 120	62	43.2	254.3	N/A	5.2	4	14.2	N/A	N/A	231.0 (0)	188.4 (0)	170.6 (0)	51.1	65.8	53.8
Japanese 10-15	51	40.5	305.1	N/A	14.2	6.9	29.3	N/A	N/A	254.7 (0)	194.9 (0)	175.1 (0)	91.9	65.8	17.5

Table 5-6: Simulation results for the load following (non hybridized) fuel cell vehicle.

[56] As defined in Equation 3-4.

5.4.2. Battery Hybrid Fuel Cell Vehicle Model

This chapter analyzes the battery hybrid version of the fuel cell vehicle introduced in the previous chapter. It should be noted that exactly the same type of fuel cell system has been assumed as in the load following case. The objective is to investigate the energy flows for this type of hybridization and the impacts on the overall vehicle fuel economy. Figure 5-6 shows the component arrangement and the major energy flows. The numbers in Figure 5-6 correspond to the columns in Table 5-9.

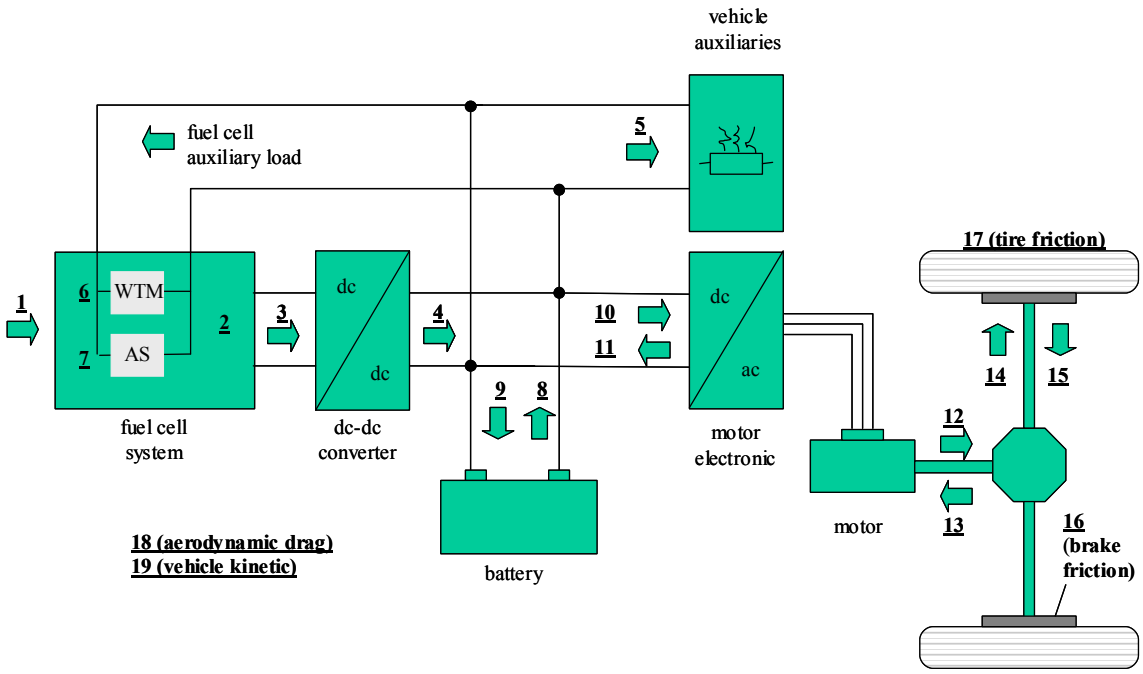

Figure 5-6: Battery hybrid fuel cell vehicle. The numbers in the diagram indicate energy flows and component efficiencies and correspond to the columns in Table 5-9.

The main differences between Table 5-6 (simulation results of the load following vehicle) and Table 5-9 (simulation results for the hybrid vehicle) are:

- Not all the energy provided by the fuel cell stack is available for the various loads. Because the fuel cell stack and the battery are linked via a dc-dc converter only a

fraction (ca. 96% depending on the drive cycle) of the energy at the stack terminals is available for future use. This fraction is listed in column 4.

- Columns 8 and 9 represent the energy discharged (8) and charged (9) into the battery storage system at the battery terminals.
- Columns 10 and 11 represent the electric energy into the electric motor (acceleration mode, 10) and from the electric motor (regenerative braking mode, 11).

With these modifications compared to the load following fuel cell vehicle, the electric energy balance for the consistency check is as follows.

The energy supplied by the dc-dc converter (at the bus side) is equal to the sum of all auxiliary loads plus the difference of charged and discharged energy at the battery terminals plus the difference of acceleration and regenerative energy at the motor terminals.

Column (4) =	column (5) + column (6) + column (7) +	// auxiliary loads
	column (9) – column (8) +	// energy storage
	column (10) – column (11)	// drive train

Columns 12 and 13 list the mechanical motor shaft power supplied by the motor to the transmission.

Columns 14 and 15 show the mechanical shaft power supplied by the transmission to the wheels. AuYeung (AuYeung 2001) reports combined cycle efficiencies of motor and transmission for the motor mode of 80 % and for the regenerative braking mode 65%. The efficiency numbers found in this work are for the motor mode 70% for the FUDS cycle and 71% for the Highway cycle and for the regenerative braking mode 67% for the FUDS cycle and 62% for the Highway cycle. While the efficiency for the regenerative

braking mode matches the efficiencies quoted by AuYeung, the efficiencies in the acceleration mode are 9 percentage points different. Although this difference is considered large, similar to the discussion for the load following vehicle, the difference could be a result of different vehicle, motor, and transmission characteristics.

The fraction of regenerative braking, defined as column (11) over column (10), is 17.6% for the ECE cycle. Nahmer (Nahmer 1996) reports for a different vehicle (Volkswagen Van) a theoretical maximum fraction of regenerative energy of 17.5% for the ECE cycle, assuming that the friction brakes are not used at all. The value found in this work of 17.6% matches well with Nahmer's findings, considering that the friction brakes had been only sparingly used and the value of 17.6% is 96% of the theoretical maximum regenerative energy (friction brake energy 3.3 Wh/mile and regenerated energy 74.1Wh/mile). However, it needs to be recognized that due to the different vehicle characteristics a strict comparison is not possible.

As a consistency check on the mechanical side, the following energy balance could be carried out.

The mechanical energy provided to the wheels minus the mechanical energy taken from the wheels during regenerative braking is equal to the sum of brake, tire and drag losses plus the energy stored in the vehicle kinetics (vehicle mass and wheel inertia).

Column (14) - column (15) = column (16) + column (17) + column (18) + column (19)

Additional checks for consistency are:

- The battery hybrid fuel cell vehicle has slightly higher tire friction than the load following fuel cell vehicle because of the higher weight of the battery hybrid vehicle

- The aerodynamic drag losses are (about) the same for all vehicle types because the body shape stays unchanged. Small differences result from the termination of the simulation (for the hybrid case) at equal states of charge of the energy storage at the beginning and the end of the cycle. Therefore the last cycle is likely to be incomplete for the hybrid cases.
- Because of the termination of the hybrid simulation at zero state of charge difference between the beginning and end of the simulation, the kinetic energy of the vehicle at the end of the simulation has to be considered. This kinetic energy is always positive or zero.
- The energy coming from the fuel cell is getting smaller and smaller with each conversion (motor terminals to wheel).
- The regenerative energy coming from the wheel is getting smaller with each conversion (wheel to motor terminals).
- For the hybrid fuel cell vehicles, the brake friction losses are always smaller than for the load following vehicle (effect of regenerative braking).
- The USO6 drive cycle, as the most dynamic drive cycle, has the highest brake friction losses for all vehicle types.
- For the low dynamic Japanese 10-15 cycle, almost all the brake friction energy of the load following case could be eliminated in the battery hybrid case. Note: The ultra-capacitor case does not allow this due to the limited capacity of the ultra-capacitor.

Operating the system in the regime of high efficiency

The effect of the hybrid control strategy on the operation of the fuel system could be seen by comparing the over the drive cycles averaged fuel cell system efficiencies for the load

following vehicle (Table 5-6, column 2) and the hybrid vehicle (Table 5-9, column 2) [57]. Figure 5-7 is a graphical representation of the above-discussed efficiencies. The efficiency averaged over one drive cycle of the fuel cell system is higher for all investigated drive cycles for the hybrid vehicle than for the load following vehicle. The highest gain in efficiency could be seen for the US 06 cycle. This more demanding drive cycle in terms of acceleration forces the fuel cell system in the load following case to operate a larger fraction of time in the high power regime at low efficiency (Figure 4-22) compared to the battery hybrid case in which the fuel cell system operates on average at low power. Skillful control of the power request from the fuel cell system is therefore one key for high fuel economy. The control strategy applied in this work tries to maximize the fuel cell system efficiency without compromising the charge and discharge losses within the battery.

In addition to the higher fuel cell system efficiency for the battery hybrid case, the comparison of the fuel cell system efficiencies over different drive cycles shows that they are more closely grouped to each other than they are for the case of the load following vehicle. This is also an effect of the control strategy and shows the effectiveness of the control strategy over a wide range of driving patterns (robustness).

[57] Both vehicles use exactly the same fuel cell system with the same maximum power and overall characteristics.

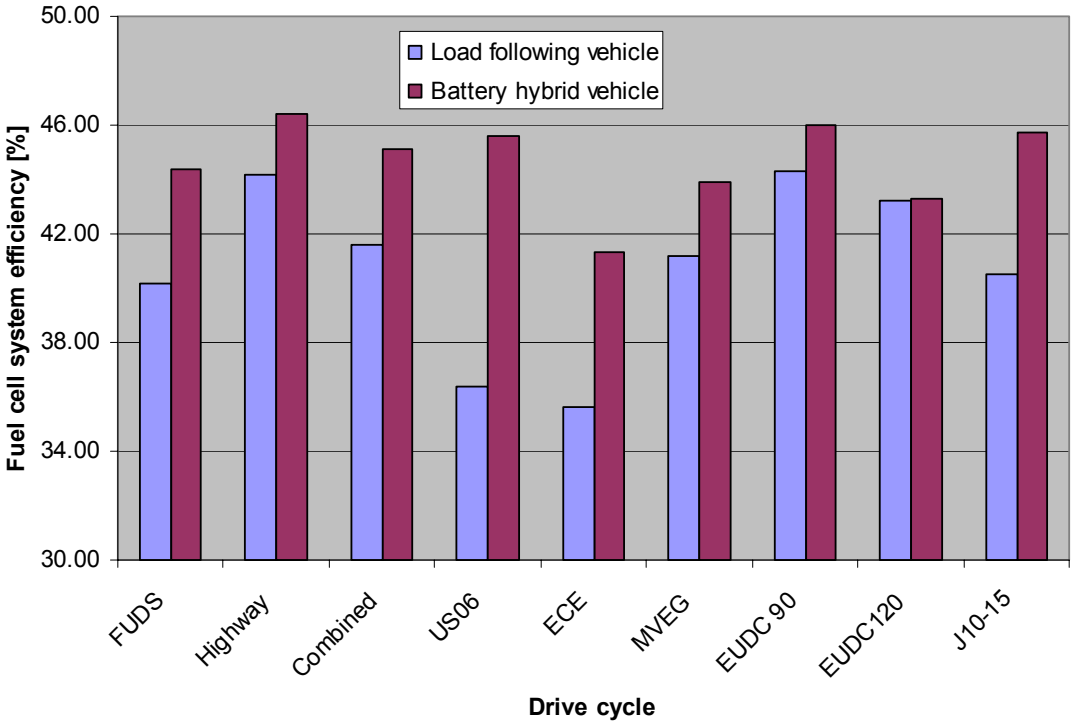

Figure 5-7: Fuel cell system efficiencies for the load following vehicle and the battery hybrid vehicle for different drive cycles. Note that the vertical axis starts at 30% efficiency and not at 0%.

Effect of regenerative braking

The second advantage of the battery hybrid vehicle is the regenerative braking ability. The kinetic energy stored in the vehicle mass and the rotational inertia (wheel, transmission, motor) could be recaptured during deceleration phases and do not have to be dissipated in the friction brakes. During the mode of regenerative braking, the motor operates in a generator mode, taking mechanical energy and converting it into electrical energy, which is then stored in the battery system or feeds directly into the auxiliary loads of the vehicle or the fuel cell system. Figure 5-8 shows the amount of regenerative braking for the different drive cycles at the wheel, the transmission, and the motor terminals. In addition, Figure 5-8 shows the energy dissipated in the friction brakes. The numbers for the standard control parameters c_0 and c_1 are quoted as defined in Table 5-3.

Table 5-7 and Table 5-8 show the fuel economy, the energy recaptured at the wheels, and the energy recaptured at the dc terminals of the motor electronic during braking for the FUDS and Highway cycles. For both cycles, the control parameters c_0 and c_1 are varied, adjusting the regenerative braking function. A detailed explanation of the parameters is provided in the chapter "vehicle controller." The following conclusions could be drawn from Table 5-7 and Table 5-8:

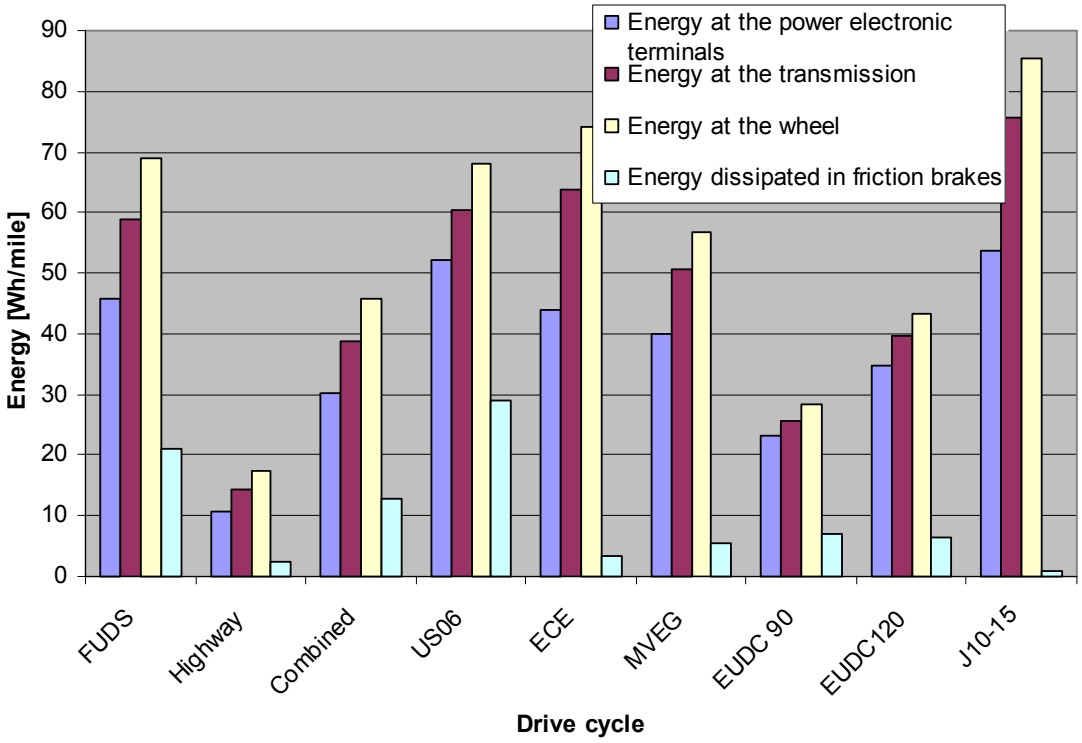

Figure 5-8: Regenerated energy at the wheel, at the motor shaft, and at the terminals of the motor power electronic for various drive cycles. Energy dissipated in the friction brakes for different drive cycles. The parameters for the control of regenerative braking are c_0=0.3 and c_1=0.5 (default parameters)

- For the FUDS cycle, it could be seen that the fuel economy varies significantly from zero regenerative braking (c_0=0, c_1=0) to the point of almost maximum regenerative braking (c_0=0.5, c_1=0.6). At the latter point, 96% of the theoretically retainable energy has been utilized (looking at the wheel). Because of

regenerative braking, the fuel economy could be improved from 47.6 miles/gallon to 58.9 miles/gallon or by 23.7% (Table 5-7 and Figure 5-9).

- For the Highway cycle the fuel economy depends less strongly on the function of regenerative braking. It increases from 67.8 miles/gallon (with zero regenerative braking) to 70.9 miles/gallon or by 4.5%. At the point of maximum regenerative braking, 97% of the energy theoretically retainable at the wheel has been utilized (Table 5-8 and Figure 5-10).
- If the regenerative braking function is only sparsely used (low parameters c_0 and c_1), the efficiency of the energy conversion from the mechanical energy at the wheel to the electric energy at the motor terminals is very poor (e.g. 7 % or 1.8Wh / 24.2 Wh for c_0=0.1 and c_1=0.1 for the FUDS cycle). The reason is that for these cases the motor and transmission are operated in the low power regime. For these operating points, the efficiency is very low compared to the maximum efficiency of each component.
- The maximum cycle efficiency for regenerative braking (the efficiency for the energy conversion from the wheel to the dc terminals of the power electronic) is 72% for the FUDS cycle and 66% for the Highway cycle. The efficiencies are similar to the cycle efficiencies for acceleration (FUDS 70% and Highway 72%).

The theoretical potential for regenerative braking is equal to the energy dissipated in the friction brakes if the function of regenerative braking is disabled. The potential increases with increasing vehicle mass and decreases with increasing aerodynamic drag and rolling friction. For the analyzed vehicle configuration, the theoretical potential for regenerative braking is 91.3 Wh/mile for the FUDS cycle and 22.3 Wh/mile for the Highway cycle.

Regenerative strength c_1 Regenerative exclusive c_0	0	0.1	0.3	0.5	0.6
0.0	**47.6**, 0.0, 0.0	**47.6**, 7.2, 0.6	**48.3,** 18.7, 4.9	**49.0**, 24.4, 9.6	**49.4**, 28.2, 12.0
0.1	**47.6**, 0.0, 0.0	**48.2**, 24.2, 1.8	**49.8**, 30.2, 12.2	**50.7**, 43.5, 23	**51.7**, 49.3 28.4
0.2	**47.6**, 0.0, 0.0	**48.9**, 18.8, 4.4	**50.9**, 40.9, 20.2	**53.3**, 57.6, 36.1	**54.5,** 63.7, 41.8
0.3	**47.6**, 0.0, 0.0	**49.4**, 22.5, 6.5	**52.2**, 50.7, 29.0	**55.2**, 68.8, 45.9	**56.3**, 75.0, 51.5
0.4	**47.6**, 0.0, 0.0	**49.8,** 26.0, 8.6	**53.9**, 58.0, 36.5	**56.7**, 76.2, 52.4	**58.9**, 88.0, 63.5
0.5	**47.6**, 0.0, 0.0	**50.5**, 29.6, 11.0	**54.7**, 64.9, 42.2	**58.2**, 82.8, 58.4	**58.9,** 88.0 63.5

Table 5-7: Recaptured energy through regenerative braking for different control parameters defining the regime of exclusive regenerative braking (c_0) and the strength of regenerative braking (c_1). The total potential energy for regenerative braking is equal to the energy dissipated in the friction brakes if the regenerative braking function is disabled. For the analyzed vehicle this potential is 91.3 Wh. All values are quoted for the FUDS cycle. For each parameter set c_0, c_1, the fuel economy [miles/gallon], the energy regenerated at the wheel [Wh/mile], and the energy regenerated at the terminals of the power electronics [Wh/mile] is stated. The values are calculated for the battery hybrid vehicle configured in Table 5-2.

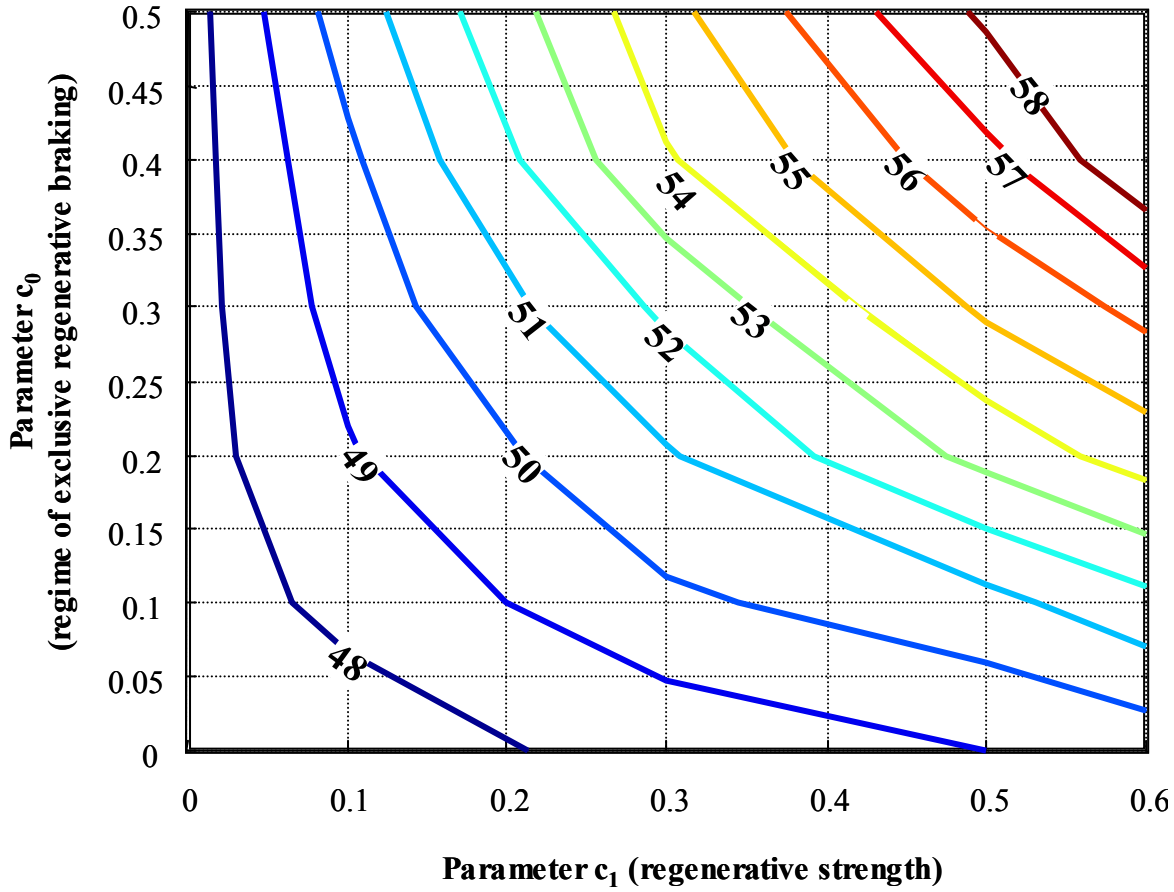

Figure 5-9: Vehicle fuel economy in the FUDS cycle in miles/gallon gasoline equivalent as a function of the regenerative braking control parameters c_0 and c_1.

All energies in the combined cycle have been derived from the equivalent energy values in the Highway and the FUDS cycle according to Equation 5-2.

$$E_{Combined} = 0.55 \cdot E_{Highway} + 0.45 \cdot E_{Fuds}$$

where:

$E_{Combined}$ = Energy in the Combined cycle[Wh/mile] **Equation 5-2**

$E_{Highway}$ = Energy in the Highway cycle[Wh/mile]

E_{Fuds} = Energy in the Fuds cycle[Wh/mile]

Regenerative strength c_1 Regenerative exclusive c_0	0	0.1	0.3	0.5	0.6
0.0	**67.8**, 0, 0	**67.8**, 1.2, 0.1	**68.0**, 5.4, 0.8	**68.1**, 7.2, 1.7	**68.2,** 13.7, 2.2
0.1	**67.8**, 0, 0	**68.2**, 8.7, 0.3	**68.9**, 9.7, 3.2	**69.0**, 13.1, 5.9	**69.4**, 14.4, 7.2
0.2	**67.8**, 0, 0	**68.7**, 7.1, 1.2	**69.2**, 8.3, 5.6	**69.3**, 16.6, 9.5	**69.6**, 17.8 10.8
0.3	**67.8**, 0, 0	**69.0**, 12.4, 1.9	**69.5**, 15.2, 7.7	**70.0**, 17.5, 10.8	**70.4**, 19.7, 12.6
0.4	**67.8**, 0, 0	**69.4**, 9.5, 2.6	**69.5**, 16.9, 9.7	**70.5**, 20.0, 12.9	**70.7**, 20.9, 13.7
0.5	**67.8**, 0, 0	**69.7,** 10.5, 3.3	**69.9,** 18.1, 10.9	**70.7**, 20.9, 13.7	**70.9,** 21.5, 14.3

Table 5-8: Energy recaptured through regenerative braking for the Highway cycle. The total potential for regenerative braking in this cycle is 22.3 Wh/mile (energy dissipated in the friction brakes if the function of regenerative braking is disabled).

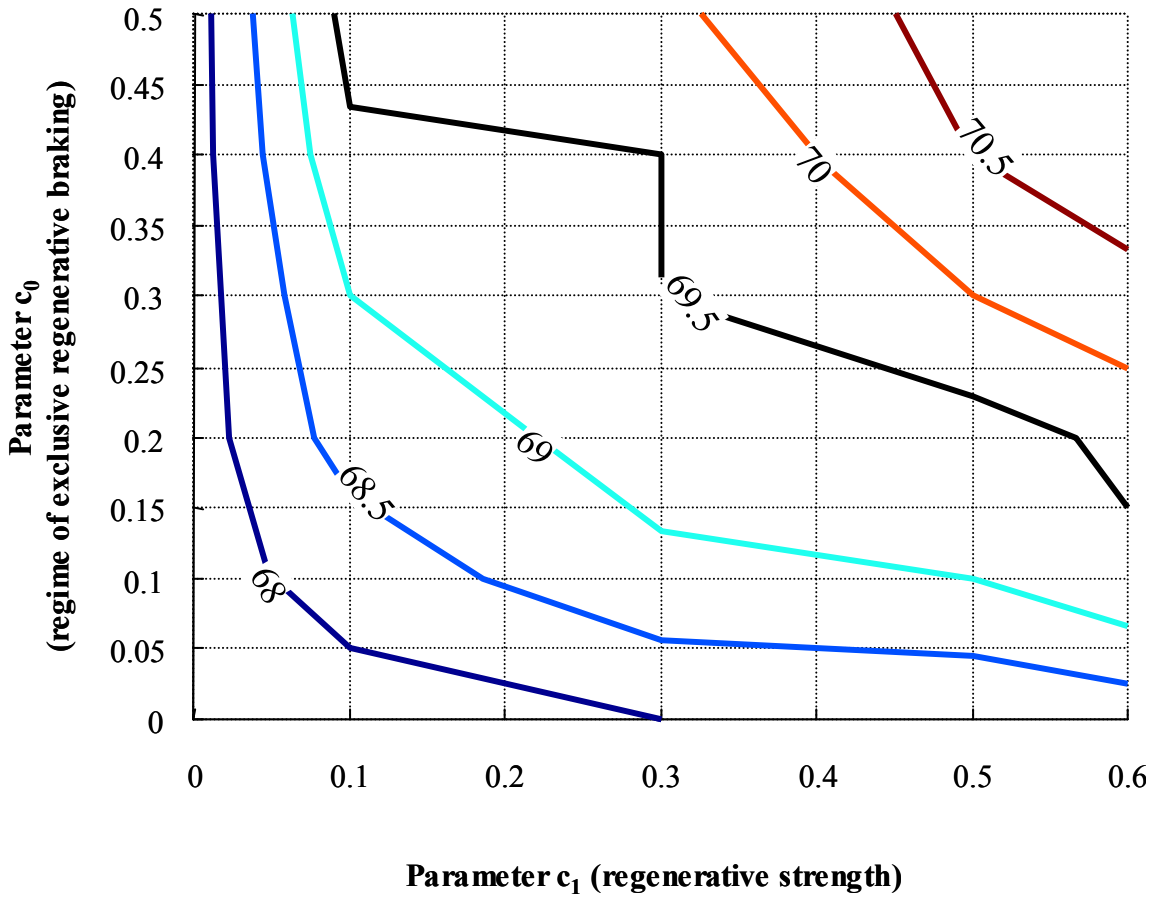

Figure 5-10: Vehicle fuel economy in the Highway cycle in miles/gallon gasoline equivalent as a function of the regenerative braking control parameters c_0 and c_1.

Summary

Compared to the pure load following vehicle the battery fuel cell vehicle shows two advantages, which finally result in higher fuel economy. These are the ability of regenerative braking and the operation of the fuel cell system in the regime of high system efficiency only.

Beyond the two advantages of the battery fuel cell vehicle over the load following fuel cell vehicle, the analysis of the energy flows reveals also one area of potential improvement for the battery hybrid case. All the electric energy generated by the fuel cell stack has to go through the dc-dc converter. The dc-dc converter allows the control of the power flow from the stack into the battery and the drive train. It therefore allows the

operating point of the fuel cell system to be determined.[58] The dc-dc converter could be seen as the actuator for the fuel cell stack current. As such it carries the full fuel cell stack power. Comparing column 3 and column 4 in Table 5-9 shows that the average efficiency of the dc-dc converter is between 94% and 96% depending on the cycle. The static efficiency map of the dc-dc converter is shown in Figure 4-39. Because all the energy fed into the drive train goes through this device, the overall fuel economy is reduced by the efficiency of the dc-dc converter (Figure 5-6).

The next chapter presents an alternative design (Figure 5-11) in which these losses are minimized by applying a different arrangement of components and the involvement of a bi-directional dc-dc converter capable of handling both directions of power flows. The expected result is a higher fuel economy because of the expected reduction in losses.

[58] The hardware configuration also allows the control of the operation point of the battery employing a different operating strategy. In reality, a mixed control strategy considering the battery and the fuel cell system is likely to be implemented.

	1	2	3	4	5	6	7	8+9	10+11	12+13	14+15	16	17	18	19
Drive Cycle	Equivalent gasoline consumption [miles/ gallon]	Fuel cell system efficiency [1][59]	Electric energy generated by the fuel cell stack [Wh/mile]	Electric energy at bus side dc-dc converter [Wh/mile]	Electric energy into vehicle auxiliaries [Wh/mile]	Electric energy for WTM [Wh/mile]	Electric energy for air supply [Wh/mile]	Electric energy discharged (charged) from (into) electric storage [Wh/mile]	Electric energy into drive train (regeneration) [Wh/mile]	Mechanical energy at motor shaft (regeneration) [Wh/mile]	Mechanical energy at wheels (regeneration) [Wh/mile]	Brake friction losses [Wh/mile]	Tire Friction losses [Wh/mile]	Aero drag losses [Wh/mile]	Kinetic Energy at simulation end [Wh/mile]
Federal Urban Driving Schedule (FUDS)	55	44.4	273.0	263.0	10	6.5	24.5	198.4 (205.1)	261.1 (45.9)	199.4 (59.0)	182.9 (68.8)	21.2	69.0	23.7	0.4
Federal Highway Cycle	70	46.4	222.5	211.4	4.2	3.6	12.0	87.6 (90.5)	199.5 (10.8)	159.3 (14.3)	144.4 (17.5)	2.5	69.0	53.7	1.7
US O6 Cycle	49	45.6	318.8	300.1	4.2	5.1	16.6	161.0 (172.0)	315.2 (52.1)	266.4 (60.3)	247.5 (68.1)	29.0	69	79.1	2.5
ECE Cycle	47	41.3	302.3	292.6	21.8	11.2	46.2	256.9 (264.2)	250.1 (44.0)	176.3 (63.9)	158.8 (74.1)	3.3	69.0	10.3	2.3
MVEG Cycle	57.5	43.9	259.6	249.2	10.4	6.6	25.1	156.6 (161.7)	241.9 (40.1)	185.7 (50.7)	169.0 (56.6)	5.4	69	36.2	1.9
EUDC 90	69	46.0	224.7	213.2	5.5	4.0	14.1	93.9 (97.4)	209.3 (23.1)	163.2 (25.6)	148.1 (28.3)	6.9	69.0	43.9	0
EUDC 120	63.7	43.3	242.6	231.0	5.2	4.3	15.2	103.9 (95.8)	233.3 (34.9)	188.8 (39.8)	172.6 (43.4)	6.5	69	53.8	0
Japanese 10-15	55	45.7	264.4	255.0	14.2	7.8	31.4	201.2 (196.5)	250.5 (53.6)	188.5 (75.7)	178.2 (85.4)	0.81	69	17.4	0

Table 5-9: Simulation results for the Battery Hybrid Fuel Cell Vehicle. The simulation was terminated after 20Ah had been charged into the battery system and the final state of charge was equal to the initial state of charge or after 10 cycles were completed (whichever occurred first).

[59] As defined in Equation 3-47.

5.4.3. Ultra-Capacitor Hybrid Fuel Cell Vehicle Model (indirect coupling)

Figure 5-11 shows an alternative design for the battery fuel cell hybrid described in the previous chapter (Figure 5-6). In this design, the electric energy storage is not directly involved in the main power path from the fuel cell stack to the electric drive train. As a consequence, the dc-dc converter connecting the fuel cell stack and the energy storage is also not involved in this path. Therefore the losses in this device and in the energy storage itself are expected to be lower than in the previous battery hybrid fuel cell design.[60]

[60] Compared to the battery hybrid fuel cell vehicle not only the component arrangement but also the energy storage itself and the control strategy have been changed. The change from batteries to ultra capacitors is considered secondary. The principal characteristics of the design in Figure 4-5 would stay unchanged if the ultra capacitor system were replaced by an adequate battery. However the change in the control strategy is significant and the difference in overall fuel economy is partly due to this change. While for the battery fuel cell vehicle the fuel cell current was the controlled variable, in the current design the storage current is controlled while the fuel cell stack current is floating. It could also be said that the battery vehicle had more the characteristic of a range extender vehicle while the current vehicle is a power assist vehicle.

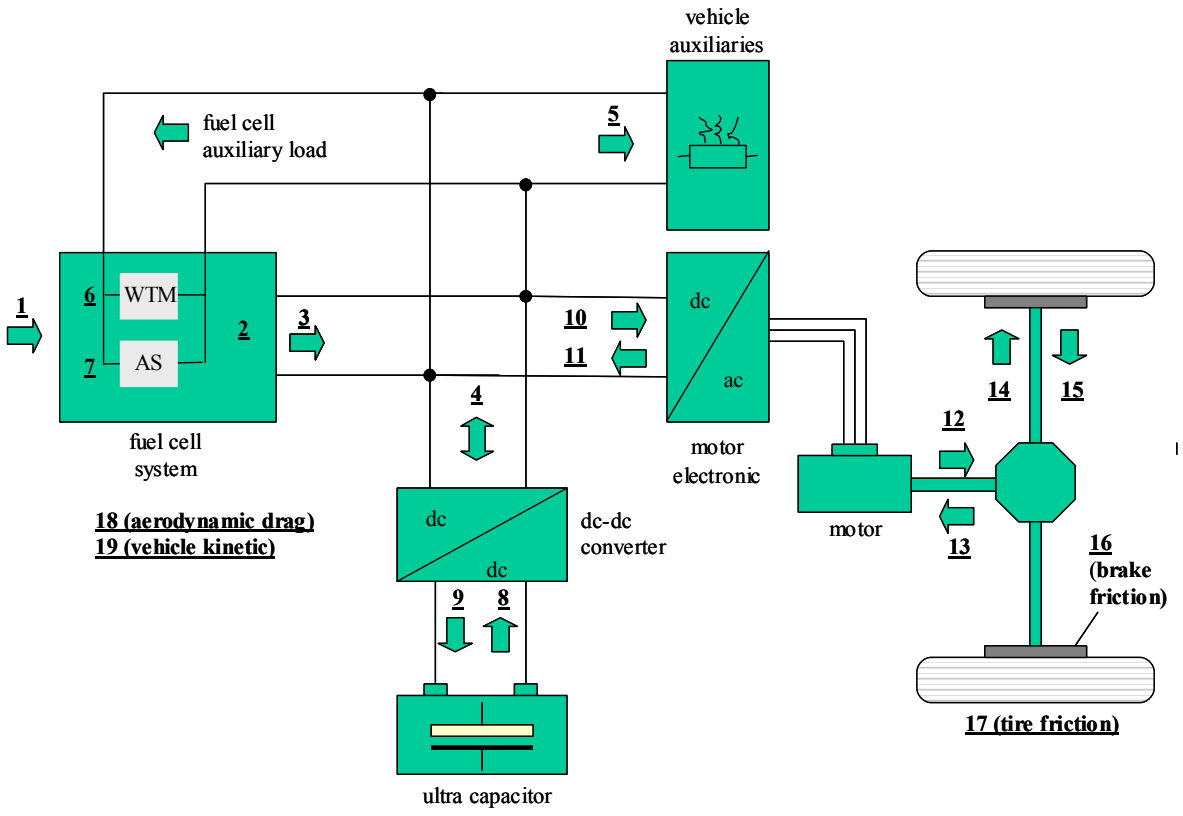

Figure 5-11: Ultra-capacitor fuel cell vehicle (indirect coupling). The numbers in the diagram indicate energy flows and component efficiencies and correspond to the columns in Table 5-10

Comparing the energy discharged and charged from the energy storage between the battery hybrid fuel cell vehicle (Table 5-9, columns 8 and 9) and the ultra-capacitor hybrid fuel cell vehicle (Table 5-10, columns 8 and 9) reveals that the energy turnaround for the battery hybrid fuel cell case is several times higher (3 times for the US06 cycle and 17 times for the ECE cycle) than for the ultra-capacitor case. The reason for the lower energy turnaround for the ultra-capacitor case is the different control strategy asking for assisting power from the ultra-capacitor storage only if the fuel cell stack voltage drops below a lower threshold.

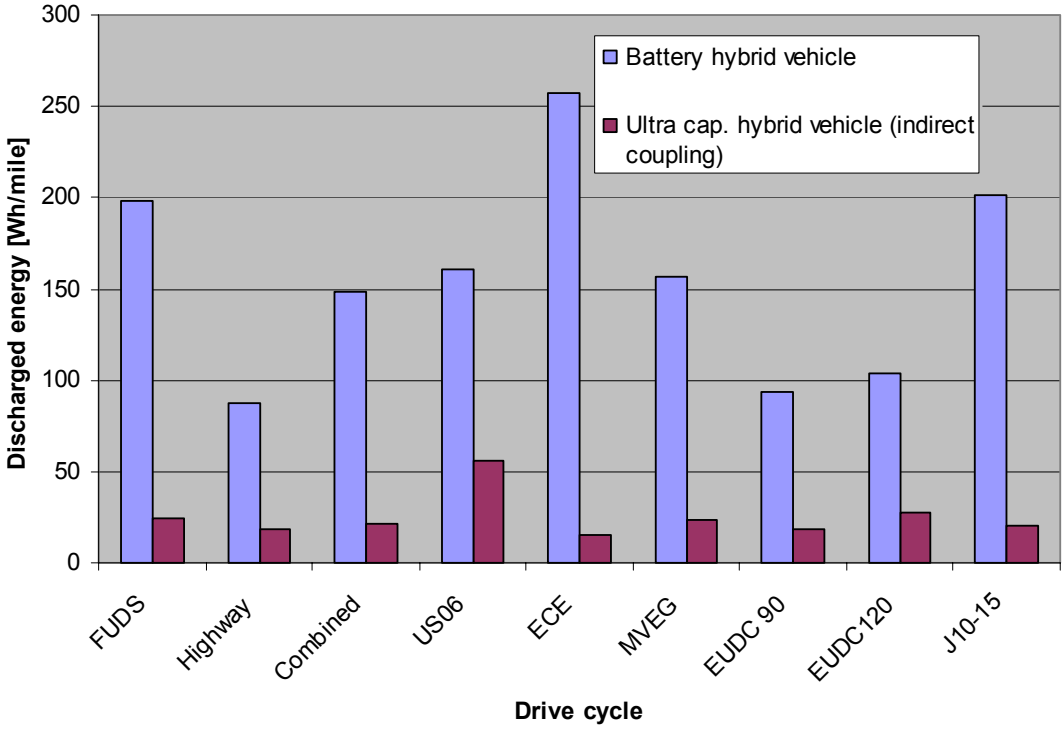

Figure 5-12: Energy per mile discharged from the storage system for different drive cycles for the battery hybrid and the ultra-capacitor hybrid fuel cell vehicle.

Figure 5-12 shows the above-discussed differences in energy turnaround in graphical form (discharged energy only). The lower energy turnaround results in significantly fewer losses and thermal and electrochemical stress and therefore longer lifetime of the energy storage. However, the lower energy turnaround in the storage system in the component arrangement shown in Figure 5-12 is not bound to the use of ultra-capacitors. Similar results are expected if the ultra-capacitor system is replaced with high power battery storage. Linked to the lower energy turnaround in the ultra-capacitor are lower losses in the dc-dc converter, which additionally benefits the fuel economy of the vehicle.

As a result of the design improvement (control strategy and component arrangement), the fuel economy for the indirect ultra-capacitor hybrid vehicle is between

2% and 10% higher for most cycles than for the battery hybrid vehicle. The highest gain (ca. 10%) could be reached in the FUDS cycle while the Japanese 10-15 cycle shows only a gain of about 2%. The only cycle showing lower fuel economy for the ultra-capacitor design than for the battery hybrid design is the US06 cycle (Figure 5-13).

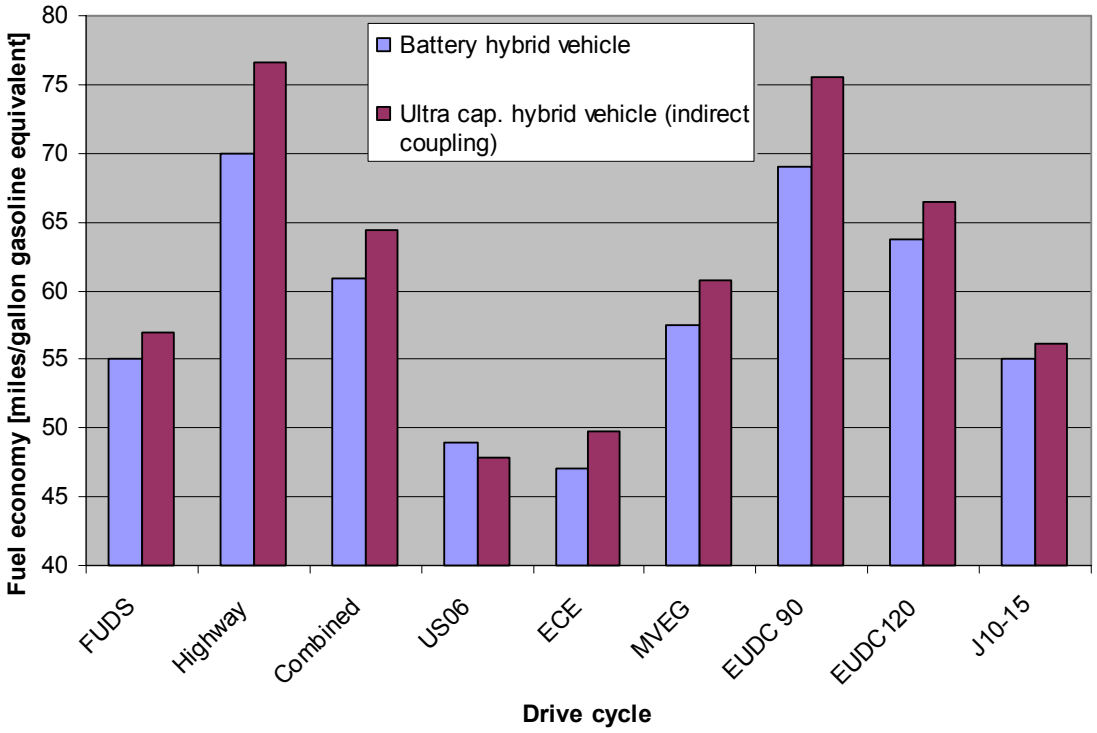

Figure 5-13: Fuel economy of the battery hybrid vehicle and the ultra-capacitor hybrid vehicle for different drive cycles in miles / gallon gasoline equivalent. Note: The vertical axis starts at 40 mpg. Therefore the differences between the cycles are magnified.

A closer look into the US06 cycle simulation reveals that the capacity of the ultra-capacitor is not high enough for a sufficient load leveling in this cycle. As a result, the fuel cell system is forced to operate more often in the regime of higher power equivalent to lower efficiency. Consequently the fuel cell system efficiency (averaged over the drive cycle) for the US06 cycle is lower for the indirect ultra-capacitor hybrid design than for the battery hybrid design. If the comparison had assumed a battery of equal size for both

cases it is expected that the fuel economy for the US06 cycle would follow the trend of the other cycles.

The disadvantage of this vehicle concept is that it relies heavily on a fast-responding fuel cell system if ultra-capacitors are used as electrical storage. If the fuel cell system is slow- responding, more energy for compensating the shortfalls has to be supplied by the ultra-capacitor system. A given size ultra-capacitor system would be more often discharged and not ready to supply the shortfall. The consequences would be performance losses in these situations together with a drop in efficiency. The performance loss is because of the drop in the bus voltage. The efficiency drop has two reasons: First, for a given cycle for slower systems, more energy will charged and discharged into and from the storage. The associated losses in the dc-dc converter and the storage itself result in lower overall efficiency and fuel economy. Second, the fuel cell system efficiency drops with the stack voltage.

An additional potential difficulty associated with the design in Figure 5-11is the only “weakly” determined bus voltage. The bus voltage, serving as main control variable, is only determined by the capacitors inside the drive train electronic. The capacity of this drive train electronic is on the order of 10,000 uF. Assuming the maximum bus current is 400A and the desired controllability for the bus voltage is 2V, the control loop including power electronics for maintaining the voltage within the 2V tolerance has to respond within 50 usec. This leads to a minimum switching frequency for the power semiconductors of 20 kHz. Although this value is not extremely high (Brosch 2000) and could be reduced with additional capacitors at the bus side or by widening the voltage tolerance, the control of the overall system bears a potential risk.

The next chapter introduces a further improvement of the current ultra-capacitor hybrid design, addressing the capacity shortage[61] and the increasing losses for the case of slower-responding fuel cell systems. In addition the problem of the only weakly determined bus voltage will be solved. The final result is a fuel cell hybrid vehicle optimized in many aspects.

[61] The replacement of the ultra capacitor system with a battery could also solve the capacity shortage.

	1	2	3	4	5	6	7	8+9	10+11	12+13	14+15	16	17	18	19
Drive Cycle	Equivalent gasoline consumption [miles/ gallon]	Fuel cell system efficiency [1][62]	Electric energy generated by the fuel cell stack [Wh/mile]	Electric energy at bus side dc-dc converter [Wh/mile]	Electric energy into vehicle auxiliaries [Wh/mile]	Electric energy for WTM [Wh/mile]	Electric energy for air supply [Wh/mile]	Electric energy discharged (charged) into (from) electric storage [Wh/mile]	Electric energy into drive train (regeneration) [Wh/mile]	Mechanical energy at motor shaft (regeneration) [Wh/mile]	Mechanical energy at wheels (regeneration) [Wh/mile]	Brake friction losses [Wh/mile]	Tire friction losses [Wh/mile]	Aero drag losses [Wh/mile]	Kinetic energy [Wh/mile]
Federal Urban Driving Schedule (FUDS)	57.0	45.8	272.8	N/A	10.3	5.5	22.2	24.4 (25.4)	261.2 (35.0)	199.6 (47.3)	183.1 (57.0)	34.0	69.4	22.8	0
Federal Highway Cycle	76.6	47.8	211.3	N/A	4.2	2.9	10.5	18.0 (18.0)	200.6 (11.6)	160.4 (15.3)	145.4 (19.1)	3.1	69.4	53.8	0
US O6 Cycle	47.8	43.5	308.2	N/A	4.2	5.2	17.0	56.0 (58.8)	315 (46.4)	265.9 (53.7)	246.9 (60.8)	36.8	69.4	80.0	0
ECE Cycle	49.7	44.2	302.8	N/A	21.1	9.3	41.1	15.2 (25.3)	253 (39.5)	180 (58.1)	166.2 (66.0)	16.4	69.4	10.5	0
MVEG Cycle	60.7	46.5	260.0	N/A	10.0	5.4	21.5	23.1 (24.9)	241.9 (26.9)	186.8 (37.5)	170.0 (41.9)	21	69.4	37.8	0
EUDC 90	75.5	48.2	216.2	N/A	5.5	3.2	12.5	18.5 (20.1)	211.9 (22.9)	165.1 (25.3)	149.9 (27.4)	9.2	69.4	43.9	0
EUDC 120	66.4	47.3	241.2	N/A	5.2	3.7	13.2	27.8 (30.8)	235.8 (26.4)	191.1 (32.6)	174.8 (35.5)	16.1	69.4	53.8	0
Japanese 10-15	56.1	46.3	280.6	N/A	14.1	6.7	28.7	20.7 (24.1)	257.4 (37.9)	194 (59.6)	177.7 (66.8)	23.4	69.4	17.5	0

Table 5-10: Table of results for the ultra-capacitor hybrid fuel cell vehicle (indirect coupling).

[62] As defined in Equation 3-47.

5.4.4. Ultra-Capacitor Hybrid Fuel Cell Vehicle Model (direct coupling)

The previous chapter introduced a fuel cell hybrid vehicle with indirect (via a dc-dc converter) coupling between ultra-capacitor and fuel cell system. In this chapter, a vehicle design is simulated with a directly (via a diode) to the stack coupled ultra-capacitor system[63] (Figure 5-14). The expected advantages for this system compared to the indirectly coupled system are:

- Increased energy storage capacity: Because no dc-dc converter is necessary a larger capacitor could be installed, maintaining the same overall vehicle weight.
- Increased efficiency: Because the design works without a dc-dc converter, the overall efficiency increases (no converter losses).
- Simplicity: The ultra-capacitor voltage determines the bus voltage. No complex and expensive control schemes are necessary for maintaining the bus voltage within the upper and lower limit.

[63] For simulation purposes only an inductor is placed in series with the diode between the fuel cell stack and the ultra capacitor.

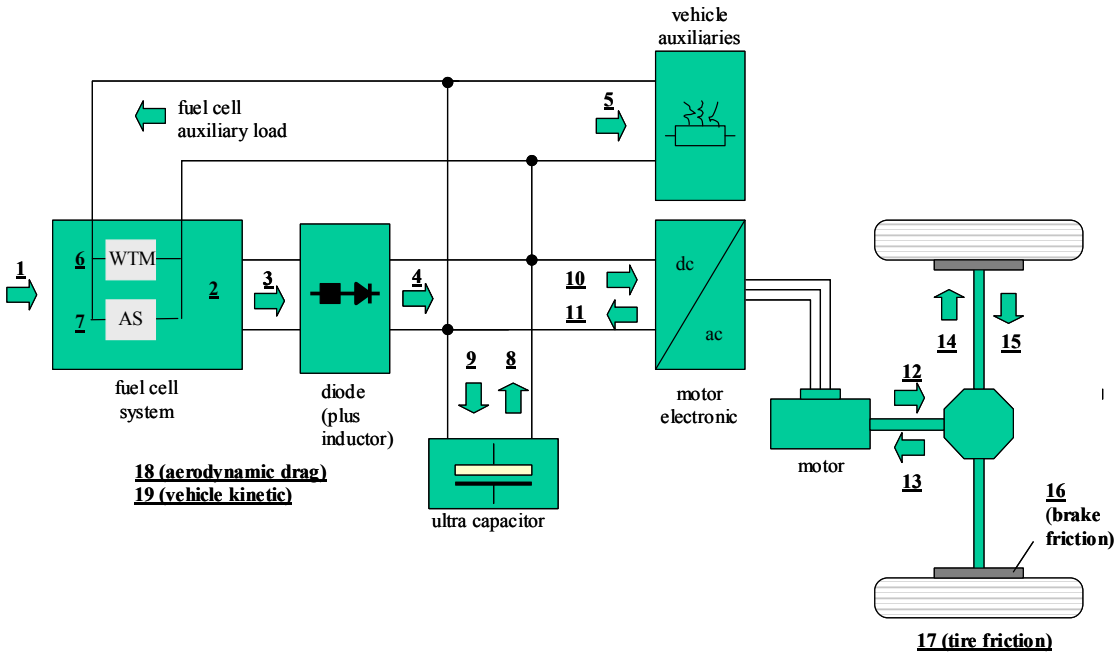

Figure 5-14 Ultra-capacitor fuel cell vehicle (direct coupling). The numbers in the diagram indicate energy flows and component efficiencies and correspond to the columns in Table 5-11.

However, similar to the previous design, the current design relies also on the transient response characteristics of the overall system. For slower responding systems, a larger capacitor has to be installed.

The comparison of the simulation results between the indirect-coupled system and the direct-coupled system reveals:

- The fuel economy for the vehicle with direct-coupled ultra-capacitor system is between 2% (EUDC 90) and 11 % (US06) higher than for the indirect-coupled system (Figure 5-15).
- The average fuel cell system efficiency is about the same for both ultra-capacitor vehicles for most drive cycles. Only the increase of 2.9 percentage points for the US06 cycle for the case of the direct-coupled system appears to be significant (Figure 5-16).

- The direct-coupled system makes a higher use of the ultra-capacitor storage device (more Wh/mile charged and discharged) than the indirect-coupled system. However, it makes still less use of the storage than the battery hybrid system.
- The energy fed into the drive train terminals is almost the same for both systems in all cycles. The largest difference (1.2% or 4 Wh/mile) can be seen for the USO6 cycle.
- The regenerated energy at the dc terminals of the power electronics (but also at the motor shaft and the wheel) is higher for the vehicle with direct-coupled ultra-capacitor system for all drive cycles except for the Highway cycle (Figure 5-17).
- The differences in regenerated energy correspond to the differences in the brake friction losses. For cycles with a significantly higher fraction of regenerative braking (comparing the indirect- and the direct-coupled design), the brake friction losses are smaller.

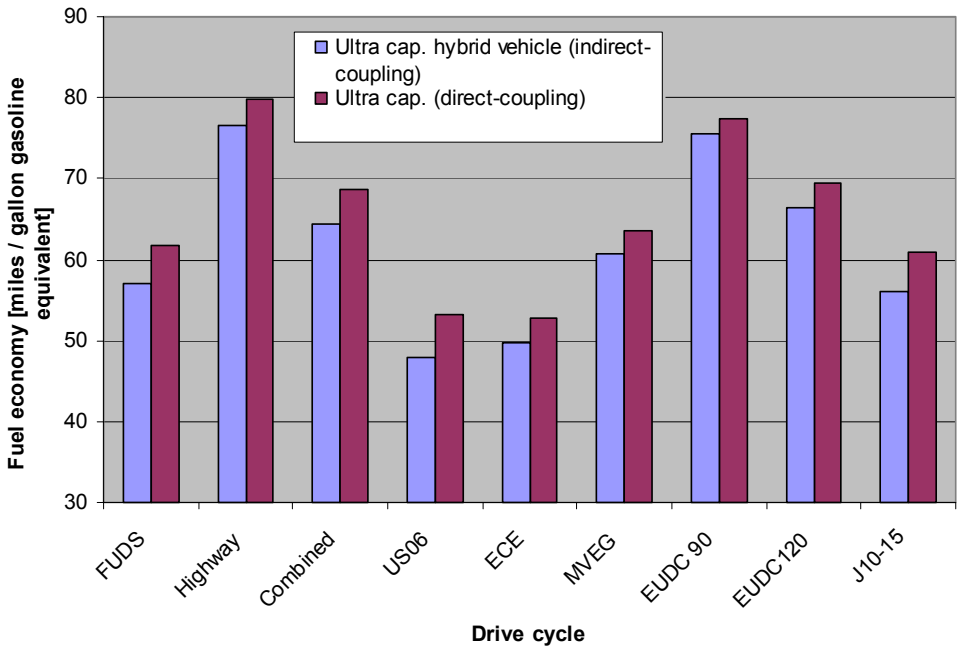

Figure 5-15: Fuel economy for the vehicles with direct-coupled and indirect-coupled ultra-capacitor systems for different drive cycles.

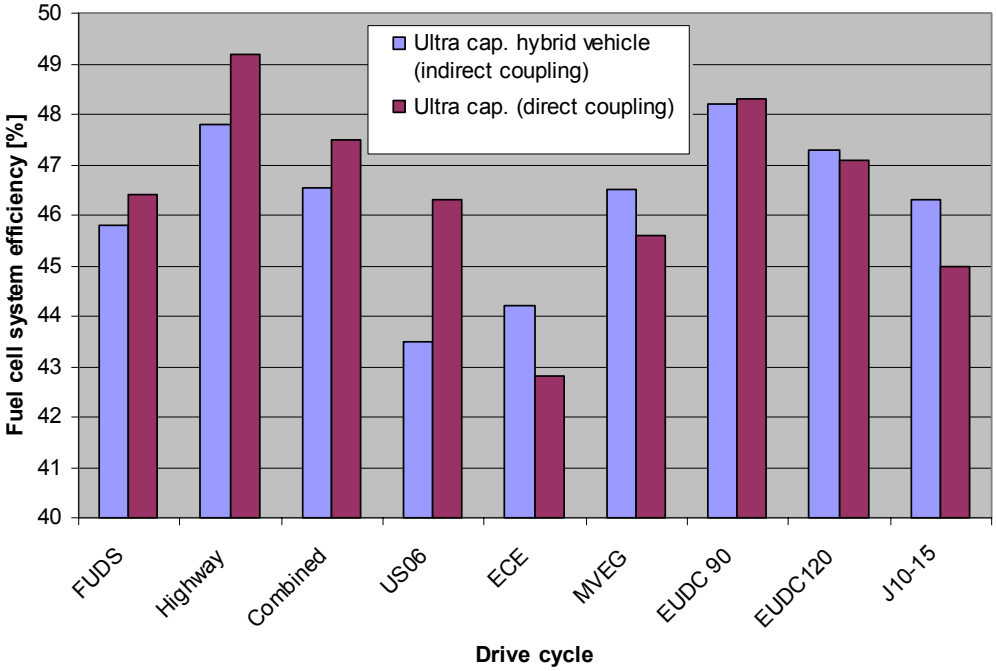

Figure 5-16: Fuel cell system efficiency for the vehicles with indirect-coupled and direct-coupled ultra-capacitor system for different drive cycles. Note that the vertical axis starts at 40%.

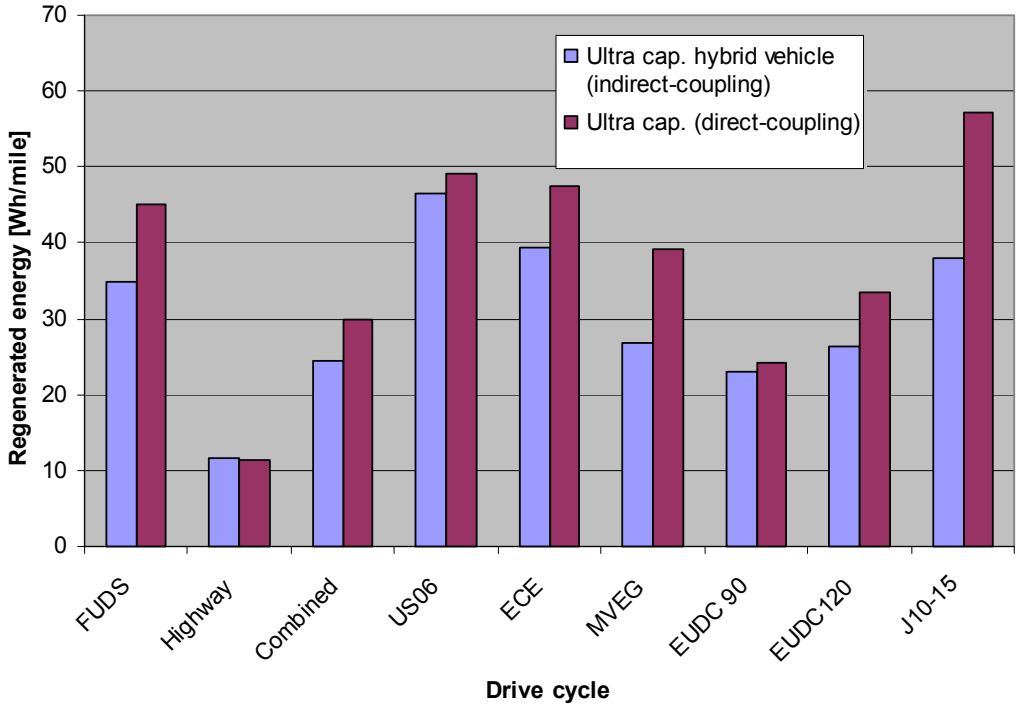

Figure 5-17: Regenerated energy for the vehicles with indirect and direct-coupled ultra-capacitor systems.

From comparing the friction brake losses for the vehicle with direct-coupled capacitor in Table 5-11, column 16 with the brake friction losses for the indirect-coupled system in Table 5-10, column 16 could be concluded that the higher fuel economy for the direct-coupled design is due to a more intense use of the regenerative braking function. The vehicle with direct-coupled ultra-capacitor system uses the mechanical friction brake more sparely for the same drive cycles. The reason for this is twofold:

- For the direct-coupled vehicle, the installed ultra-capacitor storage capacity is larger. Therefore for the case of the direct-coupled vehicle regenerative, braking was less often limited and the friction brakes were not used so often.[64]
- The control strategy for the indirect-coupled vehicle had been optimized for the satisfaction of the acceleration requirements. Therefore the control strategy aims to maintain an almost fully charged capacitor. However this is a disadvantage for regenerative braking because not all the additional energy can be accepted at all ultra-capacitor states. For decelerations in which the ultra-capacitor is already charged, the braking energy has to be dissipated in the friction brakes.[65]

Beyond this, the comparison between the direct-coupled ultra-capacitor fuel cell vehicle (Table 5-11) and the battery hybrid fuel cell vehicle (Table 5-9) reveals that the direct-coupled fuel cell vehicle suffers no constraints in regenerative braking due to limited storage capacity.

[64] A larger capacitor would also benefit the indirect-coupled design. However, the increase would also increase the weight of the overall vehicle. In this scenario, the sum of ultra capacitor and dc-dc converter weight were held constant for both designs.

[65] For the vehicle with an indirect-coupled ultra capacitor system a different control strategy maintaining a lower average voltage in the ultra capacitor might lead to improved fuel economy. However, this also leads to compromises in vehicle performance (slower acceleration).

	1	2	3	4	5	6	7	8+9	10+11	12+13	14+15	16	17	18	19
Drive Cycle	Equivalent gasoline consumption [miles/ gallon]	Fuel cell system Efficiency [1][66]	Electric energy generated by the fuel cell stack [Wh/mile]	Electric energy at bus side inductor [Wh/mile]	Electric energy into vehicle auxiliaries [Wh/mile]	Electric energy for WTM [Wh/mile]	Electric energy for air supply [Wh/mile]	Electric energy discharged (charged) into electric storage [Wh/mile]	Electric energy into drive train (regenerated) [Wh/mile]	Mechanical energy at motor shaft (regenerated) [Wh/mile]	Mechanical energy at wheels (regenerated) [Wh/mile]	Friction losses in brakes [Wh/mile]	Tire friction [Wh/mile]	Losses because of aero drag [Wh/mile]	Kinetic energy [Wh/mile]
Federal Urban Driving Schedule (FUDS)	61.7	46.4	254.8	253.1	10.3	5.0	20.8	115.7 (117.4)	260.4 (45.1)	198.4 (58.1)	181.8 (68.2)	21.5	69.4	22.8	0
Federal Highway Cycle	79.8	49.2	208.2	206.3	4.2	2.7	10.0	37.8 (38.8)	199.9 (11.4)	159.7 (15.0)	144.8 (18.7)	2.9	69.4	53.8	0
US O6 Cycle	53.1	46.3	294.6	289.3	4.2	4.4	14.9	103.8 (107.8)	310.9 (49.1)	262.3 (56.7)	243.4 (63.8)	30.1	69.4	80.2	0
ECE Cycle	52.8	42.8	276.1	274.9	21.2	8.9	39.9	122.6 (123.6)	251.5 (47.5)	178.5 (67.3)	160.8 (77.6)	3.5	69.4	10.4	0
MVEG Cycle	63.5	45.6	243.3	240.9	10.0	5.2	21.1	80.0 (77.7)	241.7 (39.2)	186.7 (49.5)	169.9 (55.2)	7.6	69.4	37.8	0
EUDC 90	77.3	48.3	211.7	209.7	5.5	3.2	12.3	41.6 (43.1)	211.4 (24.2)	164.9 (26.8)	149.6 (29.2)	7.3	69.4	43.8	0
EUDC 120	69.4	47.1	229.8	226.8	5.2	3.6	13.3	53.5 (56.3)	235.4 (33.5)	190.7 (38.2)	174.5 (41.5)	9.9	69.4	53.8	0
Japanese 10-15	61.0	45.0	250.1	249.5	14.2	6.3	27.4	125.8 (127.6)	257.1 (57.3)	193.6 (80.5)	177.2 (89.5)	0.9	69.4	17.5	0

Table 5-11: Simulation results for the ultra-capacitor hybrid fuel cell vehicle (direct coupling; simulation for 10 complete cycles, small (< 10Wh) difference in state of charge at the beginning and end of the simulation).

[66] As defined in Equation 3-47.

5.5. Summary of the Simulation Results

The results provided are by no means a complete vehicle analysis. However they reveal some interesting aspects, which will be summarized in this chapter.

Four different vehicle concepts have been simulated: a load following fuel cell vehicle, a battery hybrid fuel cell vehicle, an ultra-capacitor hybrid fuel cell vehicle with dc-dc converter between stack and ultra-capacitor, and an ultra-capacitor fuel cell vehicle with an ultra-capacitor connected directly (via a diode) to the stack terminals.

All four vehicles use exactly the same indirect methanol fuel cell system and an only slightly scaled electric drive train (Table 5-2). Differences in design are in the technology (high power batteries or ultra-capacitors), the integration of the energy storage system, and the applied control logic. The differences in the energy storage system lead also to small differences in the overall vehicle test weight. The load following vehicle weighs 1501 kg, while the battery electric vehicle weighs 1562 kg and both ultra-capacitor vehicles weigh 1583 kg (Table 5-2). All four vehicles meet or are close to the PNGV standards (Table 5-1) but do not exceed them significantly.

Applying the model described in chapter five, it has been shown that with skillful component arrangement and control of the energy flow the fuel economy could significantly be improved (Figure 5-18).

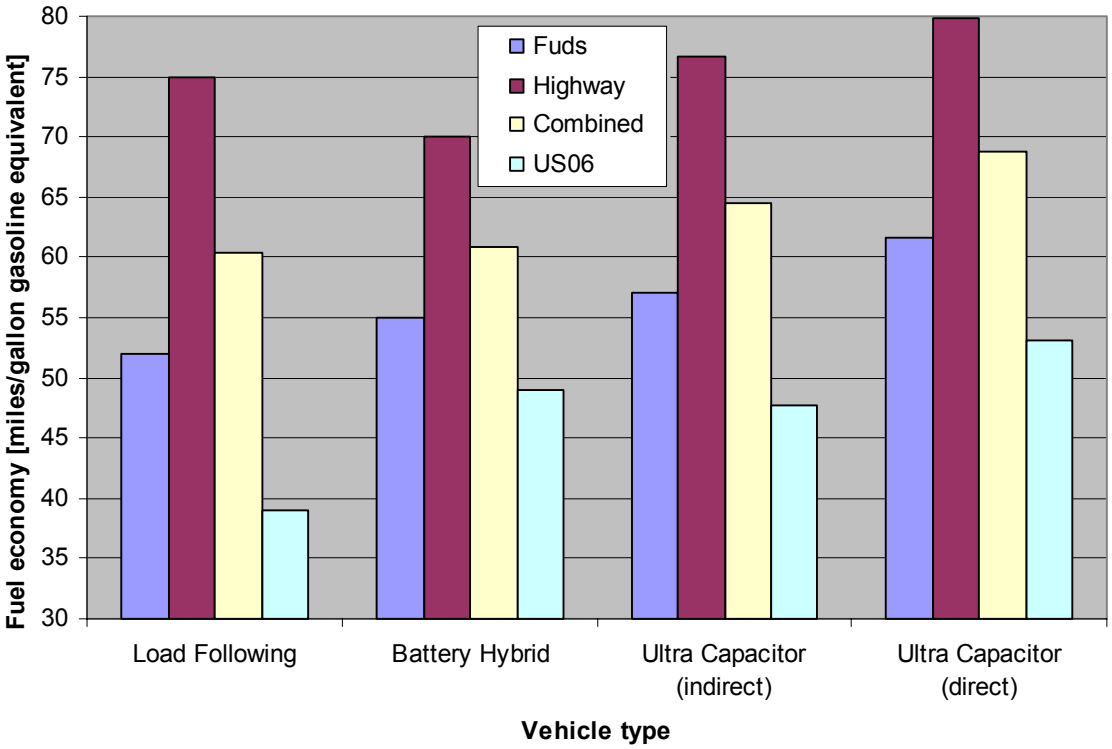

Figure 5-18: Fuel economy for the different vehicles analyzed. Vertical axis starts at 30mpg.

For the four drive cycles shown (FUDS, Highway, Combined cycle and US06), the vehicle with the directly coupled ultra-capacitor system provides the highest fuel economy. The increase relative to the load following vehicle is 18.5% for the FUDS cycle, 6.4% for the highway cycle, and 36.1% for the US06 cycle. The fuel economy improvement in the combined cycle is 14%.

Three effects are responsible for the gain in fuel economy. These are:

- The operation of the fuel cell system in the regime of higher efficiency (equivalent to the operation at low power but not very low power, Figure 4-22),
- The feature of regenerative braking,
- The integration of the energy storage into the overall vehicle design,

Figure 5-19 shows the fuel cell system efficiency for all four vehicle types for the FUDS, the Highway, the Combined, and the US06 cycle.

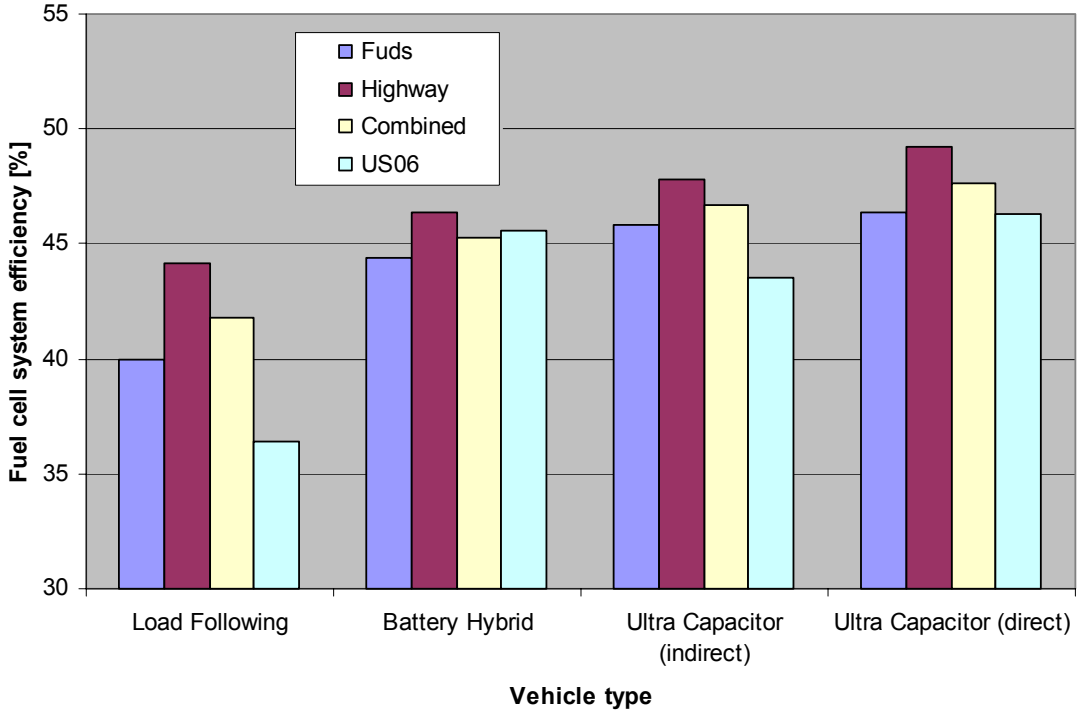

Figure 5-19: Fuel cell system efficiency for the different vehicles. Vertical axis starts at 30% efficiency.

The largest percentage point increase occurs at the transition from the pure load following vehicle to a hybrid design. For the transition from the load following design to the direct ultra-capacitor design, the gain is ca. 6 percentage points for the FUDS cycle, 5 percentage points for the Highway cycle, and 10 percentage points for the US06 cycle. The drop in efficiency from the battery hybrid design to the indirect ultra-capacitor hybrid design for the US06 cycle is a result of the capacitor limitations (regenerative braking) of the latter.

Figure 5-20 shows the fraction of the theoretical energy (brake energy) that is recaptured by the regenerative braking function. The maximum theoretical energy that

could be recaptured is the energy, which would be dissipated at the friction brakes if no regenerative braking occurs. This potential increases with the vehicle weight. The value is zero for the load following vehicle for all drive cycles because this vehicle type does not include the possibility of regenerative braking.

The drop for the indirect ultra-capacitor vehicle for the FUDS and US06 cycle is a result of the limited capacity of the ultra-capacitor together with the applied control strategy. The capacitor had been sized for meeting the acceleration requirements and not for the requirements of regenerative braking. There is no drop for the Highway cycle because the amount of regenerated energy in this cycle is significantly smaller than for the other cycles and could easily be accepted by the ultra-capacitor.

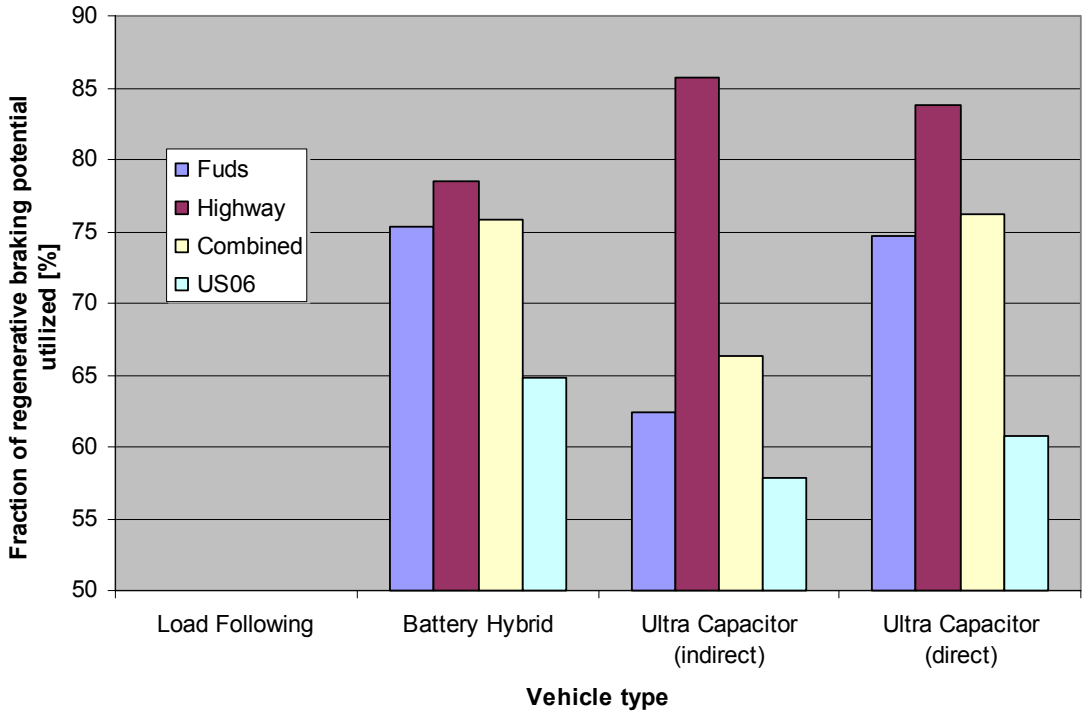

Figure 5-20: Fraction of the theoretical energy potential utilized by the regenerative braking function. The theoretical energy potential for regenerative braking is the energy that would be dissipated in the friction brakes if the regenerative braking function were disabled. The ratio is provided for the energy at the wheel. Note: The vertical axis starts at 50%.

The discussion shows that although fuel cell vehicles offer significantly higher efficiency than internal combustion engine vehicles and, if hybridized, include the feature of regenerative braking, it is still a challenge to reach the PNGV fuel economy goal of 80 miles / gallon gasoline equivalent for the combined cycle. The sensitivity analysis and the regression equations show that the reduction of the vehicle weight is the most promising measure to accomplish the PNGV 80 miles /gallon target, given that the drag coefficient and frontal area could not be further reduced for mid size passenger vehicles for 6 occupants.

Besides the improvement of fuel economy, the hybridization of fuel cell vehicles is motivated by:

- The feature of rapid drive away (battery vehicles),
- Limited fuel cell system dynamic response (battery and ultra-capacitor vehicles).

Each of the areas on its own provides enough incentive for researching hybrid fuel cell vehicles as an option to the pure load following fuel cell vehicle. The model introduced could serve as a tool for this research.

6. Verification of the Results

After the formulation and test of the model. the computed results need to be verified with experimental results or other sources of information (e.g. literature). Depending on this verification, the model could then be improved with respect to its prediction accuracy about the investigated system characteristics.

The system investigated in this work is a fuel cell vehicle in a load following and three different hybrid configurations. The expected results are fuel economies for different drive cycles as well as acceleration times, elasticity, top speed, and component stress (energy flows). In a broader sense, also, the applied control algorithms could be seen as results and transferred into existing prototyping hardware. Therefore verification in this area is also desired.

For the verification of a vehicle model some sources (Heath 1996) suggest the comparison of the overall vehicle characteristics of a prototype vehicle with the model predictions. If both match the model is considered verified. This method is only satisfying if only the total vehicle characteristics are of interest and the inside could be treated as black box. However this is not the case in this work. As stated in the previous paragraph also internal energy flows and even control algorithms are also of great interest. Therefore the model verification has to go beyond the “black box” approach.

In principle the model could be verified using three different sources of information for the verification. These are:

- Existing prototype hardware,
- Other simulation models and the results computed by them,
- Literature.

All three methods of variation have, in part, been applied in the verification process of this work.

Wheel energy

For the validation of the energy supplied to the wheels, the aerodynamic drag losses, and tire friction losses, a comparison with the simulation package Advisor 3.0 has been undertaken. The load following vehicle defined in Table 5-2 serves as basis of the comparison. However, for the comparison of the "energy at the wheel," only the vehicle weigh, the drag coefficient, the frontal area, and the tire friction coefficient have to be kept constant in both simulations. The same air density has to be assumed for getting comparable results.

The results of this comparison are summarized in Figure 6-1.

Figure 6-1 shows that almost no difference for the aerodynamic drag loss and the tire friction loss between the models exists. The remaining small differences could not be tracked down and are assumed to have their reason in the totally different calculation schemes of both models. The (significant) differences in the total energy supplied to the wheels and the brake friction losses could not be tracked down because of the complex calculation scheme in Advisor. However, it can be assumed that the differences are due to different methods of accounting the individual losses. However, a final conclusion could not be drawn.

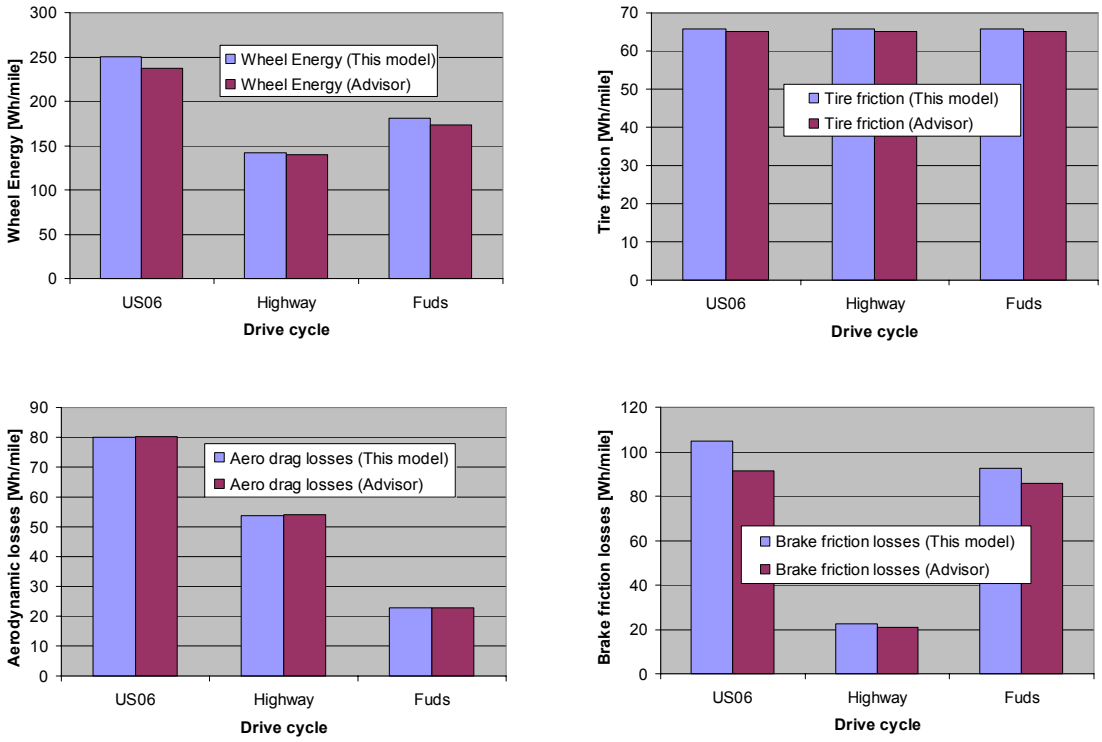

Figure 6-1: Comparison of wheel energy, tire friction losses, aerodynamic drag losses, and brake friction losses between the model developed in this work and Advisor. Note: For both cases the same air density 1.168 kg/m^3 was assumed. Advisor does not compute directly comparable friction brake losses.

Components

The energy provided to the wheels (during acceleration) as well as the regenerative energy during phases of deceleration in hybrid designs is provided by the electric motor through the transmission to the wheels. A battery or ultra-capacitor system serves as energy storage in the hybrid designs. For the validation of these components, the method of comparison of results with existing prototype hardware was applied (Table 6-1).

Component	Component model based on data from:	Component model validated with other sources?
Electric motor	Volkswagen AG	Motor efficiency, torque speed characteristic, inertia -> (Nahmer 1996)
Transmission	Volkswagen AG	Peak efficiency (Ford Ecostar 2001)
Battery	UC Davis Battery Laboratory	Manufacturer data (Shin Kobe, Ovonic, Hawker, Bolder)
Ultra-capacitor	UC Davis Battery Laboratory	Manufacturer data (Maxwell)

Table 6-1: Experimentally validated component models

The Fuel cell system includes the main components, methanol steam reformer, CO clean up stages, fuel cell stack, and the air supply system including expander. Besides these main components auxiliaries, such as the cooling system, a water management system, and anode air bleed have been modeled. All these components and processes have been validated with data from the literature.

Validation of Controls

The highest uncertainty of the model is the area of controls. This includes the controls for the processes inside the fuel cell system as well as the controls on the vehicle side.

The main control loops inside the fuel cell system are the controls for the methanol supply to the fuel processor, the methanol supply to the burner, the air compressor, the water management and the cooling system.

The main control loops outside the fuel cell system are the controls for the dc-dc converter determining the power distribution between fuel cell system and electrical energy storage (battery, ultra-capacitor), the motor controller, the controls for regenerative braking (based on the state of charge of the energy storage), and additional

safety controls for avoiding overpowering of the fuel cell system and the electric energy storage.

Because of the unavailability of data, an in-depth validation of the control elements in the model was not possible. However, the model supports such a validation process through its structure. Similar to the hardware design in existing vehicles, the model incorporates individual controllers for the electric motor, the battery, the ultra-capacitor controller, the overall vehicle, and individual components within the fuel cell system. This setup allows the validation of control algorithms through the employment of rapid prototype techniques.

The choice of control strategies and controller parameters is based on the component characteristics and the objective of achieving the highest fuel economy while maintaining the minimum performance required for meeting the minimum vehicle performance.

Complete vehicle

Several sources quote fuel economies and other vehicle properties for fuel cell vehicles of different designs (e.g. Ricardo Consultants, MIT, Princeton University). However, because of the unavailability of a complete set of data and the underlying assumptions made it has been decided not to compare this model with the literature on an aggregated vehicle level. Major shortcomings of the literature reviewed are in areas of controls, regenerative braking, and the fuel cell system characteristics.

In addition, for cases for which the data sets are more complete, the unavailability of some of the applied modeling programs (Princeton University) makes a comparison of this model on the vehicle level questionable.

A validation with existing hardware was also not possible. Reasons are:

- The high level of confidentiality,
- The fact that most (if not all) currently existing vehicles have the character of 1st prototypes, which are not optimized and are in their current state inferior to the "close to production" vehicles assumed in this work,
- The ultra-capacitor fuel cell vehicles and the battery fuel cell vehicle topologies have not been realized yet.

Hauer (Hauer 2000) compared this program qualitatively with other available programs (Advisor, Psat, Simplev, UC-Davis hydrogen). A quantitative comparison of the load following vehicle model with other programs has been done by Hoefgen (Hoefgen 2001).

7. Summary and Conclusion

In this work a new analysis tool for fuel cell vehicles and fuel cell hybrid vehicles has been developed.

The differences to existing models are:

- The modeling of the fuel cell system has been done in a dynamic manner and is not based on steady state efficiency maps.
- The modeling of the interaction between the electric drive train and fuel cell system has been done in a dynamic manner with current, voltage, and the acceleration pedal position as the interfacing variables between both systems.
- The possibility to analyze different hybrid topologies e.g. a directly to the stack connected ultra-capacitor versus via a dc-dc converter coupled ultra-capacitor.
- The more fundamental modeling of regenerative braking compared to other published models (one important aspect for the proper determination of fuel economy of hybrid vehicle designs)
- The strict separation of component models and control algorithms. This separation increases the transparency of the model and allows a more accurate analysis of existing prototype vehicles. In addition, the assignment of control algorithms to component specific control blocks prepares the model for use in a rapid prototyping development process.

In the second part of this work, the model has been applied to analyze the following vehicle concepts:

- A load following fuel cell vehicle,
- A battery hybrid fuel cell vehicle,
- An ultra-capacitor hybrid fuel cell vehicle with ultra-capacitor system coupled to the stack via dc-dc converter,
- An ultra-capacitor hybrid fuel cell vehicle with ultra-capacitor system coupled directly to the stack.

For ease of comparison, the individual vehicles have been designed on an equal performance basis (same or similar acceleration, pay load, and top speed). The tank to wheel energy analysis of the different vehicles allows the ranking of the concepts according to their fuel economy (the metric used has been the fuel economy in the FUDS, the Highway, the Combined, and the US06 cycle). All of the analyzed vehicles use exactly the same indirect methanol fuel cell system. Differences are in the size of the electric motor, the vehicle weight, and the concept itself (hybrid, non hybrid, and component arrangement).

It has been found that:

- All analyzed hybrid fuel cell vehicles show significant improvement in fuel economy over the load following case.
- The reasons for the fuel savings of the hybrid designs are the higher fuel cell system efficiency (averaged over a drive cycle) and the additional feature of regenerative braking.

- The fuel savings depend largely on the hardware and software integration (control algorithm) of the energy storage into the overall vehicle.
- The vehicle with ultra-capacitor connected directly in parallel to the fuel cell stack offers simple storage integration and the highest fuel economy of all designs. The savings of this vehicle type compared to the load following vehicle are 18% in the FUDS, 6% in the Highway, 14% in the combined, and 36% in the US06 cycle.

Besides the potential improvement of fuel economy, multiple other reasons for hybridizing a fuel cell vehicle exist. These are:

- Design simplifications in the fuel cell system because of the reduced transient fuel processor requirements in hybrid vehicles.
- The feature of rapid cold start and drive away using energy stored in the electric storage (battery).
- A potential reduction in cost as long as battery or ultra-capacitor cost per unit power are lower than fuel cell system cost.
- The provision of higher peak power (increased vehicle performance) in hybrid designs (maybe even with the same electric drive train, allowing short term overload conditions).

None of the above areas have been investigated in this work. However, they are important questions to answer on the way to an optimal fuel cell vehicle design. The

model developed in this work could serve as a tool for a systematic analysis of the optimal vehicle.

Because of the relative simplicity (compared to the hybridization of an IC engine vehicle), the potential benefits of the hybridization of fuel cell vehicles should not be dismissed.

All simulations were carried out using the same indirect methanol fuel cell system with steam reformation process. In addition to the indirect methanol system the fuel cell modeling group of the University of California, Davis provides models compatible with the vehicle model for an indirect hydrocarbon and for a direct hydrogen fuel cell system. A compatible model for a direct methanol system is planned.

8. References

Argonne National Laboratories (2000), *PSAT 4.0 CD Rom, Help Function*

Argonne National Laboratories (2000), *GCtool Help Documentation*

AuYeung F., J.B. Heywood, A. Schafer (2001), *Future Light –Duty Vehicles: predicting their Fuel Consumption and Carbon Reduction Potential*, SAE 2001-01-1081

Aerovironment (2001), *Product Information ABC 150*

Badrinarayanan, P. (2000), *The implications of water and thermal management parameters in the optimization of an indirect methanol fuel cell system*, American Institute of Aeronautics and Astronautics, paper number 2000-3046

Boeing Inc. (1999), Easy5 Demo Disk and User Guide, The Boeing Company PO Box 3707, MC 7L-46, Seattle WA 98124-2207, Internet address: http://www.boeing.com/easy5

Bosch, R. (1991), *Kraftfahrzeugtechnisches Taschenbuch*, 21.edition

Bowman, John L. and Akiva, Moshi Ben (1996) *Activity-Based Travel Forecasting*, Massachusetts Institute of Technology. (Authors email address: jlbowman@mit.edu)

Bronstein I.N., Semendjayev K.A. (1985), *Handbook of mathematics*, translation edited by K.A. Hirsch., 3rd completely rev. ed. Thun H. Deutsch ; New York

Brosch, P., J. Landrath (2000), *Leistungselektronik*, Vieweg Verlag, ISBN 3-528-03879-9

Burke, Andrew (1995), *Ultracapacitors for Electric and Hybrid Vehicles- Performance Requirements, Status of the Technology, and R&D Needs*, University of California, Davis UCD-ITS-RR-95-23

Burke, Andrew (1999), *Review of Ultra Capacitor Technologies for Vehicle Applications*, Advanced Battery Conference, Las Vegas

Burke, Andrew (2000), *Ultracapacitors: why, how, and where is the technology, Journal of Power Sources*, preprint 2000

Burke, Miller (2000), *Experimental Study of the Shin Kobe Lithium Ion Batteries for Electric and Hybrid Vehicles Applications*, non-published ITS report

California Air Resources Board (2000), *Zero Emission Vehicle Program*, Biennial Report

Cunningham J. M., M. A. Hoffman, R. M. Moore, D. J. Friedman (1999), *Requirements for a Flexible and Realistic Air Supply Model for Incorporation into a Fuel Cell Vehicle*

(FCV) System Simulation, Society of Automotive Engineers SAE Paper Number 1999-01-2912.

Cunningham J. M, (2000), *The implications of using an expander (turbine) in an air system of a PEM fuel cell engine*, Electric Vehicle Symposium 17, Montreal 2000

Cunningham, J. (2000), *The direct hydrogen fuel cell system model of the University of California*, Davis, work in progress

Daimler Chrysler (1999), *Offen fuer alle Optionen*, company brochure from Daimler Chrysler

Dessaint, L.-A.; Al-Haddad, K, (1999), *A power system simulation tool based on Simulink*. IEEE Transactions on Industrial Electronics, vol.46, (no.6), IEEE, p.1252-4.

Donelli, M. (1998), Electric Vehicle Motor Drive Simulation, Presentation available on the Internet: http://www.analogy.com/Auto/Apptech/ElecSys/ElecVehicle/index.htm

Eggert, A. (2000), *Characteristics of an indirect-methanol fuel cell system*, American Institute of Aeronautics and Astronautics, paper number 2000-3040

Eggert, A. (2001), *Simulated performance of an Indirect Methanol Fuel Cell System*, SAE 2001-01-0544

Endres, Thomas E. (1999), *Advantages of Rapid Prototyping*, Society of Automotive Engineers SAE 1999-01-3433

Friedrich, Horst, Siegfried Koehle, Peter Lueck, (1998) *The Volkswagen Electric Vehicle Objectives and Technology*, Volkswagen AG Research Center

Friedman, D.J. (1998), *Programming of a Fuel Cell Stack Model in Simulink*, private conversations and unpublished work

Friedman, D.J. (1999), *PEM Fuel Cell System Optimization*, Proceedings of the 2nd International Symposium on Proton Conducting Membrane Fuel Cells II, Electrochemical Society, Pennington, New York

Friedman, D. J. (1999), *Maximizing Direct-Hydrogen PEM Fuel Cell Vehicle Efficiency: Is Hybridization Necessary?,* SAE Society of Automotive Engineers, paper number 1999-01-0530

Friedman, D. J. (2000), *Reformate Fuel Cell Stack Characteristics And System Interactions*, Published American Institute of Aeronautics and Astronautics, IECEC conference 2000, paper number 2000-3045

Friedman D. J., A. Eggert (2001), *Maximizing the Power Output of an Indirect Methanol PEM Fuel Cell System: Balancing Stack Output and Air Supply/Water and Thermal*

Management Demands, Society of Automotive Engineers SAE paper number 2001-01-0535

Foellinger, Otto (1985), *Regelungstechnik,* 5th edition, Dr. Alfred Huethig Verlag Heidelberg

Ford Ecostar (2001), *Design specifications of the transaxle drive train*, World Wide Web: www.ecostardrives.com

General Motors Europe (1999), *Energy for Our Mobility Tomorrow, Fuel Cell Technology* ,company brochure, GM Europe international communications, P.O. Box Stelzenstrasse 4, CH-8152 Zurich Switzerland, ordernumber 0864154

Gillespie, Thomas (1992), *Fundamentals of Vehicle Dynamics,* Published by Society of Automotive Engineers

Hanselmann, Herbert (1999), *Automatische Generierung von Produktionscode fuer Seriensteuergeraete*, Proceedings of the 2nd Symposium Steuerungssysteme fuer den Antriebsstrang von Kraftfahrzeugen, Published by Ingenieuergesellschaft Auto und Verkehr GmbH, p. 233-256

Hauer, Karl-Heinz (2000), *Literature Overview About Fuel Cell Vehicle Modeling Programs,* unpublished work

Hauer, Karl-Heinz (2001), *The Hybridized Fuel Cell Vehicle Model of the University of California, Davis,* SAE World Congress 2001, SAE 2001-01-0543

Heath, R.P.G., C.Y. Mo (1996), *A Modular Approach to Powertrain Modeling for the Prediction of Vehicle Performance, Economy and Emissions,* Ricardo Consulting Engineers Ltd, SAE 960427

Huet, F. (1998), *A review of impedance measurements for determination of the state-of-charge or state-of-health of secondary batteries*, Journal of Power Sources, 70 (1998) 59-69

Hoefgen, T. (2001), *A comparison of different fuel cell vehicle models*, University of California, Davis

Hyprotech (2000), *Internet page http://www.hyprotech.com/index.html*

Idaho National Engineering and Environmental Laboratory (1993), Simplev Documentation, DOE ID-10293-2 (http://ev.inel.gov/simplev/manual.html)

Jacobson, Bengt (1995), *On Vehicle Driving Cycling Simulations,* Society of Automotive Engineers SAE 950031

Kee, Robert J. (1996), Chemkin III : *A Fortran Chemical Kinetics Package For The Analysis Of Gas Phase Chemical And Plasma Kinetics*, Sandia National Laboratories, SAND96-8216. The document is also available on the Internet at: http://stokes.lance.colostate.edu/chemkinmanualslist.html

King, Robert D. et. al. (1998), *Ultracapacitor/Battery Electronic Interface Development,* Prepared by General Electric for the U.S. Department of Energy (DOE), contract DE-FC07-96ID12406

Leonhard, Werner (1985), *Einfuehrung in die Regelungstechnik*, Vieweg Verlag, 3rd edition (German)

Leonhard, Werner (1990), *Digitale Regelungstechik,* Teubner Verlag, 1st edition (German)

Leonhard, Werner (1996), *Control of electrical drives*, Springer Verlag, 2nd completely rev. edition

Li, J.; P.H. Mellor et. al. (1999), *Modeling and evaluation of advanced traction systems and new technology vehicles with SABER*, University of Sheffield, Department of Electronic and Electrical Engineering, Electric Vehicle Symposium 1999

Lloyd, Alan (1999), *Transportation, Energy and Environmental Policy for the 21st Century*, Presentation at the Asilomar Meeting of UC Davis

MacBain, John A. (2000), *Co-Simulation of Advisor and Saber- A Solution for Total Vehicle Energy Management Simulation* , proceedings Advisor User Conference

McBroom, Scott T. et. al. (1999) *Models get tooled up*, Electric and Hybrid Vehicle Technology 99, 66-70.

Mathwork corporation (2001), *Simulink Helpdesk,* www.mathworks.com

Matthe, Roland (1999), *Electric Vehicles Powered by Fuel Cells at GM/Opel- a Global Project,* General Motors AG

Maxwell (2000), *PC 2500 Data Sheet 05-00*, Maxwell Technologies, World Wide Web: www.maxwell.com

Menne, Marcus and De Doncker, Rik W. (1999), *Non-Linear Dynamic Model of an Electric Vehicle Drivetrain*, conference proceedings on CD-Rom, Electric Vehicle Symposium 16

Moreland, J (1998), Choosing a Simulation Tool, IEE Colloquium ”Power Electronic System Simulation” 1998

Nahmer, Stephan (1996), *Antriebssysteme fuer Elektrofahrzeuge*, Dissertation, Technische Universitaet Braunschweig

National Renewable Energy Laboratory (NREL), *Advisor Documentation and Help Files*, World Wide Web: http://www.ctts.nrel.gov/analysis/download.html

National Research Council (1997), *Trends and Outlook in Motor Vehicle Transportation*, TRB Special Report 251

Ohl, Gregory Lyle (1995), *Dynamic analysis of a methanol to hydrogen steam reformer for transportation applications*, Dissertation, University of Michigan, 1995

Ogata, Katsuhiko (1998), *Modern Control Engineering*, 3rd edition

Ogden, Joan M., M. Steinbuegler, T. Kreutz (1998), *A comparison of hydrogen, methanol and gasoline as fuels for fuel cell vehicles: implications for vehicle design and infrastructure development*, Journal of Power Sources 79 (1999) 143-168

Panik, Ferdinand, Dietmar Beck (1999), *The fuel cell – A powertrain stretched between IC-Engine and alternative forms of energy*, Daimler Chrysler

PNGV (2001), *PNGV Targets*, Calstart Webpage: www.calstart.org/about/pngv/pngv-ta.html

Peters, R.,H. Duesterwald, B.Hoehlein, (1998), *Simulation of Fuel Cell Powered Vehicles*, Forschungszentrum Juelich GmbH

Ramaswamy, S. (2000), *System dynamics and efficiency of the fuel processor for an indirect methanol fuel cell vehicle*, American Institute of Aeronautics and Astronautics, paper number 2000-3048

Ramaswamy, S. (2001), *Efficiency, dynamic performance and system interactions for a compact fuel processor for indirect methanol fuel cell vehicles*, SAE 2001-01-0231

Ramaswamy, S. (2001), *Numerical model of a gasoline (Iso Octane) fuel processor*, unpublished work and private conversations

Ricardo Consultants (2000), *Brochure about Wave*, The brochure is also available on the Internet at http://www.ricardo.com/index.htm?pages/search.htm

Rousseau Aymeric (2000), Argonne National Laboratories makes the PSAT software for researchers in the field of electric and hybrid vehicles available, private conversation with Aymeric Rousseau, email: ARousseau@perilous.es.anl.gov

Sadler, Melanie (1998), *A Dynamic Model of a Fuel Cell Car*, Powerpoint Presentation at UC-Davis Fuel Cell Modeling Workshop 1998

Stobart, Richard K. (1999), *Engine and Control System Modeling to Reduce Powertrain Development Risk*

Sievert, Dietrich (1968), *Das Dynamische Verhalten der H2/O2 Brennstoffzelle und Probleme Ihrer Anwendung (Dynamic behavior of H2/O2 fuel cells and problems in applications)*, Dissertation Technische Universitaet Braunschweig

Skudelny et. al. (1993), *Antriebe fuer Elektrostrassenfahrzeuge*, Institut fuer Stromrichtertechnik und Elektrische Antriebe, Rheinisch-Westfaelische Technische Hochschule Aachen, FAT Schriftenreihe Nr. 104

Sundaresan, Meena et. al. (2000), *Steam Reformer/Burner Integration and Analysis for an Indirect Methanol Fuel Cell Vehicle,* American Institute of Aeronautics and Astronautics, IECEC conference paper 2000-3047

Springer, T.E., M.S. Wilson, S. Gottesfeld (1993), *Modeling and Experimental Diagnostics in Polymer Electrolyte Fuel Cells,* Journal of Electrochemical Society, Vol. 140,No. 12, pp. 3513-3526

Springer, T.E., T.A. Zawodzinski, M.S. Wilson, S. Gottesfeld (1996)*, Characterization of Polymer Electrolyte Fuel Cells Using AC Impedance Spectroscopy*, Journal of Electrochemical Society, Vol. 143,No. 2, pp. 587-599

The International Panel on Climate Change, Working Group I (1995), *Summary for Policymakers: The science of climate change,*
World Wide Web: http://www.ipcc.ch/pub/sarsum1.htm

UC-Davis, Fuel Cell Modeling Team (1998), *Description of the hydrogen fuel cell vehicle model,* internal document of the Institute of Transportation Studies

UC-Davis, Fuel Cell Modeling Team (2000), *Description of the indirect methanol fuel cell vehicle model,* internal document of the Institute of Transportation Studies (in progress)

Volkswagen AG (1999), *Personal conversations in the department of hybrid and electric vehicles*

Wallentowitz (1999), *Strukturvarianten von Hybridantrieben*, Institut fuer Kraftfahrwesen, University of Aachen

Wiegman, H.L.N. (2000), *Mass Transport and Direction Dependent Battery Modeling for Accurate On –Line Power Capability Prediction,* GE Corporate Research and Development 1, Published at EVS 17

Wipke, K.B. Cuddy, M.R. and Burch, S.D (1999), *Advisor 2.1: A User – Friendly Advance Powertrain Simulation Tool Using a Combined Backward/Forward Approach*, National Renewable Energy Laboratory, NREL/JA-540-26839

9. Appendix

9.1. Forwards and Backwards Looking Modeling Approach

Among the compared models two in principle different modeling techniques have been applied. These are the “forward looking” approach and the “backward looking” approach as defined by the Southwest Research Institute (McBroom, 1999). Ricardo consultants reference both cases with “dynamic transient” (forward looking) and “quasi-stationary” (backward looking) (Heath and Mo, 1996). Argonne National Laboratories reference the backward looking approach as a “Combined Backward/Forward Approach”. All terminologies are somewhat misleading and reflect only poorly the characteristics of the different approaches. A better way to distinguish both approaches would be renaming them as “causal approach” instead of forward-looking approach and “non causal” approach instead of backwards looking approach. However this work uses the terminology defined by the Southwest Research Institute because it is already established.

Figure 9-1 and Figure 9-2 are graphical illustrations of both methods.

The forward-looking approach starts with a driver that compares the desired drive cycle with the actual vehicle velocity. In case that the vehicle velocity is below the in the drive cycle specified velocity the driver requests more motor power and the extra power leads to an acceleration of the vehicle until the difference of specified and actual velocity is zero. The causal relation between driver, vehicle and components is the same as in a physical vehicle.

In the backwards-looking approach causality is reverse to physical reality starting at the wheels and ending at the most remote component in the vehicle in terms of energy flow. Because of this setup the name backwards approach has been established. A backwards-looking model answers the question: How does each component have to perform assuming that the vehicle speed is given? Unlike in a forward-looking model an explicit driver is not required.

Both modeling techniques have different advantages / disadvantages that will be discussed in more detail in this chapter. The modeling work in this dissertation is employing a forward-looking approach.

Forward approach

The forward approach assumes causality, meaning that it assumes that system inputs are known (brake pedal position, acceleration pedal position) and the system states[67] such as vehicle velocity, battery state of charge, motor speed etc. are computed (Heath and Mo, 1996, McBroom, 1999, Jacobson 1995, Wipke, 1999). The trajectories between the initial and final system states are determined by the set of differential equations describing the system. In this approach the trajectory is emphasized and leads to the final system state and vector of output variables (McBroom, 1999). This method follows the standard controls approach as described in (Leonhard, 1996, Foellinger, 1985, Ogata, 1998). The driver represents the controller for the system vehicle. The primary controlled system state is the vehicle velocity. Consequently in this approach the driver is

[67] The in this work applied definitions of system and system states is given in (Ogata, 1998). The system referred to in this context is the vehicle without the driver. System states are a set of variables that describe the condition of the vehicle (speed, state of charge, radiator temperature, state of controls …)

not part of the analyzed system. This is in accordance to experiments, such as roller bench tests, in which the vehicle is always characterized without mentioning the driver.

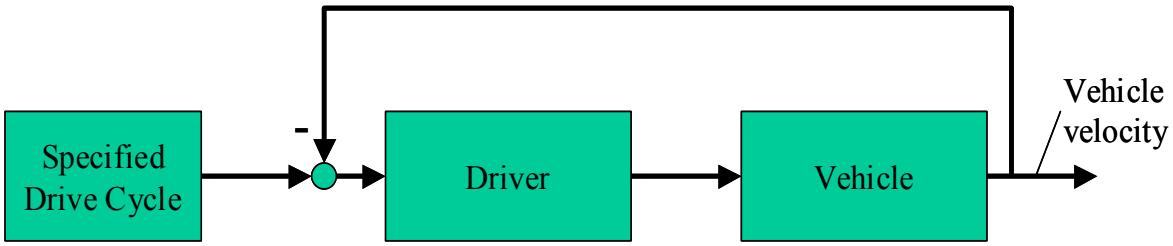

Figure 9-1: Forward approach for a vehicle model. Driver and vehicle model are separated. The controlled property of the vehicle is the vehicle velocity.

The forward approach does support the direct transfer of control algorithms from the simulation software into existing hardware (rapid prototyping). Software programs supporting this transfer for models employing a forward structure are available from various companies such as Dspace (Hanselmann, 1999).

The forward approach is followed by Ricardo Consultants (Heath, 1996, Sadler,1998) and Southwest Research Institute in the simulation programs Path and PSAT (McBroom, 1999).

Backwards approach

The backwards approach on the other hand takes the vehicle velocity as an input variable. Based on this input the required wheel torque is calculated to meet this specified velocity. The wheel torque feeds into the transmission and establishes the necessary motor torque. The motor torque is then taken for calculating the electric requirements necessary to supply the demanded motor torque and these requirements feed then into the fuel cell system and establish compressor requirements, reformer requirements etc. (Idaho National Renewable Energy Laboratories, 1993), National Renewable Research

Laboratory, 2000). At the last link of the calculation scheme the direction of information flow reverses. Starting at this last link the last component, e.g. the air compressor in a fuel cell system, responds with the fraction of the request it could supply. This supplied quantity is then taken by the component that requested it and this component, e.g. the fuel cell stack, will now take it and calculate the electricity generation based on the supplied air. The process is repeated until finally the vehicle velocity is calculated based on the supplied wheel torque. The calculation is basically done backwards starting at the wheels and ending at the fuel cell system, reversing there and going back to the wheels (Wipke 1999). However, if one component is not able to meet the requested value, e.g. the fuel cell system is not able to supply the requested motor power, the calculation has to be redone if component properties depend on the operating point. For the case that the fuel cell system is not able to supply the requested power it means that the motor calculations have to be redone because the motor effectively operates at a different operating point. However if the motor operates at a different operating point the initial request to the fuel cell system is subject to change. An accurate determination of the final operating point can only be found by employing an iteration process between the two interacting components. A task that could become increasingly complex if properly programmed. None of the backwards-looking models employs this iteration process and therefore all these models have a principle error in addition to inaccuracy of the model setup itself (Idaho National Renewable Energy Laboratories, 1993, National Renewable Research Laboratory, 2000, Wipke 1999). The additional error due to the modeling approach depends highly on the drive cycle and is smaller for drive cycles that underutilize each component, e.g.. in low demanding drive cycles. For the case of extreme acceleration the

error could become significant if component characteristics depend significantly on the operating point.

With the respect of the modeling requirements stated at the beginning of this chapter the backwards approach is less physically and mathematically sound than the forward approach. The physically soundness is not mutually given because the law of causality is not followed through within the model. Example: The wheel speed is not the causal reason that the electric motor draws electricity from the fuel cell stack. The mathematical soundness is not mutually given because the method of backwards modeling is only very limited discussed in the literature. Fundamental questions, such as stability criteria and proof for the uniqueness of the provided solution are not answered at all. Criteria for the error estimation for the case that a component is unable to meet the request are not derived yet. A tutorial paper explaining the underlying mathematics of the backwards approach could not be found.

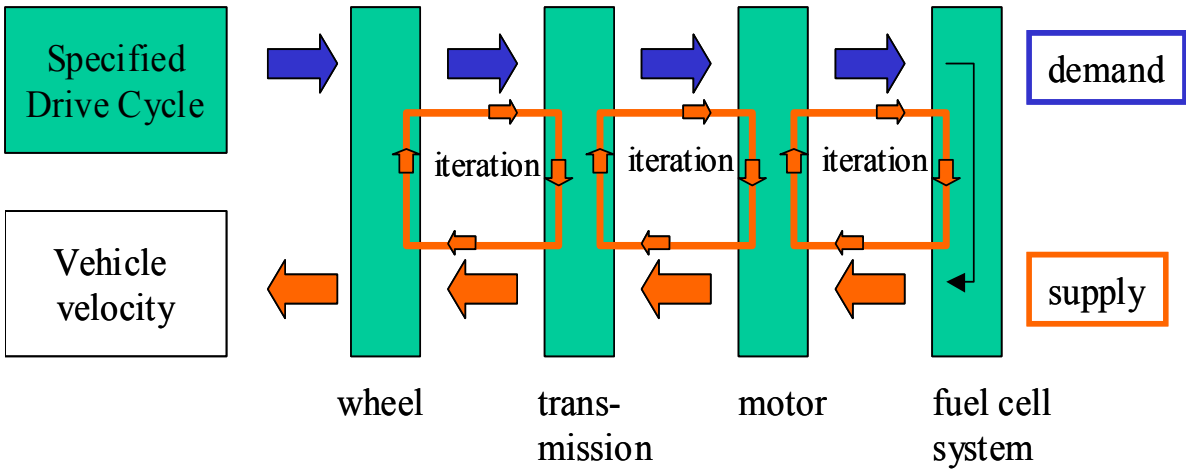

Figure 9-2: Backwards looking method. It is no explicit driver employed. The calculation is backwards starting at the wheels and working its way up to the fuel cell system. All systems respond with a supply to the previous stage. The final result is the vehicle velocity. The iterations shown in the graphics are one way to compensate for cases in which the supply falls short of the demand. However neither of the investigated models employs these additional routines.

The backwards approach does not support the direct transfer of control algorithms from the simulation software into existing hardware (rapid prototyping).

The backwards approach is taken by National Renewable Energy Laboratories with their program system Advisor, Southwest Research Laboratory in the simulation program Elvis (McBroom, 1999), University of Sheffield (Li and Mellor, 1999) and University of California Davis in their 1st generation hydrogen fuel cell vehicle model (UC Davis, Fuel Cell Modeling Team 1998).

9.2. Method of Co-Simulation

Complementary to stand alone fuel cell vehicle models exist a number of tools to assist the modeling of different aspects of fuel cell systems, such as chemical kinetics (Chemkin), process modeling (Wave, Hysis), electric drives and power electronics (Saber), or digital decisions (State flow).

For the complete fuel cell system analysis, except the vehicle, Argonne National Laboratories provides a package of specialized C-procedures named GC-tools that could be used for modeling the different fuel cell system components as well as the fuel cell system component interaction, such as air compressor and fuel cell stack. However this tool is not a complete fuel cell system-modeling program. GC-Tools is also not meant for modeling the vehicle aspects of a fuel cell vehicle. Instead it assists the user with the development of his own fuel cell system model in any C or C compatible program language. The package is commercially available under the name GC-Tool.

The Boeing Corporation commercially provides the program package Easy5. Easy5 allows the composition of systems based on basic components such as heat exchangers, compressors, valves and electric motors. However currently Easy5 does not support the simulation of fuel processors and gas clean up stages. A complete built up of a fuel cell system only using Easy5 is therefore impossible. Similar to GC-Tools, Easy5 is not meant to simulate a complete fuel cell vehicle. An overview about the different specialized software packages provides Table 9-1.

All of the currently available fuel cell vehicle models are programmed in Matlab/ Simulink[68]. Therefore the question of how the different tools could be integrated in a fuel

[68] With the exception of Simplev which is programmed in basic

cell vehicle model translates into how Matlab/Simulink interfaces with each of the tools in Table 9-1. Figure 9-3 shows the basic principle how the different complementary program packages, listed in Table 9-1, interact with Matlab/Simulink. The method is the method of co-simulation and is explained by John A. MacBain in his paper “Co Simulation of Advisor and Saber – A Solution for Total Vehicle Energy Management Simulation” (McBain, 1999). Other examples of co-simulation are given in the Matlab Helpdesk (Mathworks Corporation, 2000).

Name	Source	Description
Chemkin	Sandia National Laboratories, Livermoore (Kee 1996)	Fortran chemical kinetics package for analysis of gas phase chemical kinetics. In addition to this program Sandia provides the Fortran routine collection "Surface Chemkin" an analysis package for analyzing heterogeneous chemical kinetics at a solid-surface -- gas-phase interface. Example applications for both program routine collections are the simulation of the kinetics in the fuel processor.
Wave	(Ricardo Consultants, 2000)	1-dimensional gas dynamics simulation software. Examples for fuel cell vehicle applications are the modeling of the gas dynamics in the air supply system.
Hysim and Hysis	(Hyprotech 2000)	Process Engineering Software Hysim allows steady state process simulation and optimization while Hysys allows in addition the simulation of dynamics related to the start up and shut down of processes. Examples for fuel cell vehicle applications are the simulation of the steady state and dynamic fuel processor characteristics.
Saber	(Donelli 1998, Li 1999, Moreland 1998)	Mixed signal circuit simulation program. Applications in fuel cell vehicles are the simulation of power electronics
Power System Blockset	(Mathworks Inc. 1999, Dessaint 1999)	Simulation of electric drive systems and power electronics
Stateflow	Mathworks Inc. 1999)	Software for the development of graphical models of event-driven systems using finite state machine theory. An example in a fuel cell vehicle would is the modeling of the shift logic in a multi speed transmission.
GC-Tool	(Argonne National Laboratory 2000)	Collection of C routines supporting the simulation of fuel cell system components, such as air compressors, expanders etc.
Easy5	(Boeing Inc. 1999)	Easy5 is a program package designed for component modeling such as heat exchangers, compressors, expanders and electric motors. Possible applications in fuel cell systems are the simulation of the mentioned components

Table 9-1: Assisting program package for modeling fuel cell systems and fuel cell vehicles.

The underlying principle is that the vehicle model (programmed in Matlab Simulink) and the complementary specialized tool for modeling one aspect or component of the vehicle run in parallel on the same computer in a resource sharing mode. Each simulation step both programs are stopped and the relevant data between vehicle model (Matlab Simulink) and component model (Specialized tool) are exchanged. After this exchange of data both models are restarted until the next data exchange is required. The time between the data exchange is determined by the slowest system. For example given are:

- A power electronic with a switching frequency of 20 kHz,
- An electric drive train with a mechanical resonance frequency of 8.5 Hz[69].

Both systems are modeled using different simulation tools and applying the method of co-simulation. The time interval a data exchange is required is not determined by the more transient system (here the power electronic with a time constant in the order of magnitude of 50 μsec (1/20 kHz) but by the less dynamic characteristics of the drive system. The reason is that the less dynamic system acts as a filter for the more dynamic system. In the given example the exchange of data every 50 μsec would not influence the drive train behavior. However the more frequent data exchange would slow the simulation down.

[69] The calculation of the eigenfrequenz of a multiple mass mechanical drivetrain is discussed by Markus Menne and Rik. W. DeDoncker from the University of Aachen in their paper "Non Linear Dynamic Model of an Electric Drive Train" (Menne and DeDoncker, 1999)

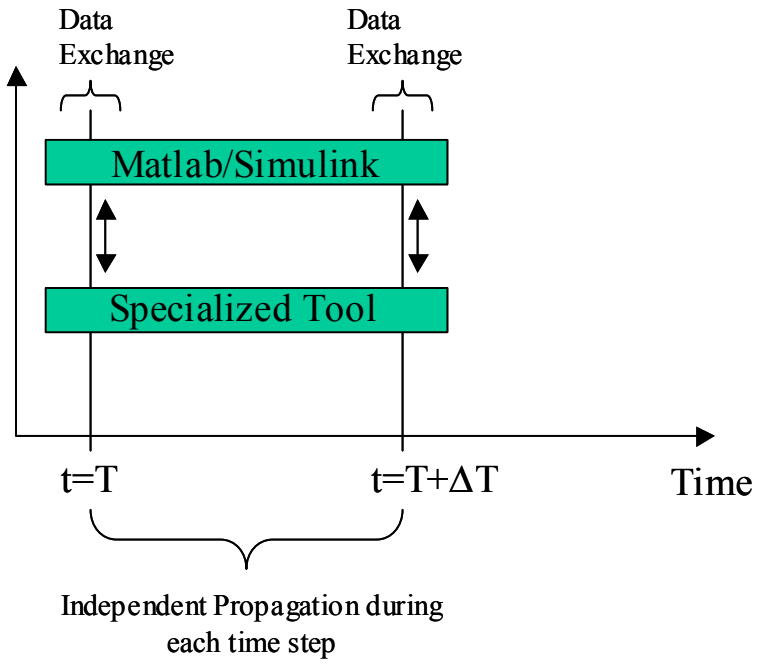

Figure 9-3: Principle of Co-simulation.

Due to the commitment the model in Matlab/Simulink none of the tools in Table 9-1 was applied in this dissertation.

Other reasons for not employing the method of co-simulation are:

- The modeling effort was driven by the macroscopic vehicle properties. Objective was to program a vehicle model answering questions about fuel economy, acceleration and emissions. Individual components such as a compressor electronic or heat exchangers are only modeled with their impact on the overall fuel economy of the vehicle. Therefore the model is not meant as a tool to assist the design of specific components considering the specific needs of each component. More specifically for the example of modeling a heat exchanger the fluid flows, temperature distribution and heat flows within the device are not modeled although important for the design of such a component. Co-simulation,

employing programs such as Easy5, would support the modeling in this level of detail and be of great value for a heat exchanger manufacturer. However the employment of Easy5 would not necessary support the accomplishment of the objectives stated above.

- The simulation run time increases significantly with co-simulation. The reasons are firstly that the coordination and data exchange between the two different programs requires overhead and secondly that the level of detail modeled increases and this increase requires additional computational time.

However the forward-looking causal program structure supports the employment of co simulation wherever necessary[70]. The main issues are that the model is forward-looking and therefore causal and secondly the strict separation of control algorithms from component descriptions. The causality eases the direct employment of additional tools and the separation of controls and component models eases the integration of highly specialized tools, such as Saber for circuit simulation, without the need to worry about how to transfer control elements into a specialized tool for component modeling. The necessary control algorithm could still be realized in Matlab/Simulink.

[70] In principle both modeling approaches allow the method of co simulation. However due to the inverse causality of the backwards approach it is necessary to employ an additional control loop that takes the request value as a controls variable. Although such a strategy is always possible the additional control loop modifies the system in an, in general case, unpredictable manner. Co-simulation for the backwards approach relies therefore heavily on empirical validation with experimental results.

9.3. *Rapid Prototyping*

Endres defines Rapid Prototyping as follows: “Rapid Prototyping is a group of advanced technologies for converting designs from computer representations directly into solid objects without human intervention.” (Endres,1999). Originally the phrase “rapid prototyping” was applied only for processes generating solid objects directly from computer data. However later it became a synonym for the direct transfer from data into hardware. The transferred data could be either CAD data for machining a on the computer designed structure or program code in any form. In this context rapid prototyping stands for the transfer of, in a computer model, tested control algorithm into an existing hardware, e.g. an engine controller (Figure 9-4).

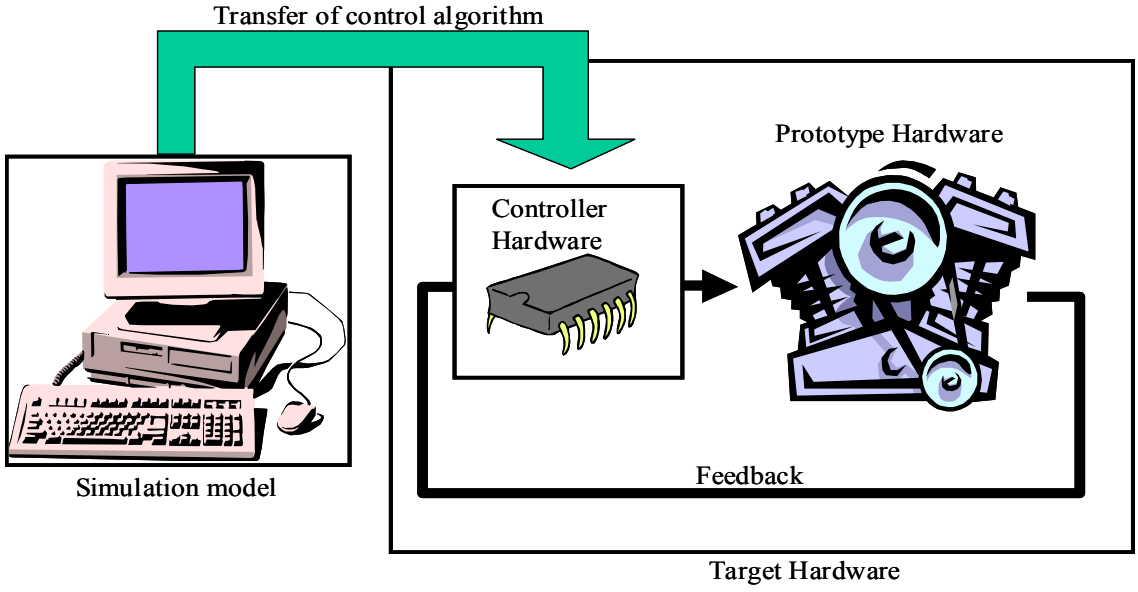

Figure 9-4: Principle of “Rapid Prototyping”

The methods of rapid prototyping and hardware in the loop are well-established tools in system development (Hanselmann, 1999). Stobart describes rapid prototyping as a “prominent feature of engine management development …” (Stobart, 1999)

Rapid Prototyping benefits:

- a faster development process because controls can be developed before hardware exists,
- a test of controls in the "safe" software environment,
- a mutual validation of the model because the model is not only used at the end of a development process but also within the development process itself. Therefore a continuous validation through the whole process takes place.

Rapid prototyping implies the separation of component models (mathematical representations of the hardware) from control algorithms. Only the control algorithms will be transferred into the existing controller hardware.

The non-causality of backwards facing models makes rapid prototyping impractical because the direct translation and transfer of control algorithms from the, non-causal, backwards facing model into the causal and forward facing prototype hardware is not possible.

9.4. Conversion Factors

	Methanol	Gasoline
Density	0.79 kg/l	0.74 kg/l
Lower Heating Value	19.7 MJ/kg	42.7 MJ/kg

Table 9-2: Conversion Factors (Bosch 1991)

9.5. Vehicle Parameters

```
% Parameter file for Vehicle and Driver
%
% Karl-Heinz Hauer
% Version 1.0
% January 2001

%*****************************************************************************************************

% Auxiliary power except fuel cell system (head lights, stereo, ...)
FCV.vehicle.auxilary_power = 200              % [W]

% Buffer for hydrogen enabled or disabled in FCS_h2buffer file


% Driver
FCV.driver.proportional=0.3;
FCV.driver.integral=0.0;                      % Set to zero to improve dynamic response on step cycle (prev = 0.05)
FCV.driver.prediction_time=0.5;               % enables the driver to base his action on the drive cycle requirements xx sec ahead [sec]
FCV.driver.prediction_factor=0.1;             % determines how strong the drivers considers the drive cycle xx sec ahead of now
FCV.driver.contr.T_const=0.2;

% Drive Cycle
IM_FUDS_c;                                    % default drive cycle
FCV.cycle.grade_in_percent=0;                 % grade in percent e.g. 10% or 20% ...

% Regnerative braking and mechanical braking
FCV.vehicle.regen_exclusive=0.3;              % the first xx% are regenerative braking. The remainder is mechanical braking
FCV.vehicle.regen_strength=0.5;               % regenerative strength parameter
FCV.vehicle.maximum_braking_force=10000;      % maximum mechanical braking force in N; Note deceleration for
                                              % passenger vehicles 5.8m/s^2
                                              % according to Bosch Kraftfahrtechnisches Taschenbuch page 600

% Vehicle Parameter
FCV.vehicle.cw=0.2;                   % aerodynamic drag coefficient
FCV.vehicle.A=2;                      % frontal area [m^2]
FCV.vehicle.r=0.3556;                 % tire radius
FCV.vehicle.teta_wheels=2;            % wheel inertia
FCV.vehicle.m=1572.9;                 % vehicle test weight [kg]
FCV.vehicle.mu=0.01;                  % includes bearing friction
FCV.vehicle.mu1=0;
FCV.vehicle.mu2=0;


% Motor parameter (75kW induction motor)
FCV.vehicle.motor_scalar = 0.9                % parameter to scale the motor up and down (if 1.0 the motor is not scaled)
FCV.motor.inertia=0.1;                        % Motor inertia in [kg*m*m]

% Motor Controller Parameter
FCV.motor.contr.proportional=0.0;             % Proportional part of motor controller
FCV.motor.contr.integral=0.1;                 % Integral part of motor controller
FCV.motor.contr.T_const=0.01;                 % Previously 0.1;
FCV.motor.contr.volt_contr_in = [200 220 250 290 300 350 400];      % limit motor power if battery voltage is too low
FCV.motor.contr.volt_contr_out = [0 0.5 1 1 1 1 1];                 % limit motor power if battery voltage is too low


% motor speed in rpm
FCV.motor.input_speed_for_max_torque = [0 500 1000 ...
    1500 2000   2500 3000 3500 4000 4500 50005500 6000 6500 7000 7500 8000 8500 9000 9500 10000 10100];

% motor voltage in V
FCV.motor.input_voltage_for_max_torque = [ 50 100 190 200 250 300 350 400];

% torque map(horizontal speed, vertical voltage)
% See Figure 4-8
```

```
% ------------------------------------------------------------------------------------------------------------
  % Motor efficiency map
% efficiency map (horizontal torque, vertical speed)
% See Figure 4-7


% input speed for motor efficiency map rpm/min
FCV.motor.input_speed_for_motor_efficiency = [200 770 1540 2310 3080 3850 4620 5390 6160 6930 7700 8470 9240 10010];

% motor torque in Nm
FCV.motor.input_torque_for_motor_efficiency = FCV.vehicle.motor_scalar *
 [-270    -253  -236  -219  -202  -185  -168  -151  -135  -118  -101  -84   -67   -50.6 -33.8 -17.5 -10   -5    -0.1...
    0.1    2     6     7.5   15.8  30.6  67.5  84.3  101.3       118.1       135   151   168   185   202   219   236   253   270];


%-------------------------------------------------------------------------------------------------------
% transmission parameter

FCV.tx.ratio=8.9;                           % transmission ratio [1]

% speed at the motor side in rpm/min
FCV.tx.input_speed_for_tx_efficiency= [200 770 1540 2310 3080 3850 4620 5390 6160 6930 7700 8470 9240 10010];

% torque at the motor side in rad/sec
FCV.tx.input_torque_for_tx_efficiency = FCV.vehicle.motor_scalar * [-270.0-253.0      -236.0      -219.0      -202.0      -185.0…
                                    -168.0-151.0      -135.0      -118.1      -101.3      -84.3 -67.5 -50.6 -33.8 -17.5 -10.0 -5.0  -1.0...
    1.0     5.0   10.0  17.5  33.8  50.6  67.5  84.3  101.3       118.1       135.0       151.0       168.0       185.0       202.0       219.0
      236.0       253.0       270.0];

% efficiency map (horizontal torque, vertical speed)
% See Figure 4-13

%-------------------------------------------------------------------------------------------------------

% DC-DC converter
% This is a generic map for a dc-dc converter efficiency
% The efficiency drops with increasing power and increasing voltage difference


FCV.dc_dc.power = 10000*[-8 -7 -6 -5 -4 -3 -2 -1 -0.1 0.1 1 2 3 4 5 6 7 8]; % dc-dc power bus side [W]

FCV.dc_dc.volt_ratio=[1.1 1.3 1.5 1.7 1.9 2.1]; %voltage ratio bus voltage over ultra-capacitor voltage [1]

% dc-dc efficiency map for both directions of energy flow
% See Figure 4-43
%-------------------------------------------------------------------------------------------------------

FCV.h2buffer.enable=1;                          % enables (external) buffer when 1
                                                % disables (external)buffer when 0

%-------------------------------------------------------------------------------------------------------

% Constants
FCV.constant.g=9.81;                            % m/s^2
FCV.constant.rho_air=1.168;                     % air density kg/m^3
F=96487;                                        % Faraday constant in As/mol
```

9.6. Battery and the Battery Controller Parameters

```
% Parameter file for Block Battery and Controller
% Battery Type: Li Shin-Kobe
% Karl-Heinz Hauer
% Version 1.0
% January 2001
% Updated February 2001 with scalar, cell mass, module mass and battery mass (Hauer)

%*************************************************************************************************

% Cell data:
% Weight: 0.3 kg
% Nominal capacity 3.6 Ah
% 4.536 Peukert constant (source Andy Burke)
% -0.0187 Peukert exponent

%-------------------------------------------------------------------------

% Battery controller

% Parameters for the current request depending on soc
FCV.battery.SOC_ini=0.85;                                   % initial soc
FCV.battery.SOC_max=0.87;                                   % maximum soc
FCV.battery.SOC_min=0.83;                                   % min soc
FCV.battery.controller.fccurrent_request_soc=75;            % requested stack current
FCV.battery.SOC_final=0.85;                                 % final soc for program termination

% Parameters for the current request depending on the average load
FCV.battery.controller.average_time=60;                 % average time for calculating the average power [sec]
FCV.battery.controller.power_treshhold=10000;           % min. power requested from fuel cell because of power average [W]
FCV.battery.controller.fccurrent_request_avg=200;       % max current requested from fuel cell because of average power

% Parameters that consider (dynamic) constraints of the fuel cell system
FCV.battery.controller.fccurrent_request_pos_slope=10;  % maximum positive stack current slope [A/sec]
FCV.battery.controller.fccurrent_request_neg_slope=-1000; % maximum negative stack current slope [A/sec]
FCV.battery.controller.fc_system_warmup_time=30;        % minimum time from start until
                                                        % a request to the fc-system is submitted [sec]

% Parameters for specifying the termination of the simulation at a specific soc
FCV.battery.controller.AH_discharged_min=20;            % minimum discharge capacity before end of simulation [Ah]
%-------------------------------------------------------------------------

FCV.battery_scalar=2;                                   % two strings of cells in parallel
% Cell data

FCV.battery.cell_mass=0.3*FCV.battery_scalar;           % kg
FCV.battery.peukert_const=4.536*FCV.battery_scalar;     % Peukert constant
FCV.battery.peukert_exp=-0.0187/FCV.battery_scalar;     % Peukert Exponent
FCV.battery.c1_capacity=4.4*FCV.battery_scalar;         % c1 capacity
FCV.battery.i1_current=4.4*FCV.battery_scalar;          % 1hour battery discharge current

% Battery Module data
FCV.battery.cells_in_module=6;                                              % number of cells per module
FVV.battery.module_mass=FCV.battery.cells_in_module*FCV.battery.cell_mass;  % kg
FCV.battery.module_number=14;                                               % number of battery modules

FCV.battery.mass=FVV.battery.module_mass*FCV.battery.module_number;
FCV.battery.rint_dis=1/FCV.battery_scalar*[0.0034 0.0032 0.0031 0.0031 ...
    0.0031 0.0031 0.0032 0.0035 0.0041];                    % discharge resistance (cell)

FCV.battery.rint_chg=FCV.battery.rint_dis;                  % charge resistance as function of soc (cell)
FCV.battery.soc=[0 0.1 0.21 0.37 0.50 0.64 0.77 0.91 1.00]; % state of charge vector (only as input for table)
FCV.battery.voc=[3.08 3.16 3.43 3.66 3.84 3.97 4.07 4.1 4.17]; % open cell voltage as function of soc
```

9.7. Ultra-Capacitor Parameters for the Directly to the Stack Coupled Ultra-Capacitor

```
% Parameter file for Block Ultra-capacitor and Controller
% Karl-Heinz Hauer
% Version 1.2
% October 2000
% Updated 03.10.2000

% Data are for Maxwell PC 2500 ,
% Reference Andy Burke and the Maxwell Webpage

%*****************************************************************************************************

FCV.vehicle.uc_scalar=1.0;                                  % scaled by Factor

% uc cell data
FCV.uc.cell_mass=FCV.vehicle.uc_scalar*0.725;               % kg
FCV.uc.cell_capacity=FCV.vehicle.uc_scalar*2500;            % Farad (was 2700 F);
FCV.uc.cell_resistance=0.0006/FCV.vehicle.uc_scalar;        % Ohm
FCV.uc.cell_voltage_max=2.7;                                % Volts
FCV.uc.cell_voltage_min= 0.5*FCV.uc.cell_voltage_max;

% uc Module data
FCV.uc.cells_in_series=136;
FCV.uc.cells_in_parallel=1;
FCV.uc.cells_number=FCV.uc.cells_in_series*FCV.uc.cells_in_parallel;
FCV.uc.module_mass=FCV.uc.cells_number*FCV.uc.cell_mass;                                          % kg
FCV.uc.module_capacity=FCV.uc.cell_capacity/FCV.uc.cells_in_series*FCV.uc.cells_in_parallel;      % Farad
FCV.uc.module_resistance=FCV.uc.cell_resistance*FCV.uc.cells_in_series/FCV.uc.cells_in_parallel;  % Ohm
FCV.uc.module_voltage_max=FCV.uc.cells_in_series*FCV.uc.cell_voltage_max;                         % Volts
FCV.uc.module_voltage_min= 0.5*FCV.uc.module_voltage_max;
FCV.uc.module_voltage_ini=1*FCV.uc.module_voltage_max;                                            % initial voltage
FCV.uc.module_charge_ini=FCV.uc.module_voltage_ini*FCV.uc.module_capacity;                        % initial charge
FCV.uc.module_nom_energy=1/3600*3/8*FCV.uc.module_capacity*...
FCV.uc.module_voltage_max*FCV.uc.module_voltage_max;                                              % energy in Wh


% Ultra-capacitor controller (not for direct coupling; for this case the ultra-capacitor is not directly controlled)
FCV.uc.controller.voltage_dcdc_on=0.70*FCV.uc.module_voltage_max;
                        % Recharge starts at 70% voltage level (not for direct coupling)
FCV.uc.controller.voltage_dcdc_off=0.80*FCV.uc.module_voltage_max;
        % Recharge stops at 80% voltage level (not for direct coupling)


FCV.uc.controller.fccurrent_request=50;                     % requested stack current for recharge
FCV.uc.controller.fccurrent_recharge_max=100                % max stack current for which recharge is allowed
FCV.uc.controller.fccurrent_request_pos_slope=15;           % maximum positive stack current slope [A/sec]
FCV.uc.controller.fccurrent_request_neg_slope=-10000;       % maximum negative stack current slope [A/sec]
FCV.uc.controller.fc_system_warmup_time=5;                  % minimum time from start until
                                                            % a request to the fc-system is submitted [sec]

FCV.uc.controller.average_time=15;                          % average time for averaging the load current

FCV.uc.controller.powersplit_in=[0 200 230 250 270 300 400 500];
                        % input vector for fuel cell stack voltage
FCV.uc.controller.powersplit_out=[0 0 0.1 0.3 0.7 1 1 1];
        % output is the fraction of load current supplied by the fuel cell system
FCV.uc.controller.min_stack_voltage=250;
%minimum stack voltage for recharging the ultra-capacitor through the fuel cell system


FCV.uc.controller.limit_acc_in =        [0.8*FCV.uc.module_voltage_min 0.9*FCV.uc.module_voltage_min
FCV.uc.module_voltage_min...
                        1.1*FCV.uc.module_voltage_min 1.2*FCV.uc.module_voltage_min];
FCV.uc.controller.limit_acc_out =       [0 0 1 1 1];
```

```
FCV.uc.controller.limit_regen_in = [0.8*FCV.uc.module_voltage_max 0.9*FCV.uc.module_voltage_max
FCV.uc.module_voltage_max...
                        1.1*FCV.uc.module_voltage_max 1.2*FCV.uc.module_voltage_max];
FCV.uc.controller.limit_regen_out = [1 1 0 0 0];
```

9.8. Ultra-Capacitor Parameters for the Via Dc-Dc Converter to the Stack Coupled Ultra-Capacitor

```
% Parameter file for Block Ultra-capacitor and Controller
% Karl-Heinz Hauer
% Version 1.2
% October 2000
% updated 03.10.2000

% Data are for Maxwell PC 2500 (2500F), Reference U3 (Andy Burke) and the Maxwell Webpage

%*****************************************************************************************************

% uc cell data
FCV.uc.cell_mass=0.725;                                          % kg
FCV.uc.cell_capacity=2500;                                       % Farad (was 2700 F)
FCV.uc.cell_resistance=0.0006;                                   % Ohm
FCV.uc.cell_voltage_max=2.7;                                     % Volts
FCV.uc.cell_voltage_min= 0.5*FCV.uc.cell_voltage_max;


% uc Module data
FCV.uc.cells_in_series=85;
FCV.uc.cells_in_parallel=1;
FCV.uc.cells_number=FCV.uc.cells_in_series*FCV.uc.cells_in_parallel;
FCV.uc.module_mass=FCV.uc.cells_number*FCV.uc.cell_mass;                                          % kg
FCV.uc.module_capacity=FCV.uc.cell_capacity/FCV.uc.cells_in_series*FCV.uc.cells_in_parallel;      % Farad
FCV.uc.module_resistance=FCV.uc.cell_resistance*FCV.uc.cells_in_series/FCV.uc.cells_in_parallel;  % Ohm
FCV.uc.module_voltage_max=FCV.uc.cells_in_series*FCV.uc.cell_voltage_max;                         % Volts
FCV.uc.module_voltage_min= 0.5*FCV.uc.module_voltage_max;
FCV.uc.module_voltage_ini= FCV.uc.module_voltage_max;                                % initial voltage
FCV.uc.module_charge_ini=FCV.uc.module_voltage_ini*FCV.uc.module_capacity;           % initial charge
FCV.uc.module_nom_energy=1/3600*3/8*FCV.uc.module_capacity*...
  FCV.uc.module_voltage_max*FCV.uc.module_voltage_max;                               % energy in Wh

% Ultra-capacitor controller
FCV.uc.controller.voltage_dcdc_on=0.70*FCV.uc.module_voltage_max;    % Recharge starts at 70% voltage level
FCV.uc.controller.voltage_dcdc_off=0.80*FCV.uc.module_voltage_max;   % Recharge stops at 80% voltage level


FCV.uc.controller.fccurrent_request=50;              % requested stack current for recharge
FCV.uc.controller.fccurrent_recharge_max=100         % max stack current for which recharge is allowed
FCV.uc.controller.fccurrent_request_pos_slope=15;    % maximum positive stack current slope [A/sec]
FCV.uc.controller.fccurrent_request_neg_slope=-10000; % maximum negative stack current slope [A/sec]
FCV.uc.controller.fc_system_warmup_time=5;           % minimum time from start until
                                                     % a request to the fc-system is submitted [sec]

FCV.uc.controller.average_time=15;                   % average time for averaging the load current

FCV.uc.controller.powersplit_in= [0 190 200 220 240 250 270 300 400];
% input vector for fuel cell stack voltage
FCV.uc.controller.powersplit_out=[0 0   0.1 0.2 0.5 0.6 0.8 1.0   1  ];
% output is the fraction of load current supplied by the fuel cell system

FCV.uc.controller.limit_acc_in =       [0.8*FCV.uc.module_voltage_min 0.9*FCV.uc.module_voltage_min ...
                        FCV.uc.module_voltage_min...
                        1.1*FCV.uc.module_voltage_min 1.2*FCV.uc.module_voltage_min];
FCV.uc.controller.limit_acc_out =      [0 0 1 1 1];

FCV.uc.controller.limit_regen_in = [0.8*FCV.uc.module_voltage_max 0.9*FCV.uc.module_voltage_max ...
                       FCV.uc.module_voltage_max...
                       1.1*FCV.uc.module_voltage_max 1.2*FCV.uc.module_voltage_max];
FCV.uc.controller.limit_regen_out = [1 1 0 0 0];


FCV.uc.controller.min_stack_voltage=230;
% Minimum stack voltage for recharging the ultra-capacitor through the fuel cell system
```

Acknowledgements

The author would like to acknowledge the discussions with and helpful input of the fuel cell modeling team at UC-Davis, which benefited this work in many aspects.

The fuel cell modeling team includes Dr. Sitaram Ramaswamy, Anthony Eggert, Meena Sundaresan, Badri Narayanan, Claudia Villa Diniz, Jose Fernando Contadini, Joshua Cunningham, David Friedman, Monterey Gardiner, Dr. M. Hoffman and the program director of the fuel cell modeling team Dr. Bob Moore.

Dr. Bob Moore and Prof. Sperling provided helpful advice for the structuring of the overall document. Their friendly and not dominating style supported independent research and the pursue of own ideas. At the same time Dr. Moore and Prof. Sperling were very valuable discussion partners from the beginning to the end to of this dissertation work.

The work was partially funded by Volkswagen AG, Chevron U.S.A. Inc., and the Institute of Transportation Studies, Davis. The author is grateful to them for their support.